

1-1-1986

## Micelle formation in block copolymer/homopolymer blends/

Dave J. Kinning  
*University of Massachusetts Amherst*

Follow this and additional works at: [https://scholarworks.umass.edu/dissertations\\_1](https://scholarworks.umass.edu/dissertations_1)

---

### Recommended Citation

Kinning, Dave J., "Micelle formation in block copolymer/homopolymer blends/" (1986). *Doctoral Dissertations 1896 - February 2014*. 710.  
<https://doi.org/10.7275/2zrg-xs53> [https://scholarworks.umass.edu/dissertations\\_1/710](https://scholarworks.umass.edu/dissertations_1/710)

This Open Access Dissertation is brought to you for free and open access by ScholarWorks@UMass Amherst. It has been accepted for inclusion in Doctoral Dissertations 1896 - February 2014 by an authorized administrator of ScholarWorks@UMass Amherst. For more information, please contact [scholarworks@library.umass.edu](mailto:scholarworks@library.umass.edu).





312066 0006 1035



MICELLE FORMATION IN BLOCK  
COPOLYMER/HOMOPOLYMER BLENDS

A Dissertation Presented

By

David John Kinning

Submitted to the Graduate School of the  
University of Massachusetts in partial fulfillment  
of the requirements for the degree of

DOCTOR OF PHILOSOPHY

September 1986

Polymer Science and Engineering

Copyright by  
© David John Kinning 1986  
All Rights Reserved



MICELLE FORMATION IN BLOCK  
COPOLYMER/HOMOPOLYMER BLENDS

A Dissertation Presented

By

David John Kinning

Approved as to style and content by:

Edwin L. Thomas

Edwin L. Thomas, Chairperson of Committee

Richard S. Stein

Richard S. Stein, Member

P. A. Monson

Peter A. Monson, Member

Julio M. Ottino

Julio M. Ottino, Member

Edwin L. Thomas

Edwin L. Thomas, Head  
Polymer Science and Engineering

DEDICATION

To my parents Darrell R. and Carol E. Kinning,  
and to my wife Lynn.

## Acknowledgements

I would like to thank Professor Edwin L. Thomas for his enthusiasm during his guidance of my research. I would also like to thank Professors Richard S. Stein, Peter A. Monson, and Julio M. Ottino for serving as committee members.

Thanks also go to Dr. Lewis J. Fetters for synthesizing the block copolymers used in this dissertation, Cam Murray and Mike Satkowski for their help with the PDP and CYBER, Dave Alward and Will McCarthy for assistance with SAXS, Lou Raboin for his help with electron microscopy, Jim Sax for assistance with transport measurements, Dave Gobran for his help with word processing, and Dr. Randal Richards for his help in setting up the non-linear least squares fitting program for SAXS data. I also thank Dr. R. J. Roe for providing a copy of his computer program to calculate theoretical micellar structure parameters.

I would also like to thank Dale Handlin, Dave Alward, Yachin Cohen, and Menas Vratsanos for helpful discussions, both scientific and otherwise. Special thanks go to John Bric, Hank Bartoni, and Joe Knight for being so easily convinced to take the afternoon off to hit the links.

Lastly, but most importantly, I thank Lynn for her love and support during the last five years.



## ABSTRACT

Micelle Formation in Block Copolymer/Homopolymer Blends

(September 1986)

DAVID JOHN KINNING

B.S., University of Minnesota

Ph.D., University of Massachusetts

Directed by: Professor Edwin L. Thomas

The goal of this dissertation is the elucidation of the formation and structure of micelles in block copolymer/homopolymer blends. A wide range of well characterized poly(styrene-butadiene) diblock copolymers and polystyrene homopolymers are employed in order that the effects of homopolymer and copolymer block molecular weights, as well as copolymer concentration, can be determined. A powerful new experimental methodology utilizing both small angle x-ray scattering (SAXS) and transmission electron microscopy (TEM) has been developed from which the structure of block copolymer/homopolymer blends exhibiting spherical micelles can be completely characterized. The SAXS from such blends has been modeled successfully using the Percus-Yevick (PY) hard sphere fluid approximation to account for the interparticle interference contributions to the scattered intensity. The combination of TEM and SAXS is a necessary part of this methodology, since TEM provides direct evidence of micelle shape, and the PY model is only applicable for the case of spherical micelles. By combining this modeling with SAXS invariant analysis and quantitative analysis of TEM images, the following struct-

ural parameters can be obtained: (1) critical micelle concentration (cmc), (2) micelle core radius, (3) polydispersity in core radius, (4) micelle corona thickness, (5) amount of homopolymer dissolved in the micelle core, (6) concentration of unaggregated copolymer, (7) concentration of homopolymer in the micelle corona, and (8) the packing mode of spherical micelles exhibiting long range order. In addition, a rigorous sample preparation technique is used to assure that equilibrium structures are obtained, enabling the predictions of the Leibler, Orland, and Wheeler (LOW) theory of micelle formation in block copolymer/homopolymer blends to be critically tested. While qualitative agreement between the experimental results and the theoretical predictions is observed, quantitative differences exist. In particular, the LOW theory predicts cmc values which are at least an order of magnitude smaller than observed experimentally.

For blends forming spherical micelles, a transition from a disordered liquid-like arrangement to a simple cubic lattice of micelles is observed at copolymer concentrations for which the micelle volume fraction exceeds about 0.5.

In addition, transitions from spherical to non-spherical micelles with increasing homopolystyrene and/or polybutadiene block molecular weight are observed by TEM, which can be explained in terms of chain packing requirements and the relative volume fractions of the micelle core and corona.

## TABLE OF CONTENTS

ACKNOWLEDGEMENTS.....	v
ABSTRACT.....	vi
LIST OF TABLES.....	x
LIST OF FIGURES.....	xi
CHAPTER	
I. INTRODUCTION.....	1
1.1 Opening Remarks.....	1
1.2 Organization of the Dissertation.....	4
II. SCATTERING THEORY.....	6
2.1 General Kinematic Scattering Theory.....	6
2.1.1 Scattering from a single particle.....	7
2.1.2 Scattering from a collection of particles...	11
2.2 Small Angle X-Ray Scattering Data Corrections....	23
2.3 SAXS Absolute Intensity.....	24
2.4 SAXS Invariant.....	29
2.5 Scattering at Large Angles.....	31
III. BLOCK COPOLYMER MORPHOLOGY.....	33
3.1 Neat Block Copolymers.....	33
3.1.1 Experimental studies.....	34
3.1.2 Thermodynamic theories.....	37
3.1.3 Lattice structure of spherical microdomains.	47
3.1.4 Ordered bicontinuous structure.....	50
3.2 Block Copolymer/Solvent Systems.....	53
3.3 Block Copolymer/Homopolymer Blends.....	61
3.3.1 Micelles in block copolymer/homopolymer	
blends.....	72
3.3.1.1 Experimental studies.....	72
3.3.1.2 Theoretical studies.....	77
IV. EXPERIMENTAL METHODS.....	86
4.1 Sample Synthesis and Characterization.....	86
4.2 Sample Preparation.....	89
4.3 Electron Microscopy.....	92
4.4 Small Angle X-Ray Scattering.....	92
V. STRUCTURE OF POLY(STYRENE-BUTADIENE) DIBLOCK COPOLYMER/ POLYSTYRENE HOMOPOLYMER BLENDS EXHIBITING SPHERICAL MICELLES.....	94
5.1 Effect of Block Copolymer Concentration.....	95
5.1.1 Critical micelle concentration.....	97
5.1.2 Blends with liquid-like packing.....	103



5.1.3	Transition to an ordered lattice of micelles	109
5.1.4	Effect of copolymer concentration on micelle core radius.....	115
5.2	Dependence of Micellar Structure on Homopolystyrene Molecular Weight.....	120
5.2.1	Critical micelle concentration.....	123
5.2.2	SAXS invariant analysis.....	124
5.2.3	Core size.....	133
5.2.4	Corona thickness.....	137
5.3	Dependence of Micellar Structure on Polystyrene and Polybutadiene Block Molecular Weights.....	142
5.3.1	Effect of PS block length.....	142
5.3.2	Effect of PB block length.....	155
5.3.3	Effect of copolymer molecular weight.....	155
5.4	Lattice Structure of Ordered Micellar Phase.....	167
VI.	COMPARISON OF EXPERIMENTAL RESULTS AND THEORETICAL PREDICTIONS FOR SPHERICAL MICELLAR SYSTEMS.....	175
6.1	Critical Micelle Concentration.....	178
6.2	Phase Mixing.....	180
6.3	Core Size.....	188
6.4	Corona Thickness.....	192
VII.	STRUCTURE OF POLY(STYRENE-BUTADIENE) DIBLOCK COPOLYMER POLYSTYRENE HOMOPOLYMER BLENDS EXHIBITING NON- SPHERICAL MICELLES.....	202
7.1	Transition in Micelle Shape with Homopolymer Molecular Weight.....	203
7.2	Transition in Micelle Shape with Polybutadiene Molecular Weight.....	212
VIII.	CONCLUSIONS AND FUTURE WORK.....	222
8.1	Conclusions.....	222
8.2	Future Work.....	226
	REFERENCES.....	229
	APPENDIX A	
	Effect of Morphology on the Transport of Small Molecule Gases in Block Copolymers.....	249
	APPENDIX B	
	BCC Lattice Structure of Diblock Copolymers Exhibiting Spherical Microdomains.....	269

## LIST OF TABLES

### Table

2.1	d spacings corresponding to the first eight reflections for common morphologies.....	13
4.1	Poly(styrene-butadiene) diblock copolymer characteristics.....	88
4.2	Polystyrene homopolymer characteristics.....	90
5.1	Root mean square end to end distances of the PS and PB blocks.....	136
5.2	Determination of lattice type for copolymer SB 20/20.	172
A1	Characteristics of poly(styrene-butadiene) block copolymers.....	255
A2	Transport data for pure components and block copolymers.....	261
B1	Molecular characteristics of block copolymers.....	271
B2	SAXS lattice spacings.....	271
B3	Comparison of intersphere distance for the various projections of SB 10/110.....	282
B4	Comparison of EM and SAXS results.....	286

## LIST OF FIGURES

### Figure

2.1	Schematic showing the scattering from a single particle.....	8
2.2	Schematic of the pair distribution function (taken from Ziman [4]).....	16
2.3	Interference function $S(hR)$ for hard sphere volume fractions of 0.1, 0.3, and 0.5.....	20
2.4	Effect of polydispersity on the interference factor	22
2.5	Schematic of SAXS geometry.....	27
3.1	Schematic showing the equilibrium domain morphology as a function of copolymer composition (from Molau [32]).....	36
3.2	Structure diagram showing the PS-PB block copolymer microdomain morphology as a function of molecular weight (given in Kg/mole) and composition predicted by Helfand's theory (taken from Helfand [74]).....	39
3.3	Structure diagram showing the regions of stability of the disordered homogeneous phase and the various ordered mesophases predicted by Leibler's theory (taken from Leibler [80]).....	45
3.4	Schematic of the ordered bicontinuous double diamond (OBDD) structure (taken from [91]). One fourth of the unit cell is shown.....	51
3.5	Schematic showing the equilibrium domain morphology as a function of copolymer composition, including the BCC lattice structure of spherical microdomains and the recently discovered ordered bicontinuous double diamond (OBDD) structure.....	52
3.6	Phase diagram of SB diblock/PS homopolymer blend obtained by Roe and Zin [126] using both SAXS and light scattering. The diblock contained 27 wt% PS and had a total molecular weight of 28,000. The homopolystyrene had a molecular weight of 2,400....	71



5.1	Schematic showing the effect of copolymer concentration on the structure of diblock copolymer/homopolymer blends.....	96
5.2	Schematic showing the structure of spherical micelles in poly(styrene-butadiene) diblock copolymer/polystyrene homopolymer blends.....	98
5.3	Determination of critical micelle concentration for copolymer SB 20/20 in 3900 PS homopolymer from SAXS	100
5.4	Electron micrographs of copolymer SB 20/20 in 3900 PS homopolymer. Copolymer concentrations are as indicated.....	101
5.5	Determination of critical micelle concentration for copolymer SB 20/20 in 3900 PS homopolymer by EM....	102
5.6	SAXS and EM results for 5.55 wt% SB 20/20 in 3900 PS homopolymer. The solid line shows the best fit to the SAXS data obtained with the PY hard sphere fluid model. The parameters of best fit are as indicated.....	107
5.7	SAXS and EM results for 11.7 wt% SB 20/20 in 3900 PS.....	108
5.8	SAXS and EM results for 17.9 wt% SB 20/20 in 3900 PS.....	111
5.9	SAXS and EM results for 24.9 wt% SB 20/20 in 3900 PS.....	112
5.10	SAXS and EM results for 30.3 wt% SB 20/20 in 3900 PS.....	113
5.11	SAXS and EM results for 49.4 wt% SB 20/20 in 3900 PS.....	114
5.12	Effect of copolymer concentration on micelle core radius for SB 20/20 in 2100, 3900, and 7400 PS homopolymer.....	117
5.13	SAXS invariants of copolymer SB 20/20 in 3900 PS as a function of copolymer concentration. The dashed line indicates the decrease in the invariant ratio due to the presence of a 20Å interface width.	119

5.14	Schematic showing the effect of homopolymer molecular weight on spherical micelle structure....	121
5.15	Effect of homopolymer molecular weight on the critical micelle concentration for copolymers SB 10/10, SB 20/20, and SB 80/80.....	125
5.16	SAXS invariants for copolymer SB 20/20 as a function of homopolymer molecular weight.....	126
5.17	SAXS and EM results for 12.5 wt% SB 20/20 in 2100 PS.....	128
5.18	SAXS and EM results for 12.5 wt% SB 20/20 in 2100 PS.....	130
5.19	SAXS and EM results for 12.3 wt% SB 20/20 in 7400 PS.....	132
5.20	Micelle core radius as a function of homopolymer molecular weight for copolymers SB 40/10, SB 10/10, SB 40/40, and SB 80/80. The scaling exponent $\gamma$ for each copolymer is as indicated.....	134
5.21	Corona thickness as a function of homopolymer molecular weight for copolymers SB 20/20, SB 40/40, and SB 80/80. The scaling exponent $\epsilon$ is indicated for each copolymer.....	139
5.22	Volume fraction of homopolystyrene in the corona as a function of homopolystyrene to PS block molecular weights for SB 20/20, SB 40/40, and SB 80/80.....	140
5.23	Effect of PS block length on the critical micelle concentration in various homopolystyrenes.....	143
5.24	SAXS invariant as a function of PS block length....	146
5.25	SAXS and EM results for 10.1 wt% SB 23/10 in 17000 PS.....	147
5.26	SAXS and EM results for 17.6 wt% SB 40/10 in 17000 PS.....	148
5.27	SAXS and EM results for 18.7 wt% SB 60/10 in 17000 PS.....	149
5.28	Micelle core radius as a function of PS block length.....	151

5.29	Corona thickness as a function of PS block length..	153
5.30	Volume fraction of homopolystyrene in the corona as a function of homopolystyrene to PS block molecular weight for copolymers SB 23/10, SB 40/10, and SB 60/10 in 7400 and 17000 PS homopolymer.....	154
5.31	SAXS invariant as a function of copolymer molecular weight for copolymers SB 10/10, SB 20/20, SB 40/40, and SB 80/80 in 7400 PS homopolymer.....	157
5.32	SAXS and EM results for 13.0 wt% SB 10/10 in 7400 PS.....	158
5.33	SAXS and EM results for 9.9 wt% SB 40/40 in 7400 PS.....	159
5.34	SAXS and EM results for 9.9 wt% SB 80/80 in 7400 PS.....	160
5.35	Core radius as a function of PB block length.....	163
5.36	Corona thickness as a function of PS block length..	165
5.37	SAXS and EM results for 17.8 wt% SB 20/20 in 2100 PS.....	168
5.38	SAXS and EM results for 24.2 wt% SB 20/20 in 7400 PS. The electron micrograph for 30.9 wt% SB 20/20 in 7400 PS is shown in the lower right corner.....	170
6.1	Comparison of experimentally determined (solid lines) and theoretically predicted (dashed lines) cmc values for SB 10/10, SB 40/10, and SB 20/20 at 115 °C.....	179
6.2	Comparison of experimentally determined (solid lines) and theoretically predicted (dashed lines) values of $\zeta$ and $\eta_B$ for SB 20/20 ( $\approx$ 12.5 wt%) at 115 °C as a function of $M_{hPS}$ .....	181
6.3	Predicted values of $\zeta$ and $\eta_B$ as a function of temperature for 12.5 wt% SB 20/20 in 2100 PS.....	183
6.4	Predicted values of $\zeta$ and $\eta_B$ as a function of temperature for 17.6 wt% SB 40/10 in 17000 PS.....	184



6.5	Predicted values of free copolymer volume fraction as a function of overall copolymer volume fraction for 12.5 wt% SB 20/20 in 2100 PS at 190 °C and 17.6 wt% SB 40/10 in 17000 PS at 300 °C.....	187
6.6	Comparison of experimentally determined (solid lines) and theoretically predicted (dashed lines) micelle core radii as a function of $M_{hPS}$ for SB 40/10, SB 20/20, and SB 80/80 at 115 °C....	189
6.7	Comparison of experimentally determined (solid line) and theoretically predicted (dashed line) core radii as a function of $M_{PS}$ for SB 10/10, SB 23/10, SB 40/10, and SB 60/10 at 115 °C.....	191
6.8	Comparison of experimentally determined (solid line) and theoretically predicted (dashed line) core radii as a function of $M_{PB}$ for SB 10/10, SB 20/20, SB 40/40, and SB 80/80 at 115 °C.....	193
6.9	Comparison of experimentally determined (solid line) and theoretically predicted (dashed line) core radii as a function of $M_{PB}$ for SB 10/10, SB 20/20, SB 40/40, and SB 80/80 at 115 °C.....	194
6.10	Comparison of experimentally determined (solid lines) and theoretically predicted (dashed lines) corona thickness as a function of $M_{ohPS}$ for copolymers SB 20/20 and SB 80/80 at 115 °C.....	195
6.11	Comparison of experimentally determined (solid line) and theoretically predicted (dashed line) corona thickness as a function of $M_{PS}$ for copolymers SB 10/10, SB 20/20, SB 40/40 and SB 80/80 at 115 °C.....	197
6.12	Comparison of experimentally determined (solid line) and theoretically predicted (dashed line) value of homopolystyrene volume fraction in the corona as a function of $M_{hPS}$ for copolymer SB 80/80 at 115 °C.....	199
7.1	Electron micrographs showing the transition from spherical micelles for the blend containing 5.7 wt% SB 20/20 in 7400 PS to cylindrical micelles for the blend containing 7.4 wt% SB 20/20 in 17000 PS.....	204

7.2	Electron micrographs of SB 40/40 in 17000 PS showing the transition from spherical to cylindrical micelles with increasing copolymer concentration (a) 5.0 wt%, (b) 9.8 wt%, and (c) 18.2 wt%.....	206
7.3	Electron micrograph showing the spherical vesicle morphology of 5.0 wt% SB 40/40 in 35000 PS.....	207
7.4	Schematic showing the arrangement of the copolymer and homopolymer chains in the spherical vesicle morphology.....	208
7.5	Electron micrographs showing the multiple layer structure of 18.4 wt% SB 10/23 in 3900 PS and the spherical micelle structure of 17.8 wt% SB 10/23 in 2100 PS (shown at the same magnification).....	215
7.6	Electron micrograph showing the lamellar structure of 13 wt% SB 10/65 in 2100 PS.....	216
7.7	Electron micrographs of the two mesophases in the blend containing 4.0 wt% SB 10/65 in 7400 PS (shown at the same magnification).....	217
7.8	Block copolymer/homopolymer micellar structure as a function of homopolymer molecular weight and copolymer composition.....	220
A.1	Structured composite having random orientation of ordered lamellar grains. The grain volume, $V_f$ , is much smaller than the volume of the sample (taken from Sax and Ottino [148]).....	250
A.2	Electron micrographs of the block copolymer samples. The letters refer to the designation given in Table A1. The magnification bar corresponds to 1000 Å except for D and E, for which it corresponds to 667 Å.....	257
A.3	Effective solubility coefficients as a function of composition. The bar in measurement C indicates representative errors.....	263
A.4	Effective diffusion coefficients as a function of composition and morphology. The bar in measurement E indicates representative errors.....	264

B.1	Corrected SAXS curves for (a) SB 10/110 and (b) SB 60/10. The solid lines show the sphere scattering fit to the data, taking into account the distribution in sphere sizes.....	272
B.2	(100), (110), (111) projections of a SC, BCC, and FCC lattice showing the unit cells (outlined) and relative projected intersphere distances. The square arrays of the (100) projections have been drawn the same size leading to different unit cell sizes for the three lattice types. Subsequent projections have been scaled accordingly.....	274
B.3	Schematic of tilting experiments performed in the electron microscope.....	275
B.4a	Electron micrograph showing the (100) projection of the BCC macrolattice for SB 10/110.....	277
B.4b	Electron micrograph showing the (111) projection of the BCC macrolattice for SB 10/110.....	278
B.4c	Electron micrograph showing the (110) projection of the BCC macrolattice for SB 10/110.....	279
B.5	Electron micrographs showing the (a) (100), and (b) (111) projections of the BCC macrolattice for SB 10/110. The dark circular regions labeled 1, 2, and 3 are 1000 Å PS spheres deposited on the section to confirm the axis and magnitude of tilt between the two projections.....	281
B.6	Electron micrographs showing the (a) (100), and (b) near (111) projections of the BCC macrolattice for SB 60/10.....	284



# C H A P T E R I

## INTRODUCTION

### 1.1 Opening Remarks

Because of their commercial utility, and intrinsic scientific interest, there has been a considerable amount of research on block copolymers since they were first synthesized in the late 1950's, particularly research on their phase separation characteristics. For sufficiently high molecular weight, and low enough temperature, the different blocks in the copolymer will be incompatible, and the system will phase separate. However, due to the chemical linking of the blocks to each other, the scale of the phase separation is restricted to occur with characteristic dimensions on the order of the radii of gyration of the copolymer blocks (typically a few hundred Å). It has long been known that, depending on the relative volume fractions of the components, microdomains of spheres, cylinders, or lamellae occur. In addition, recent work in our research group has shown that an ordered bicontinuous morphology exists for compositions between that of cylinders and lamellae. Therefore, by varying the composition of the copolymer, a wide range of morphologies, and thus physical properties, can be achieved.

A considerable amount of research has also been directed towards understanding the phase separation characteristics of block copolymer/homopolymer blends. Phase diagrams of AB block copolymers



blended with A and/or B homopolymers can be quite complex. Homogeneous mixtures, macroscopic phase separation, and the formation of different ordered mesophases (having lamellar, cylindrical, spherical, etc. microdomains) can occur, depending on temperature and composition. In addition, a micellar phase, consisting of block copolymer aggregates suspended in a homopolymer matrix with no long range order, can occur for dilute solutions of AB copolymer in A homopolymer. Recently, there has been renewed interest in such systems, due to the recognition of the important role block copolymers can play as emulsifiers (compatibilizers), impact modifiers, and surfactants in polymer blends. Furthermore, the statistical thermodynamics of block copolymer/homopolymer blends is much easier to handle than that of small molecule surfactants or copolymers in organic solvents. For example, in 1983, Leibler, Orland, and Wheeler presented a thermodynamic theory of micelle formation in AB diblock copolymer/A homopolymer blends based, in part, on the Flory-Huggins theory of polymer mixtures. These copolymer/homopolymer systems are also relatively simple from an experimental point of view. In contrast to block copolymer/selective solvent micellar mixtures which have a three-phase structure (i.e., three regions of different electron density: the micelle core, the surrounding corona region, and the solvent matrix), AB copolymer/A homopolymer blends have a two-phase micellar structure since the micelle corona and matrix regions are chemically identical. This makes the analysis of small angle x-ray scattering (SAXS) data much easier. Therefore, theoretical and experimental studies of these relatively

simple systems may provide insight as to the nature of micelle formation and the critical micelle concentration.

In this dissertation, the formation and structure of micelles in poly(styrene-butadiene) diblock copolymer/homopolymer blends will be investigated by means of both SAXS and transmission electron microscopy (TEM). A systematic series of copolymers and homopolymers will be employed in order that the effect of homopolymer and block molecular weights on the critical micelle concentration, and the micelle structure as a function of copolymer concentration, can be studied. The SAXS data from blends exhibiting spherical micelles, as evidenced by TEM, will be modeled using the Percus-Yevick (PY) hard sphere fluid approximation to account for the interparticle interference contribution to the scattered intensity. By combining this modeling with SAXS invariant analysis, the structure of the micellar phase, at a given temperature, can be completely characterized. The structural parameters which will be determined for a wide variety of copolymer-homopolymer pairs (at 115 °C) include the core radius, the polydispersity in core radius, the corona thickness, the concentration of homopolymer in the core and corona regions, and the concentration of free unaggregated copolymer. This complete experimental characterization of micellar structure in block copolymer/homopolymer blends has not been performed previously. The experimental results, including the scaling of the core radius and corona thickness with homopolymer and block molecular weights, will be compared to the predictions of recent theories of micelle formation in

block copolymer/homopolymer blends. In addition, the formation of non-spherical micelles will be investigated. The results of this study allow one to predict, a priori, the structure of the micellar aggregates from the molecular weights of the homopolymer and copolymer blocks.

## 1.2 Organization of the Dissertation

In order to provide a proper framework in which the results of this investigation can be considered, two background chapters will be presented first. Chapter II presents an overview of small angle x-ray scattering theory, with particular emphasis on the development of the equations used to analyze the scattering from block copolymers and block copolymer/homopolymer blends. Chapter III is a review of the experimental and theoretical studies on the morphology of block copolymers, and block copolymers blended with preferential solvents or homopolymers. The synthesis and characterization of the poly(styrene-butadiene) diblock copolymers, the preparation of copolymer/homopolymer blends, and the experimental TEM and SAXS techniques used in the present study are outlined in Chapter IV. Chapter V presents the experimental results for poly(styrene-butadiene) diblock copolymer/polystyrene homopolymer blends exhibiting spherical micelles, while Chapter VI compares these results to the predictions of recent theories of micelle formation in AB block copolymer/A homopolymer blends. The transition to, and structure of, poly(styrene-butadiene) block copolymer/polystyrene homopolymer blends having non-spherical micelles will be presented in



Chapter VII. The conclusions of this study, along with suggestions for future work, are given in Chapter VIII. In addition, two appendices are included. Appendix A presents a study of the effect of morphology on the transport of small molecule gases in poly(styrene-butadiene) block copolymers. The experimental results are compared to the predictions of simple theoretical models. Appendix B is an electron microscopy and SAXS study of the BCC lattice structure of poly(styrene-butadiene) block copolymers.



## C H A P T E R    I I

### SCATTERING THEORY

This chapter outlines the basics of scattering with particular emphasis on the development of the theory necessary for the analysis of small angle x-ray scattering (SAXS) data. In particular, the theory pertaining to the SAXS from a collection of spherical particles is presented. In addition, SAXS data corrections, absolute intensities, and invariants are reviewed.

#### 2.1 General Kinematic Scattering Theory

The following development of the kinematic theory of scattering [1] will be based on the assumptions that: (1) the scattering is coherent, (2) there is no multiple scattering, (3) the incident x-ray beam is monochromatic and parallel, and (4) the size of the incident x-ray beam is large compared to the interparticle distance in the irradiated sample, but small compared to the sample to detector distance.

The discussion of scattering theory begins with the interaction between the x-rays and a single electron. An incident x-ray beam of amplitude  $A_0$  impinges on a free electron and produces an emitted spherical wave with the same frequency but with an amplitude of  $A_1$  given by

$$A_1 = A_0 \frac{1}{a} \frac{e^2}{mc^2} \quad (2.1)$$

where  $a$  is the distance away from the electron,  $e$  is the charge of the electron,  $m$  is the mass of the electron, and  $c$  is the velocity of light. The angle between the directions of the incident and scattered waves is  $2\theta$ . The scattered intensity is given by the product of the amplitude and its complex conjugate

$$I_e(\vec{h}) = I_o \frac{1}{a^2} T \frac{1 + \cos^2 2\theta}{2} \quad (2.2)$$

where the subscript  $e$  refers to the scattered intensity from a single electron,  $I_o = A_o^2$ , and  $T = \frac{e^4}{m^2 c^4}$ . The factor  $\frac{1 + \cos^2 2\theta}{2}$  has been added to account for the random polarization of the x-rays. For typical  $2\theta$  encountered in small angle experiments this factor will be nearly unity. The factor  $T$  is known as the Thompson scattering factor and is equal to  $7.94 \times 10^{-26} \text{ cm}^2$ .

### 2.1.1 Scattering from a single particle

When scattering from two or more electrons occurs, such as when scattering from a particle containing many electrons, the spherical waves generated by each scattering center must be summed accounting for the phases of each wave. Figure 2.1 illustrates the diffraction from a single particle. The incident wave is  $\vec{s}_o$  and the scattered wave is  $\vec{s}_1$  with the angle between them being  $2\theta$ . The scattering vector  $\vec{s}$  is defined as  $(\vec{s}_1 - \vec{s}_o)$  and has a magnitude of  $\frac{2}{\lambda} \sin\theta$ .

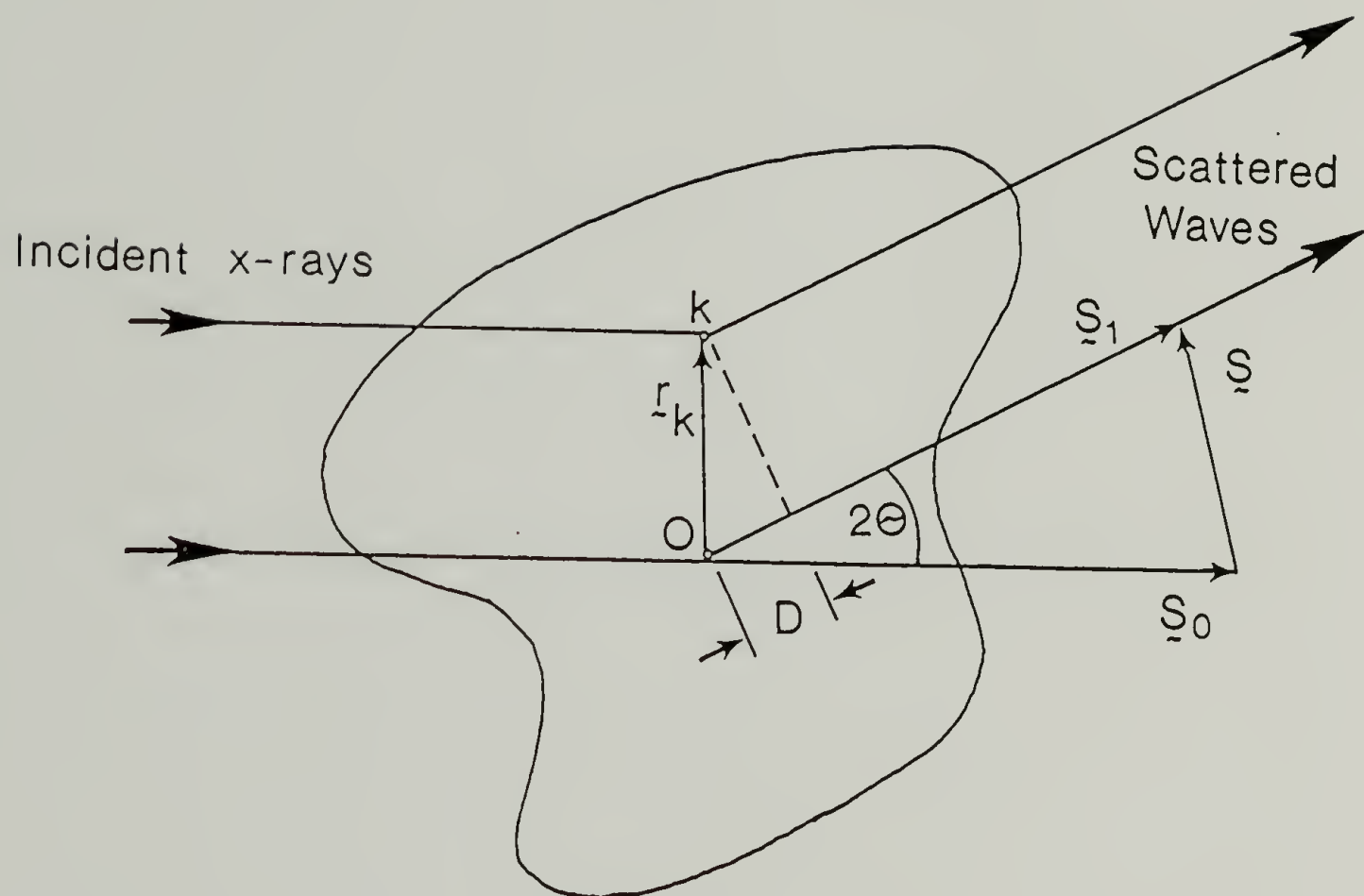


Figure 2.1 Schematic showing the scattering from a single particle.

The formula for the amplitude of radiation scattered at an arbitrary point (of scattering factor  $f_k$ ) located at  $\underline{r}$  from the origin 0 is given by

$$A_k = A_e f_k e^{-i\Delta\phi} \quad (2.3)$$

where  $A_e$  designates the amplitude scattered by one electron and  $\Delta\phi$  is the phase difference given by  $\frac{2\pi D}{\lambda}$  where  $D$  is the path length difference given by  $\lambda(\underline{s}_0 - \underline{s}) \cdot \underline{r}$  or  $\lambda(\underline{s} \cdot \underline{r})$ . Thus

$$A_k = A_e f_k e^{-i(\underline{h} \cdot \underline{r})} \quad (2.4)$$

where  $\underline{h} = 2\pi\underline{s}$ . The scattered amplitude from the entire particle is then given by summing over all points in the particle

$$A(\underline{h}) = A_e(\underline{h}) \sum_k f_k \exp[-i(\underline{h} \cdot \underline{r}_k)] \quad (2.5)$$

where  $\underline{r}_k$  is the vector from the origin to point  $k$ . The scattered intensity distribution from an isolated particle is thus

$$I(\underline{h}) = I_e(\underline{h}) \left[ \sum_k f_k \cos(\underline{h} \cdot \underline{r}_k) \right]^2 = I_e(\underline{h}) F^2(\underline{h}) \quad (2.6)$$

where  $F(\underline{h})$  is called the structure factor.

For simple shapes such as spheres, cylinders, or lamellae analytical solutions for the structure factor can be obtained [1]. For example, consider the case of a spherical particle of radius  $R$  with scattering factor

$$\begin{aligned} f_k &= 1 & r &\leq R \\ f_k &= 0 & r &> R \end{aligned}$$

The structure factor, averaged over all orientations, is given from Equation 2.7 as



$$\overline{F(\underline{h})} = \iiint \overline{\cos(\underline{h} \cdot \underline{r})} \, d\underline{r} \quad (2.8)$$

By defining  $F^2(\underline{h}) = n^2 i(\underline{h}) = v^2 \rho^2 i(\underline{h})$  where  $n$  is the total number of electrons in the particle, given by the product of the particle volume  $v$  and its electron density  $\rho$  (note that according to this definition  $i(0)$  is always unity), one can write [2]

$$i(hR) = \int_0^R \frac{\sinh r}{hr} 4\pi r^2 \, dr \quad (2.9)$$

$$i(hR) = \frac{3}{(hR)^3} (\sinh R - hR \cosh R) \quad (2.10)$$

Therefore, the scattered intensity distribution is given by

$$I(\underline{h}) = I_e(\underline{h}) v^2 \rho^2 \left\{ \frac{3}{(hR)^3} (\sinh R - hR \cosh R) \right\}^2$$

or

$$I(\underline{h}) = I_e(\underline{h}) v^2 \rho^2 \frac{9\pi}{2} \left[ \frac{J_{3/2}(hR)}{(hR)^{3/2}} \right]^2 \quad (2.11)$$

where  $J_{3/2}$  is a Bessel function of order 3/2. The scattered intensity function given by Equation 2.11 contains subsidiary maxima at  $hR = 5.76, 9.10, \dots$  so that the radius of the spherical particle can be obtained from the values of  $h$  where the intensity is a maximum. Alternatively, the radius of the spherical particle can be obtained using the Guinier approximation [1]

$$I \propto e^{\frac{-R_g^2 h^2}{3}} \quad (2.12)$$

valid for  $h^2 R_g^2 < 1$ , where  $R_g$  is the radius of gyration of the scattering particle, which is related to the spherical particle radius by  $R = \sqrt{5/3} R_g$ .

### 2.1.2 Scattering from a collection of particles

Now consider the scattering from a collection of identical particles of structure factor  $F(\vec{h})$ . The scattered intensity can be written as

$$I(\vec{h}) = I_e(\vec{h}) \overline{\sum_k \sum_j F_k(\vec{h}) F_j(\vec{h}) \cos(\vec{h} \cdot (\vec{R}_k - \vec{R}_j))} \quad (2.13)$$

where  $\vec{R}_k$  and  $\vec{R}_j$  refer to vectors between particles. Assuming there is no correlation between the positions of the particles and their orientations, Equation 2.13 reduces to

$$\overline{I(\vec{h})} = I_e(\vec{h}) \{ \bar{N} F(\vec{h})^2 + \overline{F(\vec{h})}^2 \overline{\sum_k \sum_{k \neq j} \cos[\vec{h} \cdot (\vec{R}_k - \vec{R}_j)]} \} \quad (2.14)$$

where  $\bar{N}$  is the average number of scattering particles.

The term in the double sum of Equation 2.14 can be expressed exactly for the case of a perfect crystal since the path difference follows directly from the relative positions of the scattering elements. For this case the scattered amplitude from the (hkl) plane can be written as

$$A(\vec{h}) \propto F(\vec{h}) \sum_n \exp(-2\pi i(hx_n + ky_n + lz_n)) \quad (2.15)$$

where  $x_n$ ,  $y_n$ , and  $z_n$  are the coordinates of the  $n^{\text{th}}$  scattering object with the summation performed over all of the  $n$  scattering objects in the unit cell. Examination of Equation 2.15 reveals that some of the hkl reflections may be forbidden. For example, consider the case of a body centered cubic unit cell for which the positions of the scattering

elements in the unit cell are  $(0,0,0)$  and  $(1/2,1/2,1/2)$ . Substituting these  $x_n, y_n, z_n$  values into Equation 2.14 yields

$$1 + \exp[-\pi i(h+k+l)]$$

for the term in the summation. Hence the allowed hkl reflections are those for which  $h+k+l$  is even, otherwise this term is zero. For such three dimensional periodic ordered arrangements of scattering elements, the Bragg equation

$$n\lambda = 2d_{hkl}\sin\theta \quad (2.16)$$

gives the spacing  $d$  between the hkl planes for the allowed hkl reflections where  $n$  is the order of the reflection. From the definition of the magnitude of  $\underline{s}$ , it is apparent that

$$d_{hkl} = \frac{n}{|\underline{s}|} \quad (2.17)$$

For cubic lattices,

$$d_{hkl} = \frac{a}{(h^2 + k^2 + l^2)^{1/2}} \quad (2.18)$$

and for infinitely long hexagonally packed cylinders,

$$d_{hk0} = \frac{\sqrt{3} a}{2(h^2 + k^2)^{1/2}} \quad (2.19)$$

where  $a$  is the unit cell size. The ratio of  $d$  spacings relative to the first allowed reflection for alternating lamellae, hexagonally packed cylinders, and cubic packed (SC, BCC, FCC) spheres are listed in Table 2.1. It is immediately evident that, for a scattering pattern which exhibits several reflections, ordered arrangements of spheres, cylinders, and lamellae can easily be distinguished. In addition, FCC packing should be distinguishable from BCC or SC packing of spheres. However, the first six reflections of BCC and SC have the same relative

Table 2.1

d Spacings Corresponding to the First Eight Reflections for Common Morphologies

Morphology	Reflection Number								
	1	2	3	4	5	6	7	8	
Spheres									
SC	$d_{hkl}/d_{100}$	1	0.707	0.577	0.5	0.447	0.408	0.354	0.333
	$hkl$	100	110	111	200	210	211	220	300,221
BCC									
FCC	$d_{hkl}/d_{111}$	1	0.866	0.612	0.522	0.5	0.433	0.397	0.387
	$hkl$	111	200	220	311	222	400	331	420
Cylinders									
hexagonal	$d_{hk}$	1	0.577	0.5	0.378	0.333	0.289	0.277	0.250
	$hk$	10	11	20	21	30	22	31	40
Lamellae									
	$d_n/d_l$	1	0.5	0.333	0.25	0.20	0.167	0.142	0.125
	$n$	1	2	3	4	5	6	7	8



spacings. Since only 3-4 reflections are normally observed, even under the best conditions, for block copolymers having spherical domains, it is impossible to distinguish between these two packing modes without some additional information, such as comparing the known volume fraction of the spherical domain forming component in the copolymer to that calculated for the different packing modes. The volume fraction of the spherical domains  $\phi_s$  can be calculated for SC, BCC, and FCC packing modes from the sphere radius  $R$  and the unit cell size  $a$  determined from the SAXS pattern using the following equations

$$\text{SC : } \phi_s = \frac{(4/3)\pi R^3}{(a_{\text{SC}})^3} \quad (2.20)$$

$$\text{BCC : } \phi_s = \frac{(8/3)\pi R^3}{(a_{\text{BCC}})^3} \quad (2.21)$$

$$\text{FCC : } \phi_s = \frac{(16/3)\pi R^3}{(a_{\text{FCC}})^3} \quad (2.22)$$

For the case where there is no long range order of the scattering particles, one proceeds from Equation 2.14 evaluating the term with the double sum. The result of this derivation, first given by Zernike and Prins in 1927 [3], is

$$\overline{I(h)} = I_e(h) \bar{N} F^2(h) \left\{ 1 + n \int_0^\infty [g(r)-1] \frac{\sinh r}{hr} 4\pi r^2 dr \right\} \quad (2.23)$$

where  $n$  is the number density of particles and  $g(r)$  is the pair correlation function describing the arrangement of the particles.

For the case of spherical scattering elements, the pair correlation function  $g(r)$  is related to the probability of finding a sphere a distance  $r$  away from the sphere chosen as the origin. As seen

in Figure 2.2, taken from Ziman [4],  $g(r)$  for a disordered system must be zero for distances less than the hard core diameter of the spherical particle. It then rises to a maximum at some value  $r_0$  which can be equated with the radius of the first coordination shell of particles. The average coordination number,  $z$ , is related to the area under this peak,

$$z = \int g(r) 4\pi r^2 dr \quad (2.24)$$

Similarly, the second peak in  $g(r)$  arises from the second coordination shell, with successive coordination shells becoming less well defined as  $g(r)$  approaches unity with increasing  $r$ .

For the case of spherical particles, Equation 2.23 can be written in the compact form

$$I(h) = KNP(hR)S(h) \quad (2.25)$$

where  $K = I_e(h)(\Delta\rho)^2$  and  $\Delta\rho$  is the electron density difference between the spherical particles and their surroundings. The function  $P(hR)$  is due to scattering from an isolated sphere, i.e. intraparticle scattering, and is equal to  $V^2\Phi^2$  where  $\Phi$  has already been given by Equation 2.10. The interference function  $S(h)$  is due to interparticle interference and is given by

$$S(h) = 1 + 4\pi n \int_0^\infty [g(r)-1] \frac{\sin hr}{hr} r^2 dr \quad (2.26)$$

For dilute systems, where the scattering particles are separated by large enough distances so that no interference occurs between scattering from different particles (i.e.,  $S(h) \approx 1$  for all  $h$ ), the intensity of scattered radiation is simply the product of the number of

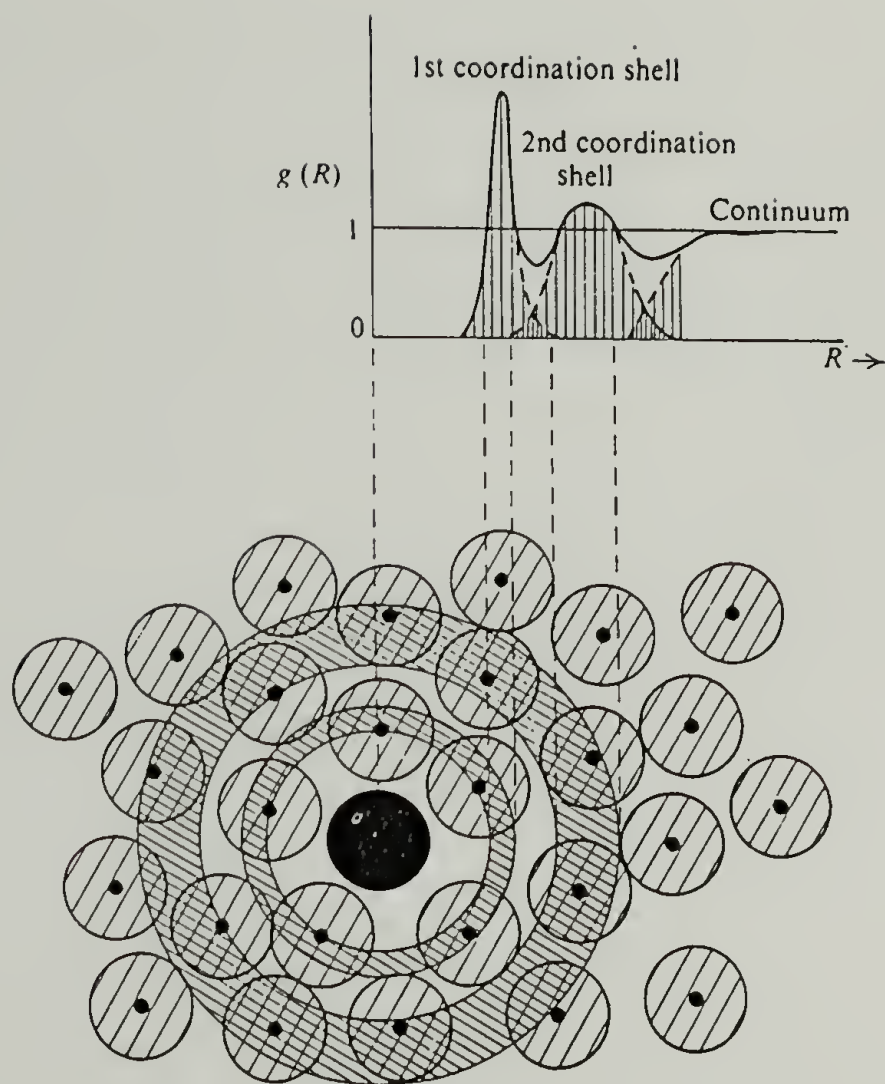


Figure 2.2 Schematic of the pair distribution function  
(taken from Ziman [4]).

scatterers and the scattered intensity of a single particle

$$I(h) = KNP(hR) \quad (2.27)$$

However, as the number density of scattering particles increases, interparticle interference becomes significant. The task now becomes one of finding  $g(r)$  for the particular system of interest so that Equation 2.26 can be solved. The exact form of  $S(h)$  will depend not only on  $h$ ,  $R$ , and  $n$  but also on the interparticle potential.

A successful approach for understanding the scattering from simple liquids is to examine the total correlation function, defined as

$$h(r_{12}) = g(r_{12}) - 1 \quad (2.28)$$

which measures the deviation of the pair distribution function from its background value due to the influence of particle 1 on particle 2 at a distance  $r_{12}$  [5]. Ornstein and Zernike [6] first proposed in 1914 that  $h(r_{12})$  could be considered to consist of a direct correlation between particles 1 and 2 and an indirect term by which the correlation is transferred to all of the neighboring particles. This is expressed mathematically as

$$h(r_{12}) = c(r_{12}) + n \int c(r_{13})h(r_{32}) dr_3 \quad (2.29)$$

The direct correlation function  $c(r_{12})$  should be of short range order since it is a correlation between particles 1 and 2, depending only on the interparticle potential, which will fall off quickly to zero with separation distance.

A useful approximation for the direct correlation function is the Percus-Yevick [7] expression:

$$c(r) \simeq (1 - e^{\theta(r)/kT})g(r) \quad (2.30)$$



Wertheim [8] and Thiele [9] independently showed that this direct correlation function has an exact closed-form solution for the classical hard-sphere fluid. For  $r > 2R$ , where  $\phi(r)$  is zero,  $c(r)$  will also be zero, while for  $r < 2R$ , where  $\phi(r)$  is infinite,  $c(r)$  has the polynomial solution

$$c(r) = -(\alpha + \beta s + \gamma s^3) \quad (2.31)$$

where

$$\alpha = (1 + 2\eta)^2 / (1 - \eta)^4 \quad (2.32)$$

$$\beta = -6 (1 + \eta/2)^2 / (1 - \eta)^4$$

$$\gamma = 1/2 \eta (1 + \eta)^2 / (1 - \eta)^4$$

$$s = r/2R$$

Here,  $\eta$  is the hard-sphere volume fraction  $4\pi R^3 \eta / 3$ . Combining the Fourier transform of the Ornstein-Zernike equation with the definition of the interference function (Equation 2.26) yields

$$S(h) = \frac{1}{1 - nC(h)} \quad (2.33)$$

where  $C(h)$  is the Fourier transform of the direct correlation function given by

$$C(h, R, \eta) = -4\pi \int_0^{2R} (\alpha + \beta s + \gamma s^3) \frac{\sinh r}{hr} r^2 dr \quad (2.34)$$

This integral is readily evaluated [10] to give

$$S(h, R, \eta) = \frac{1}{1 + 24 (G(A)/A)} \quad (2.35)$$

where  $A = 2hR$  and

$$G(A) = \frac{\alpha}{A^2} (\sin A - A \cos A) + \frac{\beta}{A^3} (2A \sin A + (2 - A^2) \cos A - 2) + \frac{\gamma}{A^5} (-A^4 \cos A + 4[(3A^2 - 6) \cos A + (A^3 - 6A) \sin A + 6]) \quad (2.36)$$

The normalized intensity can then be written as

$$I_N(h) = I(h)/I(0) = S(h)P(h)/S(0)P(0) \quad (2.37)$$

but  $\phi(0) = 1$  and  $S(0) = 1/\alpha$ , so

$$I_N(h, R, \eta) = S(h, R, \eta) \phi^2(hR) \alpha \quad (2.38)$$

Figure 2.3 shows  $S(hR)$  versus  $hR$  for hard sphere volume fractions of 0.1, 0.3, and 0.5. As the hard sphere volume fraction increases, the maxima and minima in  $S(hR)$  become more pronounced. For the case of hard spheres, the interference function calculated by the Percus-Yevick integral equation agrees rather well with that obtained by Monte Carlo or molecular dynamics computations [5].

For the systems studied in this dissertation, there will inevitably be some distribution in the size of the spherical particles as well as a finite interface region between the phase separated spherical microdomains and the surrounding matrix phase. For this case, Equation 2.25 needs to be written as

$$I(h) = KNP'(hR)S'(h) \quad (2.39)$$

where  $P'(hR)$  is the polydisperse sphere scattering function which can be written as [11]

$$P'(h) = \int_0^\infty P(R) f^2(h, R) dR / \int_0^\infty P(R) dR \quad (2.40)$$

Here,  $f(h, R)$  is the scattered amplitude of the spherical particles, modified for the case of diffuse boundaries

$$f(h, R) = [4/3\pi R^3] \phi(hR) \exp(-\sigma^2 h^2 R^2) \quad (2.41)$$

where  $\sigma$  is the parameter that characterizes the diffuseness of the phase boundaries (i.e., the width of the interface). The electron density

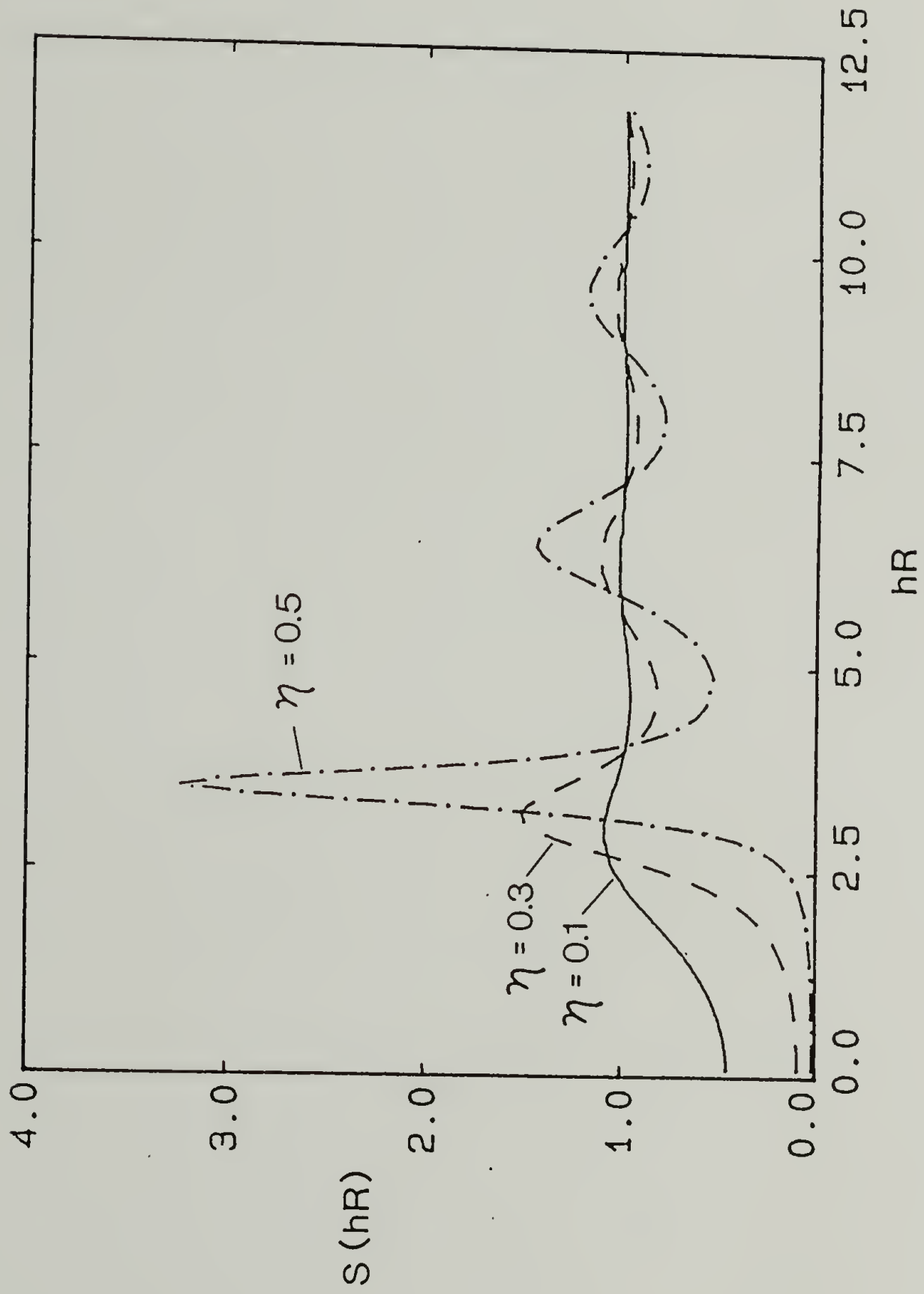


Figure 2.3 Interference function  $S(hR)$  for hard sphere volume fractions of 0.1, 0.3, and 0.5.

profile of the boundary,  $\Psi(r)$ , is given by a convolution of the density profile for a sharp boundary,  $\rho(r)$ , with a Gaussian smearing function  $k(r)$

$$k(r) = (2\pi\sigma^2)^{-3/2} \exp(-r^2/2\sigma^2) \quad (2.42)$$

from which the interfacial thickness  $t$  is defined as

$$t = (2\pi)^{1/2} \sigma \quad (2.43)$$

Note that the polydisperse sphere scattering function is a 6<sup>th</sup> moment average of the sphere radius so that the larger spheres contribute much more to the scattered intensity than do the smaller spheres. The function  $P(R)$  is normally chosen to be a Gaussian distribution about the average sphere radius  $\bar{R}$ :

$$P(R) = A \exp[-(R-\bar{R})^2/2\sigma_R^2] \quad (2.44)$$

The factor  $S'(h)$  in Equation 2.39 is the polydisperse interference function. Vrij [12] has derived an expression for the scattered intensity from a polydisperse system of homogeneous hard spheres in the Percus-Yevick approximation, from which the interference function can be obtained [13]. The effect of polydispersity on the interference function is illustrated in Figure 2.4 for the case of  $\eta = 0.30$  and  $\sigma_r/R = 0.0, 0.10, \text{ and } 0.25$ . As the polydispersity increases, the maxima and minima in  $S'(h)$  become less pronounced.

In summary, this section has presented the scattering theory for two extreme cases of order: (1) a three dimensional periodic arrangement of scattering particles (i.e., a crystal), and (2) a liquid-like arrangement of spherical scattering particles. Both cases will be of importance for analysis of the small angle scattering encountered in the



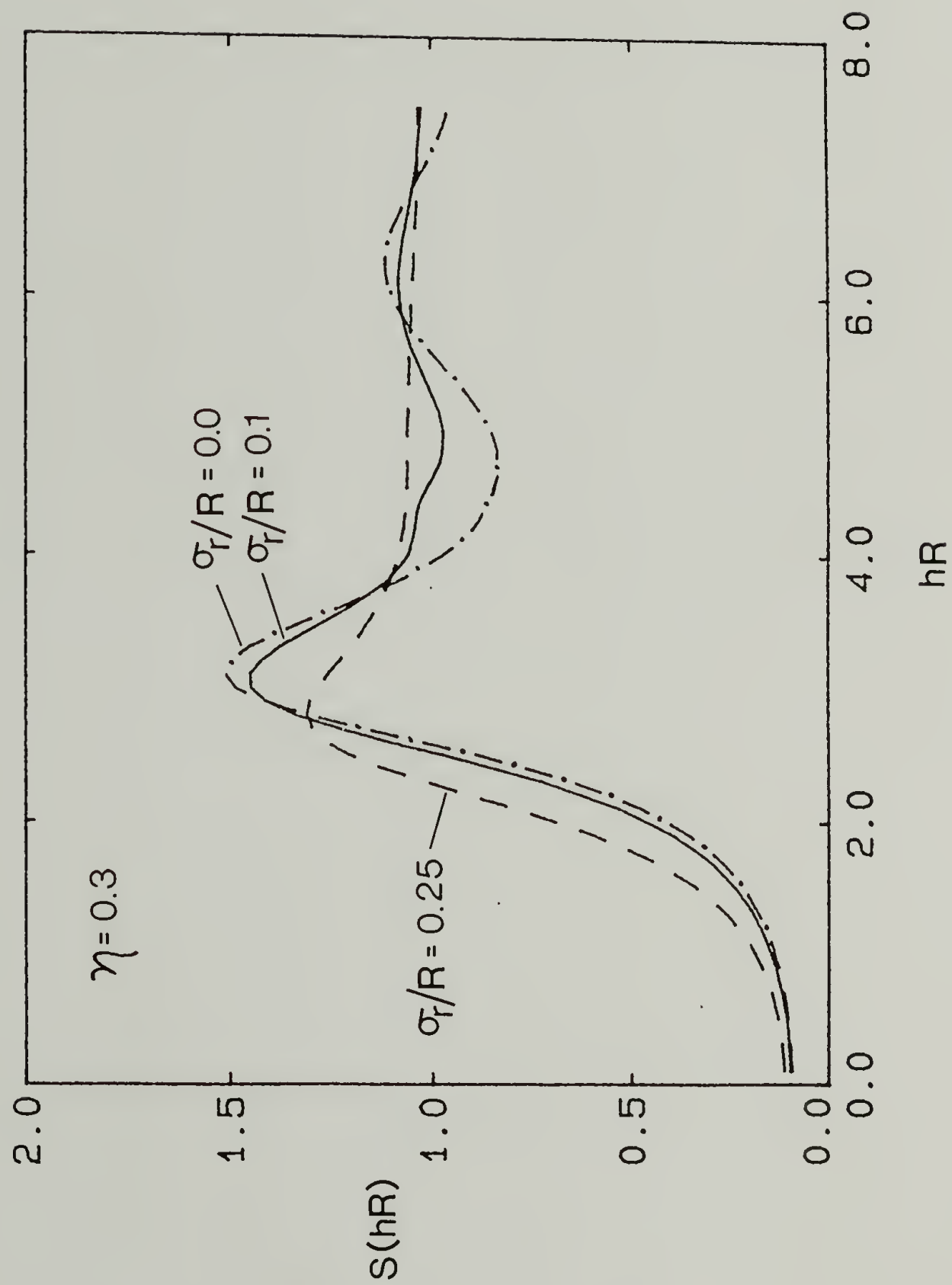


Figure 2.4 Effect of polydispersity on the interference factor.

block copolymer systems examined in this dissertation.

## 2.2 Small Angle X-Ray Scattering Data Corrections

The SAXS experiments in this dissertation utilize a Kratky camera (slit collimation) equipped with a one-dimensional position sensitive detector (see experimental section). The use of this type of experimental apparatus requires that several corrections be made to the raw data before the actual scattered intensity profile from the sample can be obtained [14]. The most important of these are the corrections for sample absorption, detector sensitivity, parasitic scattering, and slit length smearing.

Since x-rays are absorbed as they travel through any material, the raw data must first be divided by the sample transmission which is the fraction of incident x-rays which travel through the sample.

The scattering due to the camera itself, called the parasitic scattering, results primarily from scattering from the edges in the collimation assembly. This scattering must be subtracted from the raw data to obtain the scattering from the sample itself.

Since some regions (channels) of the detector can be more sensitive than others to scattered x-rays, the detector sensitivity must be measured. This can be accomplished by bathing the detector with a uniform flux of x-rays from an  $^{55}\text{Fe}$  source. The scattering from the sample must then be normalized with respect to the detector sensitivity.

The incident x-ray beam, defined by the slit collimation of the camera, is extended in the horizontal direction (see Figure 2.5), which results in a "smearing" of the data. This means that the intensity at a given detection angle is the sum of contributions from scattering all along the slit length, each contribution of which is from a different scattering angle. In other words, there is an angular superposition of the scattering information. Therefore, a mathematical deconvolution must be performed to obtain the desmeared data. Several algorithms for desmearing have been developed [15-18]. The method of Vonk [18] has been used to treat the data presented in this dissertation.

### 2.3 SAXS Absolute Intensity

Absolute SAXS intensity units have been discussed previously by several workers [19-22]; however, for the sake of clarity, they will be reviewed here since they will be needed in calculating invariants. The following section relies heavily on the derivations presented by Vonk [23] in the notes accompanying his FFSAXS data handling program.

Absolute x-ray intensities are based on the unit scattering of a single electron. For a sample consisting of  $q$  electrons, the maximum scattered amplitude is  $qA_1$  where  $A_1$  is given by Equation 2.1. However, due to destructive interference one actually measures

$$A = pA_1 \quad (2.45)$$

where  $p < q$ . The corresponding scattered intensity for  $q$  electrons is thus,

$$I = p^2 I_1 \quad (2.46)$$

where  $I_1$  is given by Equation 2.2. The primary beam intensity  $I_0$  is equal to the energy per unit time passing through a unit area. Assuming monochromatic x-rays, one count in the detector is directly proportional to energy so that the units of  $I_0$  are also (counts/area time).

The quantity  $p^2$  is called the absolute intensity  $i'$ . It has units of (number of electrons)<sup>2</sup> or simply  $n^2$ . It is the quantity of interest and is a measure of the strength of scattering from the sample relative to the scattering from a single electron. The scattered intensity can then be written as

$$I = i' \frac{I_0 T}{a^2} \quad (2.47)$$

If the incident beam intensity is not uniform, then Equation 2.47 may be written as

$$I = \frac{iT}{a^2} \int I_0 dV \quad (2.48)$$

where  $i = i'/V$  is the absolute intensity per volume of sample. For a sample of uniform thickness  $D$  in the beam direction,  $dV = DdA$ . The total power  $P$  of the x-ray beam incident on the sample is given by

$$P = \int I_0 dA \quad (2.49)$$

where  $P$  has units of (counts/second). Combining Equations 2.48 and 2.49 gives

$$I = \frac{iTDP}{a^2} \quad (2.50)$$

so that the scattered intensity is seen to have the units of ( $n^2$  counts/cm<sup>2</sup> sec).



For the case of slit collimation one measures the smeared intensity  $\tilde{I}$  instead of  $I$ . If  $F(y)$  is the power per cm length of the primary beam, measured in the plane of registration (as indicated in Figure 2.5), then  $F(y)dy$  is the power in the element  $dy$ . The following relation can be derived from Equation 2.50

$$\tilde{I} = \int_{-\infty}^{\infty} \frac{i(r)TD}{a^2} F(y) dy \quad (2.51)$$

where  $r = (x^2 + y^2)^{1/2}$  and  $x$  is the distance in the plane of registration as shown in Figure 2.5. If the primary beam is of infinite height and  $F(y)$  is a constant  $P_1$ , then

$$\tilde{I} = \tilde{i} \frac{TD}{a^2} P_1 \quad (2.52)$$

where  $\tilde{i} = \int_{-\infty}^{\infty} i(r) dy$  can be considered as the absolute smeared intensity per  $\text{cm}^3$  of sample. The units of  $\tilde{i}$  and  $P_1$  are thus  $(n^2/\text{cm}^2)$  and  $(\text{counts}/\text{cm sec})$  respectively. Note that in addition,  $\tilde{I}$  and  $I$  have the same units of  $(n^2 \text{ counts}/\text{sec cm}^2)$ .

The absolute intensity scattered from a sample can be obtained by comparing the scattering from the sample to that of a calibrated standard. A common standard is a plaque of low density polyethylene (Lupolen) [19,20]. For the Lupolen calibration sample, which is obtained from Kratky, the following information is supplied

$$\frac{\tilde{I}_c a}{P_c} = K \quad (2.53)$$

where  $\tilde{I}_c$  is the intensity of the calibration sample measured at a scattering angle corresponding to  $1/150 \text{ \AA}^{-1}$ ,  $P_c$  is the power of the primary beam per cm length in the plane of registration after absorption

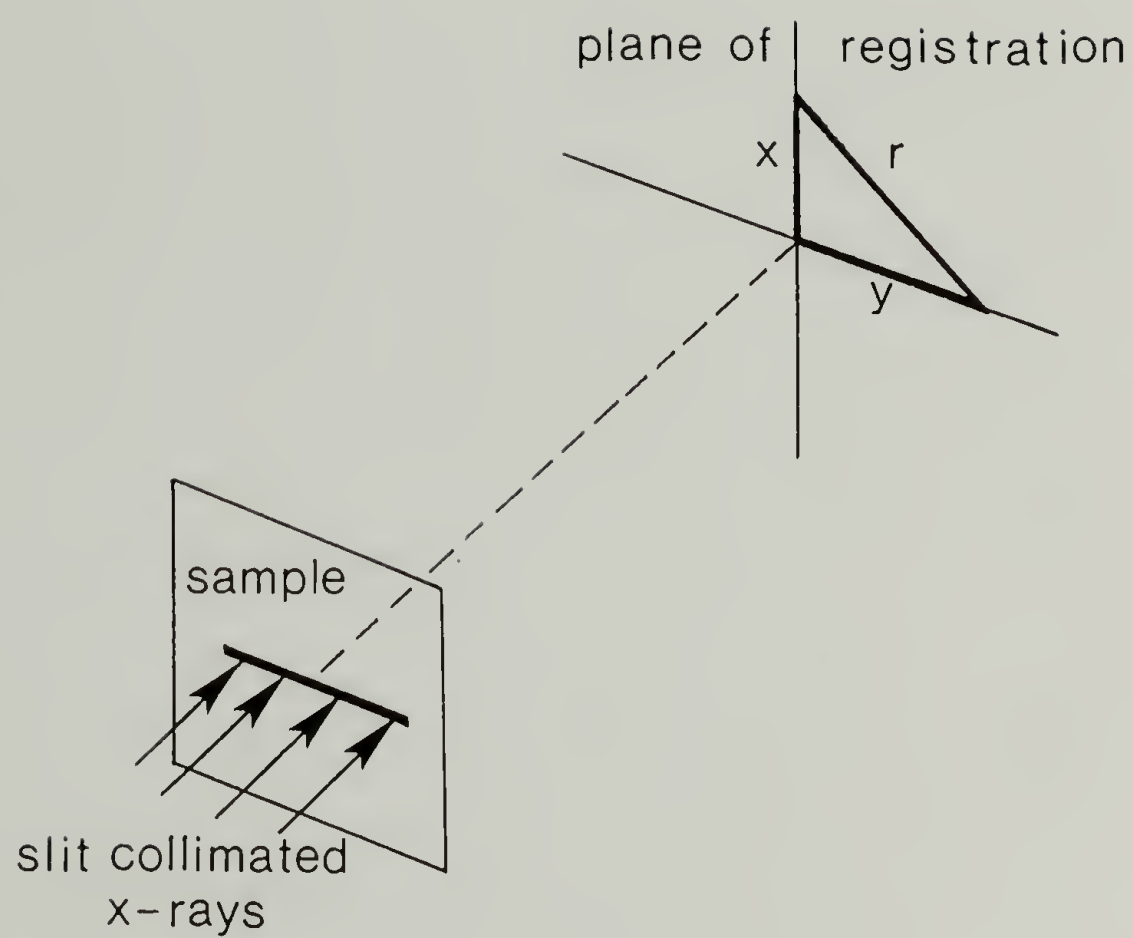


Figure 2.5 Schematic of SAXS geometry.

by the calibration sample, and  $K$  is a constant provided for the individual Lupolen calibration sample. The transmission of the calibrated sample  $A_c$  is also supplied.

In Equation 2.52 we need  $P_s$ , the value of  $P$  after absorption by the sample under consideration. It is obvious that

$$\frac{P_c}{A_c} = \frac{P_s}{A_s} \quad (2.54)$$

where  $A_s$  is the transmission of the sample. Using this relationship Equation 2.52 can be rewritten as

$$\tilde{I} = \frac{\tilde{i} TDA_s P_c}{a^2 A_c} \quad (2.55)$$

Combining this result with Equation 2.53 gives

$$\tilde{I} = \frac{\tilde{i} TDA_s \tilde{I}_c}{a A_c K} \quad (2.56)$$

so that the absolute smeared intensity per  $\text{cm}^3$  of sample is

$$\tilde{i} = \frac{\tilde{I} a A_c K}{TDA_s \tilde{I}_c} = \frac{1}{C} \left[ \frac{\tilde{I} a}{TDA_s \tilde{I}_c} \right] \quad (2.57)$$

where  $C = (1/KA_c) = 68.7$  for the UMass Lupolen standard. Similarly, for desmeared data,

$$i = \frac{1}{C} \left[ \frac{I a}{TDA_s \tilde{I}_c} \right] \quad (2.58)$$

## 2.4 SAXS Invariant

The absolute intensity scattered from a sample is proportional to  $\langle n^2 \rangle$  the mean squared fluctuation of electron density [25] where

$$\langle n^2 \rangle = \langle (\rho - \bar{\rho})^2 \rangle \quad (2.59)$$

Note that if the electron density has units of  $(n/\text{cm}^3)$ ,  $\langle n^2 \rangle$  has units of  $(n^2/\text{cm}^6)$ . The fundamental relationship is

$$\langle n^2 \rangle = 4\pi \int_0^\infty s^2 i(s) ds \quad (2.60)$$

The distance in the detector plane,  $x$ , is given by

$$x = 2a \sin \theta \quad (2.61)$$

so that Equation 2.56 can be written in terms of  $x$

$$\langle n^2 \rangle = \frac{4\pi}{a^2 \lambda^3} \int_0^\infty x^2 i(x) dx \quad (2.62)$$

Assuming an infinite slit, one may write [24]

$$\int_0^\infty x \tilde{i}(x) dx = 2 \int_0^\infty x^2 i(x) dx \quad (2.63)$$

Therefore, for smeared data

$$\langle n^2 \rangle = \frac{2\pi}{a^2 \lambda^3} \int_0^\infty x \tilde{i}(x) dx \quad (2.64)$$

Inserting the expression for  $\tilde{i}(x)$  derived previously (Equation 2.57) gives

$$\langle n^2 \rangle = \left[ \frac{2\pi}{C a^2 \lambda^3 TDA_s \tilde{I}_c} \right] \int_0^\infty x \tilde{I}(x) dx \quad (2.65)$$

This expression can also be written in terms of  $s$  as

$$\langle n^2 \rangle = \left[ \frac{2\pi}{C TDA_s \tilde{I}_c} \right] \int_0^\infty s \tilde{I}(s) ds \quad (2.66)$$



For a pure two phase system of uniform electron densities  $\rho_1$  and  $\rho_2$  having sharp interfaces, the invariant is given by [25]

$$\langle n^2 \rangle = (\rho_1 - \rho_2)^2 \theta_1 \theta_2 \quad (2.67)$$

where  $\rho_1$ ,  $\rho_2$  and  $\theta_1$ ,  $\theta_2$  are the electron densities and volume fractions of phases 1 and 2 respectively. Note that  $\langle n^2 \rangle$  does not depend on (i.e., is invariant to) the shape or arrangement of the phases. This makes the invariant extremely useful to measure since, if the volume fractions of the phases are known, the difference in the electron densities of the phases can be obtained. Conversely, if the electron densities of the phases are known, the invariant can provide compositional information. The invariant can also provide information about phase mixing. For example, if the two phases are connected by a transition layer in which the electron density varies from  $\rho_1$  to  $\rho_2$  across the interface the experimentally measured invariant will be less than the theoretical invariant. Any additional mixing of component 1 and 2 will also decrease the experimentally measured invariant since the electron density difference between the phases will decrease. It should be noted that small scale electron density fluctuations within the phases lead to additional scattering which must be subtracted from the raw data before the invariant is evaluated (see Section 4.4).

## 2.5 Scattering at Large Angles

For an ideal two phase system with sharp interfaces and random orientation, Porod [25] has shown that the scattered intensity at large angles is given by

$$K_p = \lim_{s \rightarrow \infty} (s^4 i) = \frac{2}{\pi} \lim_{s \rightarrow \infty} (s^3 \tilde{i}) \quad (2.68)$$

where  $K_p$  is the Porod constant given by

$$K_p = \frac{(S/V)(\rho_1 - \rho_2)^2}{8\pi^3} \quad (2.69)$$

The specific surface ( $S/V$ ) is the interfacial area per unit volume.

Two phase polymeric systems often exhibit systematic deviations from Porod's law due to small scale electron density fluctuations [26] which give rise to positive deviations (giving additional scattered intensity) and to the presence of diffuse phase boundaries which give rise to negative deviations from Porod's law. If the background scattering due to the small scale electron density fluctuations can be properly subtracted then the interfacial concentration profile could be obtained. More typically, a specific form of the interfacial concentration profile is assumed, and only the characteristic interfacial thickness is determined. Several excellent reviews concerning the measurement of interfacial thickness from SAXS experiments are available [11,27-30]. The main difficulty in the determination of interfacial thickness by SAXS is the uncertainty

associated with subtraction of the scattering arising from small scale electron density fluctuations.

# CHAPTER III

## BLOCK COPOLYMER MORPHOLOGY

The introduction of anionic polymerization by Szwarc [31] in 1956 enabled well defined block copolymers to be produced for the first time. Since then, a considerable amount of research has examined their properties, particularly those features connected with phase separation. This section is not intended to be a detailed review of all these previous studies; rather, it is intended to be an overview highlighting the key features concerning the phase separation and resultant morphology of amorphous two component block copolymers and blends of these block copolymers with organic solvents and homopolymers. Several excellent reviews of block copolymer morphology and properties have been published [32-36] and the reader should refer to these for a more extensive treatment.

### 3.1 Neat Block Copolymers

At temperatures below the critical temperature (the systems studied here have an upper critical solution temperature) the chemical species comprising the different blocks are incompatible, and are thus thermodynamically driven to separate into two phases. However, because the blocks are chemically linked to each other, the scale of the phase separation is restricted to occur with characteristic dimensions typically of hundreds of Angstroms, depending on the molecular weights



of the blocks. The regularity in block lengths, imparted by the anionic synthesis, leads to the formation of highly ordered equilibrium two phase morphologies.

### 3.1.1 Experimental studies

The study of the phase separation of block copolymers began soon after their discovery with the work of Skoulios et al. [37-39] who studied the structure of polystyrene-polyethylene oxide block copolymers in various solvents. It was observed, via SAXS, that these block copolymers were capable of producing well organized mesophases analogous to the lyotropic mesophases of soaps, which were also being actively investigated at this time at Strasbourg [40-42] by means of SAXS. The mesophases consisted of arrangements of three types of domains: spheres, cylinders, and lamellae.

Shortly after these initial studies, the mesophases of neat (pure) block copolymers were studied by many different groups. The development of the osmium tetroxide staining method by Kato [43,44] to selectively stain the polydiene phase led to a large number of transmission electron microscopy studies of block copolymers containing polydiene blocks [46-64]. In some instances, SAXS was also performed. The early investigations [46-52] were directed mainly at establishing the existence of the different mesophases. Typically, solvent cast films were investigated. It was recognized early on that the development of

organized structures required slow casting from dilute polymer solutions (i.e., near equilibrium conditions).

By 1970, enough evidence had been collected for Molau [32] to propose the now classic picture of domain morphology versus composition shown in Figure 3.1. The equilibrium domain shapes are: spheres of the minority component for minority volume fraction between about 0 and 0.20, cylinders of the minority component for minority volume fraction between about 0.20 and 0.40, and alternating lamellae for volume fractions between about 0.40 and 0.60. Research during the present dissertation has revised this picture (see Section 3.1.4).

Subsequent investigations were directed mainly toward the development and characterization of the long range microdomain order [53-64]. Again, the importance of driving the system towards its thermodynamic equilibrium was noted, which necessitated the avoidance of preferential solvents, quick casting, or thermoforming techniques. Generally, near equilibrium microstructures can be realized by slow casting of thin films from dilute solutions of the copolymer in a non-preferential solvent, followed by annealing above the glass transition temperature of both components (but below the critical temperature). Keller et al. [65,57,66] have developed another technique to promote the development of long range order, that of extrusion or mechanical shearing. A macrolattice structure having a single crystal texture for cylindrical and lamellar domains has been produced by several workers using this technique [65-68].

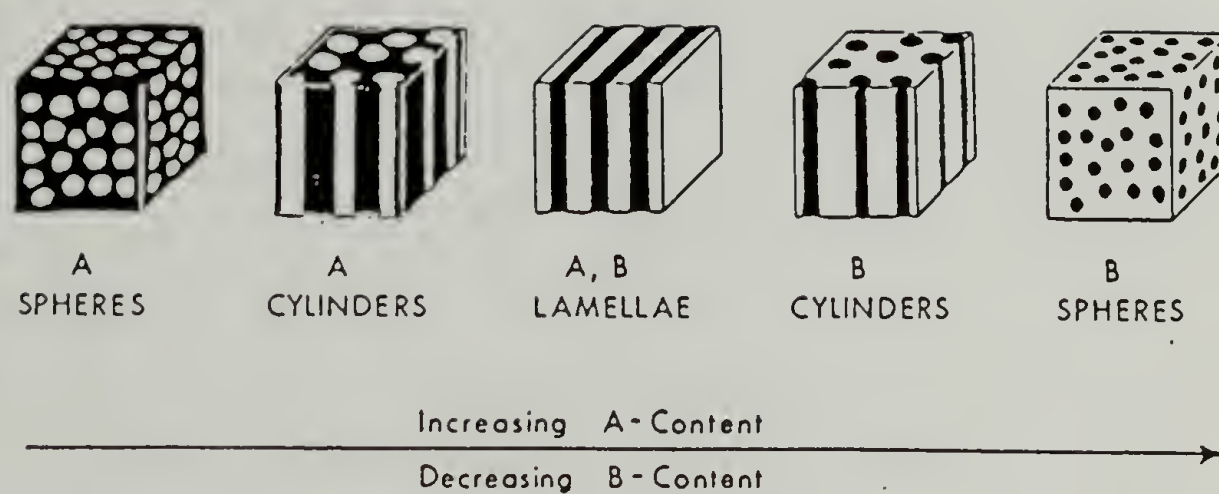


Figure 3.1 Schematic showing the equilibrium domain morphology as a function of copolymer composition (from Molau [32]).

These studies have established that the cylindrical domains are arranged on a two dimensional hexagonal lattice and the spherical domains are arranged on a three dimensional cubic lattice. However, up to the work of this dissertation, the exact nature of the cubic packing (i.e. SC, BCC, or FCC) had not been conclusively determined (see Section 3.1.3).

### 3.1.2 Thermodynamic theories

Several statistical thermodynamic theories have been presented to predict such features as the size, shape, and distance between domains, the lattice type, and the temperature at which the microphase separation takes place, as a function of the molecular properties, i.e., molecular weight, chemical composition, and degree of incompatibility of the different blocks. These theories can be classified into two main categories: (1) those which predict the domain structure after the phase separation has taken place, and (2) those which predict the energetically favored domain structure at the onset of the microphase separation.

Most notable among the first category are the theories of Helfand [69-74] and Meier [75-78]. These theories are based on determining the structural parameters for which the total free energy of the system is minimized. The driving force for the growth of the domains is the repulsive enthalpic interactions between the A and B segments characterized by the Flory-Huggins interaction parameter  $\chi = \Delta V_{\text{ref}}/kT$



where  $\Delta$  is the interaction energy energy density and  $V_{\text{ref}}$  is the average volume of the A and B segments. As the domains increase in size, the surface to volume ratio decreases, thus decreasing the interfacial free energy of the system. However, as the domain grows it creates a density deficiency toward the center of the domain unless the chains stretch to fill this region. This stretching involves the loss of conformational entropy and this opposes domain growth. In addition, the loss of entropy from confining the junction between the blocks to the interfacial region between the A and B microphases will also increase as the domains grow since the volume fraction of interface decreases; this factor also opposes domain growth. Therefore, the equilibrium domain structure is determined by a balance of these opposing factors.

At thermodynamic equilibrium, the system should choose to assume the domain morphology which corresponds to the lowest free energy. For example, Figure 3.2, taken from Helfand [74], shows the predicted structure diagram showing the regions of stability of the spherical, cylindrical, and lamellar domains calculated for poly(styrene-butadiene) diblock copolymers at a temperature of 90 °C. It is immediately apparent that the most important parameter in determining the microdomain morphology is the composition of the copolymer; the total molecular weight of the copolymer has much less of an impact. Provided the copolymer molecular weight is sufficiently high, for compositions between 0 to 0.15 volume fraction of polystyrene (polybutadiene), the stable structure is predicted to be that of polystyrene (polybutadiene) spheres in a matrix of polybutadiene (polystyrene). For polystyrene

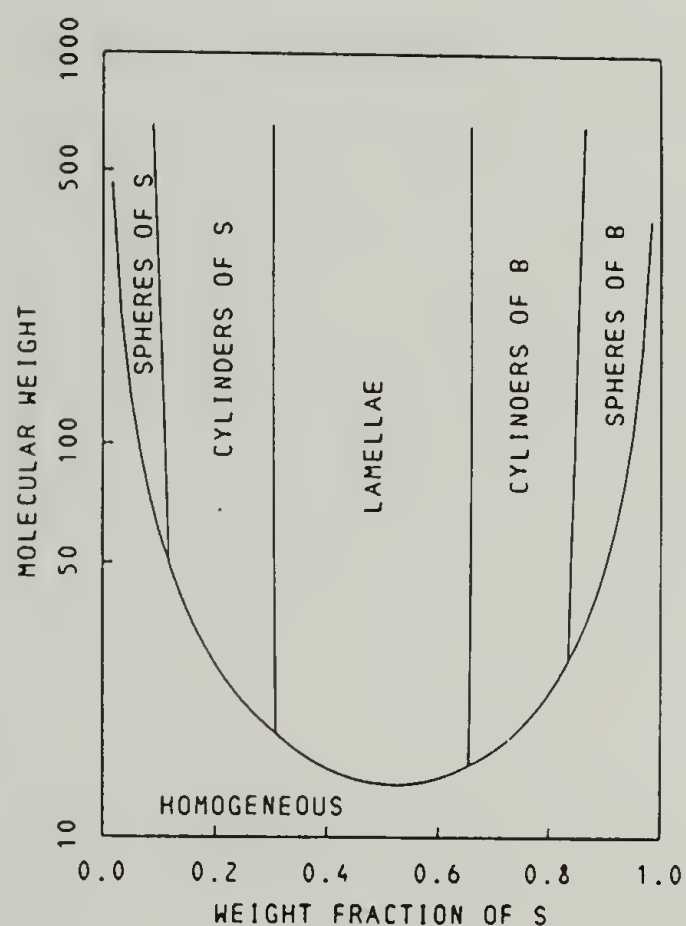


Figure 3.2 Structure diagram showing the PS-PB block copolymer micro-domain morphology as a function of molecular weight (given in Kg/mole) and composition predicted by Helfand's theory (taken from Helfand [74]).

(polybutadiene) volume fractions between 0.15 and 0.30 the stable structure is predicted to be that of polystyrene (polybutadiene) cylinders, while for polystyrene (polybutadiene) volume fractions between 0.30 and 0.70 the stable structure is predicted to be alternating polystyrene and polybutadiene lamellae. Concerning the arrangement of these domains into a unit cell, it should be remarked that the only geometries considered in this free energy minimization were close-packed spheres, hexagonally packed cylinders, and alternating lamellae. It is conceivable that other structures which were not considered, such as a bicontinuous structure, could also be possible (see Section 3.1.4).

The size of the microphase separated domains  $D$  and the interdomain distance  $d_{\text{int}}$  are predicted to follow the scaling laws

$$\begin{aligned} D &= K_1 M_d^a \\ d_{\text{int}} &= K_2 M_t^a \end{aligned} \quad (3.1)$$

where  $M_d$  and  $M_t$  are the molecular weights of the domain forming blocks and the total molecular weight of the copolymer respectively. Meier predicts  $a = .56$  while Helfand predicts  $a = .67$  (compared to the value of .50 for a random coil). Several researchers have compared their experimentally determined domain sizes as a function of molecular weight to these theoretical predictions [11,79,85,95,96]. In addition, Helfand and Wasserman have compared their calculations of domain size and spacing with the experimental results found in the literature for lamellae [71], cylinders [73], and spheres [72]. In general, these comparisons have shown that both the magnitude and the molecular weight



scaling predicted by the theories of Helfand are in good agreement with the experimental results for the case of lamellar and cylindrical domains. However, the general trend is that the experimentally determined sphere sizes are smaller than predicted by theory. Only block copolymers having low molecular weight and high rubber content closely follow the predicted behavior. This discrepancy has been attributed to a non-equilibrium structure being "frozen in" during solvent evaporation [11]. Adjustment of the spherical domain size requires transport of the minority block through the matrix phase, while the lamellar and cylindrical domains are able to approach equilibrium size more closely because the phases are not isolated, and adjustment of domain size can occur by transport of segments within the domain. The energy barrier to this transport should increase as the solvent evaporates, and the viscosity increases, during the casting process. Eventually a concentration is reached at which the solvent/polystyrene phase is below its glass transition temperature so that chain transport is effectively stopped. Increasing the rate of diffusion of the blocks by annealing above the  $T_g$  of the polystyrene should allow an equilibrium structure to be obtained given enough time. This time will be highly dependent on the molecular weight of the blocks.

The characterization of the interface boundary in block copolymers has received considerable attention in recent years due to the recognition of the important role it plays in determining mechanical properties. According to the theory of Helfand, the density profile of



the different segments across the interface, in the limit of infinite molecular weight, is given by

$$\rho(x) = 1/2 [1 - \tanh(2x/a_I)] \quad (3.2a)$$

$$a_I = \frac{2b}{(6x)^{1/2}} \quad (3.2b)$$

where  $a_I$  is the parameter which describes the interface thickness and  $b$  is the Kuhn statistical length (approximately 0.6 nm for styrene-diene block copolymers). According to the definition of interface width  $t$  presented by Hashimoto (Equation 2.43),  $a_I = (2/\pi)t$ . For a typical value of  $x$  for styrene-diene block copolymers at 100 °C (0.1) this gives an interface width  $a_I$  of 1.5 nm. Note that since  $x$  is inversely related to temperature, the interface width is predicted to increase with temperature. For example, Helfand and Sapse [132] predict that the interface width for poly(styrene-isoprene) block copolymers increases from 1.4 nm at 25 °C to 1.6 nm at 90 °C. Typical values of interface width determined from SAXS [11,29,30] and SANS [84,85,95,97] experiments fall in the range of  $a_I = 1.0 - 2.0$  nm which agrees rather well with the theoretical predictions. Experimental studies of the temperature dependence of the interphase thickness are somewhat inconclusive. Fujimura et al. [98] report an increase in interphase width measured by SAXS from  $t = 2.1$  to 2.5 nm on going from 25 to 180 °C for a spherical domain forming poly(styrene-isoprene) diblock copolymer. On the other hand, Roe et al. [30] have reported that they observed little change in interface width with temperature, also measured by SAXS, for a poly(styrene-butadiene) diblock. In fact, their data actually shows a slight decrease in the interfacial width from 1.5 nm at 20 °C to 1.2 nm

at 200 °C. This discrepancy is probably due to the fact that values of interphase width as measured by SAXS are not very accurate due to the uncertainty associated with subtraction of the scattering arising from small scale electron density fluctuations [94].

Also shown in Figure 3.2 is the predicted phase boundary for the transition from a microphase separated structure to a homogeneous mixture found by setting the change in free energy equal to zero for a given copolymer composition and molecular weight. It must be pointed out however that one of the assumptions of this type of theory is that the width of the interface region is small compared to the size of the domains. It seems plausible that near the transition there will be extensive mixing of the A and B segments, and the concept of a narrow interface loses its validity.

This leads one to the second type of theory first proposed by Leibler [80] and later extended by Hong and Noolandi [81]. Leibler has attempted to construct a theory of the fluctuations in composition about the homogeneous state, from which the microphase separation transition temperature can be located as a function of molecular weight and copolymer composition. The relevant parameters of the theory are the product  $\chi N$ , where  $N$  is the polymerization index of the copolymer, and  $f$ , the fraction of A monomers in the copolymer. In this theory, the density correlation function in the homogeneous melt is studied using the "random phase approximation" method of de Gennes [82,83]. It is found that as the critical point is approached a certain Fourier component of the monomer density fluctuation diverges, marking the

microphase separation transition. The structure diagram of the system is obtained by calculating the regions of stability of the disordered homogeneous phase and the various ordered mesophases in a plane with coordinates  $\chi N$  and  $f$ . The result, taken from [80], is shown in Figure 3.3. The critical value  $(\chi N)_c$  for  $f = 0.50$  is found to be 10.5 (compared to 2 for a blend of two homopolymers [82,83]). For a typical value of  $\chi = 0.1$ , this transition corresponds to a polymerization index  $N$  of about 100, or in other words, a polystyrene block molecular weight of about 5,000. The periodicity of the stable mesophase is given by  $2\pi/q^*$ , where  $q^*$  is the magnitude of the scattering wave vector at which the density correlation function diverges, and is of the order  $2/R_g^0$  where  $R_g^0$  is the unperturbed radius of gyration of the copolymer.

As seen in Figure 3.3, the structure which is predicted to appear first (except when  $f = 0.50$ ) as  $\chi N$  becomes larger than  $(\chi N)_c$  is a mesophase with the symmetry of a body centered cubic lattice of spheres, followed by mesophases with hexagonal and lamellar symmetries. At a given value of  $\chi N$ , the dependence of the structure on the copolymer composition is qualitatively similar to that predicted by Helfand and Meier in that, as  $f$  is increased, one expects to observe, respectively, a cubic, hexagonal, and lamellar mesophase. However, the predicted composition ranges over which these structures should occur are quite different. In addition, contrary to the results of Helfand (see Figure 3.2), Leibler predicts that the mesophase structure is highly dependent on the molecular weight of the copolymer, especially when  $\chi N$  is near  $(\chi N)_c$ . It should be remarked that this type of theory is really only



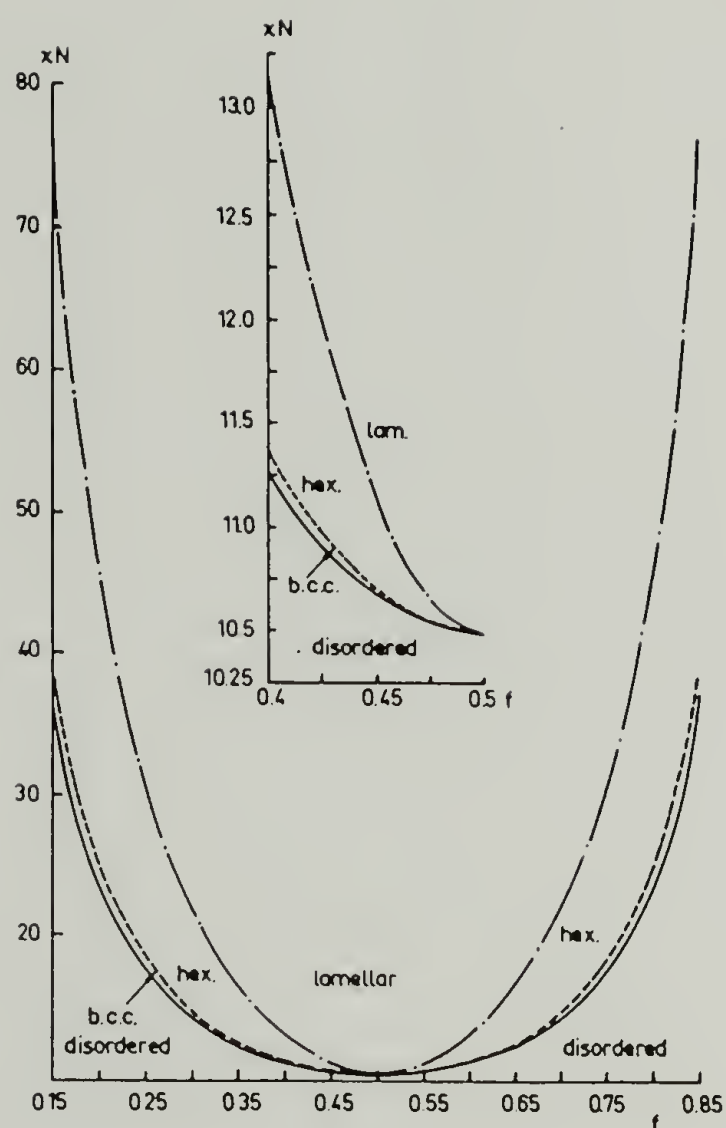


Figure 3.3 Structure diagram showing the regions of stability of the disordered homogeneous phase and the various ordered mesophases predicted by Leibler's theory (taken from Leibler [80]).



valid near the microphase separation transition since the theory looks at the fluctuations at the transition point and ideal chain behavior is assumed. From the previous discussion it is evident that the chains in domain space are perturbed from that of an ideal chain. It should also be noted that Leibler only considers mesophases with SC, FCC, BCC, or rhombohedral symmetry as possible three dimensional structures. However, other mesophases such as the ordered bicontinuous double diamond structure discussed in Section 3.1.4 could occur.

Roe et al. [30] have used SAXS to study the thermal transition from an ordered microdomain structure to a disordered homogeneous phase for poly(styrene-butadiene) block copolymers. On raising the temperature, the interference peak intensity (and the invariant) decreases steadily over a wide temperature range (100-200 °C). This indicates that the microdomain structure is destroyed over a very broad range of temperature, implying that the phase transition may not be first order. As mentioned previously, the thickness of the interface is not found to change appreciably with temperature. This leads to a model in which the disappearance of the microdomains proceeds by gradual intermixing of the blocks into the opposite phases. For a diblock copolymer having 25 weight% polystyrene and total molecular weight of 27,000, the transition temperature found by Roe was about 400 °K compared to the value predicted by Leibler of about 580 °K [99]. For a triblock SBS copolymer having the same composition, but 57,000 total molecular weight, the transition temperature was found to be higher (about 470 °K). While this trend is qualitatively predicted by

Leibler's theory, it is evident that the absolute temperature of the transition is not predicted very well. In addition, Leibler's theory predicts an abrupt transition in structure at the microphase separation transition temperature, which is in disagreement with the experimental findings.

### 3.1.3 Lattice structure of spherical microdomains

As mentioned previously, studies of the type of lattice structure exhibited by spherical domain forming block copolymers is still an active and somewhat controversial topic of study. The statistical thermodynamic treatments of Meier and Helfand both assume a priori a close packed array of spheres and proceed to calculate sphere size and intersphere distance as a function of block length and composition. The more recent theory by Leibler predicts a stable ordered spherical domain regime with body centered cubic lattice structure dependent on molecular weight, composition, and interaction parameter.

Based on their SAXS results for poly(styrene-isoprene) diblock copolymers containing 13-22% polyisoprene, Hashimoto et al.[11] concluded that the macrolattice was either simple cubic or cubic close packed. This assignment was based on the relative positions of the observed interparticle interference peaks (usually only two). Roe and coworkers [30] examined an SB and an SBS copolymer both containing 25% polystyrene. Two interparticle interference peaks were observed in the SAXS patterns, but their relative spacings did not correspond to any

particular lattice. Nevertheless, on the basis of the polystyrene volume fractions calculated for SC, BCC, and FCC lattices, (based on sphere size and intersphere distance obtained from the position of the sphere scattering and lattice peaks respectively) the authors concluded that either an FCC or BCC structure best fit their data. Douy and Gallot [86] proposed that a BCC lattice was consistent with their SAXS and EM studies on styrene-butadiene block copolymers containing between 10 and 15% polybutadiene. Richards and Thomason [84,85] studied a series of SI and SIS block copolymers by electron microscopy and SANS. Although their spherical domain forming samples exhibited only a single broad interparticle interference peak, and their electron micrographs revealed a lack of long range order, they concluded from volume fraction calculations that an FCC lattice best fit their data.

One of the most convincing identifications of lattice type in spherical domain forming styrene-diene block copolymers using scattering methods was presented by Bates et al. [88] who examined an SB diblock containing 14% polybutadiene by SANS. The published electron micrograph revealed a well ordered arrangement of the polybutadiene spheres. This observation of long range order is borne out in the SANS curve which displays three distinct lattice reflections whose relative positions coincide with those predicted for a SC or BCC lattice (these have the same relative spacings until the seventh order reflection). Volume fraction calculations strongly favored the BCC lattice.

One of the earliest investigations of spherical domain lattice structure was that by Pedemonte and coworkers [87] who used electron



microscopy to examine a polystyrene-polyisoprene-polystyrene triblock copolymer containing 10% polystyrene. The authors observed hexagonal, rectangular, and square projections which they assigned to the (111), (110), and (100) projections of a BCC lattice. This assignment was based on the relative spacings between domains in the three projections which were in good agreement with the relative spacings predicted for a BCC lattice. These different projections were, however, obtained by searching the microtomed sections to locate ordered grains which were in the correct orientation to give one of the three aforementioned symmetrical projections. A better method would be to obtain these projections by performing tilting experiments in the microscope on a single ordered grain. This is desirable for two reasons. The first is that deformation of the section during microtoming can cause changes in lattice spacings as well as shearing of the macrolattice. Another reason is that the lattice spacings may vary within the sample. Because the assignment of a macrolattice is based in part on the distance between domains, comparisons of spacings obtained from different grains is thus ill-advised. Such a quantitative tilting study using a single grain, performed as an adjunct study to this dissertation, is presented in Appendix B. Two different poly(styrene-butadiene) diblock copolymers, one having polybutadiene spheres and one having polystyrene spheres, were examined and the results proved that both samples had a BCC lattice structure. This result is consistent with most of the previous studies which, taken collectively, prove conclusively the



existence of a BCC lattice structure for ordered diblock copolymers containing spherical microdomains.

#### 3.1.4 Ordered bicontinuous structure

Recently in our laboratory, a new equilibrium domain morphology for block copolymers (other than the classical spheres, cylinders, or lamellae) has been discovered [91]. The basic unit of this structure is a tetrahedral arrangement of short rods of the minority component. Such units are interconnected on a cubic lattice having the symmetry of the  $Pn3m$  space group. The resultant structure consists of two translationally displaced, mutually interwoven, but unconnected three dimensional networks of these short rods embedded in the majority component. Each of the two separate minority phase continuous networks exhibits the symmetry of a diamond cubic lattice; thus, this morphology is called the ordered bicontinuous double diamond (OBDD) structure. A schematic of this structure is shown in Figure 3.4.

Initially, this structure was observed in poly(styrene-isoprene) star block copolymers having 30-36 wt% polystyrene outer blocks [89-92] as well as in inverted stars (polyisoprene outer blocks) having 30 wt% polyisoprene [93]. Recently, this OBDD structure has also been identified in linear poly(styrene-diene) diblock copolymers containing between 62 and 66 volume percent polystyrene [93].

All observations indicate that the OBDD structure exists in a narrow composition window between that of the hexagonally packed

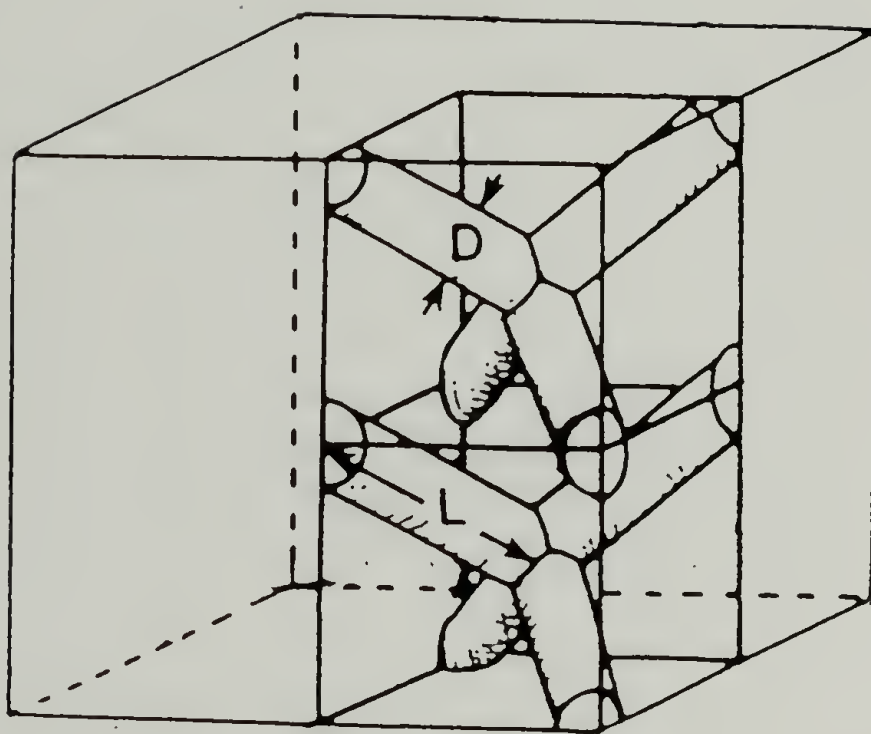


Figure 3.4 Schematic of the ordered bicontinuous double diamond (OBDD) structure (taken from [91]). One fourth of the unit cell is shown.

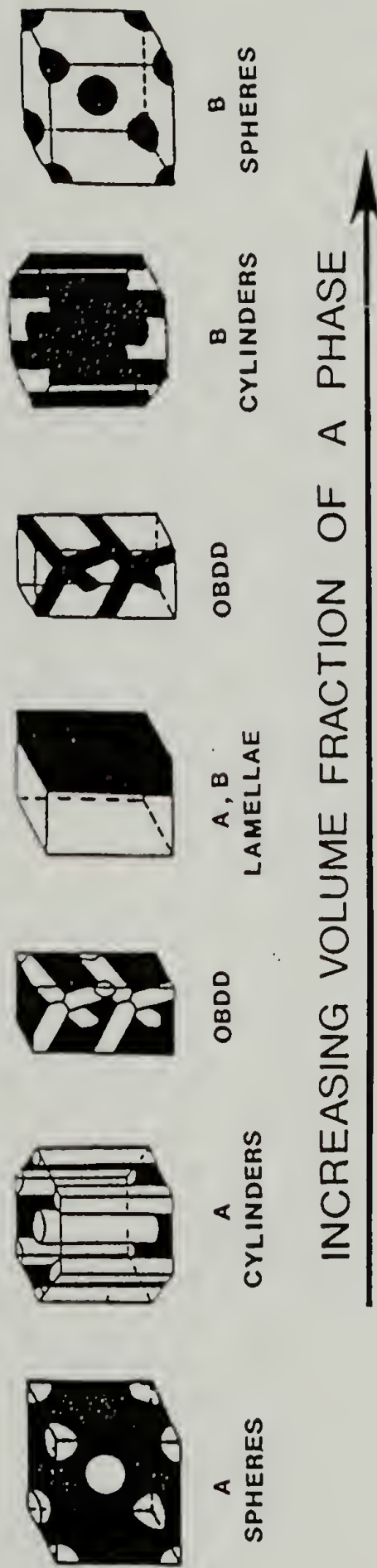


Figure 3.5 Schematic showing the equilibrium domain morphology as a function of copolymer composition, including the BCC lattice structure of spherical microdomains and the recently discovered ordered bicontinuous double diamond (OBDD) structure.

cylinders and the lamellar structures. The picture of block copolymer domain structure versus composition proposed by Molau (Figure 3.1), thus needs to be modified, taking into account both the BCC packing of the spherical domains and the existence of the OBDD structure, as shown in Figure 3.5.

### 3.2 Block Copolymer/Solvent Systems

As mentioned previously, the first investigations of the mesophase structure of block copolymers were for block copolymer/solvent systems [37-39]. Depending on the nature of the solvent, concentration of solvent, temperature, and composition of the copolymer, a myriad of structures are possible. For the most part, the following discussion will be limited to the case of a preferential solvent for one of the blocks (i.e., a good solvent for one of the blocks, but a poor or non-solvent for the other block).

For these systems, Sadron [64] has shown that the structure as a function of solvent concentration is closely related to the structures observed in systems of soap and water [40-42]. In general, three regions may be observed: (1) at very low concentrations of copolymer ( $<0.1\%$ ) a homogeneous solution is obtained in which the copolymer is molecularly dispersed in the solvent, (2) as the copolymer concentration is increased a point is reached where the less soluble block precipitates to form aggregates, or micelles, each containing many copolymer molecules, (3) above a certain copolymer concentration the



system is organized in a regular periodic structure, similar to those found for neat block copolymers.

Regions 1 and 2 have been treated in review articles by Tuzar [100] and Price [101,102]. Tuzar has presented the evidence for the micellization being a closed association process characterized by an equilibrium between a single molecularly dispersed molecule and aggregates made up of  $n$  ( $n$  is on the order of 100) copolymer molecules. This closed association model assumes the existence of a critical micelle concentration (cmc) which has been observed in the micellization of soaps and ionic and nonionic surfactants [103]. The critical micelle concentration is defined as the concentration at which micelles first appear; thus, it marks the division between regions 1 and 2 as defined by Sadron [64].

Structural studies of these block copolymer micelles has been performed using x-ray scattering [104,105], light scattering [106-109], and neutron scattering [110]. Some of these studies have also employed electron microscopy [106,107] although these studies examined the structure after the solvent was removed. The micelles are found to contain a core region, consisting mainly of the insoluble block, surrounded by a corona region containing the soluble blocks highly swollen with solvent.

Plestil and Baldrian [105] investigated the structure of a poly(styrene-butadiene) diblock containing 24% polystyrene in dilute solutions of heptane, which is a selective solvent for polybutadiene, by SAXS. Measurements were made at four temperatures ranging from 18 to 50

°C. The scattering curves exhibited a slight shoulder at about 0.003 rad, which was attributed to interparticle interference, and a weak maximum within the range 0.0130 to 0.0145 rad, which was attributed to intraparticle interference. Absolute intensity measurements were extrapolated to zero angle (using Guinier's law), from which the average molecular weight of the micelles was obtained. The number of copolymer chains per micelle was thus determined to decrease from 190 at 18 °C to 100 at 50 °C. In addition, the degree of swelling of the individual components was determined from an invariant analysis. The degree of swelling of the polybutadiene chains with solvent was observed to increase with increasing temperature; the polybutadiene volume fraction in the corona decreased from about 0.20 at 18 °C to about 0.12 at 50 °C. The swelling of the polystyrene core with solvent remained unchanged with temperature; the polystyrene volume fraction in the core was about 0.80. A two phase concentric sphere model for the micelles was also used to calculate the diameter of the micelle cores and the overall diameter of the micelles from absolute intensity measurements.

Noolandi and Hong [111] have compared the results of Plestil and Baldrian to the predictions of their theory for block copolymer micelles in solution. This theory is an extension of that presented by Leibler et al. [112] which will be discussed in more detail in Section 3.3. Briefly, the free energy of the system is minimized with respect to the length scales  $l_A$ ,  $l_B$ , and  $R$  for a given copolymer molecular weight, composition, and concentration, where  $l_A$  is the thickness of the corona region,  $l_B$  is the radius of the micelle core ( $l_A$  and  $l_B$  are the average

end to end distances of the A and B blocks), and  $R$  is the radius of the unit cell which encloses the entire micelle as well as some pure solvent. Three interaction parameters are required for the calculations:  $\chi_{AS}$ ,  $\chi_{BS}$ , and  $\chi_{AB}$  where  $S$  refers to solvent. The comparison of the theoretical predictions to the experimental results shows good agreement to the extent of correctly predicting the qualitative trends with changes in temperature of the radius of gyration, the degree of swelling of the two blocks, and the number of copolymer molecules per micelle. However, the predicted values of the number of copolymer molecules per micelle do not decrease nearly as fast with increasing temperature as do the experimental values. This may be due to the fact that the temperature dependence of the polybutadiene/*n*-heptane  $\chi$  parameter was neglected in the calculations. The decrease of the aggregation number with increasing temperature can be attributed to a decreasing interaction parameter between the A and B blocks, which leads to less segregation of the chains and favors smaller core sizes. According to the theory, the overall size of the micelle and the size of the core should scale as  $Z_c^{2/3}$ , while the number of copolymer chains per micelle should scale as  $Z_c$ , where  $Z_c$  is the total degree of polymerization of the block copolymer. These exponents had previously been calculated by de Gennes [113].

Kotaka et al. [109] have investigated how the solvent quality effects the micellar structure. Three different polystyrene/polymethylmethacrylate (PS/PMMA) diblock copolymers having .24, .49, and .69 weight fractions of PS in a mixture of toluene and *p*-cymene solvents



were examined by light scattering. Toluene is a good solvent for both blocks while p-cymene is a good solvent for PS but a nonsolvent for PMMA. By varying the relative amount of each of these solvents, the solvent quality could be gradually changed. The observed behavior could be classified into three categories: (1) in the region of low p-cymene content the block copolymer molecules are in a state of molecular dispersion, (2) for intermediate p-cymene content spherical or nearly spherical micelles with PMMA cores are assumed to be present, and (3) for high p-cymene content micelles of large size and unknown morphology are present. For a given p-cymene/toluene ratio, the results for spherical micelles indicate that the PMMA blocks in the core are nearly unstretched while the PS chains in the corona are considerably extended in the radial direction. The core radii of the micelles were found to be larger for those having larger PMMA blocks, although no comparisons to scaling predictions were made. As the p-cymene content is increased, much larger aggregates are observed. The authors attribute this to a change of core shape from spherical to a more extended ellipsoidal or cylindrical shape. Indeed, such a transition has been observed by Canham et al. [107] for SBS triblock copolymers having 30% polystyrene in ethyl acetate, which is a selectively poor solvent for polybutadiene. As the temperature of these solutions was increased, a cloud point occurred, and as the temperature was raised even further the solutions became clear again. Light scattering and electron microscopy studies (the EM studies were performed on samples prepared by staining the solution with osmium tetroxide, followed by evaporation of the solvent)



suggested that the onset of cloudiness was due to a reversible transition from spherical to worm-like micelles. The clearing of the solutions on raising the temperature further occurred because the micelles dissociated to form copolymer molecules molecularly dispersed in the solvent. This transition in micelle shape was attributed to an increasing degree of swelling of the polybutadiene core as the temperature was raised. The authors state that the formation of worm-like and lamellar micelles is a general phenomena expected to occur in systems for which the solvent is selectively bad for the larger block in the copolymer. Indeed, Tuzar et al. [114] have reported similar results for SBS triblock copolymers (containing about 30 wt% PS) in isopropyl acetate, which is a selective solvent for PS.

In the region of larger block copolymer concentration (i.e., region 3 as defined by Sadron), the system is organized in regular periodic structures similar to those found for pure block copolymers. This region has been extensively investigated by the Orleans group [53,59,60,63,64,115]. The microdomain structure in solutions were primarily investigated by SAXS and electron microscopy. In order to perform the microscopy, preferential solvent monomers which could be polymerized by UV light were employed [64] so that solidified solutions could be obtained, which could then be microtomed, stained, and studied in the microscope. It was hoped that the structure formed after the polymerization of the monomer was the same as that before polymerization. Although no large changes were reported in the SAXS patterns upon polymerization, it will be shown in subsequent sections of

this dissertation that the molecular weight of the homopolymer matrix can have a marked effect on the structure.

In general, the structures observed are the same as those observed for neat block copolymers; namely, spheres, cylinders, and lamellae. It seems that the principle put forth by Molau [32] for the case of neat copolymers regarding the volume fractions over which each type of structure is observed can be generalized to include the case of block copolymer/solvent systems if the volume fractions considered are those of the insoluble block phase and the soluble block/solvent phase. For example, consider a neat block copolymer exhibiting lamellar morphology. As a preferential solvent S for the A block is added, the successive structures encountered will be: alternating lamellae of B and (A+S), B cylinders on a hexagonal lattice in (A+S), and B spheres on a cubic lattice in (A+S). Of course, as more solvent is added a disorganized arrangement of spherical micelles having B cores is expected to be present. For a given structure, the interdomain distance will increase in a regular manner with increasing solvent content [64].

The transitions in structures for pure block copolymers as well as block copolymer/solvent systems as a function of the relative block lengths (i.e., molecular volumes of the blocks) can be intuitively understood in terms of packing requirements of the chains in the domain space and interface curvature. Consider first the situation where the two blocks have nearly the same volume and form the lamellar structure where the interface is planar, and the space available to the blocks on either side of the interface is comparable. Now let one of the block

lengths increase relative to the other. The interface surface now becomes curved so that the space available on the convex side of the interface is larger than that available on the concave side; thus, cylindrical or spherical microdomains are formed with the smaller block occupying the concave side of the interface. The addition of solvent preferentially to one of the blocks just increases its effective volume.

Recently, Shibayama et al. [116] have studied the microdomain structure of an SB diblock copolymer containing 30% polystyrene in *n*-tetradecane (a good solvent for polybutadiene, but a poor solvent for polystyrene) as a function of concentration and temperature using SAXS. For polymer concentrations up to 60%, a spherical polystyrene microdomain structure was observed (the pure copolymer exhibited polystyrene cylinders). It was observed that below a polymer volume fraction of 0.08 the spherical domains possessed liquid-like packing as evidenced by a lack of higher order SAXS interference peaks. However, for volume fractions greater than about 0.08, an ordered cubic structure with relative SAXS interparticle interference peak positions of  $1:(2)^{1/2}:(3)^{1/2}$  were observed. As discussed in Chapter 2, this indicates that the spheres are packed in either a SC or BCC lattice. From volume fraction calculations, which assumed that there was no solvent in the polystyrene core, the SC packing mode seemed more probable (recall that spherical domain forming neat copolymers exhibit a BCC packing mode).



### 3.3 Block Copolymer/Homopolymer Blends

The literature concerning the structure and thermodynamics of block copolymer/homopolymer blends is quite extensive. The following review is restricted to the case of AB and ABA type block copolymers blended with either A homopolymer or B homopolymer, which could be considered as a special case of selective solvent.

One of the earliest experimental studies of the structure of such systems was performed by Molau in 1968 [117] who studied poly(styrene-butadiene) block copolymers in polystyrene homopolymers. Samples were prepared by dissolving the copolymer in styrene monomer (a non-selective solvent), followed by solidification of the solution by polymerization of the styrene. The samples could then be microtomed, stained, and examined in the electron microscope. It should be kept in mind that the phase separation takes place as the polymerization of the styrene monomer proceeds. Thus, the structure will be "frozen in" at some time during the polymerization of the styrene since the polymerization was carried out at room temperature, well below the  $T_g$  of even low molecular weight (2,000) polystyrene. The matrix molecular weight distribution at the time of this structure formation was unknown.

In any event, micrographs of 5% of a block copolymer containing 30% polybutadiene in 95% styrene monomer, in which the styrene monomer had been polymerized to completion, show both polybutadiene cores of spherical micelles, and larger "elliptical" structures which were



attributed to cross sectional views of cylinders. These elliptical structures appear actually to be vesicles with a polybutadiene outer shell, having homopolystyrene both inside and outside of the vesicle. It was noted by Molau that the thickness of the polybutadiene walls of the elliptical structures were similar to the diameter of the spherical polybutadiene micelle core. Therefore, the vesicle walls are likely to be composed of a double layer of polybutadiene blocks. In addition, some short rodlike (cylindrical) polybutadiene phases having about the same thickness as the vesicle walls were also present. Thus, spherical, cylindrical, and lamellar (vesicle) polybutadiene shapes are observed simultaneously, which is indicative of a non-equilibrium structure being induced by the sample preparation technique.

Inoue et al. [118] performed electron microscopy on toluene cast films of poly(styrene-isoprene) diblock copolymer blended with various amounts of homopolystyrene or homopolyisoprene. No sample annealing was performed subsequent to the sample casting so it is likely that equilibrium was not achieved. In any case, it was generally found that when the copolymer was mixed with a homopolymer having molecular weight less than or comparable to that of the corresponding block in the copolymer, solubilization of the homopolymer into the domain of the corresponding block took place. For example, 40,000 molecular weight homopolyisoprene was added to a lamellar forming copolymer having a 31,000 molecular weight polyisoprene block. As the concentration of the homopolyisoprene increased, the domain structure changed systematically from lamellae, to polystyrene rods (30% added homopolymer and 30% total

polystyrene content), to polystyrene spheres (70% added homopolymer and 15% polystyrene content). This change in structure follows that seen by Sadron [64] in block copolymer/solvent systems as a function of the volume fractions of the two phases. When the molecular weight of the homopolymer was significantly higher than that of the corresponding block, the copolymer behaved as if it were incompatible with the homopolymer, and the homopolymer formed its own phase.

Bradford [119] has stated that the domain morphology in block copolymer/homopolymer blends does not always follow the volume fraction rule proposed by Molau. He studied toluene cast films of SB and SBS block copolymers blended with polystyrene homopolymers using electron microscopy of ultramicrotomed sections. Again, no annealing was performed subsequent to sample casting. It was observed that a blend of 50% SB copolymer having 380,000 and 250,000 molecular weight polystyrene and polybutadiene blocks respectively (the pure copolymer had a lamellar morphology) in 50% 250,000 molecular weight homopolystyrene exhibited the morphology of "elongated, tangled strands" (i.e., cylinders) of polybutadiene. Since the polybutadiene content was about 20%, Bradford expected to observe polybutadiene spheres. However, his published micrograph shows that a macrophase separation of the homopolystyrene had taken place. Therefore, the actual polybutadiene content in the microdomain phase was actually higher than 20% (somewhere between 20 and 40%), in which case the volume fraction rule of Molau is still valid within the microphase separated phase. Evidently, some homopolystyrene must have been solubilized by the polystyrene block of the copolymer

since the pure copolymer exhibited lamellar domains. A SBS triblock of molecular weight 44,000/78,000/44,000 containing 47% polybutadiene and having lamellar domain structure was also blended with a 250,000 molecular weight homopolystyrene. Even for the case of 99% added homopolymer, spherical polybutadiene particles were not observed. Instead, polybutadiene "ribbons" were seen. These structures appear to be similar to the vesicles observed by Molau [117] except that they have a multilayer structure, similar to that of an onion, with a spacing similar to that seen in the original lamellar structure of the pure copolymer. This indicates that very little homopolymer had been solubilized in the microdomain structure; rather, it formed its own macrophase. This type of structure was also seen in the case of 99% added 52,000 molecular weight homopolystyrene. However, the spacing between the polybutadiene layers increased, indicating that a larger amount (but still small) of 52,000 homopolymer was solubilized in the microdomain structure. This follows the general rule put forth by Inoue [118].

This onion-type structure has also been observed by Gebizlioglu et al. [120] and Argon et al. [121] in blends of K-Resins (poly(styrene-butadiene) star copolymers) containing 23% polybutadiene and high molecular weight polystyrenes.

The first attempt at quantifying the effect of homopolymer molecular weight on the amount of homopolymer which can be incorporated into the block copolymer microdomain structure was made by Meier [122] in 1977, extending his earlier work on the theory of block copolymers



[75-78]. The block copolymer was assumed to be an A-B diblock copolymer having equal molecular weight blocks. The volume of solubilized A homopolymer relative to the volume of the A blocks ( $V_{HA}/V_A$ ) was shown to decrease rapidly with the molecular weight of the homopolymer, in agreement with the earlier experimental results; however, the predicted amount of homopolymer that could be solubilized was quite a bit smaller than observed experimentally. For example, for  $M_H/M_A = 1$ , ( $V_H/V_A$ ) is predicted to be about 0.05 while experiments suggested that ( $V_H/V_A$ ) was about 1. Meier attributed this discrepancy to a non-equilibrium domain structure being "frozen in" during the evaporation of the solvent cast films.

A more quantitative experimental study of homopolymer solubilization was later performed by Hashimoto et al. [123] in 1981. These authors studied, by means of electron microscopy and SAXS, the change in microdomain structure of toluene cast films of poly(styrene-isoprene) diblock copolymer with the addition of homopolystyrene. The original copolymer contained 22% polyisoprene and exhibited the morphology of polyisoprene spheres in a polystyrene matrix. The molecular weights of the polystyrene and polyisoprene blocks were 250,000 and 71,000 respectively, and the homopolystyrene molecular weight was 81,000, i.e., about one third that of the corresponding block in the copolymer. The samples were cast at 30 °C over a period of one week; however no annealing was performed. Blends containing 0, 30, 60, and 90% homopolymer were prepared, all of which had the morphology of polyisoprene spheres. SAXS results showed that all of the samples,



except for the 90% homopolymer sample, exhibited a main interference peak accompanied by a broad shoulder (the sample containing 90% homopolymer gave a SAXS pattern which decreased monotonically with angle) indicating a large degree of disorder in the paracrystalline packing of the polyisoprene spheres; the electron micrographs confirm this. Undoubtedly, this lack of long range order is due to non-equilibrium effects due to the large molecular weights and the lack of an annealing treatment. Indeed, the sizes of the spherical domains were found to be almost half that predicted by theory.

In addition, it was found that as the concentration of homopolymer increased, the average sphere radius, obtained from the location of the sphere scattering peaks at higher angles, decreased slightly. This means that the number of copolymer molecules per domain was decreasing; it was not known whether this was an equilibrium effect or an artefact of the sample casting. Also, the average intersphere distance, obtained from the location of the main interference peak, was seen to increase with homopolymer concentration as expected. However, the rate of increase was not nearly as rapid as predicted assuming complete solubilization of the homopolymer into the domain structure. Therefore, incomplete solubilization was suspected; however, macrophase separation of the homopolystyrene was not reported to be observed by microscopy. It was also found that the domain boundary thickness did not change with the addition of homopolymer.

Bates et al. [95] have studied the structure of poly(styrene-butadiene) diblock copolymer/homopolystyrene blends exhibiting spherical

polybutadiene domains by SANS. Samples were slowly cast from dilute solutions in a mixture of 30% methyl ethyl ketone and 70% tetrahydrofuran at 80 °C followed by annealing at 120 °C for 24 hours. Several different diblocks, having polybutadiene minority component, and homopolystyrenes were employed. Only the lowest molecular weight copolymer (80,000 polystyrene block and 12,000 polybutadiene block) exhibited lattice-like packing of the spherical domains (see section 3.1.3). All of the other diblock and diblock/homopolymer blends exhibited a lack of long range order. Indeed, the SANS curves of some of these samples have been effectively modeled by Kinning and Thomas [124] using the Percus-Yevick hard sphere fluid model. Since the weight fractions of homopolystyrene in these blends was generally around 50%, it is expected that the spherical domains should exhibit long range order under equilibrium conditions. However, the fact that sphere radii were found to be proportional to the .37 power of the polybutadiene molecular weight indicates that the method of sample preparation, combined with the high molecular weights of the polystyrene blocks and homopolymers, caused a non-equilibrium structure to be developed. Nevertheless, the authors attributed the lack of long range order in the blends to the presence of the homopolymer. In addition, the interfacial thickness was found to be essentially independent of molecular weight and homopolymer content, in agreement with the results of Hashimoto et al. [123].

In the hopes of avoiding non-equilibrium effects, Roe and Zin have used low molecular weight samples to study the phase equilibria in

mixtures of poly(styrene-butadiene) diblock copolymer in homopolystyrene or homopolybutadiene. Both SAXS [125] and light scattering [126] methods have been employed. The most extensively studied system is that of a SB diblock containing 27 wt% polystyrene with total copolymer molecular weight of 28,000 in 2,400 molecular weight homopolystyrene, although 3,500 molecular weight homopolystyrene and 26,000 molecular weight homopolybutadiene were also used.

SAXS curves at low temperatures exhibited two interference peaks indicating the presence of an ordered microdomain structure; however, as the temperature was increased, the secondary peak disappeared completely and the main peak became very weak and broad. The authors concluded that, similar to the case of pure block copolymers that they studied [30], there was a gradual transition, over a temperature range of 50–200 °C, from the ordered microdomain structure to a disordered homogeneous structure, and that the transition proceeds through an intermediate structure in which the styrene and butadiene blocks gradually dissolve into the microdomains of the opposite block; this occurs without the domain boundary becoming more diffuse. The temperature at which this transition occurred was seen to increase from about 130 °C for the pure copolymer to about 160 °C with the addition of 30 wt% added 2,400 homopolystyrene. The value of the scattering vector of the main interference peak,  $s_{\max}$ , for the low temperature structure was seen to decrease with the weight fraction of added homopolystyrene up to a homopolymer weight fraction of about 0.4. Addition of further homopolymer had no effect on  $s_{\max}$  indicating that the homopolymer was at



first soluble in the microdomain structure, but eventually the solubility limit was reached (0.4 wt. fraction homopolymer), after which the excess homopolymer macrophase separated. In addition, it was found that the ratio of the angle of the second interference peak to that of the main interference peak varied continuously from about 1.3 for the pure copolymer to 1.8 for the blend containing 0.4 weight fraction added homopolymer. The authors attributed this to a gradual transition from spherical, to cylindrical, to lamellar polystyrene domain structure (the expected ratios for these structures are 1.41, 1.73, 2.00). The failure to attain the precise crystallographic ratios was taken to be indicative of a lack of long range order or possibly the simultaneous existence of different domain morphologies. However, no electron microscopy was performed to validate these claims.

The phase diagrams of these blends were also investigated by light scattering. Cloud point measurements indicated that the solubility of the homopolymers in the corresponding microdomains ( $V_{HA}/V_A$ ) increased from about 0.3 to 0.75 as the ratio of homopolymer to block molecular weight  $M_{HA}/M_A$  decreased from 1.2 to 0.32. The results suggested that the homopolymer would be soluble in the block copolymer at all concentrations for  $M_{HA}/M_A$  below about 0.3. Thus, the solubility limits found in this study were about an order of magnitude larger than predicted by the theory of Meier [122]. Recent theories by Hong and Noolandi [81] and Whitmore and Noolandi [127] of phase equilibria in block copolymer/homopolymer blends indicate that the amount of homopolymer which can be solubilized can be quite large depending on the



molecular weight of the homopolymer as well as the product  $\chi N$  and the composition of the copolymer. For example, for a poly(styrene-butadiene) diblock having block molecular weights of 7,300 and 3,800 respectively, about 40% 3,800 molecular weight polybutadiene is predicted to be solubilized in the microdomain structure at temperatures less than 160 °C.

From their cloud point curves and SAXS results, Roe and Zin have constructed phase diagrams with temperature and composition as the independent variables. Figure 3.6, taken from their work [126], shows the results for the case of 2,400 molecular weight homopolystyrene. The phase diagram was drawn so as to satisfy the rules of thermodynamics for first order phase transitions, namely: (1) any region containing  $p$  phases must be bounded by regions containing  $p \pm 1$  phases and (2) boundaries of one-phase regions must meet with curvatures such that the boundaries extrapolate into the adjacent two-phase regions. Observed cloud points are marked with circles while the temperatures of transition from an ordered microdomain structure to a homogeneous melt, determined by SAXS, are shown as squares. The different mesophases of the phase diagram are defined as:  $M_1$  is an ordered mesophase structure in which the microdomains are swollen with dissolved homopolymer,  $M_2$  is a micellar phase in which aggregates of block copolymer are suspended in homopolymer with no long range order, and  $L_1$  and  $L_2$  are liquid phases in which the block copolymer is molecularly dispersed. Qualitatively similar phase diagrams have been predicted by Whitmore and Noolandi [127]. The boundaries between the different regions in the lower right



corner of the phase diagram, which have been drawn as dotted lines, are more speculative than the rest. This is the region of the phase diagram which will be addressed in this dissertation.

### 3.3.1 Micelles in block copolymer/homopolymer blends

#### 3.3.1.1 Experimental studies

The first reported work on the quantitative study of the structure of block copolymer micelles in homopolymer solution was performed by Selb et al. [128] in 1983. These authors performed SANS on dilute solutions of poly(styrene-butadiene) diblock copolymers, having deuterated polystyrene blocks, in low molecular weight (1,600 to 6,500) polybutadiene homopolymers. The SANS patterns at low concentrations ( $\leq 5\%$  diblock) exhibited two to three smeared maxima which were attributed to form factor scattering from the polystyrene cores of spherical micelles. The scattering curves were well modeled using a log normal distribution of sphere sizes having a standard deviation ranging from 11 to 16% of the average radius (i.e.,  $S(h)$  was set equal to unity). Evidently, the contribution of interparticle interference to the scattering was small for these concentrations. The structure proposed was that of spherical micelles in which the core was made up of the d-polystyrene blocks surrounded by a shell of polybutadiene blocks, highly swollen with homopolybutadiene, in a matrix of homopolybutadiene. For 10% of a diblock having 23,000 and 46,000 molecular weight



polystyrene and polybutadiene blocks respectively in 1,600 molecular weight polybutadiene homopolymer, an interparticle interference maximum, accompanied by a secondary shoulder was observed. This was attributed to increased interparticle interference with concentration, although the authors made no attempt to model this low angle region of the scattering curve. The influence of different parameters on the average core radius  $R$  was examined and the following observations were made: (1)  $R$  increased with the molecular weight of the polystyrene block, as expected, (2) for copolymers with the the same molecular weight polystyrene blocks,  $R$  decreased with increasing molecular weight of the polybutadiene block, which was attributed to an increase in copolymer "solubility" within the matrix, (3) for a given copolymer,  $R$  increased with increasing molecular weight of the polybutadiene matrix, which was attributed to an increasing incompatibility between the PB matrix and PS chains, and (4)  $R$  decreased with copolymer concentration.

Rigby and Roe [129] have also studied micelle formation in blends of poly(styrene-butadiene) diblock copolymer and polybutadiene homopolymer. These authors used the SAXS technique to investigate the effect of temperature and copolymer concentration on micelle structure of a 25,000 molecular weight copolymer containing 52 wt% polystyrene in 2,350 molecular weight homopolybutadiene. Copolymer concentrations as high as 8% were studied. The scattering patterns presented in this paper exhibited monotonically decreasing intensity with angle. Neither low angle interference peaks or higher angle single particle scattering maxima were observed. The micelles were assumed to consist of a



polystyrene core surrounded by a shell containing the polybutadiene block. No electron microscopy could be performed since the low molecular weight polybutadiene was a viscous liquid at room temperature. The radius of gyration  $R_z$  of the micelle cores, determined from a Guinier analysis, showed that for temperatures below about 70 °C,  $R_z$  increased slightly with copolymer concentration, although the increase was barely beyond the experimental error. At all concentrations,  $R_z$  decreased slightly with temperature for temperatures between 30 and 60 °C, but then increased rapidly at higher temperatures. This was attributed to swelling of the micelle core with homopolymer and the eventual dissolution of the micelles. The onset of the swelling occurred at higher temperatures as the copolymer concentration increased.

The critical micelle concentrations, which were obtained from a plot of scattered intensity at zero angle (found from extrapolating the Guinier plots to zero angle) versus temperature, were found to be about 0.25% for temperatures between 30 and 60 °C, but then increased rapidly to about 1.75% at 100 °C. The SAXS invariant for all concentrations was seen to decrease steadily with temperature indicating that mixing of the components was occurring. From mass balance arguments, taking the cmc into account, it was calculated that the volume fraction of homopolymer in the core increased steadily from almost zero at 30 °C to about 0.8 at 90 °C. Concomitantly, the number of copolymer molecules per micelle decreased from about 200 to 70.

A very recent study by these same authors [130] examined the effect of block lengths on micelle structure. Three different block

copolymers all having about 25,000 molecular weight, but containing 25 wt% (25/75), 50 wt% (50/50), or 75 wt% (75/25) polystyrene were used. The homo-polymer was the same as used in the previous study. It was found at room temperature that the critical micelle concentrations were 7.8%, 0.26%, and 0.10% for the block copolymers having 25, 50, and 75 wt% polystyrene respectively. This was attributed to an increasing solubility of the copolymer in the polybutadiene homopolymer with decreasing polystyrene content. The composition ranges studied were 7.5 to 22 wt% 25/75 copolymer, 0.5 to 8 wt% 50/50 copolymer, and 0.5 to 3 wt% 75/25 copolymer. The only mixtures which exhibited an interparticle interference maximum in the SAXS patterns were those containing 6 and 8 wt% of the 50/50 copolymer. However, even for the 8% sample, this interference peak was extremely broad. In addition, there was a lack of any well defined maxima resulting from single particle scattering. Spherical micelles were assumed for all mixtures, although no electron microscopy was performed to confirm this. Nevertheless, the SAXS curves were fit with a model of polydisperse spherical micelles interacting with each other according to the Percus-Yevick hard sphere fluid approximation. This is the same model used previously by Kinning and Thomas [124] to fit the SANS pattern presented by Bates et al. [95] for a blend of a poly(styrene-butadiene) diblock and homopolystyrene exhibiting a disordered arrangement of spherical domains. The following quantities were evaluated by Rigby and Roe as a function of temperature and copolymer concentration: (1) average core radius, (2) polydispersity of core radius, (3) critical micelle concentration, (4) degree of



swelling of the core with homopolymer, (5) number density of micelles, and (6) the apparent hard sphere radius of interaction.

The effect of temperature on the radius of gyration of the core was qualitatively similar, for all three copolymers, to the results of their previous study [129], except that the temperature at which the radius of gyration abruptly increased was seen to decrease with increasing polybutadiene content in the copolymer, as expected from solubility arguments. It was also seen that the radius of the core increased with the molecular weight of the polystyrene block, and the cmc increased with temperature, as expected. A similar analysis as in the first paper revealed that the calculated volume fraction of homopolymer in the micelle core increased steadily with temperature for all three copolymers. However, the temperature at which this swelling was first observed to occur increased markedly with increasing polystyrene content in the copolymer; again this was attributed to an increasing incompatibility of copolymer and homopolymer.

It must be remarked that since the interparticle interference peaks were either very diffuse or, for the most part, nonexistent, the values of the effective hard sphere radii of interaction determined from the modeling will have a very large uncertainty associated with them, since large changes in the hard sphere radius result in relatively small changes in the predicted SAXS patterns. Nevertheless, the ratios of the hard sphere radii to the average core radii were found to be 2.0, 1.7, and 1.4, independent of concentration, for the samples 25/75, 50/50, and 75/25 respectively. These ratios follow the expected trend predicted

from the relative block lengths. The polydispersity in core size, which is required to rid the simulated SAXS patterns of sphere form factor peaks, as measured by the ratio of the weight average to number average core volume, was found to be 2.8, 1.4, and 1.3 for the 75/25, 50/50, and 25/75 copolymers respectively. No explanation for the very broad distribution of the 75/25 sample was given.

### 3.3.1.2 Theoretical studies

A theory of micelle formation in block copolymer/homopolymer blends was presented first by Leibler, Orland, and Wheeler in 1983 (hereafter referred to as the LOW theory) [112] which was later extended by Whitmore and Noolandi in 1985 [131]. Since these theories are very similar, and are expected to yield similar results, only the LOW theory will be reviewed here.

The LOW theory considers a liquid mixture of A homopolymer with polymerization index  $N_h$  and an A-B diblock containing  $N_B$  monomers of type B and  $N_A$  monomers of type A. For simplicity, only the case where  $N_A = N_B = N/2$  is explicitly considered. It is also assumed that the A homopolymer chains are shorter than the A block of the copolymer, i.e., the parameter  $\alpha = N/N_h$  is greater than 2.

Spherical micelles of radius  $R$  and containing  $p$  copolymer chains are assumed to be made up of two uniform regions: a core of radius  $R_B$  containing only B monomers, and the outer shell or corona of thickness  $R_A = R - R_B$  containing only A monomers. Only a fraction  $\eta$  of



A monomers in the corona belong to copolymer chains, the rest,  $(1-\eta)$ , belong to homopolymer chains.

The free energy of a single micelle,  $F$ , is given by the sum of three contributions.

$$F = F_i + F_d + F_m \quad (3.3)$$

The first term is the interfacial energy

$$F_i = 4\pi R_B^2 \gamma \quad (3.4)$$

where  $\gamma$  is the interfacial tension. Assuming a narrow interfacial thickness, Helfand and Sapse [132] give the following relationship

$$\gamma = \frac{(kT)}{a^2} \frac{(x)}{6}^{1/2} \quad (3.5)$$

where  $a$  is the monomer length and  $x$  is the A-B monomer interaction parameter. This also assumes that the interface width is independent of molecular weight and that both the A and B monomers have the same length  $a$ . The second term is due to loss of entropy, or the so called elastic energy, arising from the deformation of copolymer chains

$$F_d = 3/2 kT p \left[ \frac{R_B^2}{(N/2)a^2} + \frac{(N/2)a^2}{R_B^2} + \frac{R_A^2}{(N/2)a^2} + \frac{(N/2)a^2}{R_A^2} - 4 \right] \quad (3.6)$$

In writing Equation 3.6, it is assumed that in the micelle, the A and B blocks of the copolymer have the average end to end distance of the order  $R_A$  and  $R_B$  and are deformed with respect to their unperturbed dimensions  $(N/2)^{1/2}a$ . Again,  $a$  is taken to be identical for both the A and B monomers. The last contribution,  $F_m$ , is the entropy of mixing of homopolymer chains and A copolymer blocks inside the micelle corona

$$F_m = 4/3\pi \frac{(R^3 - R_B^3)}{a^3} kT \frac{1-\eta}{N_h} \ln(1-\eta) \quad (3.7)$$

The entropic effect of localizing the A-B junctions at the interface has been neglected since its contribution to  $F$  is found to be small.

Assuming incompressibility also allows one to write

$$\begin{aligned} 4/3\pi R_B^3 &= p(N/2)a^3 \\ 4/3\pi(R^3 - R_B^3)\eta &= p(N/2)a^3 \end{aligned} \quad (3.8)$$

which allows Equation 3.3 to be recast in terms of  $p$  and  $\eta$  as the independent variables.

The model allows for a fraction of the copolymer chains to remain free in a homogeneous mixture with the homopolymer chains. The fraction of copolymer chains which aggregate into micelles is  $\zeta$ , and the overall concentration of copolymer monomers is  $\phi$ . The total free energy of the micellar phase is then given by

$$F_M = (\Omega\phi\zeta/pN)F + F_{\text{mix}} - TS_m \quad (3.9)$$

where  $\Omega$  is the total number of A and B monomers in the system, and  $F$  is given by Equation 3.3. The  $F_{\text{mix}}$  term is due to the free energy of mixing of homopolymer and copolymer outside the micelle and is given by the Flory-Huggins mean field model

$$F_{\text{mix}}/kT = \Omega(1-\xi\phi\zeta)\{(\phi_1/N \ln\phi_1) + (1-\phi_1)/(N/2)\ln(1-\phi_1) + 1/2 \times \phi_1(1-\phi_1/2)\} \quad (3.10)$$

where  $\xi = (1 + \eta)/(2\eta)$ , and  $\phi_1 = \phi(1 - \zeta)/(1 - \xi\phi\zeta)$  is the concentration of copolymer monomers outside the micelles. The last term in Equation 3.9 is due to the translational entropy of the gas of micelles

$$S_m/k = -\Omega\{\phi\zeta/pN \ln(\xi\phi\zeta) + (1 - \xi\phi\zeta)/\xi pN \ln(1 - \xi\phi\zeta)\} \quad (3.11)$$

The equilibrium values of  $p$ ,  $\eta$ , and  $\zeta$  are found by minimizing  $F_M$  with respect to these quantities for a fixed  $\phi$ . It is predicted that the critical micelle concentration increases with decreasing homopolymer or

copolymer molecular weight. It is also predicted that the micelle core radius increases with increasing molecular weight of the copolymer or homopolymer. In addition, the concentration of homopolymer in the micelle corona is predicted to increase as the ratio of homopolymer to copolymer molecular weight decreases.

Recently, Roe [133] has extended this theory to take into account the possibility that the homopolymer may penetrate into the micelle core, and to allow explicitly for the case of unsymmetric block copolymers. In addition, the free energy equations have been recast in terms of the molecular volumes,  $v$ , and the root mean square end to end distances,  $r$ , of the individual homopolymer and copolymer blocks, through the relations (assuming Gaussian chains)

$$r^2 = Na^2 \quad (3.12)$$

$$v = Na^3$$

thereby avoiding the concept of segment size,  $a$ , and the number of segments,  $N$ , per copolymer molecule. End to end distances can be written as  $r = (\text{constant})M^{1/2}$  with the constant available in the literature for both polystyrene and polybutadiene. In addition, the molecular volume follows directly from the specific volume and molecular weight of the polymer.

Roe has also replaced the interaction parameter  $\chi$  with  $\Delta$ , the interaction energy density, which is related to  $\chi$  by

$$\chi = \Delta V_{\text{ref}}/kT \quad (3.13)$$

where the reference volume  $V_{\text{ref}}$  is usually taken to be the volume of a solvent molecule (if there is solvent present) or some average of the



volumes of repeat units in the polymers. Since this definition may be somewhat ambiguous, Roe prefers to use  $\Delta$  instead of  $\chi$ . Roe and Zin [134] had previously determined  $\Delta$  for polystyrene-polybutadiene from cloud point measurements of several blends of polystyrene homopolymer and polybutadiene homopolymer or poly(styrene-butadiene) block copolymers. Cloud point curves were fit to the following form of  $\Delta$  as a function of composition and temperature

$$\Delta = \lambda_0 + \lambda_1 \phi_1 + \lambda_T T \quad (3.14)$$

where  $\lambda_0$ ,  $\lambda_1$ , and  $\lambda_T$  are the fitted constants,  $\phi_1$  is the volume fraction of component 1, and  $T$  is the temperature in  $^{\circ}\text{C}$ . The compositional dependence of  $\Delta$  was generally found to be small with both positive and negative values of  $\lambda_1$  being found. On the other hand, the temperature dependence was very consistent with values of  $\lambda_T$  being between  $-0.00088$  and  $-0.0026$ . Neglecting any compositional dependence, the average functional form of  $\Delta$  was found to be

$$\Delta(\text{cal/cm}^3) = 0.718 \pm 0.051 - (0.0021 \pm 0.00045)(T-150 \text{ } ^{\circ}\text{C}) \quad (3.15)$$

Roe [133] has compared the results of the LOW theory, modified as discussed above, to the data of Rigby and Roe [130]. While "semi-quantitative" agreement was found, several experimental observations were not predicted by the theory. For example, the predicted micelle core radii changed little with temperature compared to the sudden increase observed experimentally just below the dissolution temperature. This was attributed to the fact that the theory was developed for the case of high incompatibility between the A and B segments, and this assumption may break down near the dissolution temperature. In



addition, although the observed trend of increasing cmc with polystyrene content in the copolymer was also predicted correctly, the theory predicts cmc values which are at least an order of magnitude lower than those observed experimentally. Another discrepancy is the amount of swelling of the core by the homopolymer. While theory predicts that at most 4% of the core will be homopolymer over the temperatures studied, it was found experimentally that up to 70% of the core was homopolymer just prior to dissolution. The theory predicts that the majority of phase mixing which takes place as the temperature is increased is due to an increasing amount of copolymer which does not aggregate but instead remains free in solution with the homopolymer matrix.

Leibler and Pincus [135] have extended the LOW model to calculate the interaction energy between two micelles  $U(r)$  as a function of the distance  $r$  between the centers of the micelles

$$U(r) = F(r) - 2F_0 \quad (3.16)$$

which is equal to the difference between the free energy  $F(r)$  of the complex built up of two overlapping micelles and the free energy  $2F_0$  of two nonoverlapping micelles. The essential result of this calculation is that the interaction energy between two micelles is strongly repulsive, even when the micelles are only slightly overlapping. This repulsion is found to arise mainly from the decrease in homopolymer concentration as the micelles start to overlap, which reduces the entropy of the system and is thus energetically unfavorable. The range of interaction is essentially determined by the molecular weight and degree of swelling of the micelle corona block. The degree of swelling

is predicted to increase as the homopolymer molecular weight is decreased due to an increased contribution from the entropy of mixing of block copolymer and homopolymer inside the corona region.

A useful approximation to the intermicelle potential then is that of hard spheres. As noted by Leibler and Pincus, it is well known, for systems with two-body interactions [5] that an ordered crystalline solid phase is expected to form for particle volume fractions greater than about 0.5. Therefore, one would expect the formation of an ordered macrolattice of micelles at copolymer concentrations for which the micelle volume fraction is greater than about 0.5. The type of packing in this macrolattice structure cannot be predicted by the theory however. In any case, the rheological behavior of the blends should be quite different for copolymer concentrations above and below the concentration at which this ordering takes place. A transition from viscous liquid to gel-like (solid) behavior (i.e., a large increase in relaxation time) is expected.

Whitmore and Noolandi [131] have compared the micelle core sizes determined experimentally by Selb et al. [128] to the predictions of their micelle theory, which is essentially the same as the LOW theory. In all cases, the predicted core radii were within 21% of that predicted by the theory. In addition, the scaling of the core radii with the molecular weights of the copolymer blocks and homopolymer was qualitatively predicted: the core radius increased with increasing polystyrene block molecular weight, but decreased with increasing molecular weight of the polybutadiene block or polybutadiene

homopolymer. The scaling dependence of the radii with component molecular weights can be written as

$$R \sim M_{PS}^{\alpha} M_{PB}^{\beta} M_{hPB}^{\gamma}$$

The results of Selb et al. gave  $\alpha = -.17$ ,  $\beta = .75$ , and  $\gamma = .19$ , compared to the theoretical predictions of  $\alpha = -.08$ ,  $\beta = .70$ , and  $\gamma = .06$ . It should be noted however, that the exponents derived from the data of Selb et al. were determined with only two data points; therefore, there is a large degree of uncertainty in these values.

In summary, there are several outstanding problems or controversies concerning the structure of micelles in block copolymer/homopolymer blends, many of which will be addressed in this dissertation. One of the goals is to make a critical inquiry of the scaling of both the core radius and corona thickness of spherical micelles with the homopolymer and copolymer block molecular weights. These scaling exponents, in addition to the magnitude of the core radius and corona thickness, will be compared to the predictions of the existing theories of micelle formation in block copolymer/homopolymer blends. In addition, the degree to which different types of phase mixing occur (concentration of homopolymer in the micelle core and concentration of free copolymer) will also be explored, from which the nature of the cmc phase transition will be examined. Another topic to be investigated is the transition from a disordered liquid-like to an ordered arrangement of spherical micelles with increasing copolymer concentration, particularly the type of lattice formed. The formation of non-spherical micelles is another topic which deserves attention.

The blends which will be studied in this dissertation consist of poly(styrene-butadiene) diblock copolymers in homopolystyrene matrices. This system was chosen because it is amenable to both SAXS and electron microscopy studies.



## C H A P T E R   I V

### EXPERIMENTAL METHODS

In this chapter the experimental methods employed in this dissertation will be presented. In particular, the synthesis and characterization of poly(styrene-butadiene) block copolymers and polystyrene homopolymers, the preparation of copolymer/homopolymer blends, and the electron microscopy and small angle x-ray scattering techniques used will be discussed.

#### 4.1 Sample Synthesis and Characterization

Synthesis of the poly(styrene-butadiene) diblock copolymers was performed by Dr. Lewis J. Fetters of Exxon Research and Engineering Company via the usual anionic technique employed for styrene-diene block copolymers [136-139]. Purified styrene (or butadiene) monomer, solvent (10% benzene and 90% cyclohexane), and sec-butyl lithium initiator were allowed to react completely at 30 °C under high vacuum, after which a small sample was removed from the reaction flask for later analysis. The second purified monomer was then added to the reactor and allowed to react completely, after which the reaction was terminated with the addition of degassed methanol.

The molecular weight distributions of the block copolymers and the samples removed from the reactor after polymerization of the first block (usually polystyrene) were obtained by Dr. Fetters with a Waters 150C Gel Permeation Chromatograph, which had been carefully calibrated with several polystyrene standards. In addition, the copolymer compositions were determined (by the author) by UV absorption in tetrahydrofuran at a wavelength of 260 nm. The molecular weights of the second block could then be calculated.

The characterization results are given in Table 4.1. Number average molecular weights are reported. The polydispersities, as measured by the ratio of weight to number average molecular weights, of the polystyrene blocks as well as the copolymers were all found to be less than or equal to 1.05. Although the microstructure of the polybutadiene was not determined for these samples, typical microstructures obtained from such anionic polymerizations contain approximately 90% mixed 1,4 cis and trans (40% cis and 50% trans) configurations with 10% 1,2 addition [137].

The copolymer samples can be divided into three groups: (1) those for which the polybutadiene block molecular weight was kept relatively constant at about 10,000 and the polystyrene block length was varied, (2) those for which the polystyrene block molecular weight was kept relatively constant at about 10,000 and the polybutadiene block length was varied, and (3) those for which the composition was kept relatively constant at about 50% PS and the overall molecular weight was varied.

TABLE 4.1Poly(styrene-butadiene) diblock copolymer characteristics

Sample Designation	M <sub>n</sub> PS (Kg/mole)	M <sub>n</sub> PB (Kg/mole)	wt% PS	vol% PS
SB 60/10	56.6	10.9	83.9	81.8
SB 40/10	42.0	10.3	80.3	77.9
SB 23/10	22.2	9.0	71.2	68.2
SB 10/10	12.0	10.0	54.7	51.2
SB 20/20	20.5	20.5	50.0	46.5
SB 40/40	42.3	45.0	48.2	44.7
SB 80/80	81.0	74.5	52.1	48.6
SB 10/23	10.2	23.7	30.1	26.9
SB 10/65	10.7	63.1	14.5	12.7

The molecular weights were kept relatively low in order to be able to achieve equilibrium structures more easily.

Polystyrene homopolymers of various molecular weights were obtained from Pressure Chemical Company which also supplied the characterization data shown in Table 4.2. The number average molecular weights and polydispersity indices supplied for each sample are shown in the second and third columns. Also listed in the last two columns of Table 4.2 are the values obtained by Dr. Fetters using the same GPC setup used to characterize the block copolymers. The agreement is fairly good, although differences in molecular weight of up to 18%, in the case of 7400 PS, were found.

#### 4.2 Sample Preparation

Prior to their use, the polystyrene homopolymers were heated at 160 °C under vacuum (at which temperature they foamed) for 30 minutes to ensure that any solvent or residual styrene monomer or oligomer were removed. The GPC traces of the homopolystyrenes before and after this treatment showed no differences.

Films of block copolymer/homopolymer blends for electron microscopy and SAXS investigations were prepared by solvent casting from a 3% w/v solution of the block copolymer and homopolymer in toluene, a relatively non-preferential solvent for polystyrene and polybutadiene.



TABLE 4.2

Polystyrene homopolymer characteristics

polystyrene homopoly- mer designation	$\langle M_n \rangle$	$\langle M_w \rangle / \langle M_n \rangle$	$\langle M_n \rangle$ (Fetters)	$\langle M_w \rangle / \langle M_n \rangle$
2100 PS	1,800	< 1.06	2,100	1.09
3900 PS	3,600	< 1.06	3,900	1.08
7400 PS	9,050	< 1.06	7,400	1.08
17000 PS	15,100	< 1.06	17,000	1.05
35000 PS	34,100	< 1.06	—	—
46000 PS	45,500	< 1.06	—	—

Glass casting dishes, two inches in diameter, were cleaned in a KOH solution and then treated with dimethyldichlorosilane prior to their use. This treatment lowers the surface energy of the glass, thereby allowing for easy removal of the cast films. Solutions containing the desired ratios of copolymer to homopolymer were placed in the treated casting dishes which were then placed in an oven at 35 °C under atmospheric pressure. Evaporation of the toluene required approximately one week. Due to the glassy nature of the polystyrene, a small amount of solvent remained in the film at this point. This needed to be removed prior to annealing in order to avoid foaming of the samples. After two weeks under vacuum to remove this solvent, the samples were annealed at 115 °C (i.e., about 25 °C above the glass transition temperature of the polystyrene) for one week. This sample preparation method was designed to provide, as near as possible, samples with equilibrium morphologies.

After annealing, the beakers containing the blends were quenched to room temperature in liquid nitrogen. Since the time required for the polystyrene to fall below its glass transition temperature should be about 2 seconds, based on heat transfer calculations, it was expected that the quenched films would possess a structure characteristic of 115°C, except for the small volume contraction on cooling to room temperature. At this time, the glassy films, which had a uniform thickness of about one mm, could be pulled out of the casting dish with tweezers and used for electron microscopy or SAXS studies.

### 4.3 Electron Microscopy

Thin sections, approximately 500 Å thick, for transmission electron microscopy were obtained by cryoultramicrotomy at  $-110^{\circ}\text{C}$  using a AO Reichert Ultracut microtome with an FC4 cryo attachment. A Diatome<sup>R</sup> diamond knife having a stainless steel boat was used. Sections were floated off onto n-propanol and picked up on 700 mesh copper grids. These sections were then exposed to vapors of a 2% osmium tetroxide-water solution for approximately four hours. The osmium tetroxide selectively reacts with the double bonds in the polybutadiene, thereby increasing the density of the phase containing the polybutadiene block and, hence, providing mass thickness contrast between the phases. A JEOL 100CX TEMSCAN electron microscope operated at 100 Kv, and calibrated with a 2160 lines/mm replica grating, was used to examine the sections. Bright field imaging using, in most cases, a 150 micron objective aperture was employed, and the images were recorded on Kodak SO-163 film.

### 4.4 Small Angle X-Ray Scattering

Small angle x-ray scattering was performed using a nickel filtered copper  $K_{\alpha}$  source with the generator set at 40 Kv and 30 mA. A Kratky camera equipped with a 40 micron entrance slit, 16 mm beam limiter, and 50 cm flight path was used. Scattered radiation was recorded with a Braun one-dimensional position sensitive detector operated at 10 bar

pressure of 90% argon/10% methane flow through gas and 3.8 Kv, for which the spatial resolution is approximately 50 microns.

The scattering data were corrected for sample absorption, detector wire sensitivity, and parasitic scattering as described in section 2.3. In addition, the scattering from polystyrene homopolymer was subtracted from the sample scattering to account for the scattering due to small scale electron (thermal) density fluctuations. Slit length desmearing was performed using Vonk's FFSAXS version 3 program [23]. Some smoothing of the data prior to desmearing was necessary, especially at higher angles where the number of counts was small. Absolute intensities were obtained using a calibrated Lupolen standard, which was supplied by O. Kratky. Further details concerning the UMass Kratky geometry, flight path design, alignment, and data treatment can be found in the dissertation by D. B. Alward [140].



## C H A P T E R V

### STRUCTURE OF POLY(STYRENE-BUTADIENE) DIBLOCK COPOLYMER/POLYSTYRENE HOMOPOLYMER BLENDS EXHIBITING SPHERICAL MICELLES

In this chapter, the structure of poly(styrene-butadiene) diblock copolymer/polystyrene homopolymer blends exhibiting spherical micelles will be examined by means of SAXS and electron microscopy. In all cases, the homopolystyrene molecular weight will be less than that of the polystyrene block in the copolymer. The effect of copolymer concentration will be examined in Section 5.1, using a typical case of copolymer SB 20/20 in 3900 PS homopolymer as an example. In addition, this section will outline the analysis necessary to extract the critical micelle concentration (cmc) and the structural parameters of spherical micelles (i.e., core radius, polydispersity in core radius, corona thickness, etc...) from the electron microscopy (EM) and small angle x-ray scattering (SAXS) data. In section 5.2, the effect of homopolystyrene molecular weight on the cmc, the structure of the spherical micelles, the concentration of homopolymer in the micelle core and corona regions, and the concentration of free unaggregated copolymer as a function of overall copolymer volume fraction will be examined. The effect of polystyrene (PS) and polybutadiene (PB) block lengths, as well as the overall copolymer molecular weight, on these micelle parameters will be investigated in Section 5.3. Finally, Section 5.4 examines the lattice structure of the ordered spherical micellar phase.

### 5.1 Effect of Block Copolymer Concentration

The effect of copolymer concentration on the structure of diblock copolymer/homopolymer blends predicted by the existing theories [112,131,135] is illustrated in Figure 5.1 for the case of AB copolymer in A homopolymer. At small copolymer concentrations, a homogeneous phase occurs in which the copolymer is molecularly dispersed in the homopolymer. However, as the copolymer concentration is increased beyond the critical micelle concentration (cmc), the B blocks aggregate to form micelles, in which the core contains the B blocks and the corona contains both the A blocks and A homopolymer. These micelles are dispersed in the homopolymer matrix (which contains a small amount of dissolved copolymer) with no long range ordering. Although the micelles depicted in Figure 5.1 are spherical, it will be shown in subsequent sections that, under certain conditions, other shapes are possible. As the copolymer concentration is increased further, a point is reached at which the coronae from neighboring micelles begin to overlap. At this point, the repulsion between micelles, as described by Leibler and Pincus [135], forces them to assume an ordered (cubic) packing arrangement. Increasing the copolymer concentration still further may induce a transition in micelle shape from spherical to cylindrical to lamellar depending on the composition of the copolymer. This change in structure with copolymer concentration is analogous to that proposed by Sadron [64] for the case of block copolymer/preferential solvent systems. The present case is unique in that the preferential solvent is

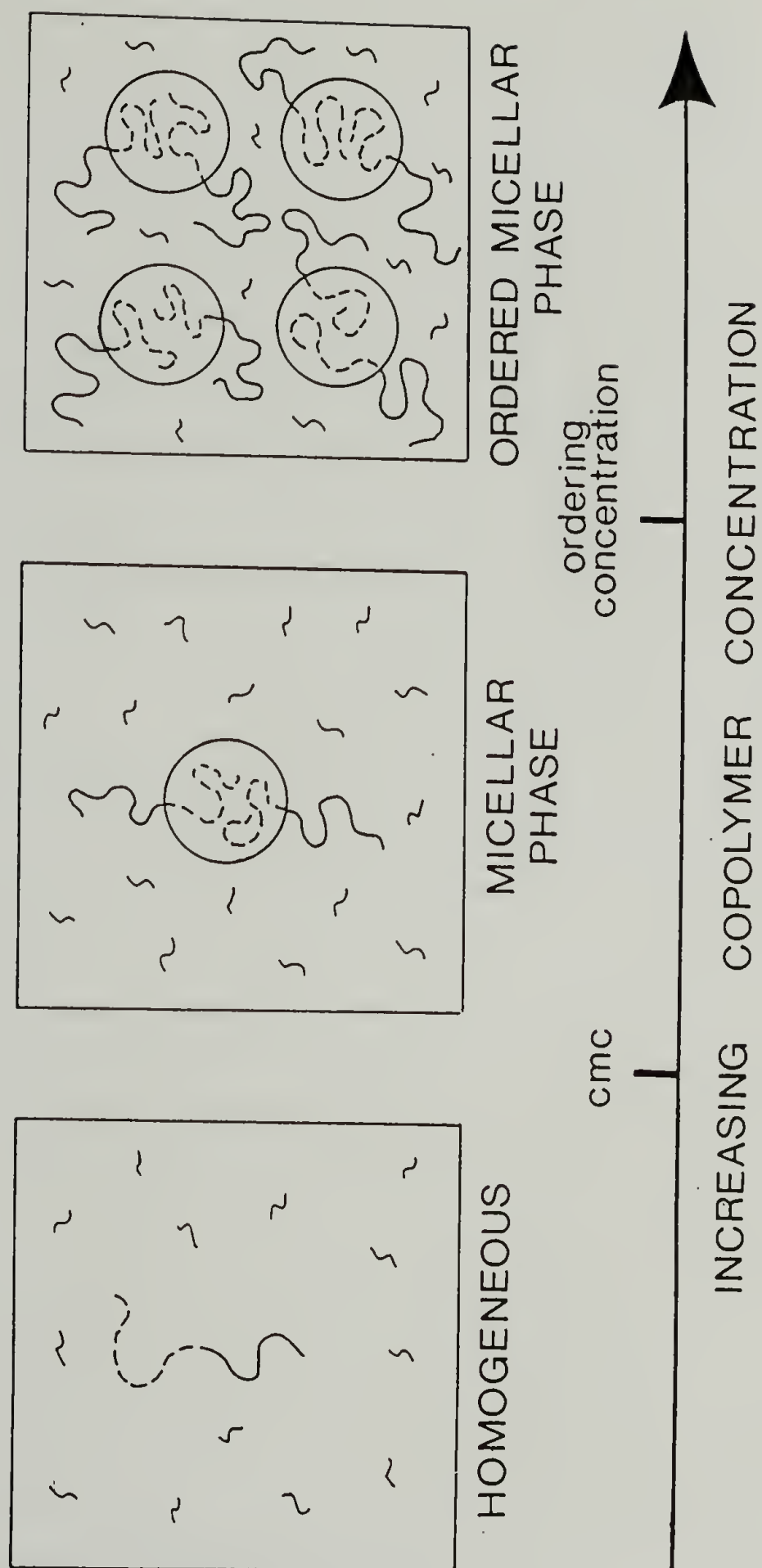


Figure 5.1 Schematic showing the effect of copolymer concentration on the structure of diblock copolymer/homopolymer blends.

chemically identical to one of the blocks of the copolymer, and is therefore a theta solvent for that block.

The structure of a spherical micelle, for the case of poly(styrene-butadiene) block copolymer/polystyrene homopolymer blends is shown in more detail in Figure 5.2. Three different regions can be identified: (1) the micelle core, of radius  $R_c$ , contains mostly PB block, although some PS homopolymer may be dissolved in the core, (2) the micelle corona region, of thickness  $L_c$ , contains PS block chains swollen with PS homopolymer, and (3) the homopolymer matrix which contains a small amount of molecularly dispersed copolymer. Also shown in Figure 5.2 is the electron density profile. Since the PS homopolymer and PS block chains have very nearly the same electron density, the difference in electron density, which will be probed during SAXS experiments, arises from the core region only. This will greatly simplify the analysis of the SAXS patterns.

#### 5.1.1 Critical micelle concentration

The critical micelle concentration can be determined by either SAXS or electron microscopy. As predicted by Equation 2.25, the scattered intensity at zero angle from a dilute suspension of spherical micelles will be directly proportional to the number of micelles per unit volume. Therefore, a plot of  $i(0)$  versus copolymer concentration can be employed to determine the concentration (cmc) at which  $i(0)$  falls to zero. Figure 5.3 shows an example of such a plot, obtained for the



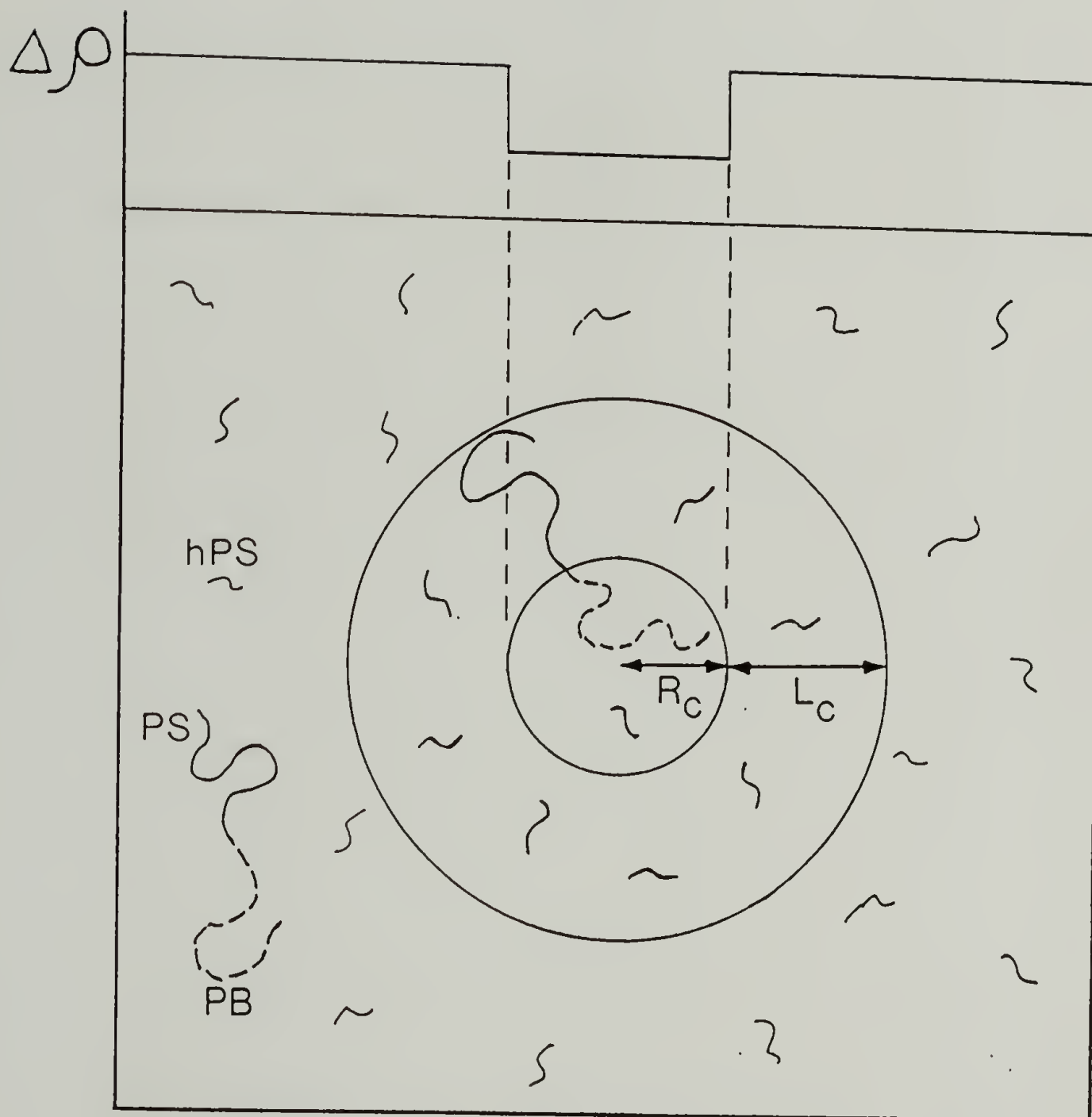


Figure 5.2 Schematic showing the structure of spherical micelles in poly(styrene-butadiene) diblock copolymer/polystyrene homopolymer blends.

copolymer SB 20/20 blended with 3900 PS homopolymer. The  $i(0)$  values were all obtained from extrapolating Guinier plots to zero angle, except for the blend containing 5.55 wt% copolymer, which exhibited an interparticle interference peak. The value of  $i(0)$  for this mixture was obtained from the single sphere scattering function used in modeling the SAXS data with the Percus-Yevick hard sphere fluid model (see Figure 5.6). A least squares fit to the data points gives a cmc of  $0.20 \pm 0.05$  wt% copolymer. It should be noted that the radii of gyration of the micelle cores, determined from the slope of the Guinier plots, for the blends containing 0.83, 1.28, and 2.66 wt% copolymer, were 123, 129, and 124 Å respectively. Since the radius of a spherical particle is related to its radius of gyration  $R_g$  by the relationship  $R = \sqrt{5/3} R_g$ , the core radii determined from the Guinier plots are thus 159, 167, and 160 Å. For a polydisperse system of spheres, a Guinier analysis gives the  $z$  average radius so that the number average core radii, which will be determined subsequently from the SAXS single particle form factor scattering at higher angles, are expected to be somewhat smaller than these values.

A more direct method of obtaining the cmc is by electron microscopy whereby a series of samples with varying copolymer concentrations are examined. Figure 5.4 shows a series of micrographs for the same SB 20/20 in 3900 PS blend examined previously by SAXS. The dark circular regions are the spherical PB micelle cores which have been stained with osmium tetroxide. It is immediately apparent that the cmc

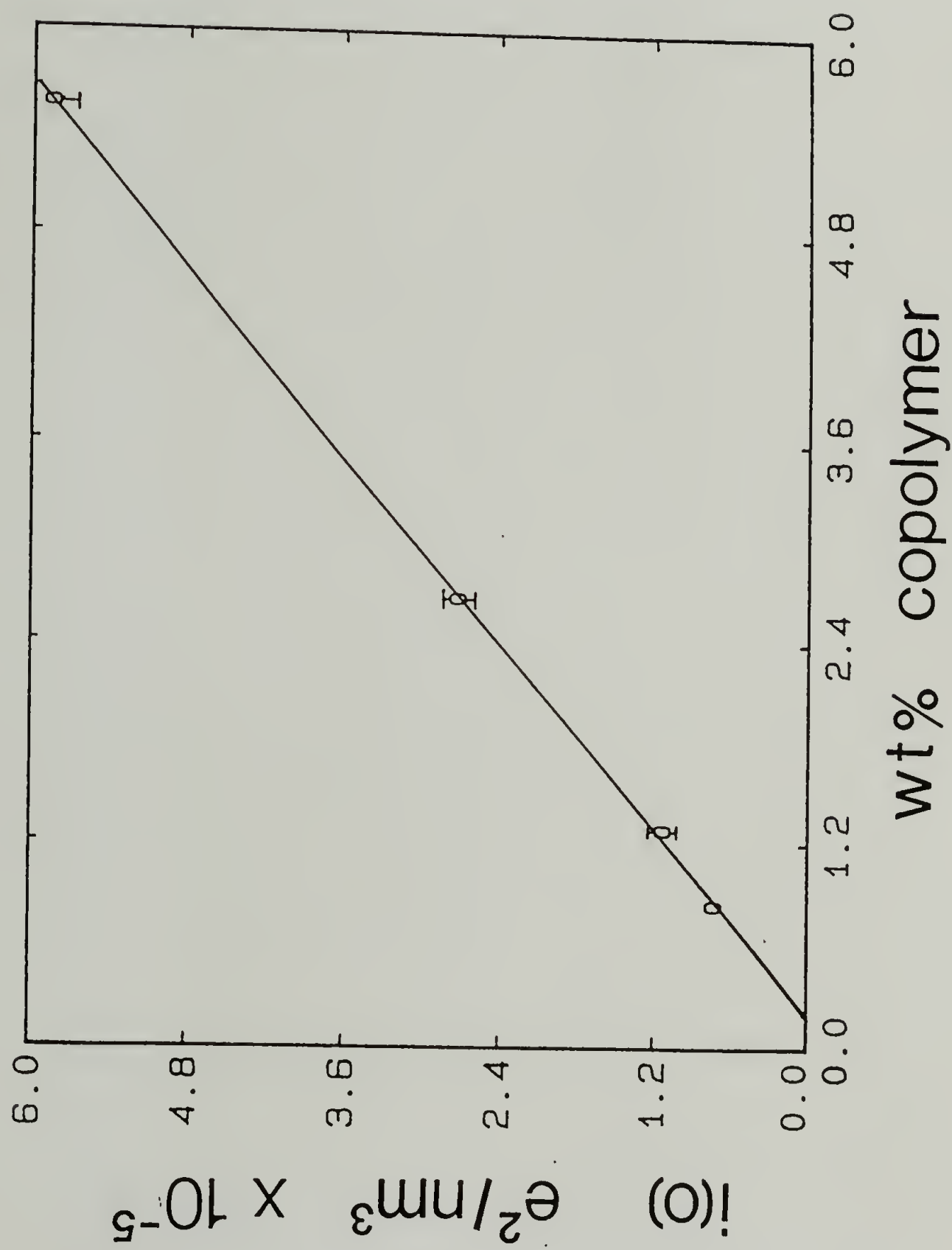


Figure 5.3 Determination of critical micelle concentration for copolymer SB 20/20 in 3900 PS homopolymer from SAXS.

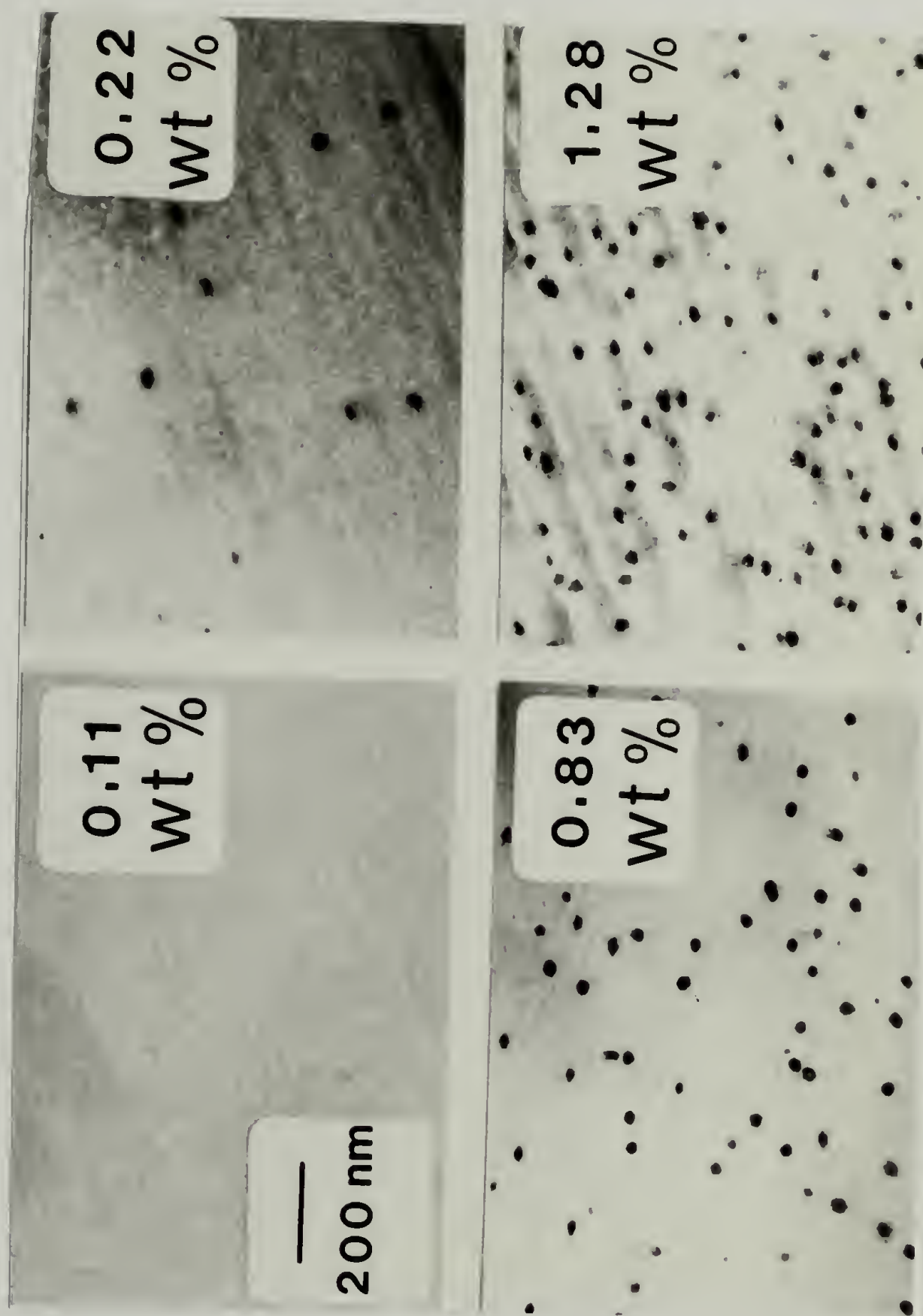


Figure 5.4 Electron micrographs of copolymer SB 20/20 in 3900 PS homopolymer. Copolymer concentrations are as indicated.



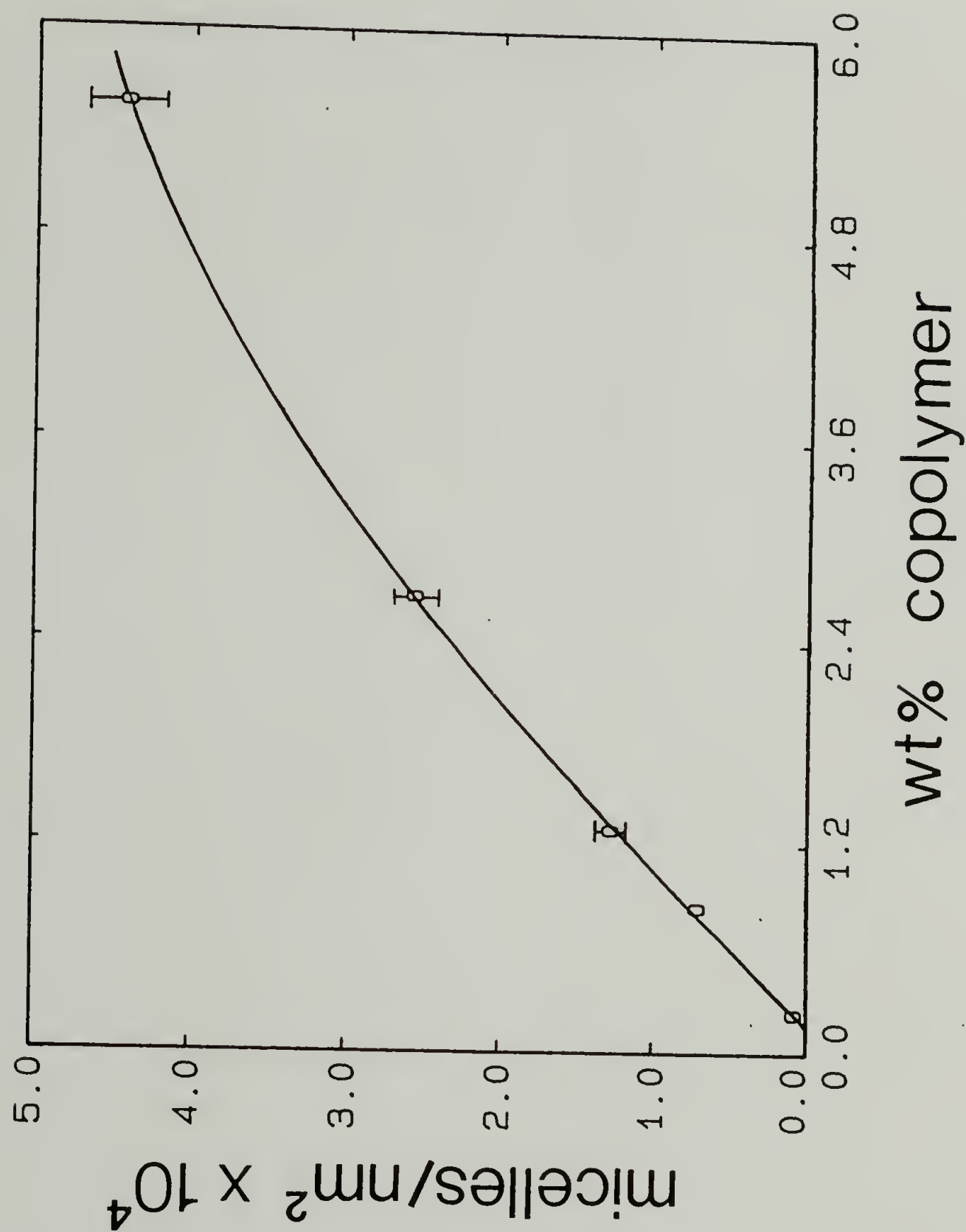


Figure 5.5 Determination of critical micelle concentration for copolymer SB 20/20 in 3900 PS homopolymer by EM.

is somewhere between 0.11 and 0.22 wt% copolymer. By constructing a plot of the number of micelles per unit area versus copolymer concentration, as shown in Figure 5.5, the cmc can be determined more accurately; a value of  $0.16 \pm 0.04$  wt% copolymer is obtained, in agreement with the SAXS result. The number of micelles per unit area was obtained by counting the number of micelle cores in an area approximately the size depicted in the micrographs of Figure 5.4. In order to obtain sufficient counting statistics, at least 50 samplings were taken. The standard deviation of the number of micelles per area obtained in this manner is indicated by the error bars in Figure 5.5. This type of analysis assumes of course that the sections are all of the same thickness.

#### 5.1.2 Blends with liquid-like packing

The micrographs in Figure 5.4 show that the spherical micelles are dispersed in the homopolymer with liquid-like packing. As the copolymer concentration is increased, and the number density of micelles increases, the contribution of interparticle interference to the scattered intensity also increases. As shown in Figure 5.6, when the concentration of SB 20/20 in 3900 PS reaches 5.55 wt%, a distinct low angle interparticle interference maximum develops in the SAXS pattern (indicated by the dots). In addition, a broad sphere scattering maximum is observed at higher angles. Also shown in Figure 5.6 is an electron

micrograph, showing the disordered arrangement of spherical micelle cores.

As discussed in Section 3.3.1.2, a hard sphere potential should be a good approximation to the actual intermicelle potential, which is expected to be steeply repulsive. Therefore, the experimental SAXS curves from these micellar systems should be modeled well using the Percus-Yevick hard sphere fluid model described in Section 2.1.2. The solid line in Figure 5.6 shows the best fit of this model to the experimental scattering data. The fitting was accomplished using a non linear least squares fitting procedure following the one presented by Bevington [141]. For the present case, the independent variables to be fit are: (1)  $R_c$ , the average core radius, which is the radius used in calculating the sphere scattering function  $P(h)$ , (2)  $\sigma_r$ , the standard deviation of the gaussian function describing the distribution in core size, (3)  $R_{hs}$ , the effective hard sphere radius used in calculating the interparticle interference function  $S(h)$ , and (4)  $K$ , a constant factor which is multiplied by the predicted scattering to scale it to the absolute scattered intensity of the sample. The hard sphere volume fraction  $\eta$  used in calculating the polydisperse interparticle interference function is obtained from

$$\eta = (R_{hs}/R_c) \phi_c \quad (5.1)$$

where  $\phi_c$  is the volume fraction of micelle cores. The weight fraction of micelle cores  $w_c$  is given by

$$w_c = (w_{\text{cop}} - w_{\text{cmc}}) w_{\text{PB}} \quad (5.2)$$

where  $w_{\text{cop}}$  is the total weight fraction of diblock copolymer in the blend,  $w_{\text{cmc}}$  is the critical micelle concentration (wt fraction copolymer), and  $w_{\text{PB}}$  is the weight fraction of polybutadiene in the copolymer. Equation 5.2 assumes that the core consists entirely of the PB block, i.e., no homopolystyrene resides in the micelle core. It also assumes that the weight fraction of free (unaggregated) copolymer equals the cmc for all copolymer concentrations greater than the cmc. As will be shown later, this restriction may not always be applicable. The volume fraction of micelle cores  $\phi_c$  can then be calculated from the weight fraction of micelle cores thus calculated and the densities of the PS and PB components. Since the SAXS experiments were carried out at 25 °C, the pure component densities used in the calculations are the densities at this temperature. The density of polybutadiene at 25 °C is given in the Polymer Handbook [142] as 0.895 g/cm<sup>3</sup>. The density of polystyrene as a function of molecular weight and temperature has been determined by Richardson and Savill [143]. For the range of molecular weights utilized in the present study (2.1 – 81 Kg/mole), the molecular weight dependence of the density was found to be very small, and will therefore be neglected. At 25 °C, the polystyrene density was found by Richardson and Savill to be 1.046 g/cm<sup>3</sup>.

For the case of 5.55 wt% SB 20/20 in 3900 PS homopolymer, the value of  $\phi_c$  thus calculated is 0.0314, and the parameters for which the best fit to the experimental scattering data was obtained are  $R_c = 132 \pm$



3 Å,  $\sigma_r = 18 \pm 2$  Å, and  $R_{hs} = 230 \pm 7$  Å. The good agreement between the experimental and modeled SAXS data is immediately apparent, indicating that, in terms of predicting  $S(h)$ , the Percus-Yevick (PY) hard sphere fluid model is a good representation of the micellar system. The effective hard sphere (i.e., micelle) volume fraction was found to be 0.17, which is much larger than the volume fraction of copolymer in the mixture. This indicates that the PS block chains in the micelle corona are highly swollen with homopolymer. By equating the effective hard sphere radius to the overall radius of the micelle, one can obtain an estimate of the thickness of the corona  $L_c$

$$L_c = R_{hs} - R_c \quad (5.3)$$

which for the present blend is  $98 \pm 15$  Å. It should be noted at this point that the core radius determined from the modeling is about 30 Å (20%) smaller than that obtained earlier for this copolymer/homopolymer blend from a Guinier analysis. This is expected since the modeling provides a number average core radius while the Guinier analysis provides a z average core radius.

Figure 5.7 shows the EM and SAXS results for 11.7 wt% SB 20/20 in 3900 PS. As expected, an increased number density of micelles is observed in the electron micrograph. In addition, the interparticle interference peak in the SAXS pattern is sharper and more intense than for the blend containing 5.55 wt% copolymer. Again, a good fit to the experimental SAXS data is obtained using the Percus-Yevick hard

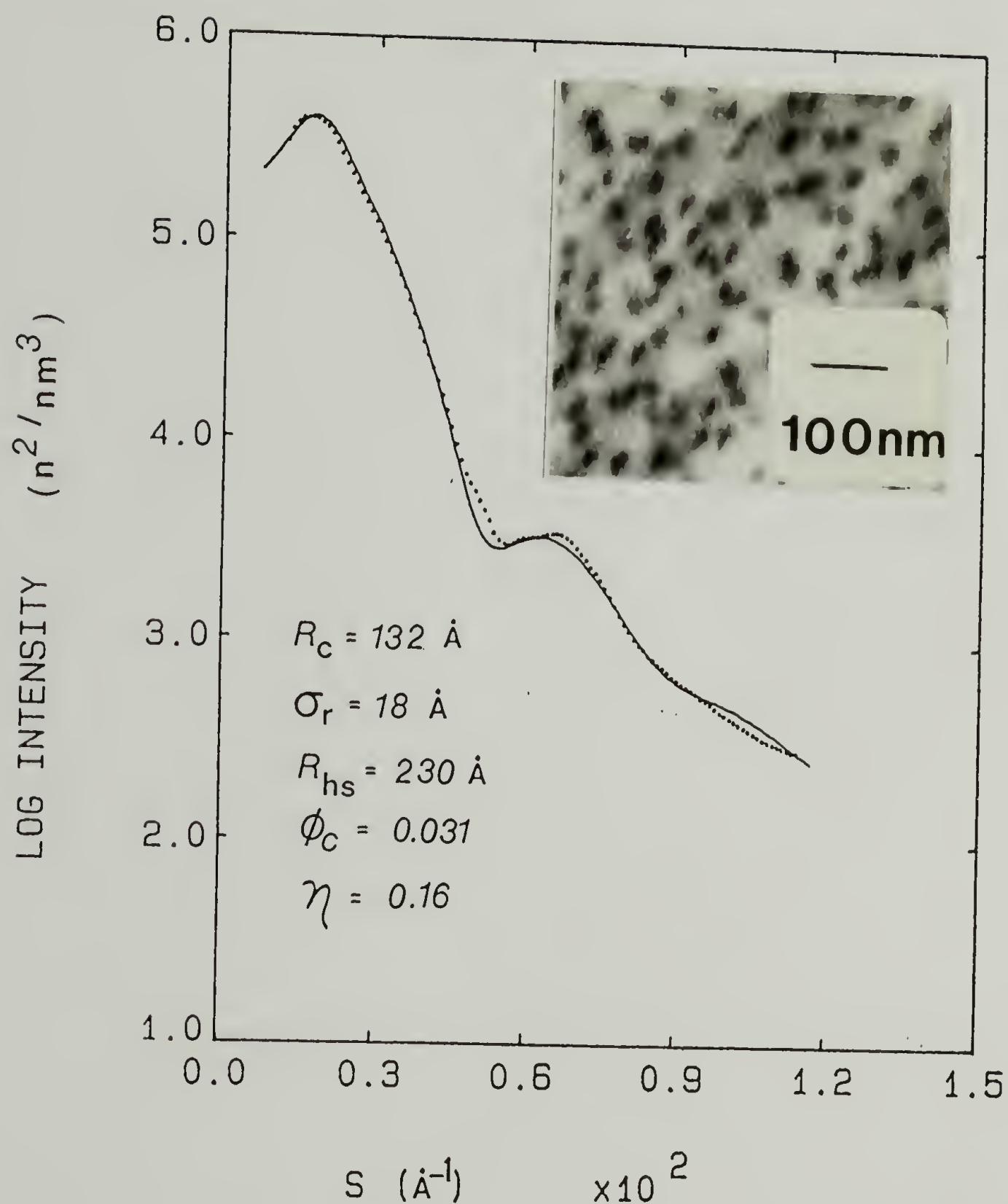


Figure 5.6 SAXS and EM results for 5.55 wt% SB 20/20 in 3900 PS homopolymer. The solid line shows the best fit to the SAXS data obtained with the PY hard sphere fluid model. The parameters of best fit are as indicated.

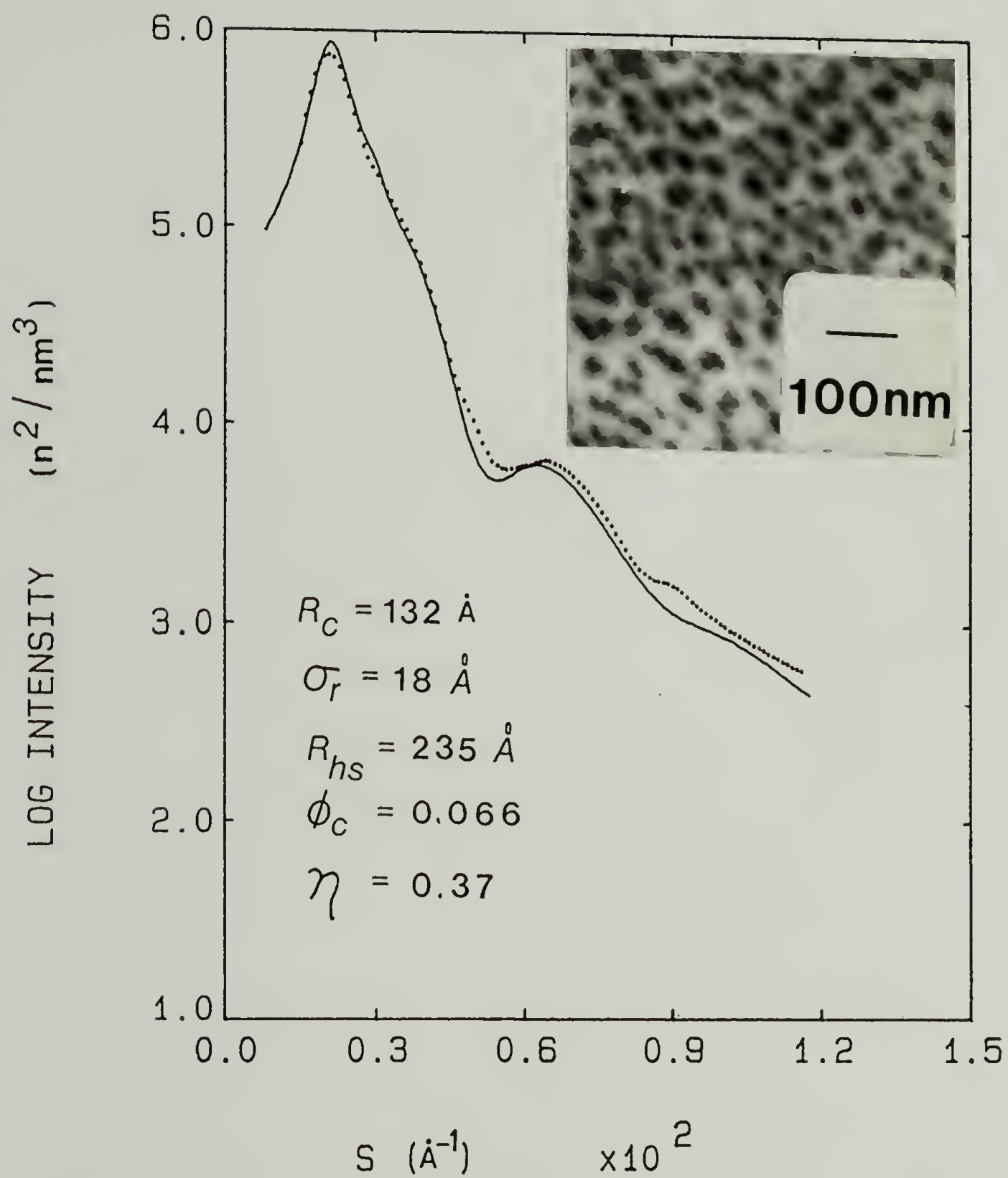


Figure 5.7 SAXS and EM results for 11.7 wt% SB 20/20 in 3900 PS.

sphere fluid model. Note that the average core radius, the standard deviation in core radius, and the effective hard sphere radius are the same as for the previous blend; however, the effective hard sphere volume fraction, i.e. the volume fraction of micelles, has increased from 0.17 to 0.38.

### 5.1.3 Transition to an ordered lattice of micelles

For a concentration of 17.9 wt% SB 20/20 in 3900 PS, the results of Figure 5.8 show that the PY hard sphere fluid model does not predict the interparticle interference region of the SAXS pattern very well. The best fit is found for  $R_c = 137 \pm 3 \text{ \AA}$ ,  $\sigma_r = 23 \pm 3 \text{ \AA}$ , and  $R_{hs} = 240 \pm 7 \text{ \AA}$ . These values are very similar to those found at lower concentrations. The corresponding micelle volume fraction is 0.55 so that one might expect that an ordered lattice of micelles should be present considering that the results of statistical mechanical modeling of hard sphere fluids [5] indicate that a solid (ordered) phase should appear for hard sphere volume fractions greater than about 0.45. The arrows in the figure mark the expected relative positions of the first four lattice peaks for a BCC or SC packing mode. It is evident that the higher order lattice peaks are not very prominent, which is borne out by the electron micrograph. Although "short rows" of aligned cores are seen, there is a lack of any significant long range order.

However, when the copolymer concentration is increased to 24.9 wt% the micelles possess a high degree of long range order as evidenced in



both the electron micrograph and SAXS pattern shown in Figure 5.9. The SAXS curve exhibits three well defined lattice peaks whose relative positions agree well with those predicted for a SC or BCC packing mode (marked by the arrows). The SAXS data at higher angles, where  $S(h)$  is nearly unity, has been fit to the scattering predicted for a polydisperse system of spherical particles (solid line), neglecting the contribution of interparticle interference to the scattered intensity.

Similar results are shown in Figure 5.10 for the case of 30.3 wt% SB 20/20 in 3900 PS. Four well defined lattice reflections are observed whose relative positions also agree well with those predicted for a SC or BCC lattice. The determination of which of these two packing modes is present for these micellar systems will be presented in Section 5.4. For the moment, suffice it to say that volume fraction calculations favor the existence of a SC lattice.

The EM and SAXS results for 49.4 wt% SB 20/20 in 3900 PS are presented in Figure 5.11. Five lattice peaks are observed in the SAXS pattern, whose relative positions match those predicted for hexagonally packed cylinders (see arrows). In addition, both axial and longitudinal projections of hexagonally packed cylinders are seen via electron microscopy (see micrograph in Figure 5.11). Therefore, a transition from spherical to cylindrical domain shape with increasing copolymer composition is observed. This is expected considering that the volume fraction of PB for this sample is 0.28. According to the general rule proposed by Molau [32] for neat block copolymers, and later by Sadron [64] for block copolymer/solvent systems, such a transition should occur

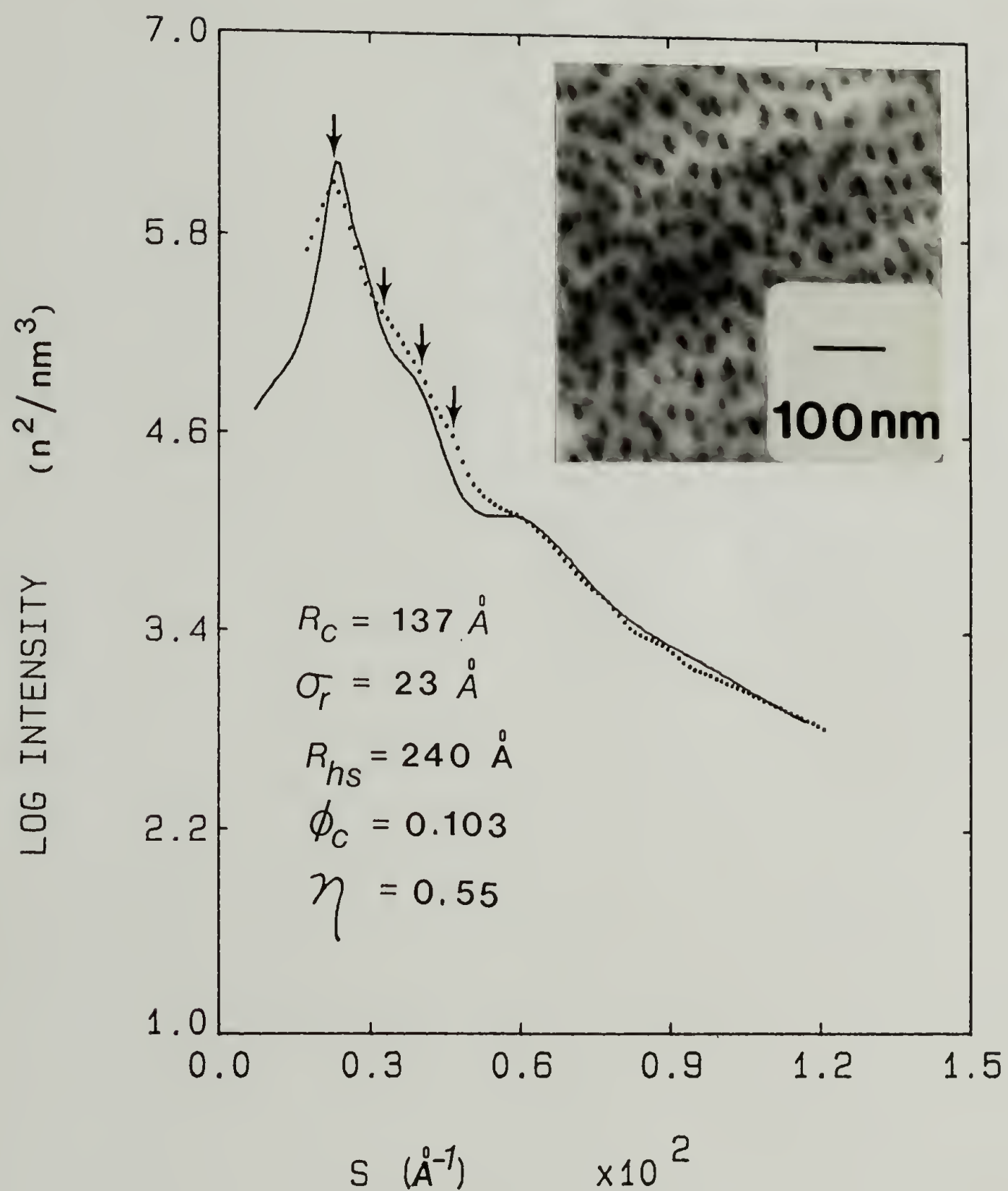


Figure 5.8 SAXS and EM results for 17.9 wt% SB 20/20 in 3900 PS.

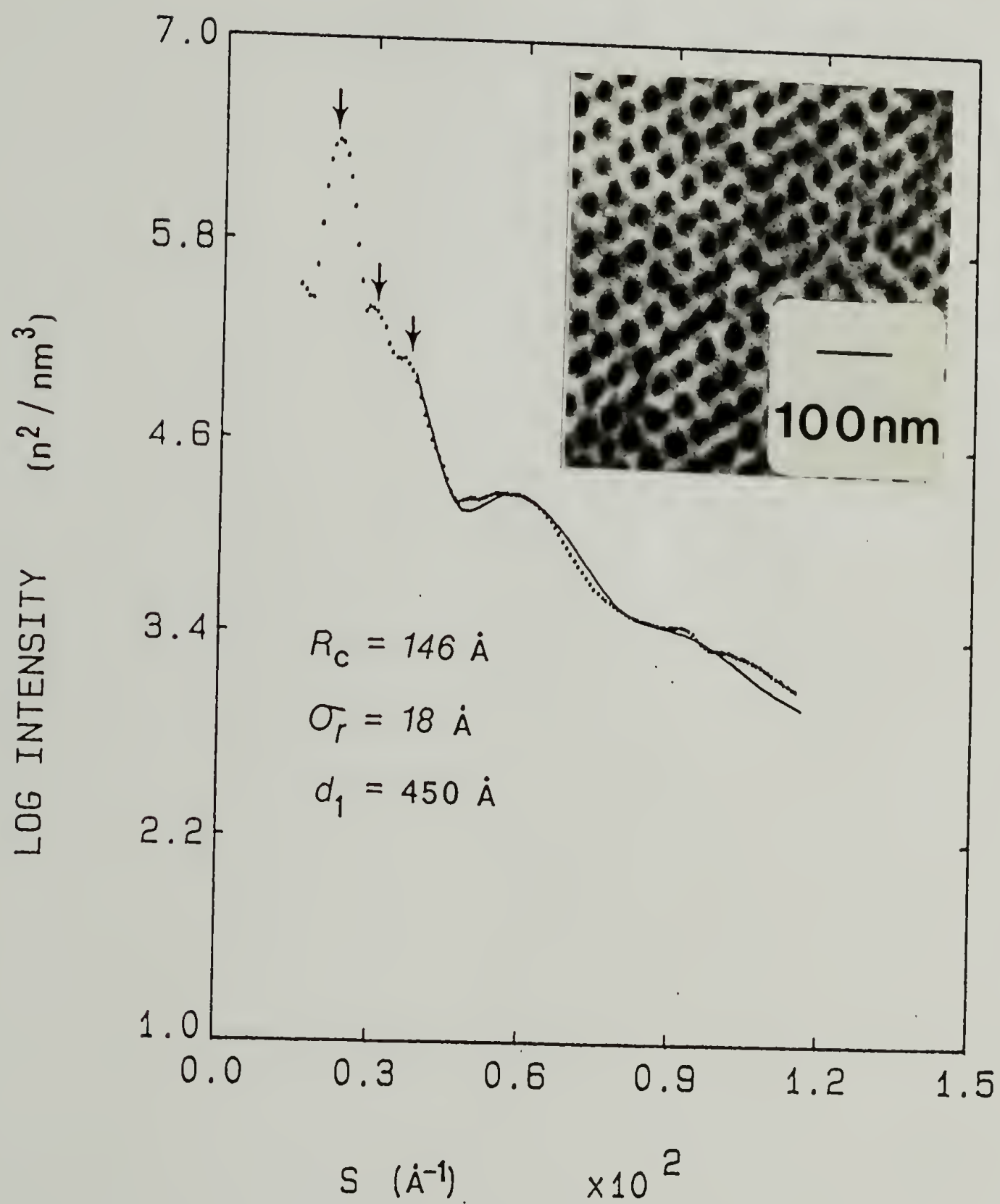


Figure 5.9 SAXS and EM results for 24.9 wt% SB 20/20 in 3900 PS.

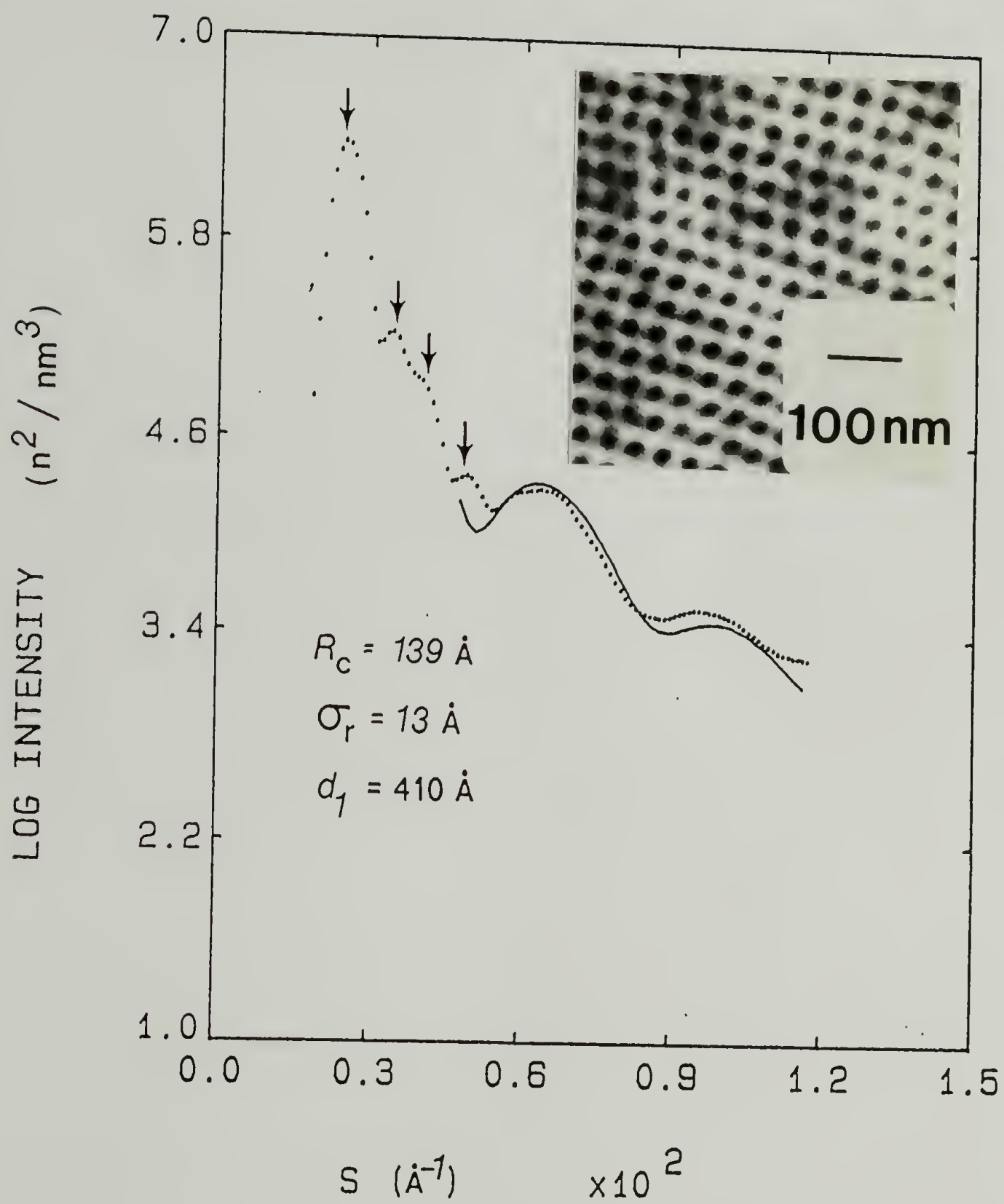


Figure 5.10 SAXS and EM results for 30.3 wt% SB 20/20 in 3900 PS.



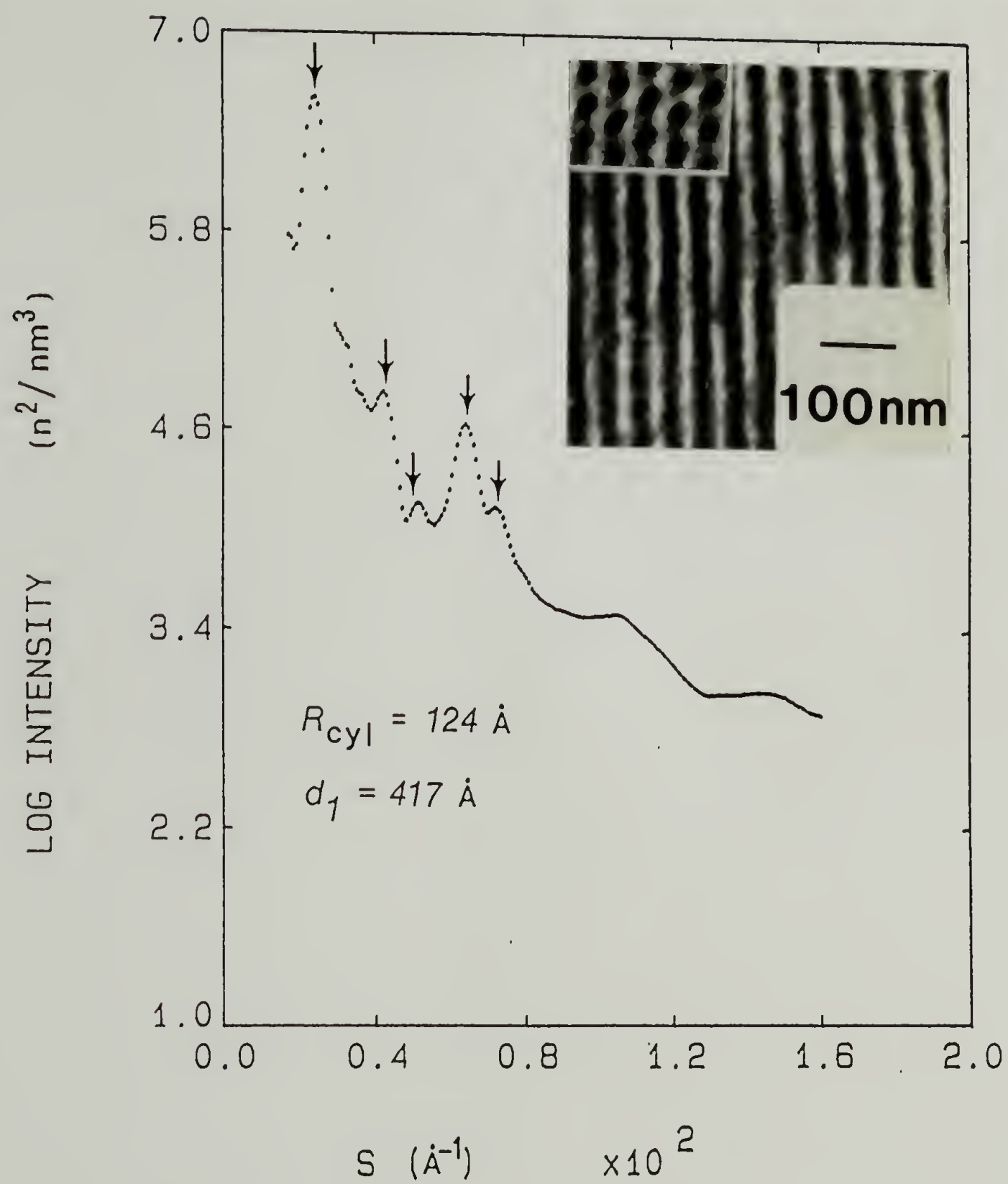


Figure 5.11 SAXS and EM results for 49.4 wt% SB 20/20 in 3900 PS.

when the volume fraction of the minority phase is about 0.20. From the positions of the second and third cylindrical scattering peaks at higher angles (the location of the first cylindrical form factor scattering peak is somewhat obscured by the presence of the third, fourth, and fifth lattice peaks at about the same location) the cylinder radius is determined to be 124 Å, while the spacing of the first lattice peak is 417 Å corresponding to a unit cell size of 481 Å, calculated from Equation 2.18. From the relation

$$\phi_{\text{cyl}} = 2\pi/\sqrt{3} (R_{\text{cyl}}/a)^2 \quad (5.4)$$

the cylindrical volume fraction is calculated to be 0.24, which compares favorably to the actual volume fraction of polybutadiene (0.28).

Although not explored experimentally, it is expected that a transition from cylindrical to lamellar morphology would occur upon increasing the copolymer concentration even further since the neat block copolymer SB 20/20 possesses a lamellar structure (see Figure A.2 in Appendix A).

#### 5.1.4 Effect of copolymer concentration on micelle core radius

The effect of copolymer concentration on the micelle core radius, as measured by SAXS, is shown in Figure 5.12 for copolymer SB20/20 in 2100 PS, 3900 PS, and 7400 PS homopolymer. For all three homopolystyrenes the general trend is a slightly increasing core radius

with copolymer concentration. For example, in the case of 3900 PS, the core radius increases from 128 Å at 2.66 wt% copolymer to 139 Å at 30.3 wt% copolymer. This corresponds to an increase in the number of copolymer molecules per micelle,  $p$ , from 231 to 295, calculated from the relationship

$$\frac{4}{3}\pi R_c^3 = p v_{PB}^3 \quad (5.5)$$

where  $v_{PB}$  is the molecular volume of the PB blocks, given by

$$v_{PB}(\text{\AA}^3) = M_{PB}/\rho_{PB}(\text{g/cm}^3) \cdot 602 \quad (5.6)$$

A key question to ask is whether this is an equilibrium effect or an artefact of the sample preparation (i.e. solvent casting) technique. The thermodynamic theories for micelle formation in block copolymer/homopolymer blends presented by Leibler et al. [112] and by Whitmore and Noolandi [131] predict a relatively constant value of  $R_c$ , independent of copolymer concentration. However, these predictions are based on the assumption of a concentration independent interaction energy density. If the interaction energy density increased with copolymer concentration (i.e., the concentration of PB) this would explain the slight increase in core radius observed, since increasing the interaction energy between the PS and PB components causes smaller surface to volume ratios, or in other words larger cores, to be energetically favored. This would also explain the slight decrease in

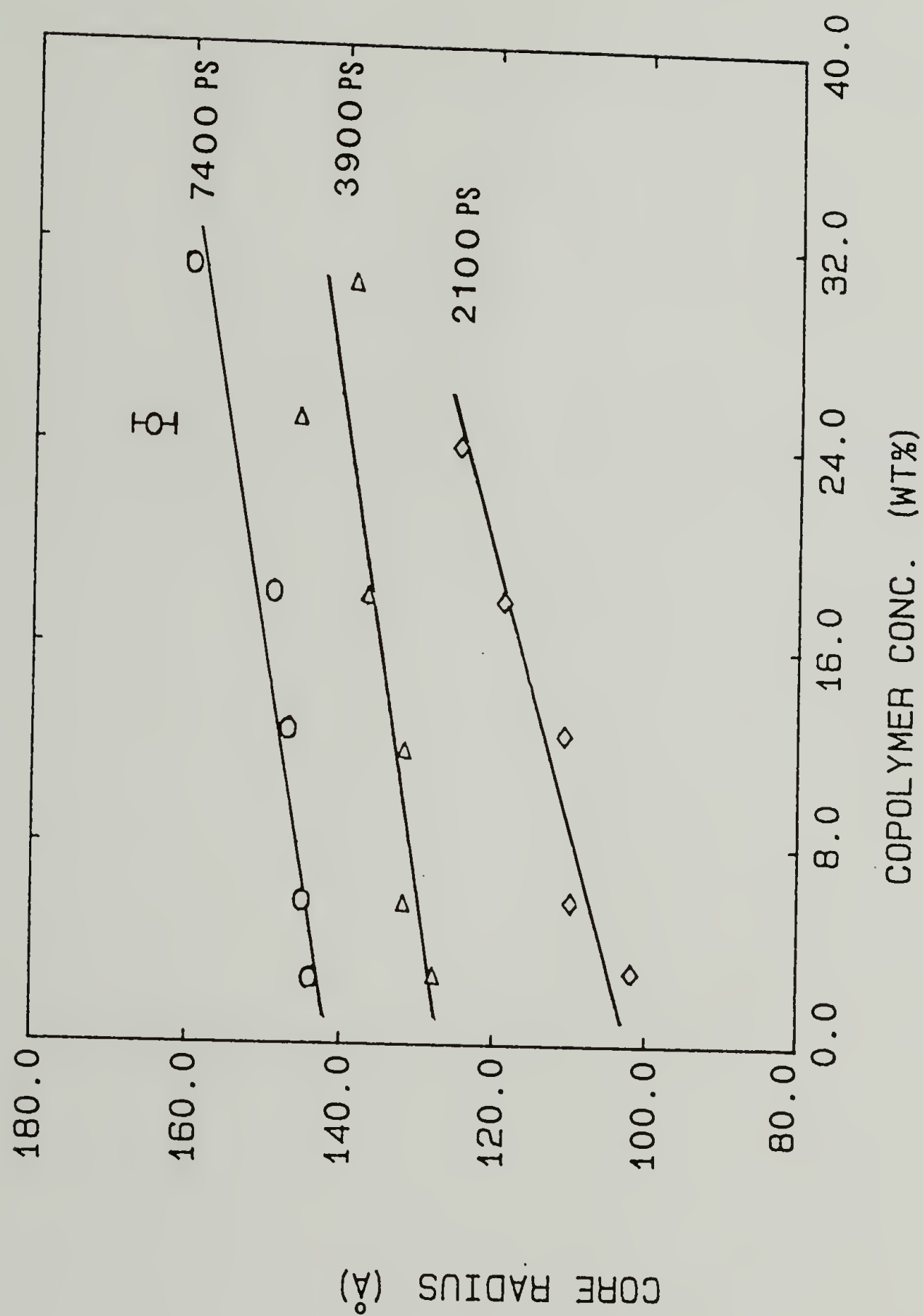


Figure 5.12 Effect of copolymer concentration on micelle core radius for SB 20/20 in 2100, 3900, and 7400 PS homopolymer.



micelle core radius with increasing copolymer concentration observed by Selb et al. [128] for poly(styrene-butadiene)/polybutadiene homopolymer blends. However, the results of Roe and Zin [134] (see Section 3.3.1.2) indicate that the compositional dependence of the interaction energy density is quite small.

An alternative explanation for the increasing core size with copolymer concentration could be an increasing swelling of the core with polystyrene homopolymer. However, as shown in Figure 5.13, the ratio of the experimentally measured invariant to the theoretically predicted invariant according to Equation 2.66, taking the cmc into account, is very nearly constant at approximately 0.9. The dotted line in Figure 5.13 indicates the decrease in this ratio from unity, predicted using Equations 2.38 to 2.43, as a result of a 20 Å interface width ( $t$ ) between the PB core and PS corona. Because of insufficient statistics in the Porod region, interface thickness measurements could not be obtained from the experiments reported here; however, a value of approximately 20 Å has been found consistently for styrene-diene block copolymers [11,29,30,95,97,123,125]. Within the error of the invariant measurements, the ratio of experimental to theoretical invariant, taking the interfacial thickness into account, is nearly unity, indicating that the amount of homopolystyrene in the core of the micelle is very small ( $\leq 5\%$ ) for all concentrations of copolymer SB 20/20 in 3900 PS homopolymer at 115 °C.

To summarize, the results of this section demonstrate that at small copolymer concentrations, a homogeneous mixture of copolymer and

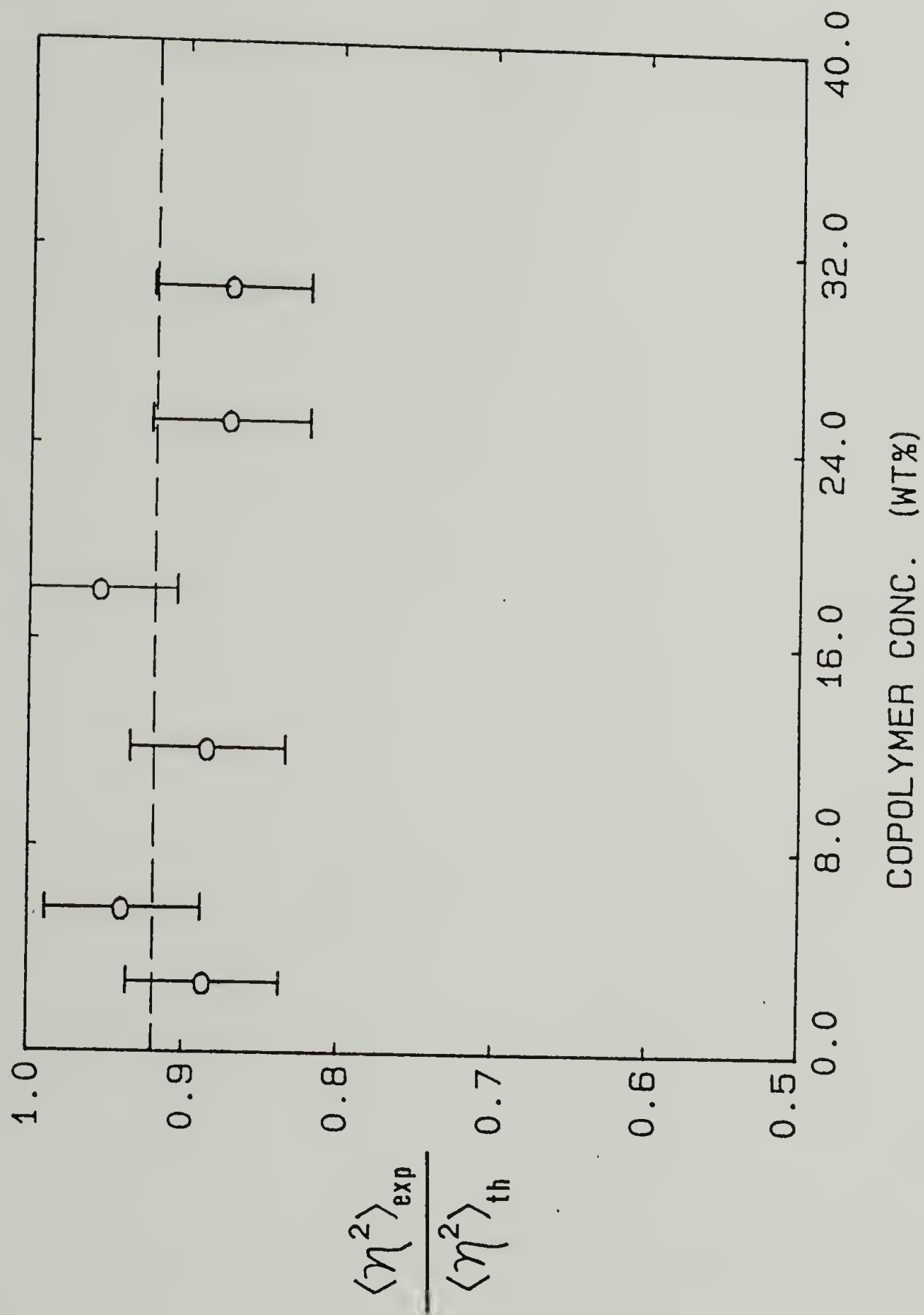


Figure 5.13 SAXS invariants of copolymer SB 20/20 in 3900 PS as a function of copolymer concentration. The dashed line indicates the decrease in the invariant ratio due to the presence of a 20Å interface width.

homopolymer molecules occurs. However, as the concentration of copolymer is increased beyond the cmc, spherical micelles form, having PB cores surrounded by coronae consisting of PS block chains highly swollen with homopolystyrene. As the copolymer concentration is increased even further, an ordered (cubic) lattice of micelles develops. Depending on the composition of the copolymer, further increases in the copolymer concentration may result in the formation of cylindrical or lamellar structures. The SAXS from spherical micelles exhibiting a lack of long range order can be well modeled using the Percus-Yevick hard sphere fluid approximation to obtain the interparticle interference contribution to the scattered intensity. From the modeling, the structural parameters of the micelles (i.e., the core radius, polydispersity in core size, corona thickness, etc...) can be determined. For example, it was found that the core radius increases slightly with copolymer concentration. In the next section, the effect of homopolymer molecular weight on micellar structure will be examined.

## 5.2 Dependence of Micellar Structure on Homopolystyrene Molecular Weight

As evidenced by the results of Figure 5.12, the molecular weight of the homopolystyrene can have a marked effect on the structure of the block copolymer micelles. The expected qualitative effects of homopolymer molecular weight on the structure of the micelles are illustrated schematically in Figure 5.14. As the homopolymer molecular

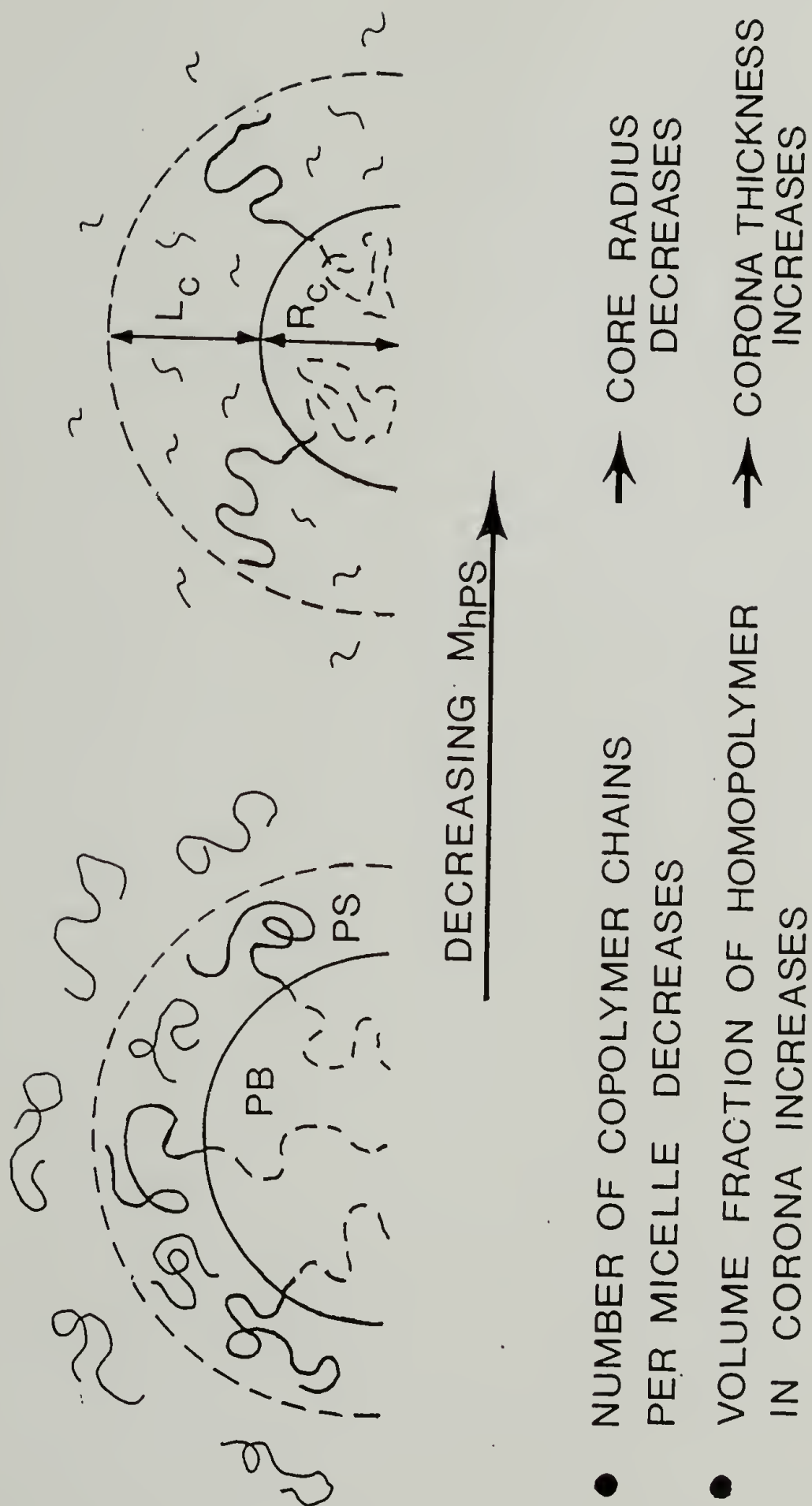


Figure 5.14 Schematic showing the effect of homopolymer molecular weight on spherical micelle structure.



weight decreases, two main effects are expected: (1) the volume fraction of homopolymer in the corona region increases, leading to radial stretching of the PS block chains in the corona, and thus a larger corona thickness, and (2) the number of block copolymer chains per micelle decreases leading to smaller micelle cores, and thus, a larger surface area per copolymer junction at the core-corona interface.

The first effect can be explained as follows. As the ratio of homopolystyrene to PS block molecular weight decreases, the gain in entropy on mixing the PS block chains and PS homopolymer in the corona region increases, causing an increased concentration of homopolystyrene in the corona. In other words, the homopolymer would like to attain a uniform value of concentration in order to maximize its entropy. This is easily understood by examining the form of Equation 3.7 in which  $F_m$ , the entropy of mixing of homopolymer and PS blocks in the corona, decreases inversely with homopolystyrene molecular weight. However, the concentration of homopolymer which can be solubilized in the corona region is limited since the stretching of PS chains accompanying the mixing causes a loss of conformational entropy (see Equation 3.6). Therefore, the concentration of homopolymer in the corona, i.e. the thickness of the corona, is determined, more or less, by a balance of these two opposing effects.

The explanation for the second effect of homopolymer molecular weight is more subtle. As shown in Figure 5.12, as the core increases in size, the PB chains must stretch to uniformly fill all of the core. This is of course energetically unfavorable due to the loss of

conformational entropy. However, the accompanying decrease in the surface to volume ratio, and the subsequent decrease in interfacial interactions, is energetically favored. Therefore, the core radius is primarily determined by a balance of these two opposing effects. Nevertheless, an additional factor in determining the core radius is the molecular weight of the homopolymer. As the molecular weight of the homopolymer decreases, the entropy effects tending to drive the homopolymer density towards a uniform value will increase. A more uniform value of homopolymer density can be obtained by maximizing the volume fraction of the corona region, which can be accomplished by either swelling of the PS corona blocks with homopolymer, resulting in an increased corona thickness, or by decreasing the radius of the core, thereby increasing the number of micelles per unit volume. A more uniform value of homopolymer concentration can also be obtained by increasing the amount of unaggregated copolymer. The degree to which each of these effects dictates the micelle structure is determined by a delicate energy balance. This will be explored in the subsequent sections.

#### 5.2.1 Critical micelle concentration

The effect of homopolymer molecular weight on the critical micelle concentration is shown in Figure 5.15 for copolymers SB 10/10, SB 20/20, and SB 80/80. The cmc values shown were determined by the electron microscopy method described previously in Section 5.1.2. The general

trend observed for all three copolymers is an increasing cmc with decreasing homopolymer molecular weight  $M_{hPS}$ . This means that the copolymer becomes more compatible with the homopolymer as  $M_{hPS}$  decreases. This is the trend predicted by the LOW theory; an examination of Equation 3.6 reveals that when the homopolymer molecular weight is decreased, and the stretching of the PS corona block (i.e.  $R_A$ ) increases, the elastic energy  $F_d$  will also increase. Therefore, the total free energy of the micellar phase also increases, making the homogeneous phase more stable relative to the micellar phase.

Also evident from Figure 5.15 is the fact that the cmc increases with decreasing copolymer molecular weight, especially at the lower copolymer molecular weights investigated. This will be discussed further in Section 5.3.3.

### 5.2.2 SAXS invariant analysis

The effect of homopolymer molecular weight on the experimentally measured SAXS invariant is illustrated in Figure 5.16 for the case of copolymer SB 20/20 (at a copolymer concentration of about 12.5 wt%). The dashed line in the figure indicates the calculated decrease in the ratio of experimental to theoretical invariant due to the presence of a typical (20 Å) interface thickness. This line is sloped due to the changing ratio of  $(t/R_c)$  with homopolymer molecular weight. For the blends containing 3900 PS and 7400 PS homopolymer, the ratio of the measured invariant to the theoretically calculated invariant, taking the

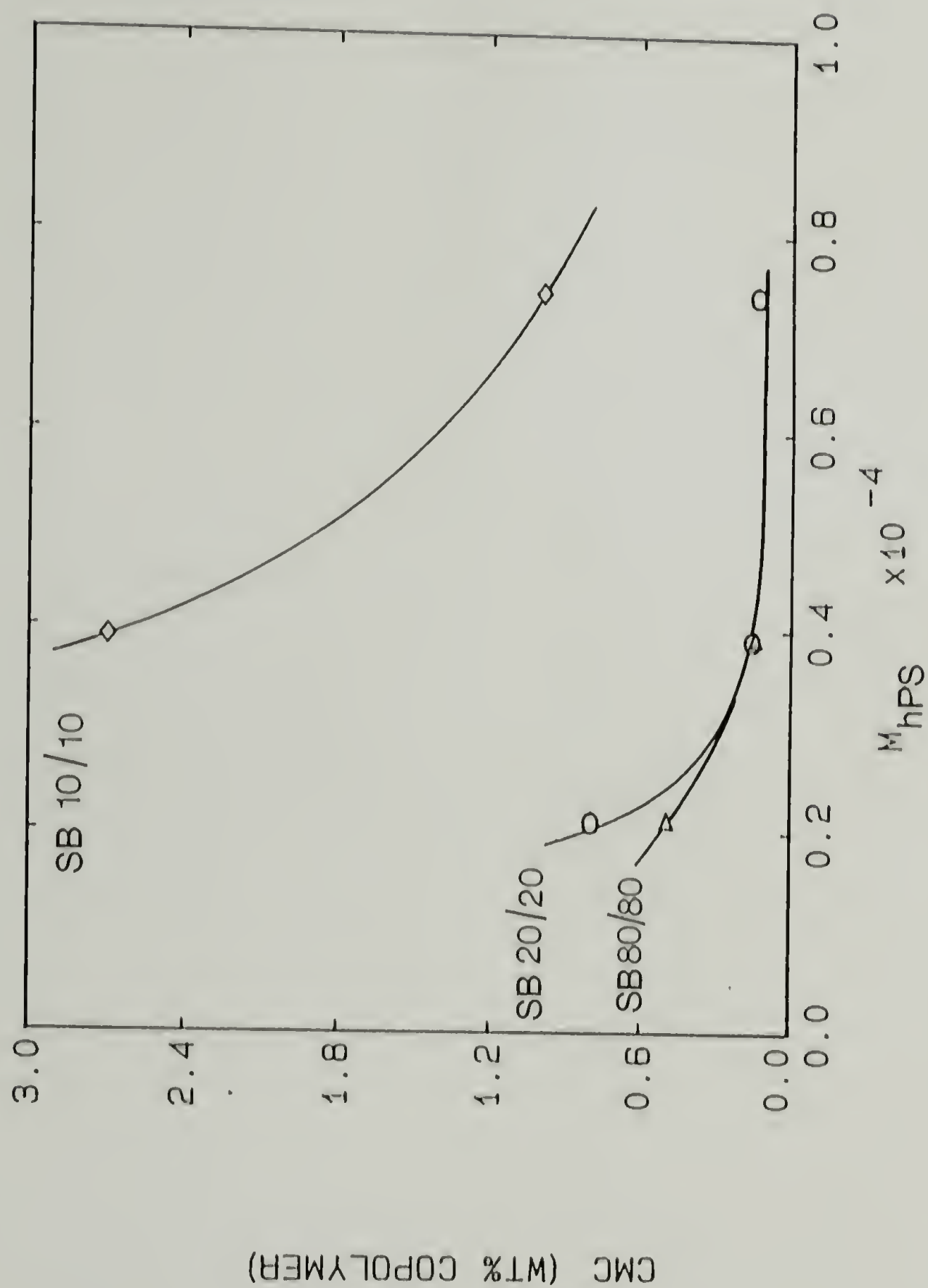


Figure 5.15 Effect of homopolymer molecular weight on the critical micelle concentration for copolymers SB 10/10, SB 20/20, and SB 80/80.



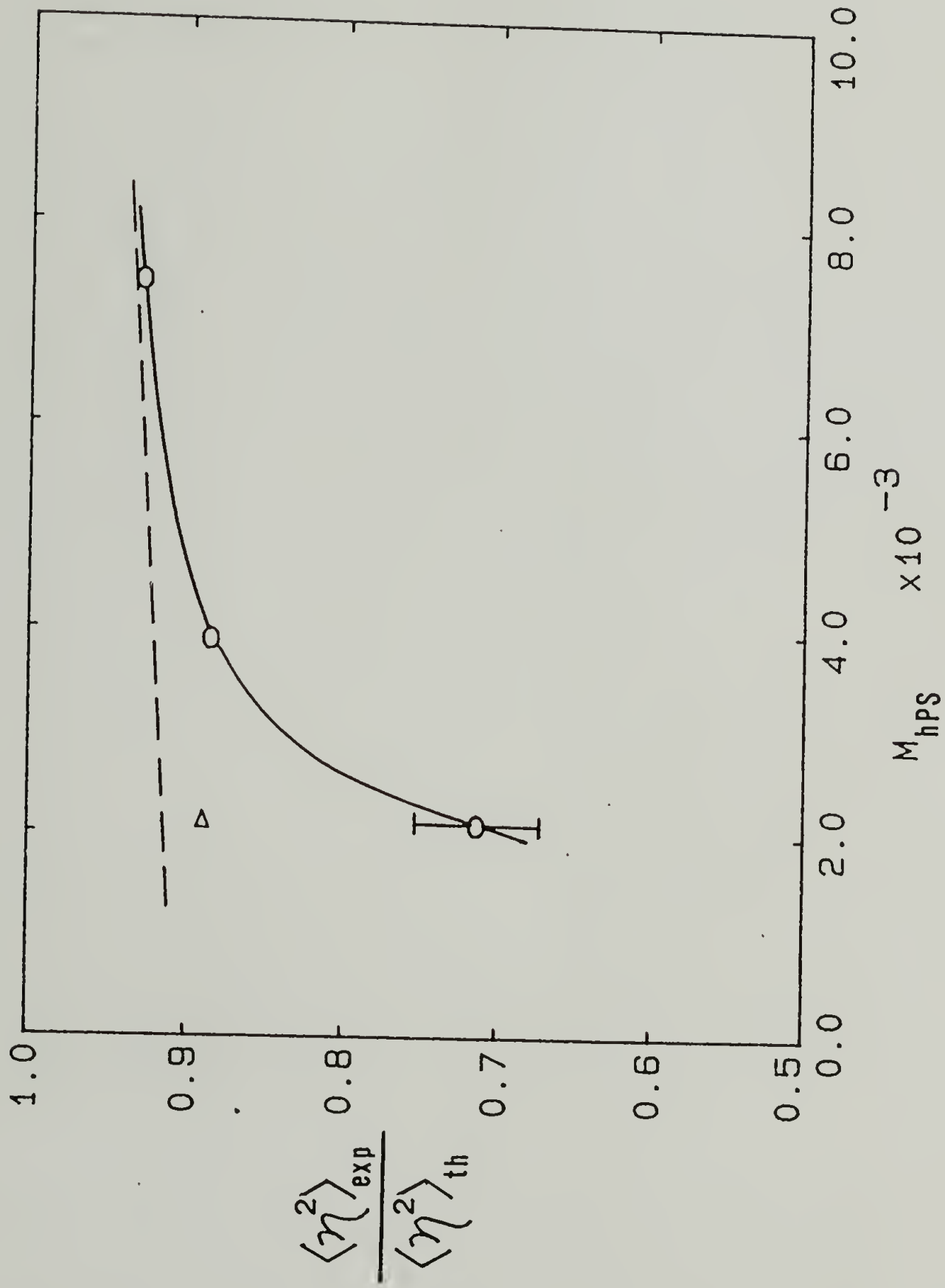


Figure 5.16 SAXS invariants for copolymer SB 20/20 as a function of homopolymer molecular weight.

cmc into account, are, within the error of the measurements, equal to that predicted for a completely phase separated system with a 20 Å interface thickness. However, for the blend containing 2100 PS homopolymer there is a marked falloff in the experimental invariant to only about 75% of the predicted value. This decrease could arise from three different types of phase mixing: (1) an increase in interface width, (2) mixing of homopolystyrene into the micelle core, and (3) an increase in the amount of free copolymer above the critical micelle concentration. As discussed previously, measurements of interface thickness utilizing the SAXS data presented here are not possible due to the lack of sufficient statistics in the Porod region. Nevertheless, interface measurements performed for block copolymer/homopolymer blends utilizing a wide range of block copolymer and homopolymer molecular weights indicate that the interface thickness is relatively constant at about 20 Å [95,123,125]. Therefore, the decrease in the invariant is not due to an increasing interface thickness. Differentiating between the second and third types of phase mixing is not possible without some additional information. The modeling of the SAXS patterns using the PY hard sphere fluid model is capable of providing this additional information. Figure 5.17 shows an electron micrograph and the accompanying SAXS pattern for 12.5 wt% SB 20/20 in 2100 PS. Also shown is the best fit (solid line) to the data obtained for the PY hard sphere fluid model, assuming there is no homopolymer in the micelle core, and that the concentration of free copolymer is equal to the cmc. It is

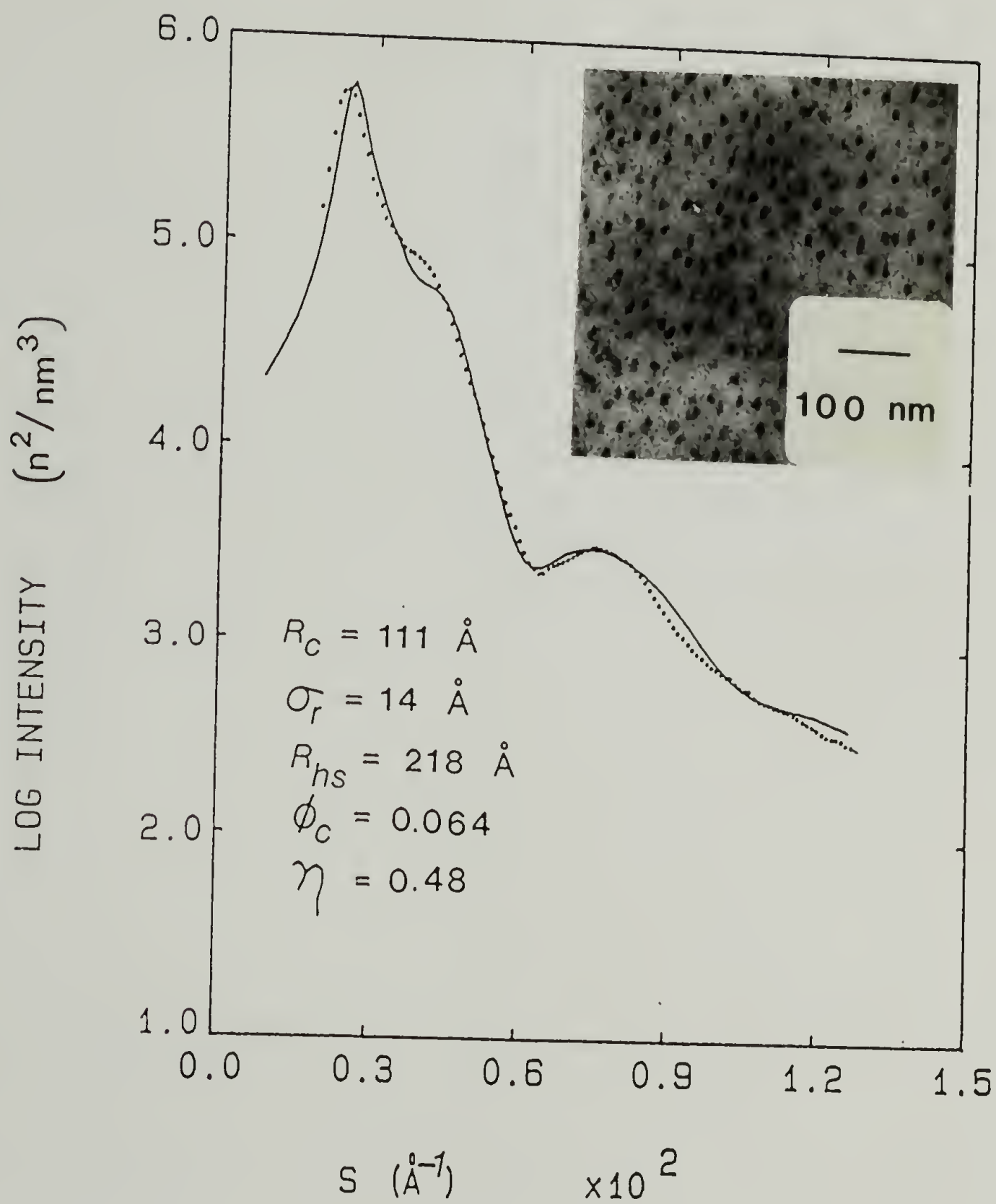


Figure 5.17 SAXS and EM results for 12.5 wt% SB 20/20 in 2100 PS.

immediately apparent that the interparticle interference scattering in the low angle region is not predicted very well. The  $s$  values of the main interference peak and the accompanying shoulder are smaller than predicted by the modeling. Assuming that there is homopolymer present in the micelle core means that the volume fraction of micelle cores used in the modeling,  $\phi_c$ , must be increased from that given by Equation 5.2. From Equation 5.1 it is evident therefore, that the hard sphere radius of the micelle used in the modeling will decrease. These two factors both serve to decrease the average distance between micelles, and thus, the model calculations would predict that the interparticle interference peaks would shift to even higher values of  $s$ . This is opposite to the result desired. Another possible reason for the disagreement between the modeling and the experimental data is incomplete solubilization of the homopolymer. However, if some of the homopolymer formed its own phase, the average distance between the micelles would be smaller than expected, which would also shift the interference peaks to larger values of  $s$ .

If however, one assumes that the concentration of free copolymer is larger than the critical micelle concentration, then the value of  $\phi_c$  used in the modeling must be decreased according to Equation 5.2, replacing the cmc with the actual amount of free copolymer. This means that the number density of micelles must be decreased. This also means that a larger value of the effective hard sphere radius must be employed in the modeling. These two factors both serve to increase the average distance between micelles, thereby decreasing the predicted values of  $s$



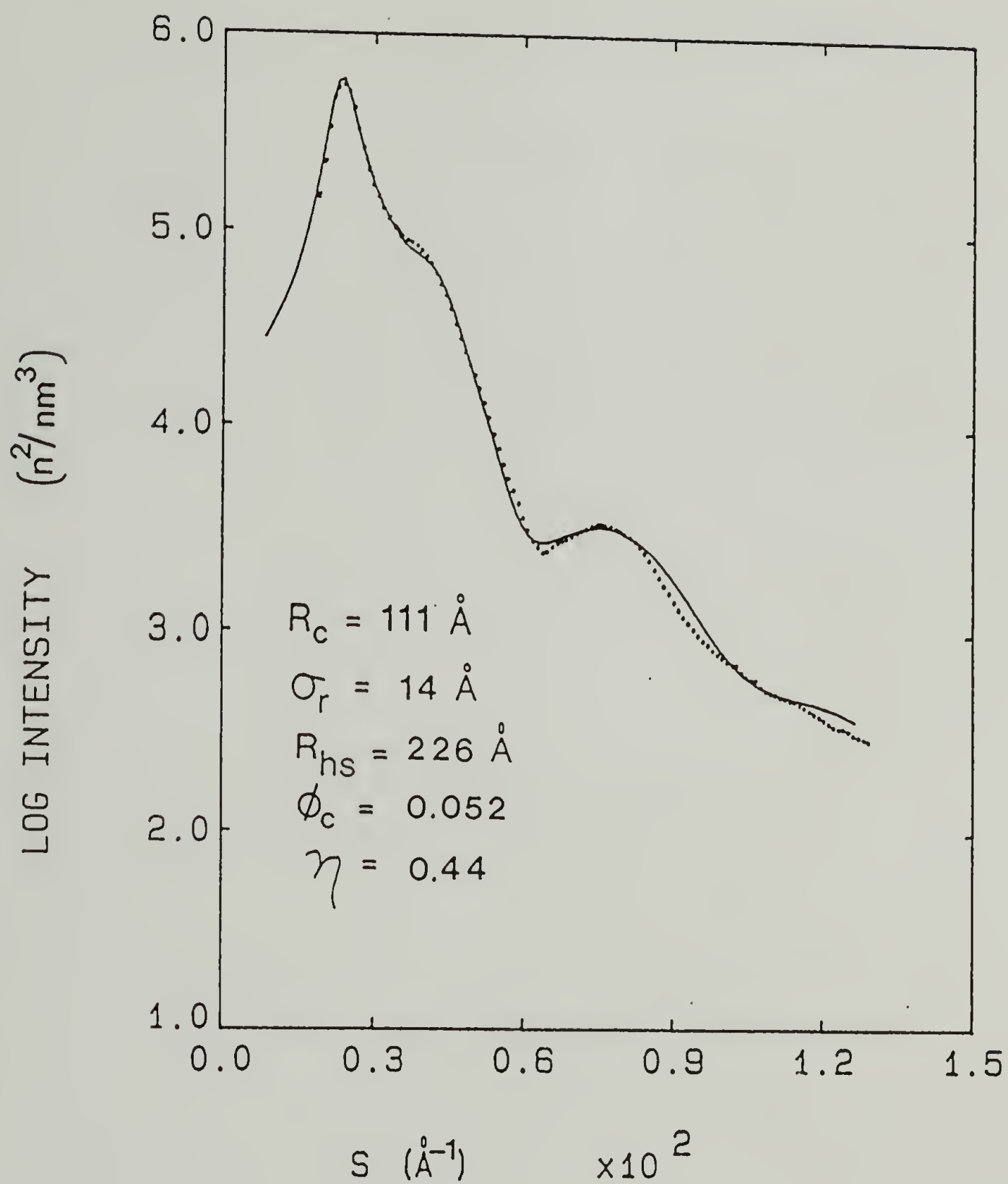


Figure 5.18 SAXS and EM results for 12.5 wt% SB 20/20 in 2100 PS.

for the interference peaks. This is the result desired. Figure 5.18 shows the best fit to the SAXS data for 12.5 wt% SB 20/20 in 2100 PS following this procedure. The experimental and calculated SAXS patterns now agree remarkably well. The volume fraction of the core is allowed to be an additional variable to be determined by the non linear least squares fitting program. A value of  $\phi_c = 0.053$  was determined, which corresponds to 3.5 wt% free copolymer compared to the critical micelle concentration of 0.8 wt% copolymer. The ratio of experimental to predicted invariant, taking this free copolymer into account, is very nearly that predicted assuming no homopolymer resides in the core as shown by the triangular data point in Figure 5.16.

The PY modeling is thus shown to be a powerful tool which allows one to say that the main type of phase mixing causing the decrease in the invariant for copolymer SB 20/20 with decreasing homopolymer molecular weight is an increase in the concentration of free copolymer above the cmc. For this copolymer the amount of homopolymer in the micelle core is found to be small ( $\leq 5\%$ ) for the temperature (115 °C) and homopolymer molecular weights studied.

For completeness, the EM and SAXS results of 12.3 wt% SB20/20 in 7400 PS are shown in Figure 5.19. The value of  $\phi_c$  used in the modeling was the value calculated assuming that the concentration of free copolymer equaled the cmc and that there was no mixing of homopolymer into the core. Again, very good agreement between the experimental data and the predictions of the modeling are obtained.

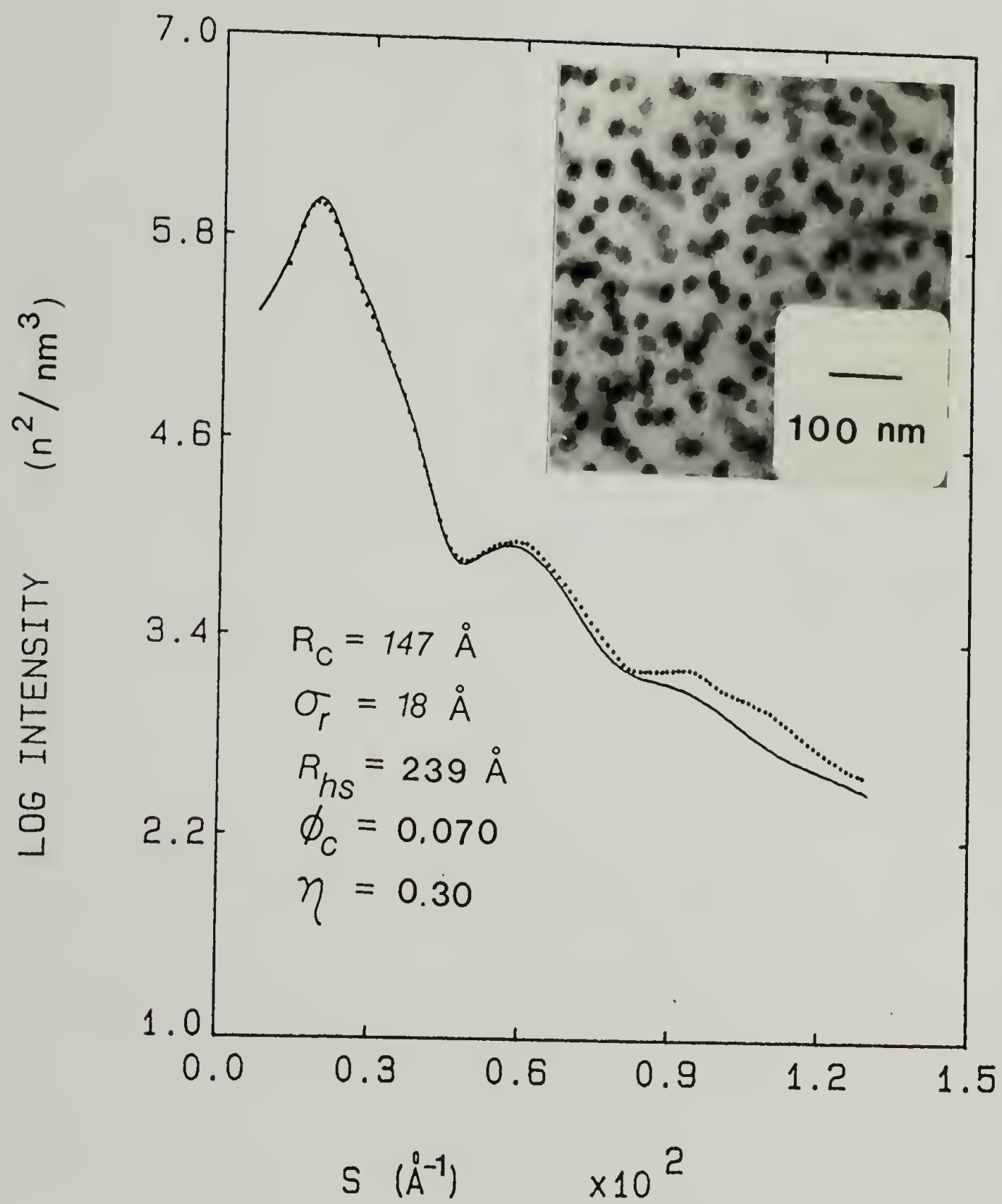


Figure 5.19 SAXS and EM results for 12.3 wt% SB 20/20 in 7400 PS.

From the SAXS results of Figures 5.7 and 5.17-5.19, it is apparent that, at a given copolymer concentration, the volume fraction of micelles increases with decreasing homopolymer molecular weight, even though the volume fraction of micelle cores may decrease. This is a direct result of the increasing swelling of the PS blocks with homopolymer, and indicates that the blend containing lower molecular weight homopolymer should form an ordered lattice of micelles at lower copolymer concentrations. An increase in corona thickness from 92 to 115 Å is observed on going from 7400 to 2100 PS homopolymer, which is outside the error of the measurements ( $\pm 7$  Å). In addition, the ratio of  $\sigma_r/R_c$  is approximately constant at 0.13 so that the polydispersity in core size is not effected by the homopolymer molecular weight. The core size however, is seen to increase from a value of 111 Å for 2100 PS to 147 Å for 7400 PS homopolymer. This increase is also evident in the electron micrographs of these blends, and is the topic of the next section.

### 5.2.3 Core size

The effect of homopolymer molecular weight on micelle core size, as measured by SAXS, is illustrated further in Figure 5.20 for copolymers SB 20/20, SB 40/40, SB 80/80, and SB 40/10 (for copolymer concentrations of about 10 wt%). The core radii measured from electron micrographs are approximately 10% smaller than those obtained by SAXS. This is in accord with the results of Berney et al. [145] which showed



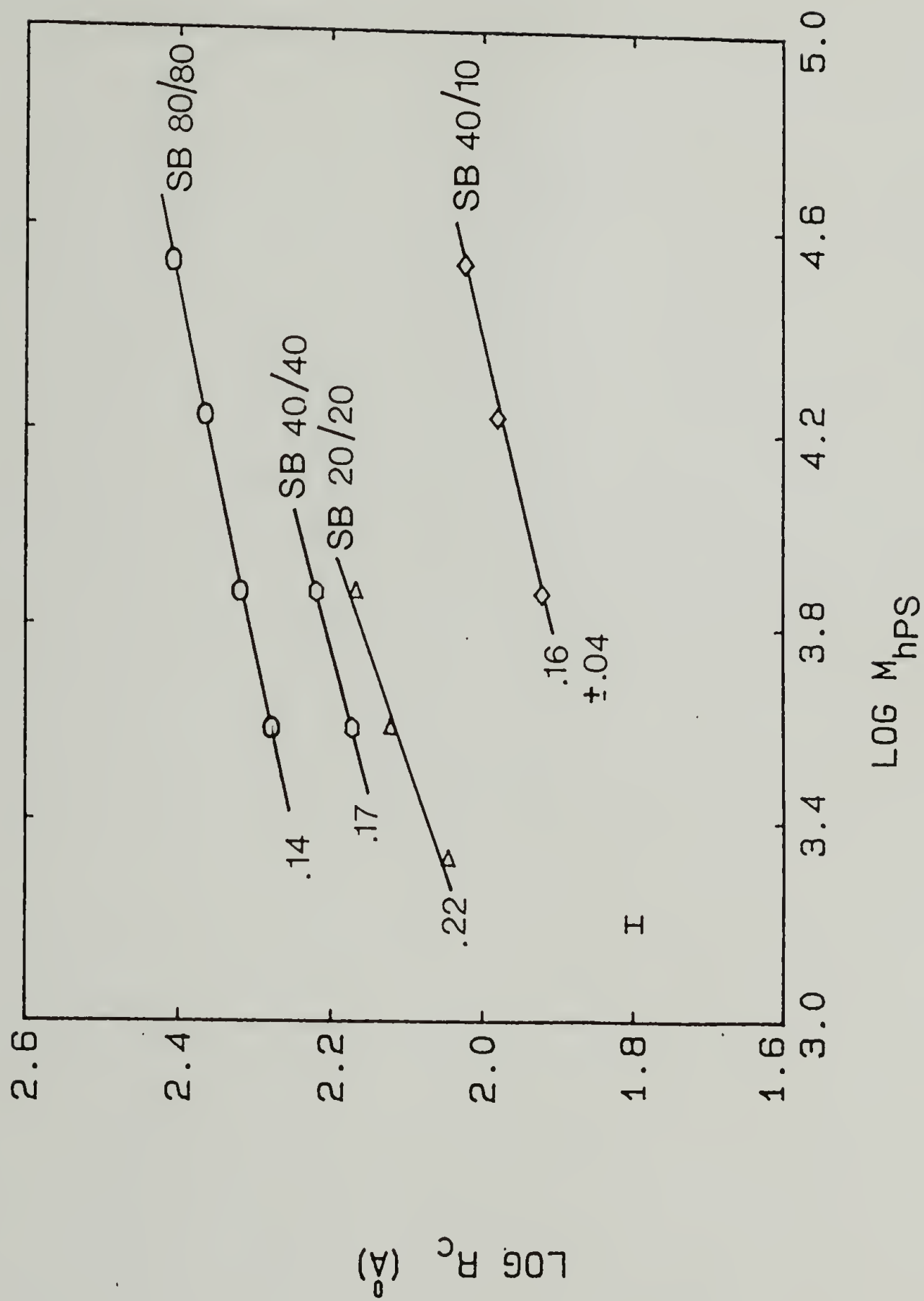


Figure 5.20 Micelle core radius as a function of homopolymer molecular weight for copolymers SB 40/10, SB 10/10, SB 40/40, and SB 80/80. The scaling exponent  $\gamma$  for each copolymer is as indicated.

that osmium tetroxide stained PB spheres in blends of poly(styrene-butadiene) copolymer and polystyrene homopolymer, as measured by EM, were  $\sim 20\%$  smaller than the values obtained using small angle neutron scattering. The core radius is seen to increase with increasing  $M_{hPS}$  for all copolymers. In addition, the scaling behavior described by the relation  $R_c \propto M_{hPS}^\gamma$  is similar for all copolymers with an average value of  $\gamma = 0.17 \pm 0.04$ . This agrees rather well with the value of  $\gamma = 0.19$  determined from the data of Selb et al. [128] for blends of poly(styrene-butadiene) diblock copolymers in low molecular weight polybutadiene homopolymers. The unperturbed root mean square end to end distances of the PS [142] and PB [142,144] block chains, calculated from the relationships

$$\langle r^2 \rangle_{PS}^{1/2} = 0.67 M_{PS}^{0.5} \quad (5.7a)$$

$$\langle r^2 \rangle_{PB}^{1/2} = 0.89 M_{PB}^{0.5} \quad (5.7b)$$

are listed in Table 5.1 for the copolymers used in the present study. A comparison of the core radii shown in Figure 5.20 to the end to end distances of the respective PB blocks reveals that the ratio  $R_c / \langle r^2 \rangle_{PB}^{1/2}$  is smaller than unity for low molecular weight homopolystyrene matrices, and larger than unity for the higher molecular weight homopolystyrene matrices. For example, this ratio increases from 0.87 to 1.16 for SB 20/20 in 2100 and 7400 PS respectively.

TABLE 5.1Root mean square end to end distances of the PS and PB blocks

Block Copolymer	$\langle r^2 \rangle_{\text{PS}}^{1/2}$ (Å)	$\langle r^2 \rangle_{\text{PB}}^{1/2}$ (Å)
SB 10/10	73	89
SB 20/20	96	127
SB 40/40	138	189
SB 80/80	191	243
SB 23/10	100	84
SB 40/10	137	90
SB 60/10	159	93

Equation 5.5 shows that for a given copolymer, the number of copolymer chains per micelle,  $p$ , scales with  $R_C^3$ ; therefore, the experimental results give  $p \propto M_{hPS}^{3\gamma} \propto M_{hPS}^{0.51 \pm 0.12}$ . The average surface area occupied by each copolymer junction,  $S$ , is given by  $4\pi R_C^2/p$  so that  $S \propto p^{-1/3} \propto R^{-1} \propto M_{hPS}^{-0.17 \pm 0.04}$ . Also evident from Figure 5.20 is the fact that the micelle core size increases with PB block length. This will be discussed further in Section 5.3.3. It should also be mentioned that increasing the homopolymer molecular weight beyond that shown in Figure 5.20 for copolymers SB 20/20, SB 40/40, and SB 80/80 results in the formation of non-spherical (cylindrical or lamellar) micelles. These transitions in micelle shape will be discussed in Chapter 7.

#### 5.2.4 Corona thickness

The effect of homopolymer molecular weight on the corona thickness, obtained from the effective hard sphere radius determined from modeling the SAXS data, is shown in Figure 5.21 for copolymers SB 20/20, SB 40/40, and SB 80/80. For all copolymers, the corona thickness decreases with increasing  $M_{hPS}$  according to the scaling law  $L_C \propto M_{hPS}^\epsilon$  where  $\epsilon$  is found to be  $-0.17 \pm 0.07$ , being the same for all copolymers within the error of the measurements. The magnitude of the corona thickness decreases to about the unperturbed end to end distance of the PS block chain (see Table 5.1) for the highest homopolymer molecular weights studied (before the transition to non-spherical micelles occurs). For example, the ratio  $L_C / \langle r_{PS}^2 \rangle^{1/2}$  decreases from 1.20



to 0.96 for SB 20/20 in 2100 and 7400 PS respectively. Similar results are found for other copolymers. The copolymer concentrations for which  $L_c$  are reported (10-20 wt%) are those for which  $\eta$  is fairly large ( $\approx 0.30-0.50$ ) in order that the most accurate measure of  $L_c$  could be obtained. Nevertheless, the uncertainty in  $L_c$  is significant compared to the change in  $L_c$  with  $M_{hPS}$ ; this accounts for the large uncertainty in the experimentally determined value of  $\epsilon$ . Figure 5.21 also shows that the corona thickness increases with the molecular weight of the PS block as expected. This will be discussed further in Sections 5.3.1 and 5.3.3.

The volume fraction of homopolystyrene in the corona ( $1-\eta_a$ ) can be calculated from the relationship

$$\eta_a = \frac{P v_{PS}}{4/3\pi(R_{hs}^3 - R_c^3)} \quad (5.8)$$

where  $\eta_a$  is the volume fraction of polystyrene blocks in the corona, and  $v_{PS}$  is the molecular volume of a single PS block. Figure 5.22 shows a plot of the volume fraction of homopolystyrene in the corona ( $1-\eta_a$ ) versus the ratio of homopolystyrene to polystyrene block molecular weight for several block copolymer/homopolymer pairs. As expected, the concentration of homopolymer in the corona decreases with increasing  $M_{hPS}/M_{PS}$ , from a value of about 0.9 at  $M_{hPS}/M_{PS} = 0.1$  to about 0.7 at  $M_{hPS}/M_{PS} = 0.5$ . This reflects the decreasing homopolymer solubility due

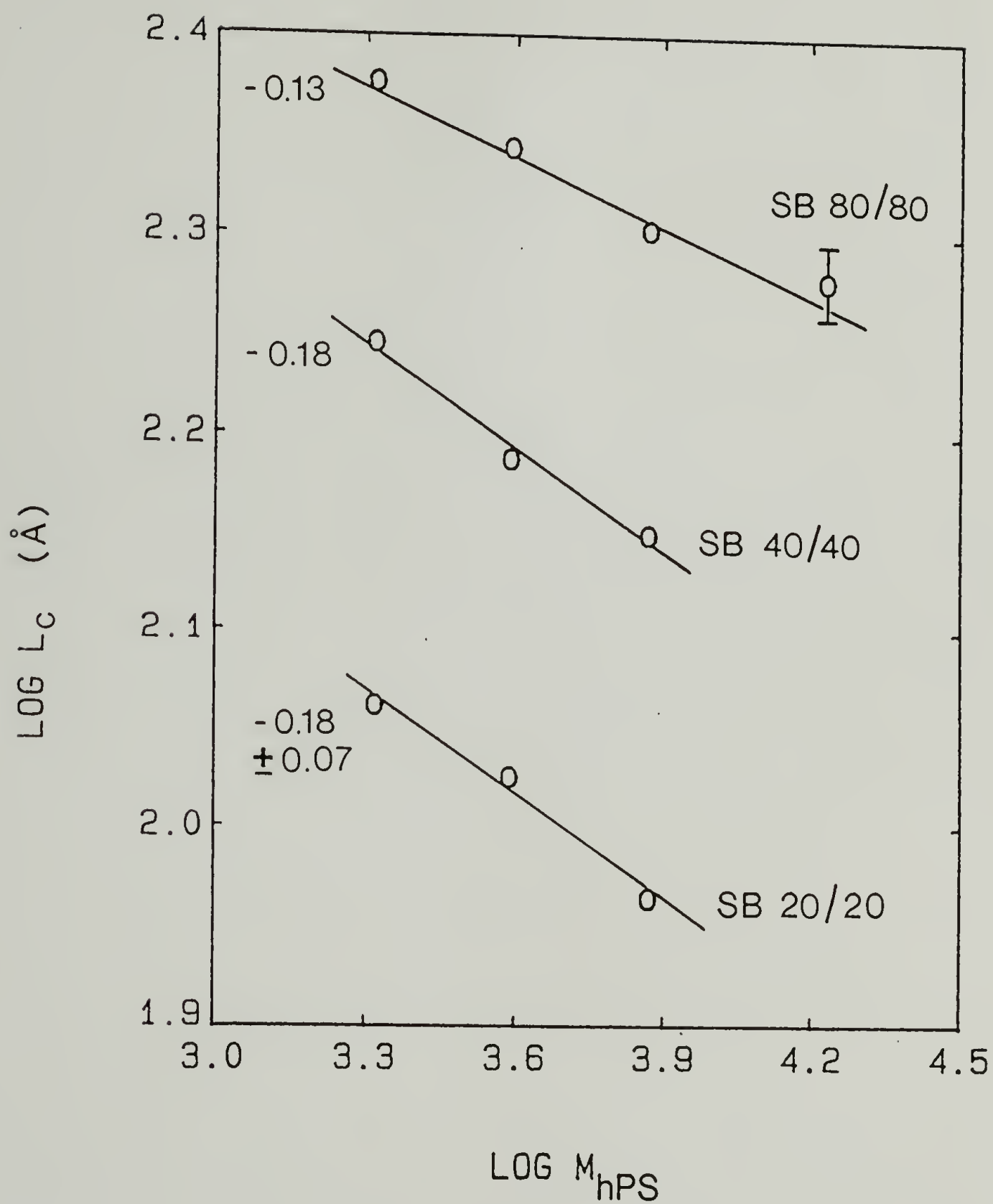


Figure 5.21 Corona thickness as a function of homopolymer molecular weight for copolymers SB 20/20, SB 40/40, and SB 80/80. The scaling exponent  $\epsilon$  is indicated for each copolymer.

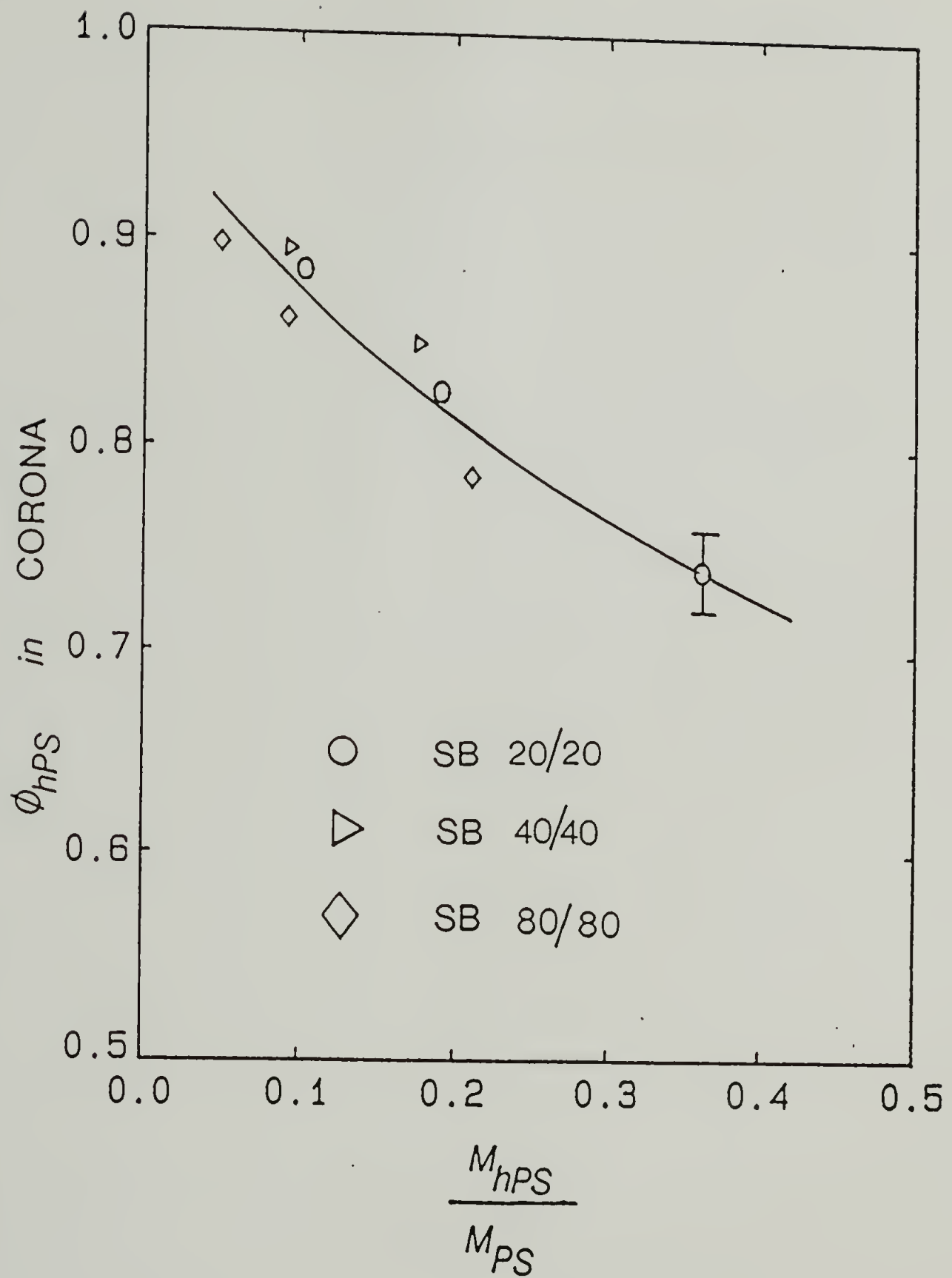


Figure 5.22 Volume fraction of homopolystyrene in the corona as a function of homopolystyrene to PS block molecular weights for SB 20/20, SB 40/40, and SB 80/80.

to the decreasing entropy of mixing with increasing  $M_{hPS}$ . Hence, performing the PY modeling of SAXS patterns allows for a quantitative assessment of the homopolymer solubility in the corona, which would be unavailable otherwise.

In summary, the results of this section have shown that the homopolymer molecular weight has a marked effect on the micellar structure of block copolymer/homopolymr blends. For instance, the critical micelle concentration was observed to increase with decreasing homopolymer molecular weight as a result of increasing compatibility between the copolymer and homopolymer. It was also observed that the SAXS invariant decreased with decreasing homopolymer molecular weight, indicating an increasing amount of mixing of PB block and PS homopolymer. By combining the invariant analysis with the PY hard sphere modeling of SAXS data, it was determined that this decrease in invariant was due mainly to free (unaggregated) copolymer, in excess of the cmc. The concentration of PS homopolymer in the PB micelle core was found to be very small. In addition, it was observed that the spherical PB micelle core radii increased with increasing homopolymer molecular weight according to the scaling law  $R_c \propto M_{hPS}^{0.17 \pm 0.04}$  while the corona thickness decreased with increasing homopolymer molecular weight according to the scaling law  $L_c \propto M_{hPS}^{-0.17 \pm 0.07}$  over the range of copolymer and homopolymer molecular weights investigated. Therefore, the number of copolymer molecules per micelle increases and the concentration of homopolymer in the micelle corona decreases with increasing homopolymer molecular weight as a result of decreasing



entropy of mixing of homopolystyrene and PS copolymer block. Perhaps the most striking effect of increasing homopolymer molecular weight is the transition from spherical to non-spherical micelles. This will be the topic of Chapter VII. The next section will examine the effect of PS and PB block lengths on the structure of spherical micelles.

### 5.3 Dependence of Micellar Structure on Polystyrene and Polybutadiene Block Molecular Weights

Three different sets of poly(styrene-butadiene) diblock copolymers, listed in Table 4.1, have been studied: (1) those for which the PB block molecular weight is kept relatively constant at about 10,000 while the PS block length is varied (SB 10/10, SB 23/10, SB 40/10, and SB 60/10), (2) those for which the PS block molecular weight is kept relatively constant at 10,000 while the PB block length is varied (SB 10/10, SB 10/23, and SB 10/65), and (3) those for which the composition is kept relatively constant at 50% while the overall molecular weight is varied (SB 10/10, SB 20/20, SB 40/40, and SB 80/80). With these three sets of samples it is possible to independently determine the effect of PS block length, PB block length, and overall molecular weight of the copolymer on the micellar structure.

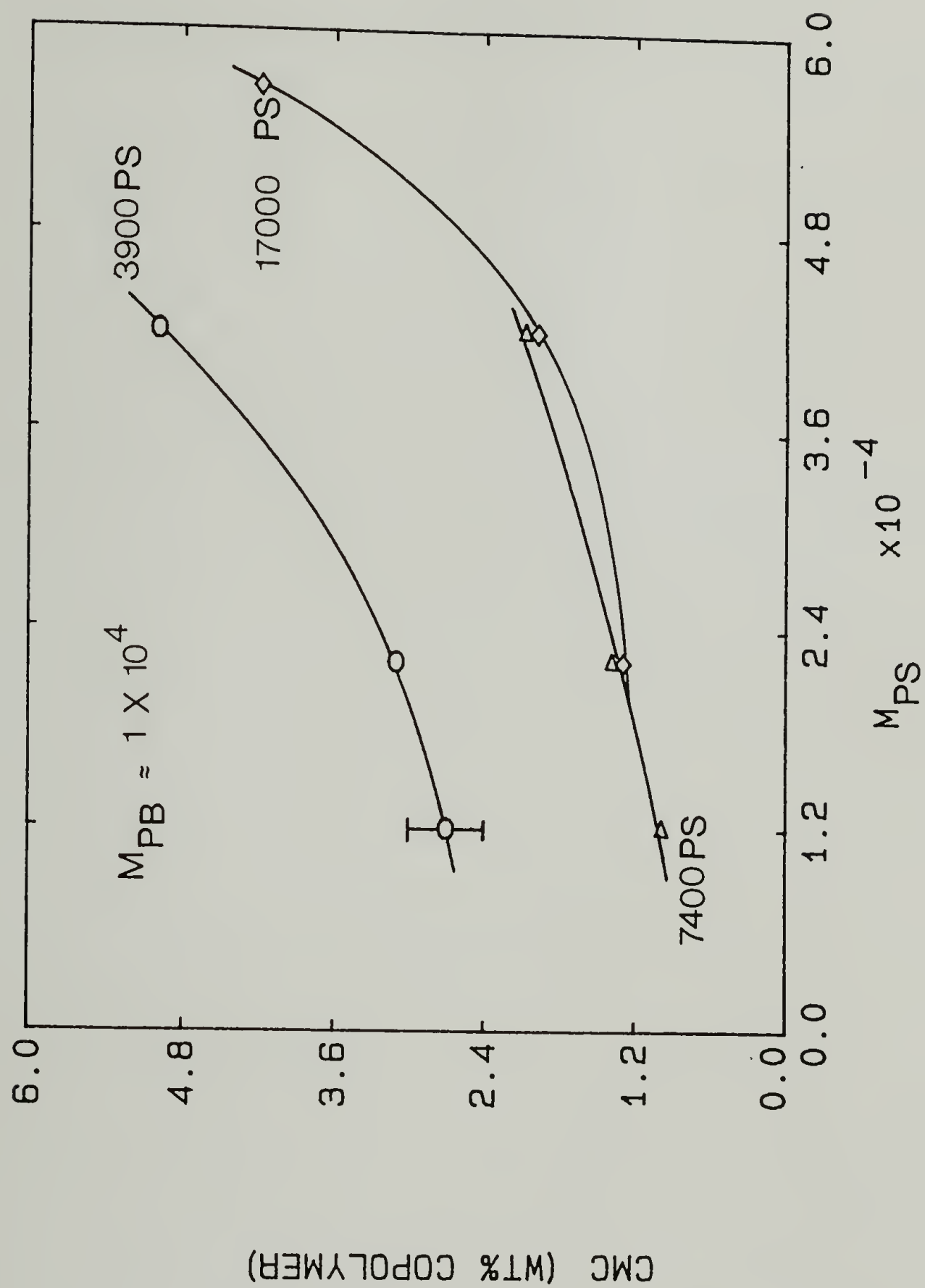


Figure 5.23 Effect of PS block length on the critical micelle concentration in various homopolystyrenes.

### 5.3.1 Effect of PS block length

The effect of PS block length on the critical micelle concentration (at 115 °C) is shown in Figure 5.23 for three different homopolymer molecular weights. The cmc values shown were obtained using the electron microscopy method outlined previously. As observed previously, the cmc decreases with increasing molecular weight of the homopolymer. In addition, the cmc also increases as the molecular weight of the PS block increases. For example, for 3900 PS homopolymer, the cmc increases from  $2.7 \pm 0.2$  wt% copolymer for SB 10/10 to  $5.0 \pm 0.5$  wt% copolymer for SB 40/10. For this molecular weight homopolymer, no micelles were observed for copolymer SB 60/10 up to a concentration of 10 wt% copolymer. Even at 17,000 molecular weight homopolymer, the cmc for SB 60/10 is still rather high ( $4.2 \pm 0.4$  wt%). This increase in cmc with PS block length is a result of increasing solubility of the copolymer in the homopolymer. This can be rationalized very simply in terms of the copolymer composition. For a given amount of copolymer, the amount of polybutadiene which must be solubilized decreases with increasing PS block length. However, this reasoning oversimplifies the situation. While increasing the cmc decreases the free energy contribution due to the micelles themselves (since the total number of micelles is reduced), it increases the free energy of mixing of homopolymer and copolymer outside the micelles. Therefore, the actual amount of free copolymer is determined by the subtle energy balance given by Equation 3.9.

The effect of PS block length on the measured SAXS invariants is shown in Figure 5.24 for the case of SB 23/10 (10.1 wt %), SB 40/10 (17.6 wt %), and SB 60/10 (18.7 wt %) in 17000 PS homopolymer (solid line). The invariant is seen to decrease from 71% of the value predicted for SB 23/10, taking the cmc into account, to 51% of the value predicted for SB 60/10. These values are well below the values predicted assuming a 20 Å interface (see dashed line). Therefore, there is significant mixing of the PS and PB components, either by (1) mixing of homopolymer into the micelle core and/or (2) additional mixing of copolymer, above the cmc, into the homopolymer matrix. As before, modeling the SAXS patterns with the PY hard sphere liquid theory can help to determine the type of phase mixing occurring. The SAXS and EM results for these three blends are given in Figures 5.25 to 5.27. Similar to the case of copolymer SB 20/20 in 2100 PS, the positions of the SAXS interparticle interference peaks predicted from the modeling, assuming that the concentration of free copolymer equaled the cmc and that no homopolymer resided in the micelle core, were at higher values of  $s$  than those of the actual data. As discussed previously, this can only be attributed to a free copolymer concentration which is larger than the cmc. By allowing  $\phi_c$  (i.e., the amount of free copolymer) to be an adjustable parameter, better fits between the model predictions (solid line) and the actual SAXS data were obtained. The parameters of best fit are listed in Figures 5.25–5.27. The values of  $\phi_c$  were found to be 0.020, 0.021, and 0.013, corresponding to 4.1, 9.5, and 11.8 wt% free copolymer (compared to the cmc values of 1.3, 2.0, and 4.2 wt%)



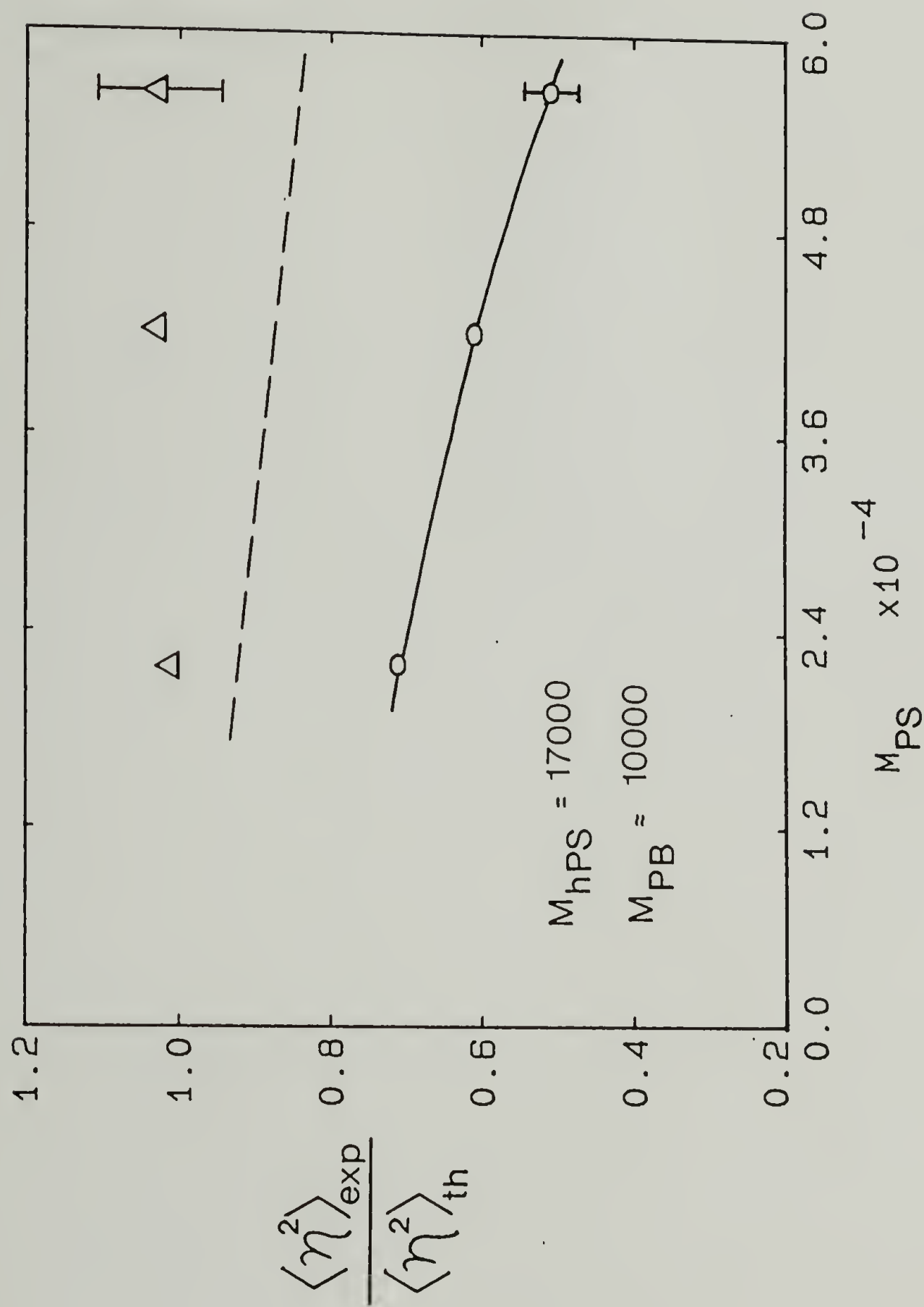


Figure 5.24 SAXS invariant as a function of PS block length.

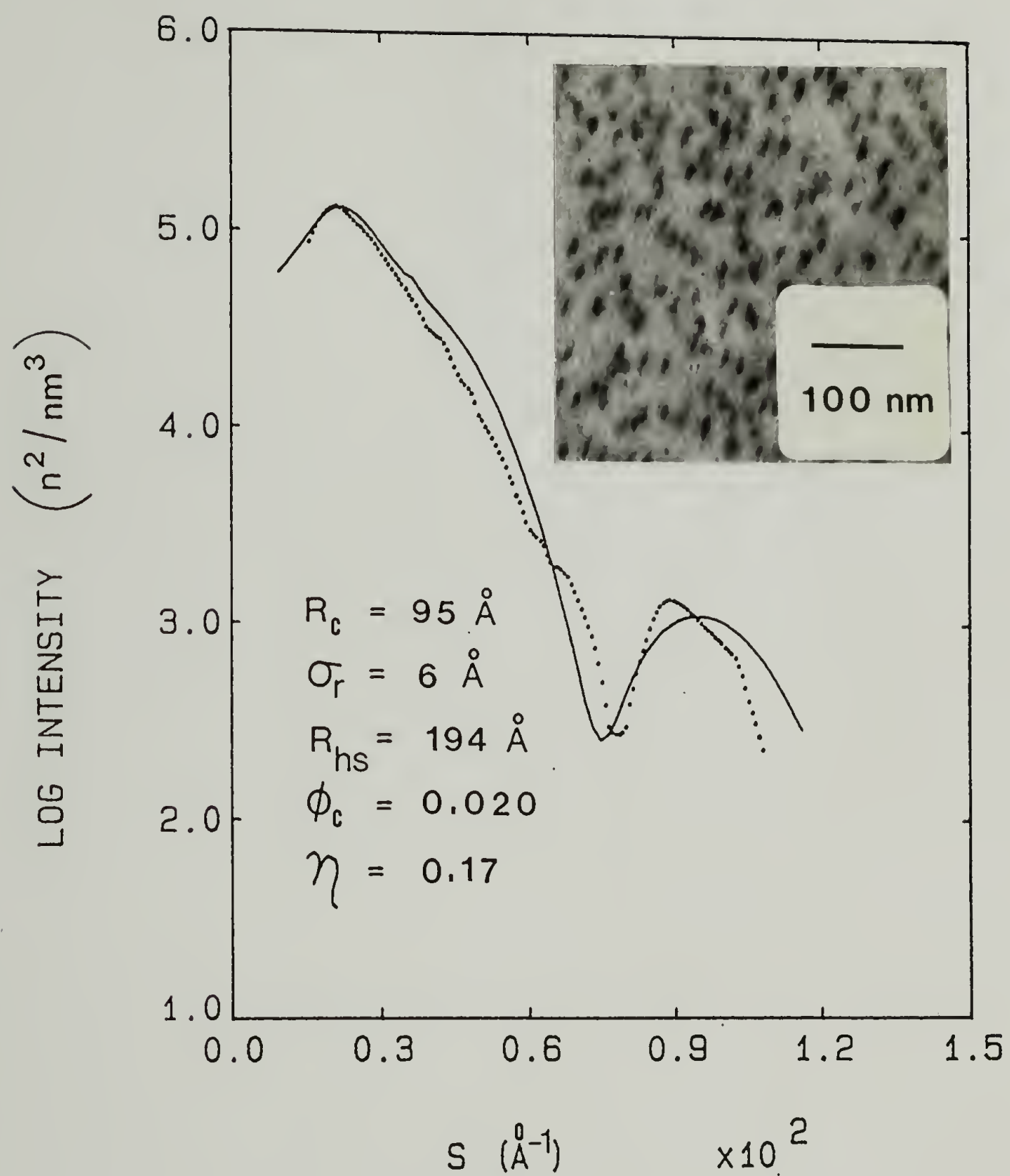


Figure 5.25 SAXS and EM results for 10.1 wt% SB 23/10 in 17000 PS.

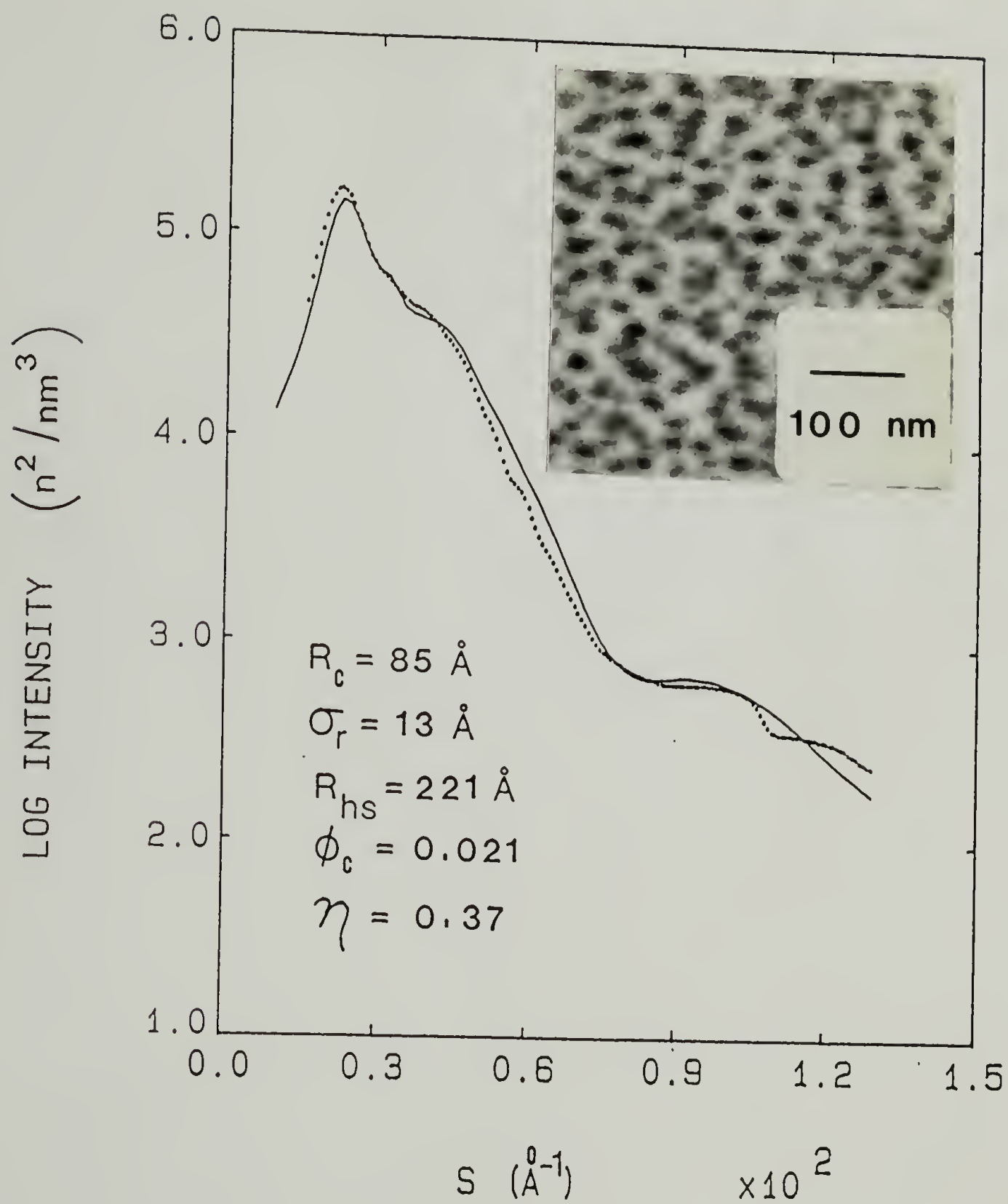


Figure 5.26 SAXS and EM results for 17.6 wt% SB 40/10 in 17000 PS.

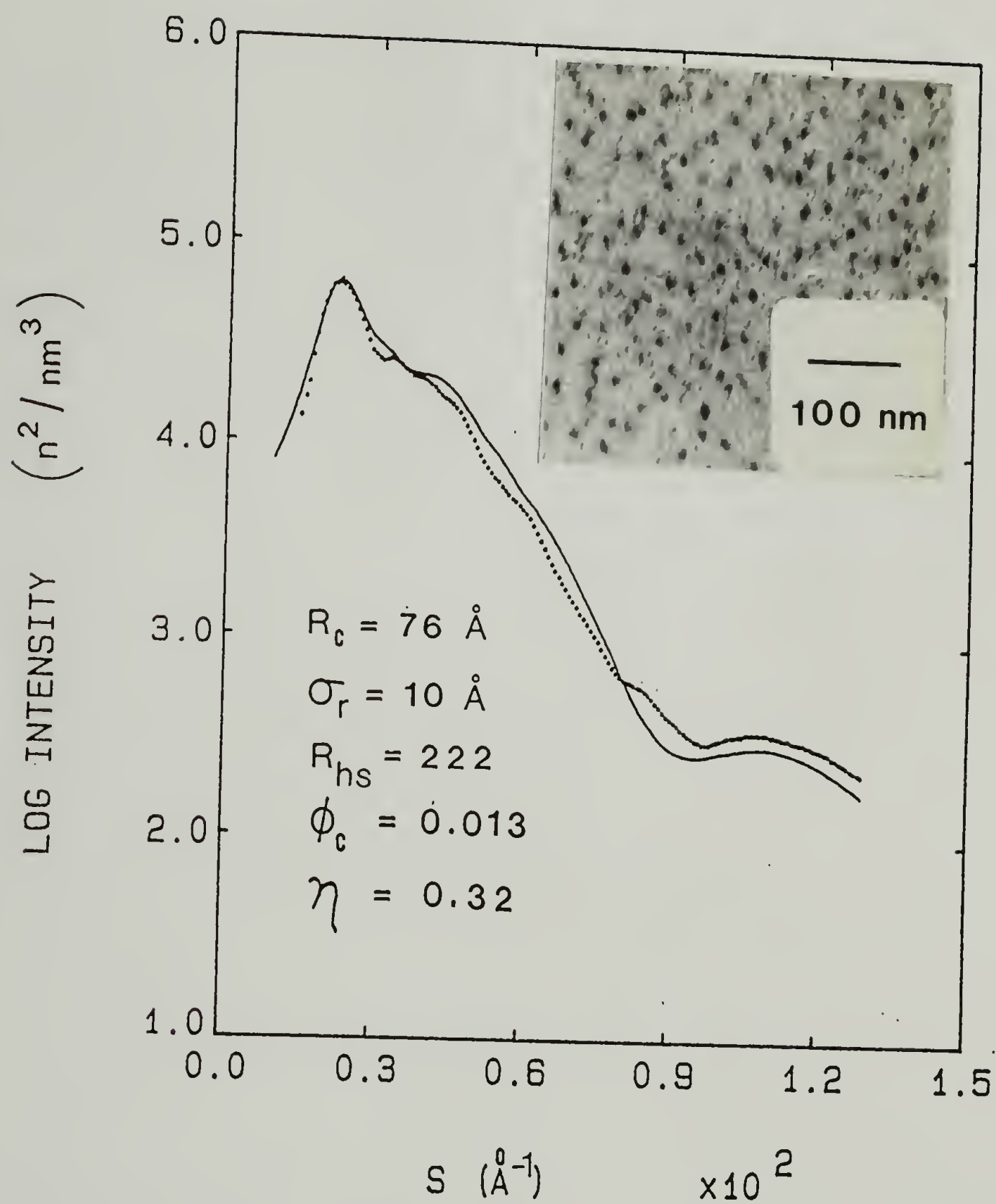


Figure 5.27 SAXS and EM results for 18.7 wt% SB 60/10 in 17000 PS.



for SB 23/10, SB 40/10, and SB 60/10 respectively. The ratio of experimental to theoretical invariants for these blends, taking these free copolymer concentrations into account, are all near unity as the triangular data points of Figure 5.24 show. Therefore, at 115 °C, the majority of phase mixing occurring for these blends is due to mixing of the copolymer into the homopolymer matrix, not mixing of homopolymer into the PB micelle core. These results are consistent with those found previously for the case of SB 20/20 in 2100 PS. In addition, from the parameters of best fit for these three blends it is evident that the core radius decreases and the corona thickness increases with increasing PS block length.

Figure 5.28 shows a log-log plot of  $(R_c / M_{hPS}^{0.17})$  versus polystyrene block molecular weight. The core radii were all determined from the PY modeling of the SAXS data, although the core radii measured from electron micrographs were generally in good agreement with those obtained from SAXS (within 10%). The core radii have been scaled according to the homopolystyrene molecular weight dependence found previously in Section 5.2.3 in order that core radii for different molecular weight homopolymers (7400 PS and 17000 PS) could be plotted on the same graph. It is immediately apparent that the core radii decrease with increasing PS block length. The scaling dependence of the core radii with polystyrene block length can be written as  $R_c \propto M_{PS}^{\alpha}$  where  $\alpha$  is found to be  $-0.20 \pm 0.05$ . This agrees rather well with the value of  $\alpha = -0.17$  determined from the data of Selb et al. [128] for SB

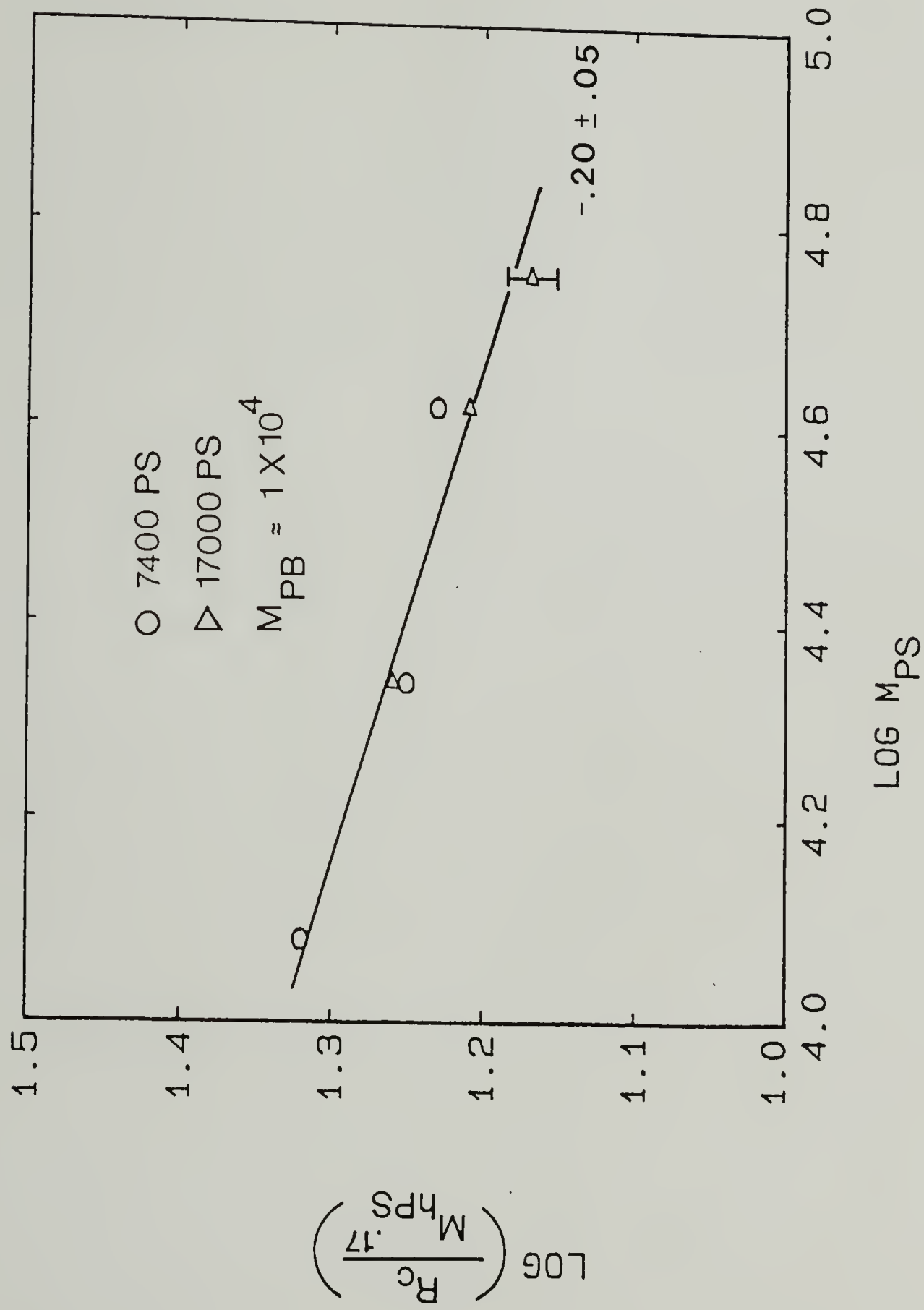


Figure 5.28 Micelle core radius as a function of PS block length.

copolymer/PB homopolymer blends. This phenomenon can be attributed to the same entropy of mixing effects which cause the core radius to decrease with decreasing homopolymer molecular weight. As the ratio of PS block to PS homopolymer molecular weight increases, the entropy of mixing effects tending to drive the homopolymer density towards a uniform value increase. As explained earlier, this will cause the volume fraction of corona to increase, partly by a reduction of the micelle core size. A comparison of the PB block end to end distances listed in Table 5.1 to the core radii for 7400 PS homopolymer reveals that the ratio  $R_c / \langle r^2 \rangle_{PB}^{1/2}$  decreases systematically from 1.08 for SB 10/10 to 0.84 for SB 60/10.

Figure 5.29 shows a log-log plot of  $(L_c / M_{hPS}^{-0.17})$  versus polystyrene block molecular weight. The corona thickness has been scaled with the homopolystyrene molecular weight dependence found previously in Section 5.2.4 in order that corona thicknesses found for different homopolystyrenes (7400 PS and 17000 PS) could be plotted on the same graph. As expected, the corona thickness increases with the molecular weight of the PS block. The scaling can be described by  $L_c \propto M_{PS}^\delta$  where  $\delta$  is found to be  $0.56 \pm 0.12$ . From the core radius, corona thickness, and molecular volumes of the PS and PB blocks, it is possible to calculate the volume fraction of homopolystyrene in the corona region. Figure 5.30 shows a plot of this volume fraction versus the ratio of homopolystyrene to PS block molecular weight. As expected, the solubility of homopolymer in the micelle corona decreases with increasing homopolymer molecular weight. However, even when  $M_{hPS} / M_{PS}$

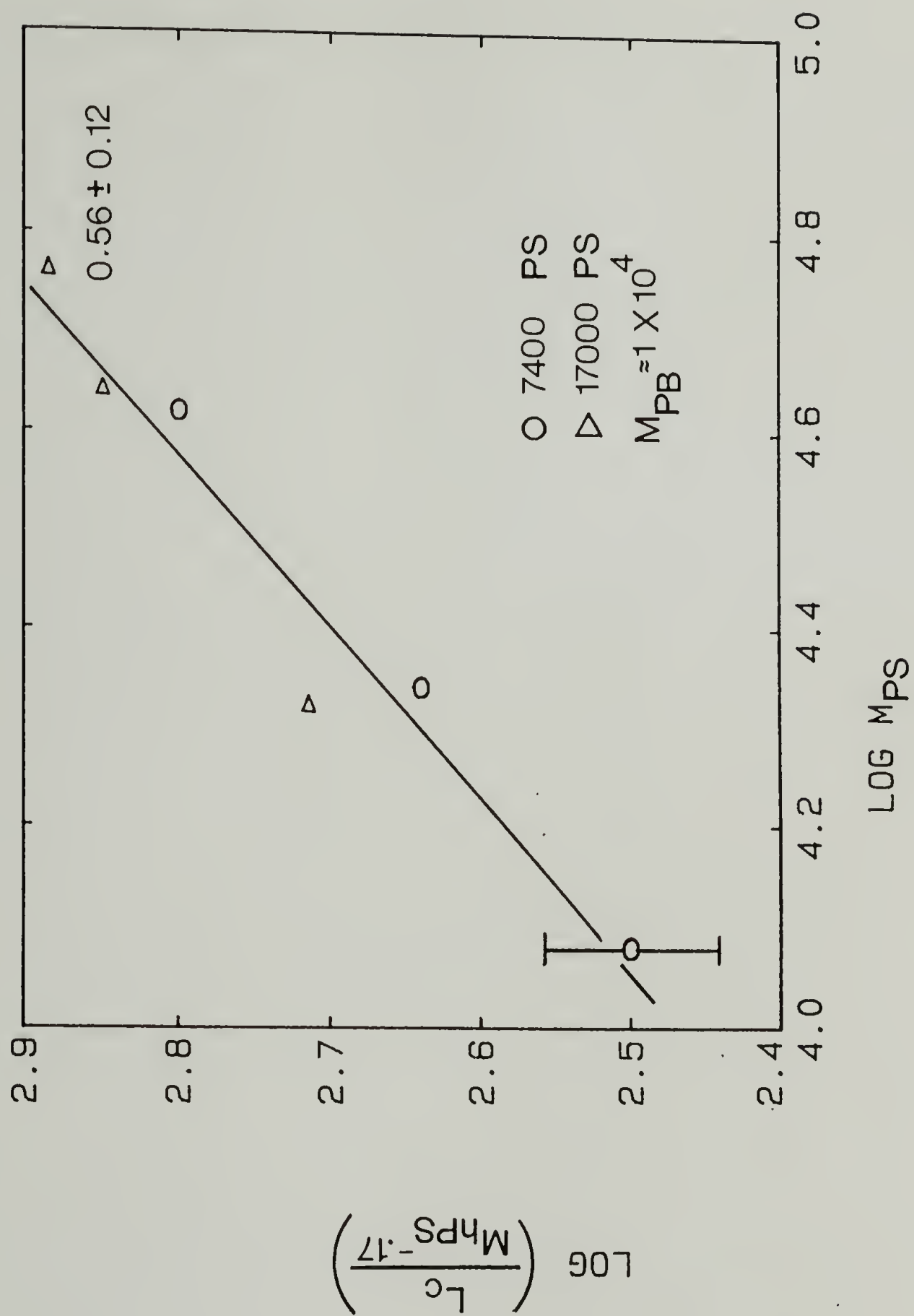


Figure 5.29 Corona thickness as a function of PS block length.



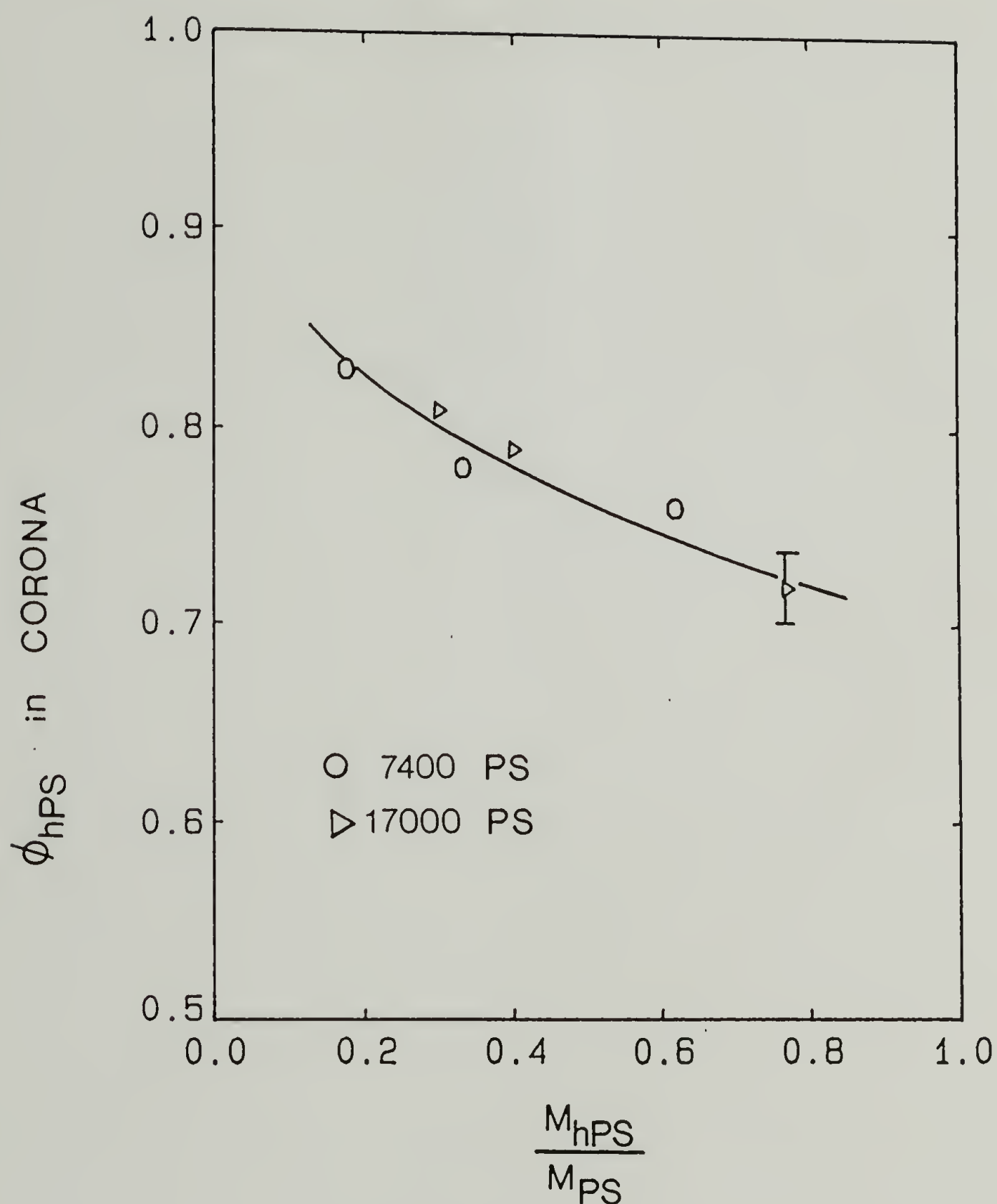


Figure 5.30 Volume fraction of homopolystyrene in the corona as a function of homopolystyrene to PS block molecular weight for copolymers SB 23/10, SB 40/10, and SB 60/10 in 7400 and 17000 PS homopolymer.

approaches unity, the volume fraction of homopolymer in the corona is still quite large (0.7). This means that the PS blocks should be stretched somewhat in the radial direction. Indeed, the ratio  $L_c / \langle r^2 \rangle_{PS}^{1/2}$  for 7400 PS increases from 0.96 to 1.06 as the PS block molecular weight is increased from 12,000 (SB 10/10) to 56,600 (SB 60/10). Therefore, one would expect that the value of  $\delta$  should be greater than the value of 0.5 for gaussian chains. This was indeed found to be the case, although the uncertainty in  $\delta$  is rather large.

### 5.3.2 Effect of PB block length

The copolymers SB 10/23 and SB 10/65 did not exhibit spherical micelles (except for SB 10/23 in 2100 PS); rather, wormlike (cylindrical) or lamellar micelles (e.g., spherical vesicle structures) were observed by electron microscopy. (This transition in micelle shape will be explored fully in Chapter VII.) Therefore, the effect of polybutadiene block length on the structure of spherical micelles could not be studied with these samples.

### 5.3.3 Effect of copolymer molecular weight

With copolymers SB 10/10, SB 20/20, SB 40/40, and SB 80/80, the effect of total copolymer molecular weight on the spherical micelle structure, at constant copolymer composition, can be examined. The data of Figure 5.15 show that at constant homopolymer molecular weight, the

cmc decreases with increasing copolymer molecular weight. This is the general trend predicted by the LOW and Whitmore-Noolandi theories of micelle formation in block copolymer/homopolymer blends. For example, for 3900 PS, the cmc for SB 10/10 and SB 20/20 are 2.7 and 0.16 wt% respectively. However, increasing the copolymer molecular weight further has much less of an effect on the cmc, except at lower homopolymer molecular weights.

Figures 5.32-5.34 show the EM and SAXS results for copolymers SB 10/10 (13.0 wt%), SB 40/40 (9.9 wt%), and SB 80/80 (9.9 wt%) in 7400 PS homopolymer. Recall that the results for copolymer SB 20/20 (12.3 wt%) in this same homopolystyrene were presented earlier in Figure 5.19. The ratio of the experimentally measured SAXS invariant to the invariant predicted assuming no phase mixing, other than the cmc, as a function of copolymer molecular weight for these four blends are shown as the circular data points in Figure 5.31. The dashed line indicates the decrease in this ratio calculated assuming a 20 Å interface thickness. All of the measured invariants are less than predicted (except for the blend containing SB 20/20) indicative of some additional phase mixing. In addition, the invariant ratio increases with increasing copolymer molecular weight. Once again, the modeling of the SAXS patterns can provide some insight as to the type of phase mixing occurring. Attempts at modeling the scattering patterns in Figures 5.32-5.34, assuming that there was no homopolymer in the micelle core, and that the concentration of free copolymer equaled the cmc, were

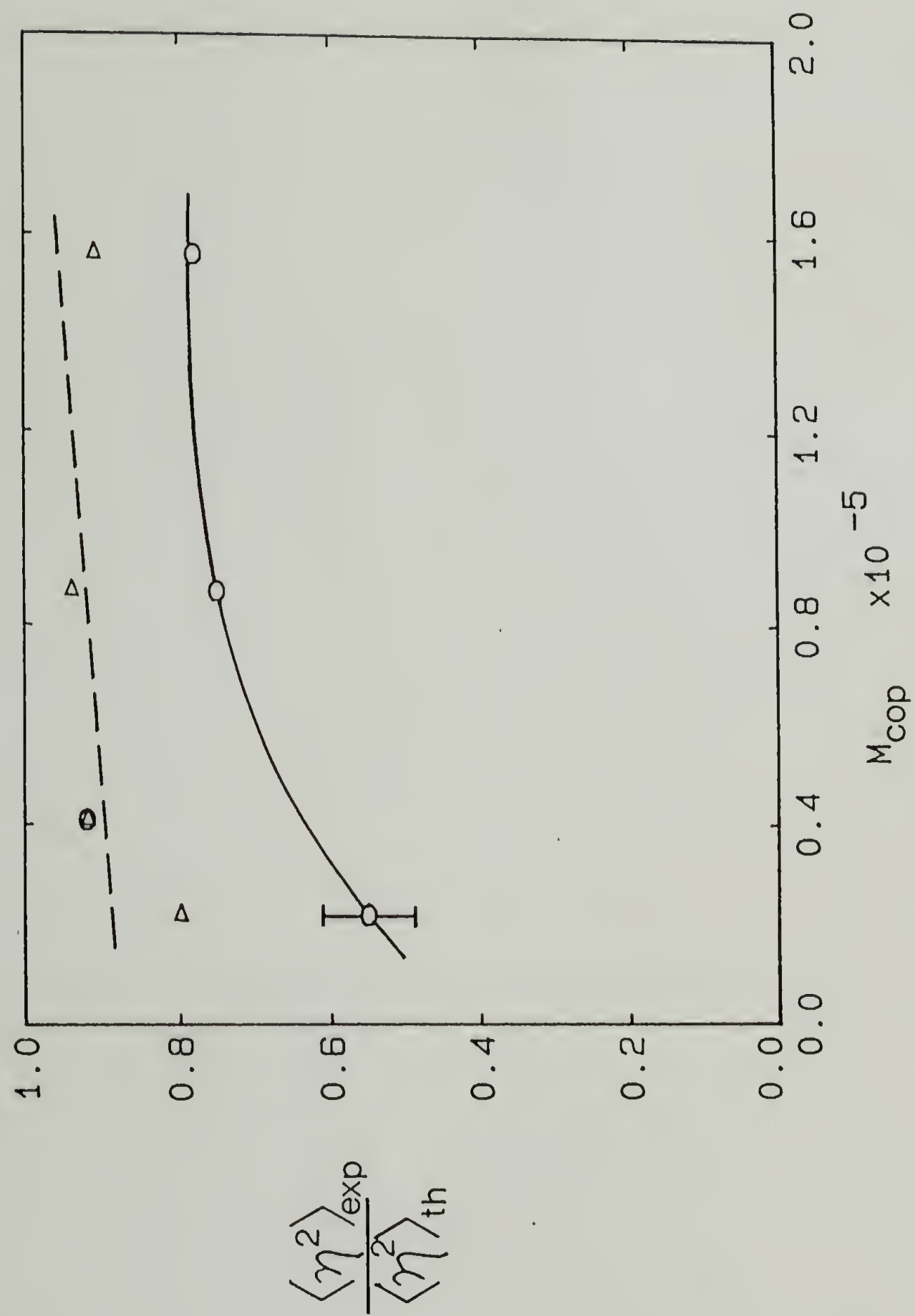


Figure 5.31 SAXS invariant as a function of copolymer molecular weight for copolymers SB 10/10, SB 20/20, SB 40/40, and SB 80/80 in 7400 PS homopolymer.



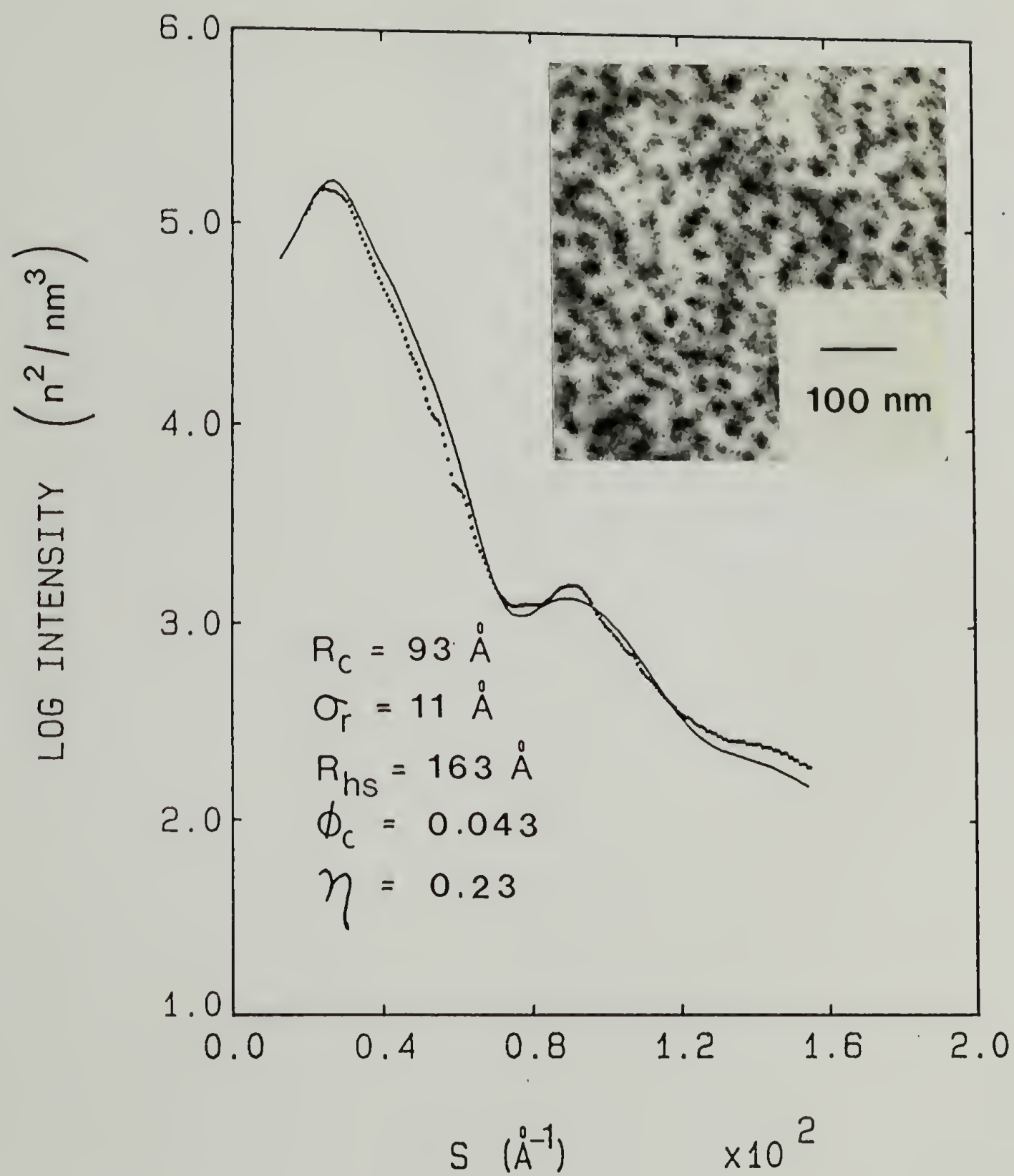


Figure 5.32 SAXS and EM results for 13.0 wt% SB 10/10 in 7400 PS.

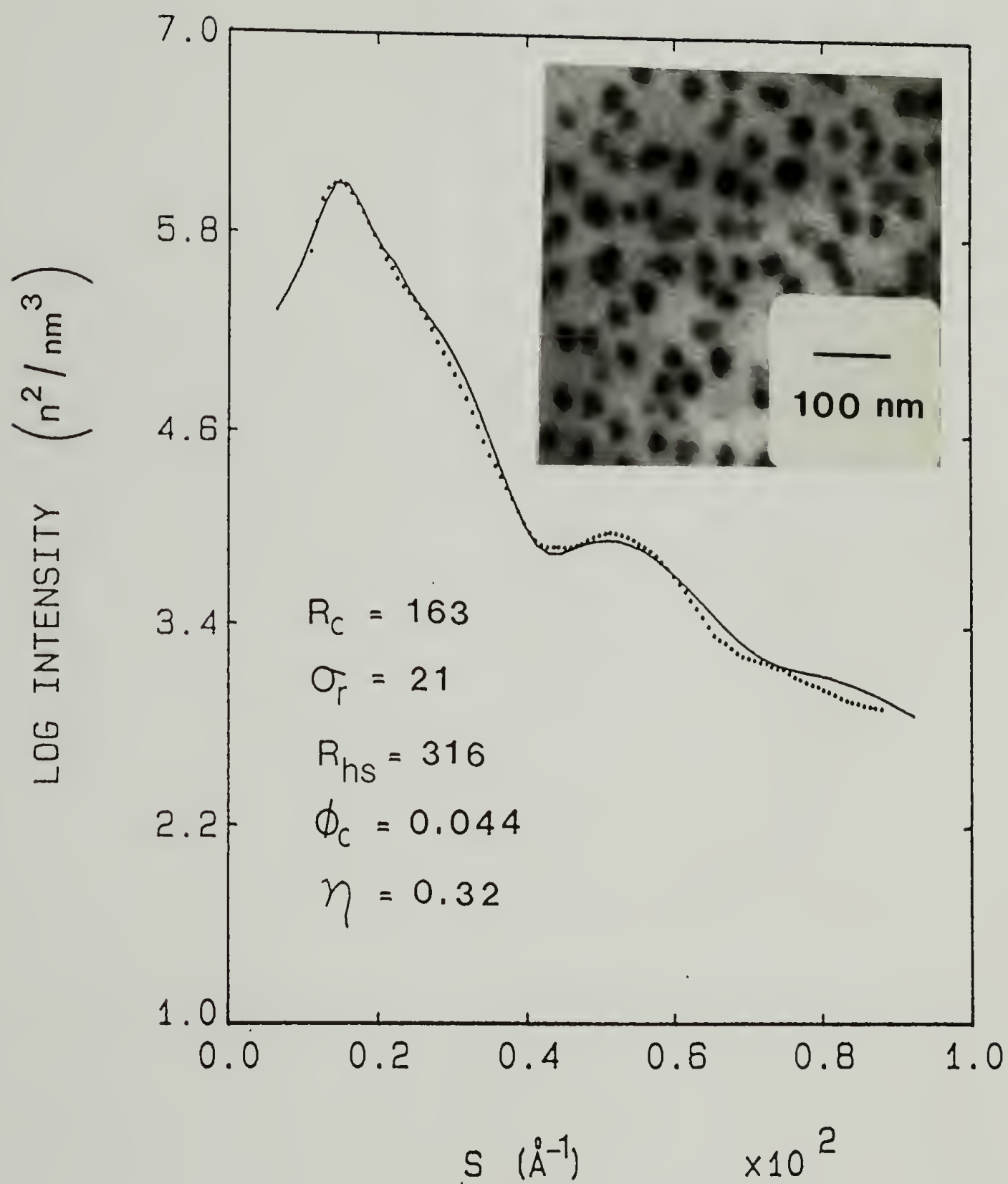


Figure 5.33 SAXS and EM results for 9.9 wt% SB 40/40 in 7400 PS.

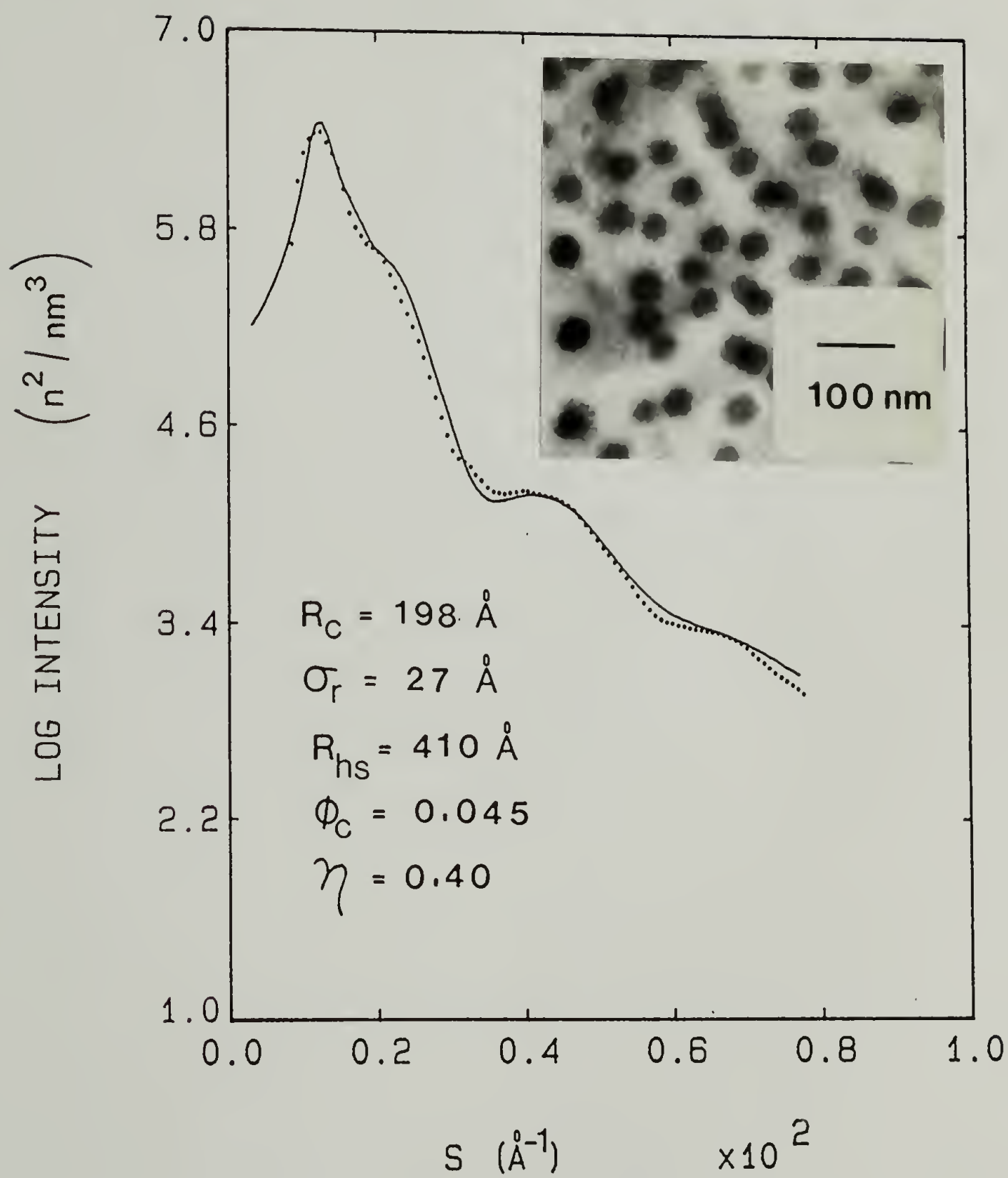


Figure 5.34 SAXS and EM results for 9.9 wt% SB 80/80 in 7400 PS.

unsuccessful at predicting the scattering in the interparticle interference region. For all three blends, the predicted positions of the interparticle interference peaks were at higher values of  $s$  than exhibited by the experimental data. Again, as discussed previously, this indicates that the amount of free copolymer must be greater than the cmc. By allowing  $\phi_c$ , i.e. the amount of free copolymer, to be an adjustable parameter, good fits between the predicted (solid lines) and actual data could be obtained. The results of the modeling indicate that the concentrations of free copolymer are 4.8, 2.7, and 2.0 wt% compared to the cmc values of 1.0, .15, and .13 wt% for copolymers SB 10/10, SB 40/40, and SB 80/80 respectively. The reason that the free copolymer concentration for copolymer SB 20/20 in 7400 PS is so low is not clear. Recall however, that for 12.5 wt% SB 20/20 in 2100 PS homopolymer, the concentration of free copolymer (3.5 wt%) was also found to be appreciably greater than the cmc (0.8 wt%). The ratios of experimental to theoretical invariants, taking these free copolymer concentrations into account, are shown as the triangular data points in Figure 5.31. They are very nearly equal to that predicted assuming a 20 Å interface thickness, except for the case of SB 10/10 for which the invariant is slightly less than the predicted value. Therefore, a small amount ( $\leq 10$  wt%) of homopolystyrene could be dissolved in the micelle core for this blend. The concentration of homopolymer in the core for higher copolymer molecular weights is negligible at the temperature studied (115 °C). As demonstrated in Section 5.2.2 for SB 20/20, the concentration of free copolymer decreases with increasing homopolymer



molecular weight. The same trend is observed for other copolymers. For example, the concentration of free copolymer for 10 wt% SB 80/80 in 17000 PS, determined from PY hard sphere modeling, is 0.9 wt%, compared to 2.0 wt% for 9.9 wt% SB 80/80 in 7400 PS.

As illustrated previously in Figure 5.20, the micelle core radius of copolymers SB 20/20, SB 40/40, and SB 80/80 in various molecular weight homopolystyrenes increases with copolymer molecular weight, as expected. For example, the core radius determined by SAXS for copolymers SB 10/10, SB 20/20, SB 40/40, and SB 80/80 in 7400 PS are 93, 147, 163, and 198 Å respectively (at about 10 wt% copolymer). This increase in core size can also be seen in the electron micrographs of these blends, from which the measured core radii are approximately 80, 130, 150, and 180 Å, in relatively good agreement with the values determined by SAXS. The polydispersity in core size, given by the ratio  $\sigma_r/R_c$ , is relatively constant ( $0.13 \pm 0.01$ ) for these four blends, implying that the polydispersity is not dependent on copolymer molecular weight.

The effect of PS block length on micelle core size has been found previously to follow the scaling law  $R_c \propto M_{PS}^{-0.20}$ . This relationship allows one to obtain the effect of the PB block length on core size, using copolymers SB 10/10 through SB 80/80. This is accomplished by normalizing the core radii with respect to  $M_{PS}^{-0.20}$ , as demonstrated by the data in Figure 5.35. In addition, the core radius has been shown to scale with  $M_{hPS}^{0.17}$ . Therefore, by normalizing the core radii with respect

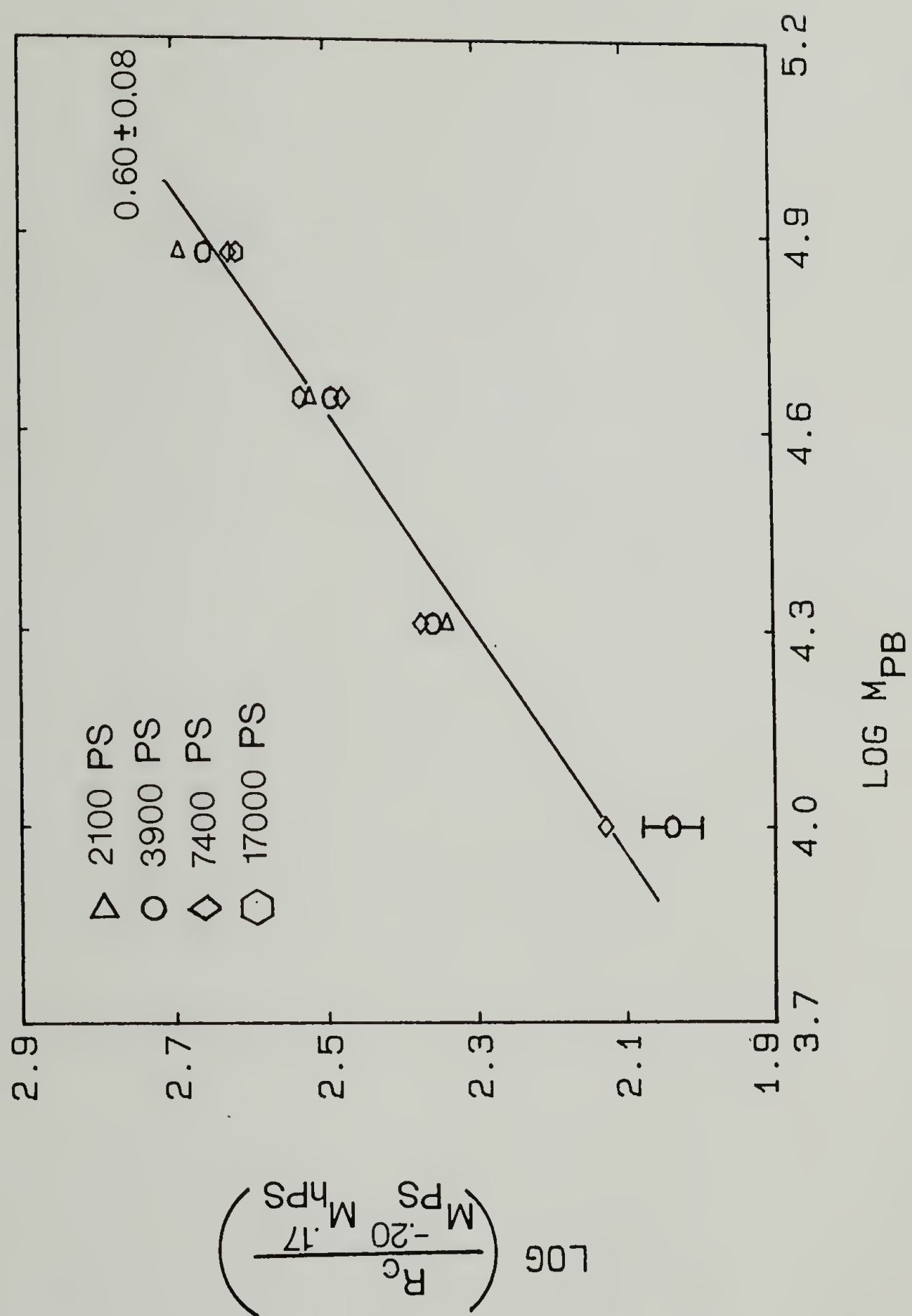


Figure 5.35 Core radius as a function of PB block length.

to  $M_{\text{hPS}}^{0.17}$ , core radii for several different molecular weight homopolymers can be employed to determine the scaling behavior of  $R_c$  with  $M_{\text{PB}}$ . From the log-log plot of  $(R_c/M_{\text{PS}}^{-0.20}M_{\text{hPS}}^{0.17})$  versus  $M_{\text{PB}}$  shown in Figure 5.35, it can be seen that  $R_c \propto M_{\text{PB}}^\beta$  where  $\beta = 0.60 \pm 0.08$ . This is slightly less than the value of 0.75 determined from the data of Selb et al., however, it falls within the range predicted by the theories of micelle formation [112,131]. The comparison between the experimental results presented in this chapter and the predictions of these micelle theories will be explored more fully in the next chapter.

As demonstrated by the data in Figure 5.21, the thickness of the micelle corona increases with the molecular weight of the copolymer. This increase is expected to occur as a result of increasing PS block length. Figure 5.36 shows a log-log plot of  $(L_c/M_{\text{hPS}}^{-0.17})$  versus  $M_{\text{PS}}$  for copolymers SB 10/10 through SB 80/80 in several different molecular weight homopolystyrenes. The corona thickness has been scaled by  $M_{\text{hPS}}^{-0.17}$  to account for the effect of homopolymer molecular weight on corona thickness determined previously (see Figure 5.21). It is assumed that the PB block length has little influence on the corona thickness. Within the error of the measurement of  $L_c$ , this assumption is found to hold. The scaling of corona thickness with PS block length is determined to be  $L_c \propto M_{\text{PS}}^\delta$  where  $\delta = 0.60 \pm 0.06$ , which is in good agreement with the scaling behavior observed previously for the series of copolymers in which the PS block length was varied and the PB block length was kept constant (see Figure 5.29). A value of  $\delta = 0.5$  would apply if the PS block chains possessed gaussian conformations. A value

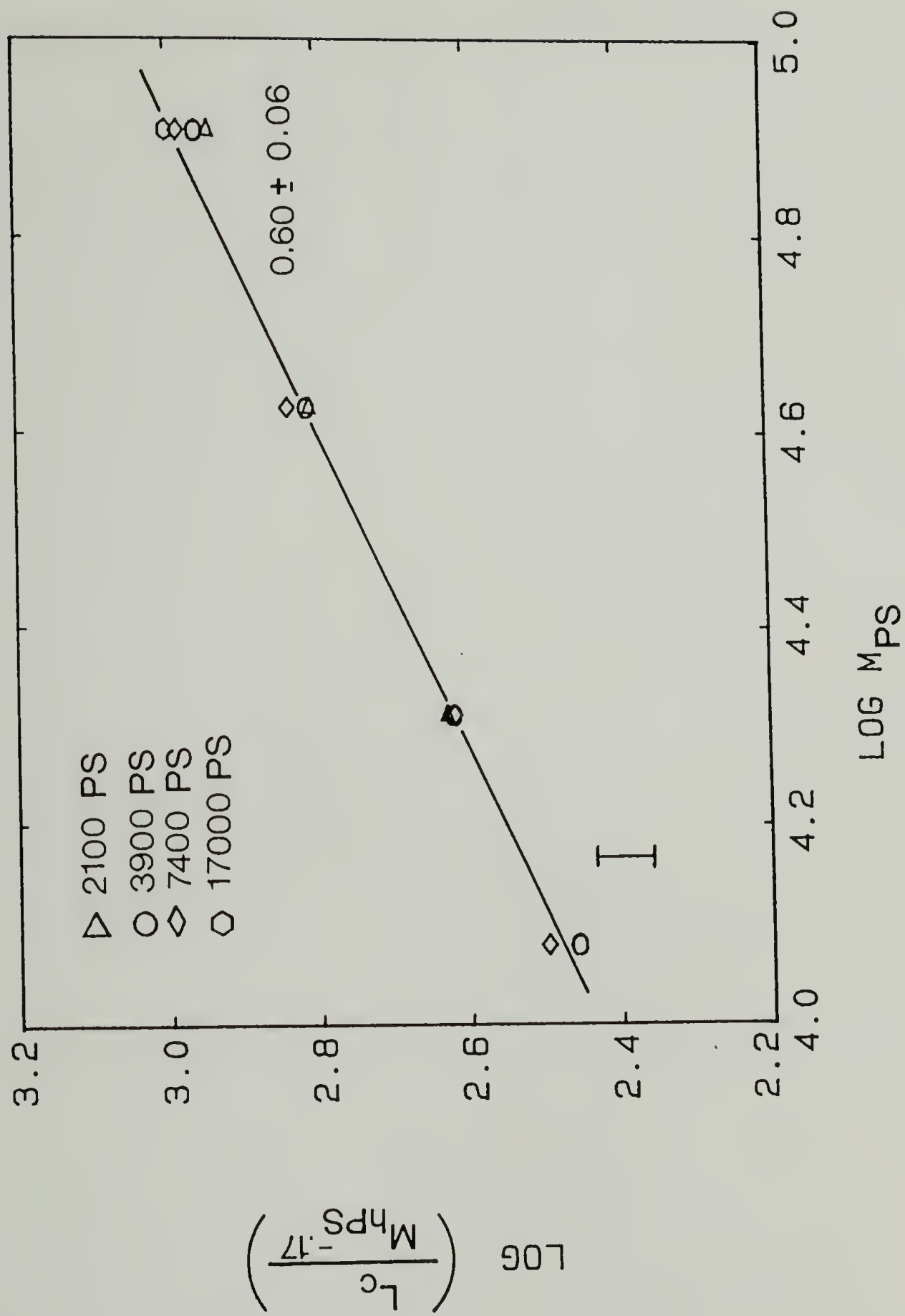


Figure 5.36 Corona thickness as a function of PS block length.



greater than 0.5, such as that observed here, implies that the PS block chains are stretched in the radial direction.

In summary, this section has examined the effect of PS block length, PB block length, and overall copolymer molecular weight on the micellar structure of poly(styrene-butadiene) diblock copolymer/polystyrene homopolymer blends. For a given homopolymer molecular weight, the critical micelle concentration was observed to increase with increasing amount of PS in the copolymer or decreasing overall copolymer molecular weight (at a fixed copolymer composition), as a result of increasing compatibility of copolymer and homopolymer. In addition, the SAXS invariant was found to decrease with increasing PS block length (at a fixed PB block length) or decreasing overall copolymer molecular weight (at a fixed copolymer composition), indicating an increased mixing of the PB block and PS homopolymer. By combining the invariant analysis with PY hard sphere modeling of the SAXS data, it was determined that this decrease in the invariant was due mainly to an increase in the amount of free copolymer, above the cmc, with increasing copolymer concentration. The amount of PS homopolymer in the PB micelle core was found to be small for all copolymer/homopolymer blends investigated. It was also observed that the spherical PB micelle core radius increased with increasing PB block length, according to the scaling law  $R_c \propto M_{PB}^{0.60 \pm 0.08}$ , and decreasing PS block length, according to the scaling law  $R_c \propto M_{PS}^{-0.20 \pm 0.05}$ , over the range of block molecular weights studied. In addition, the thickness of the micelle corona was observed to increase with increasing

PS block length according to the scaling law  $L_c \propto M_{PS}^{0.60 \pm 0.06}$ . It was also noted that a transition from spherical to non-spherical micelles occurred with increasing amount of PB in the copolymer. This will be discussed further in Chapter VII. The experimental results for the copolymer/homopolymer blends exhibiting spherical micelles will be compared to the predictions of the LOW theory of micelle formation [112] in the following chapter, but first, the evidence for a SC lattice structure in block copolymer/homopolymer blends exhibiting an ordered arrangement of spherical micelles will be presented.

#### 5.4 Lattice Structure of Ordered Micellar Phase

As discussed in Section 5.1, a transition from a disordered liquid-like to an ordered lattice arrangement of spherical micelles is expected to occur as the copolymer concentration is increased, and the coronae from neighboring micelles begin to overlap. This was indeed found to be the case for copolymer SB 20/20 in 3900 PS homopolymer; the electron micrographs and SAXS patterns for copolymer concentrations of 24.9 wt% (Figure 5.9) and 30.3 wt% (Figure 5.10) clearly showed the existence of an ordered lattice of micelles. From the relative positions of the SAXS lattice peaks, it was determined that either a SC or BCC lattice existed (these two lattice types have the same relative spacings until the seventh order).

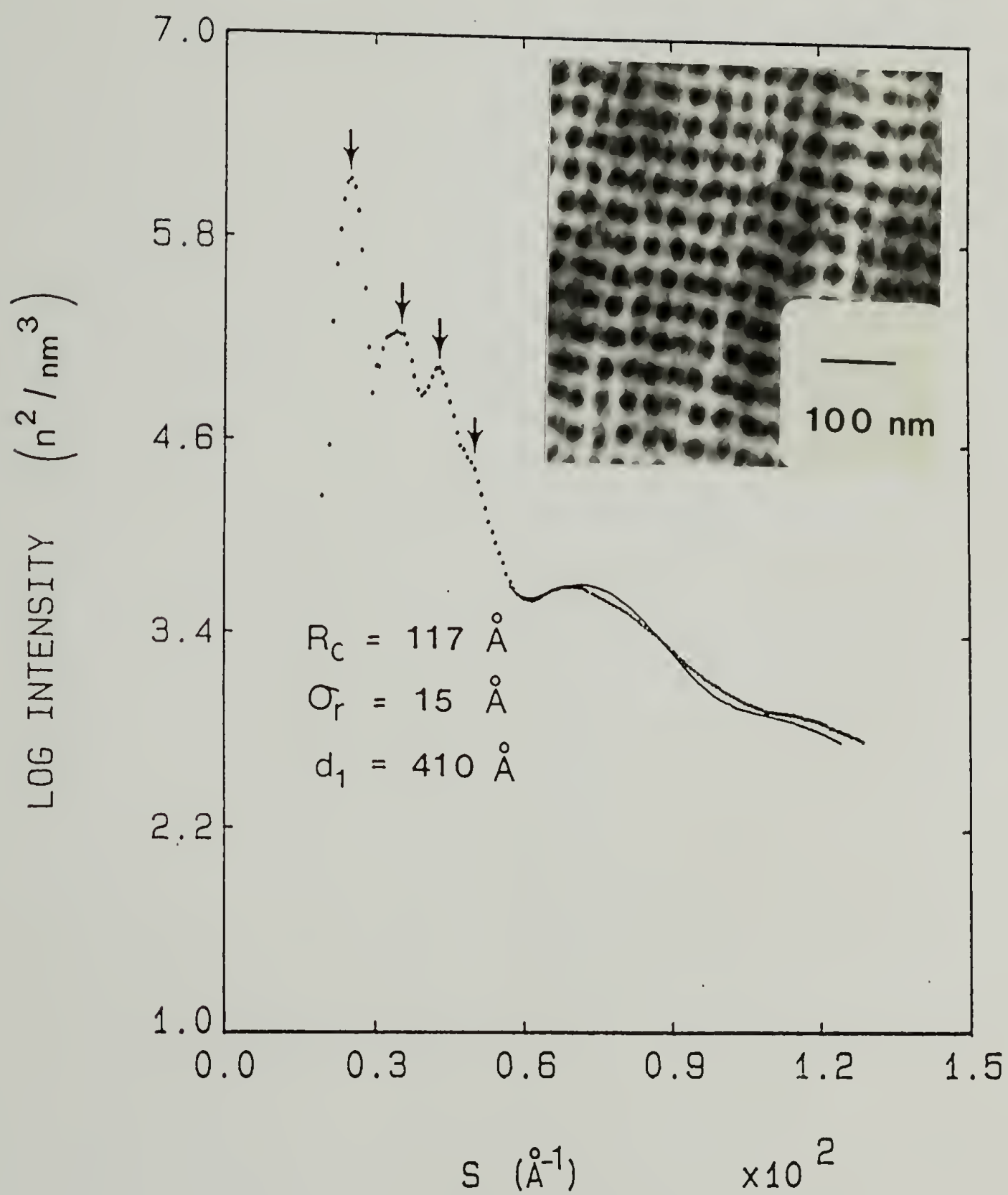


Figure 5.37 SAXS and EM results for 17.8 wt% SB 20/20 in 2100 PS.

Ordered micellar structures have also been observed for other copolymer/homopolymer pairs; for example, Figure 5.37 shows the EM and SAXS results for 17.8 wt% SB 20/20 in 2100 PS. The electron micrograph shows an ordered (square) array of PB micelle cores, while the SAXS pattern exhibits four lattice reflections whose relative spacings agree with those predicted for a SC or BCC lattice (marked by the arrows). The solid line shows the best fit to the data using a model for a polydisperse system of spheres, neglecting interparticle interference effects (i.e., setting  $S(h)=1$ ).

The EM and SAXS results for 24.2 wt% SB 20/20 in 7400 PS are shown in Figure 5.38. It is evident that the second and third lattice peaks are not nearly as well defined as those of the previous sample; nevertheless, they are in the predicted positions for a SC or BCC lattice (see arrows). This observation is borne out in the electron micrograph (upper right corner of Figure 5.38) which shows that the lattice is not very well developed, although small regions of local order are present. When the copolymer concentration is increased to 30.9 wt%, the long range order is greatly increased, as evidenced by the electron micrograph in the lower right corner of Figure 5.38. In addition, the SAXS pattern (not shown) for the blend containing 30.9 wt% copolymer, exhibits three well defined lattice peaks, similar to those of Figure 5.37. It appears therefore, that for SB 20/20 in 7400 PS, a copolymer concentration of 24.2 wt% is very nearly the concentration at which the transition from a disordered liquid-like to ordered lattice arrangement of micelles occurs. Using the corona thickness of  $92 \pm 7$  Å,



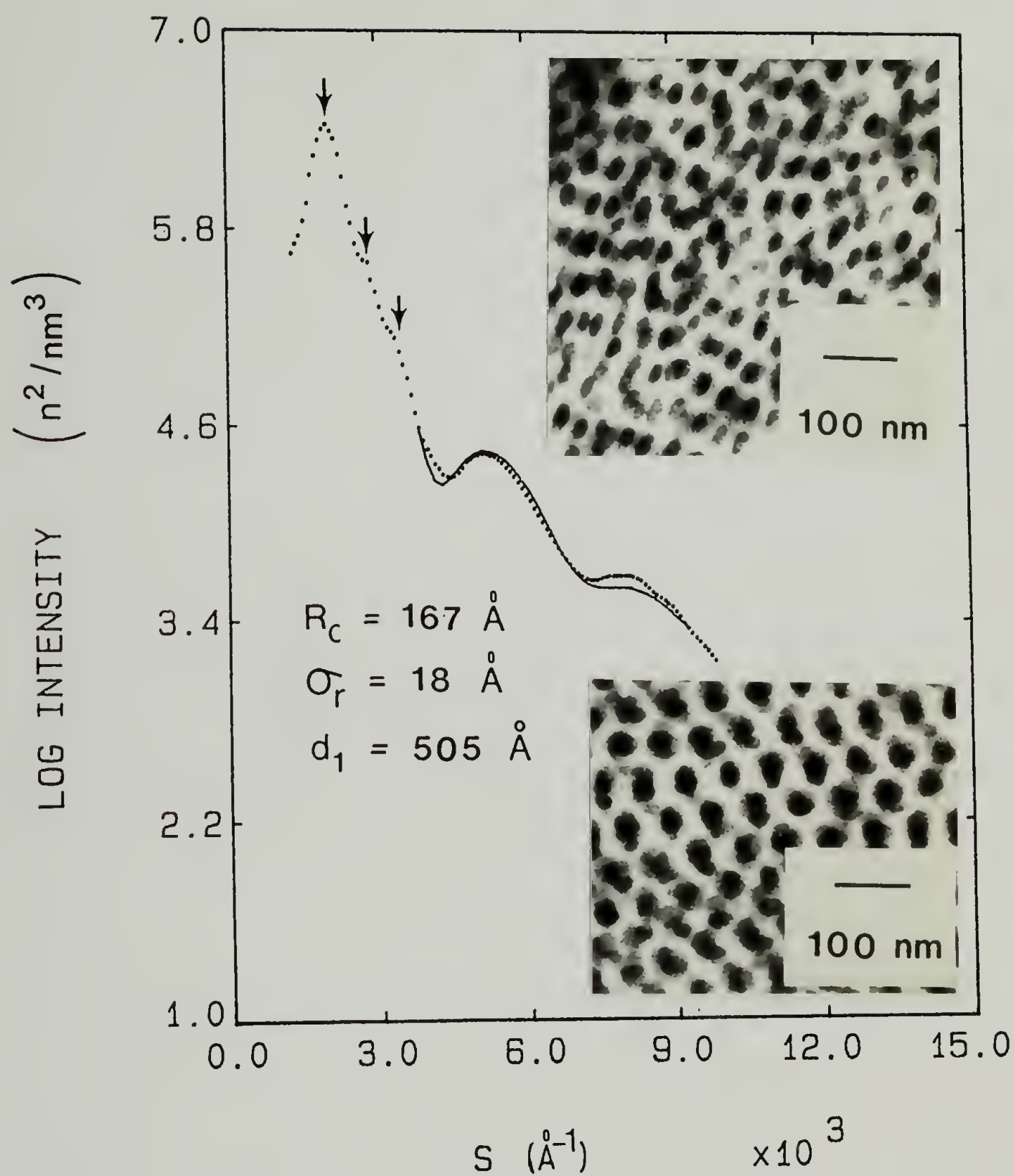


Figure 5.38 SAXS and EM results for 24.2 wt% SB 20/20 in 7400 PS. The electron micrograph for 30.9 wt% SB 20/20 in 7400 PS is shown in the lower right corner.

determined previously for 12.3 wt% SB 20/20 in 7400 PS, and a core radius of 167 Å, determined from fitting the scattering in the higher angle region (solid line in Figure 5.38), a value of  $0.52 \pm 0.06$  for the micelle volume fraction is calculated. As discussed in Section 3.3.1.2, statistical mechanical modeling of systems of hard spheres indicates that a first order liquid-solid phase transition should occur for an overall hard sphere volume fraction greater than about 0.50. It is not known whether the ordering transition of the spherical micelles observed here is a first order phase transition, i.e., whether phases with disordered arrangements (liquid phase) and ordered arrangements (solid phase) of micelles exist simultaneously. In any case, the volume fraction of micelles at which the ordering is found to occur is very nearly that predicted for a system of hard spheres undergoing a liquid to solid first order phase transition.

Table 5.2 lists the spacings of the first lattice peak  $d_1$  and the average radii of the micelle cores  $R_c$ , determined by SAXS, for copolymer SB 20/20 in 2100 PS (17.8 wt%), 3900 PS (24.9 and 30.3 wt%), and 7400 PS (24.2 wt%). The volume fraction of micelle cores calculated from these values for both SC ( $\phi_{SC}$ ) and BCC ( $\phi_{BCC}$ ) lattices are also listed. It was determined previously that the amount of homopolymer in the micelle cores for these blends was very small; therefore, in the analysis that follows, it will be assumed that there is no homopolymer in the cores. The invariant analysis and SAXS modeling also indicated that the amount of free copolymer for the blends having 3900 and 7400 PS homopolymer was

TABLE 5.2

Determination of lattice type for copolymer SB 20/20

$M_{hPS}$	wt% copolymer forming micelles	$\phi_c$	$d_1$ (Å) ( $\pm 10$ )	$R_c$ (Å) ( $\pm 3$ )	$\phi_{SC}$	$\phi_{BCC}$
2100	14.3	0.083	410	117	0.097	0.069
3900	24.7	0.141	450	146	0.143	0.101
3900	30.1	0.172	410	139	0.163	0.115
7400	24.1	0.139	505	167	0.151	0.107

very nearly equal to the critical micelle concentration. On the other hand, blends with 2100 PS homopolymer were found to contain free copolymer in excess of the critical micelle concentration. The amount of free copolymer for the 17.8 wt% SB 20/20 in 2100 PS blend cannot be determined using the PY hard sphere fluid model since it is an ordered system. However, on the assumption that the concentration of free copolymer for the 17.8 wt% blend is equal to that for the blend containing 12.5 wt% copolymer (3.5 wt%), the ratio of experimental to predicted invariant is 0.89, compared to the value of 0.92 calculated for the case of a 20 Å interface width. Therefore 3.5 wt% seems like a reasonable approximation of the concentration of free copolymer for the blend containing 17.8 wt% copolymer.

The volume fraction of micelle cores can then be calculated from the wt% copolymer forming micelles and the densities of PS and PB (at 25 °C). A comparison of the volume fraction of micelle cores thus determined to the volume fraction of micelle cores calculated assuming a SC or BCC lattice shows that the SC lattice is favored in the case of 3900 PS and 7400 PS homopolymer. The results for 2100 PS homopolymer are less conclusive however. The value of  $\phi_c$  is about halfway between the volume fractions calculated for the SC and BCC lattices. It should be remarked that the values of  $\phi_{SC}$  and  $\phi_{BCC}$  have a large degree of uncertainty associated with them since  $d_1$  and  $R_c$  are both cubed in the volume fraction calculations (see Equations 2.20 and 2.21). Therefore, any errors in these values will be greatly magnified. For example, by increasing  $d_1$  by 10 Å and decreasing  $R_c$  by 3 Å, a value of  $\phi_{SC} = 0.084$



is obtained (compared to 0.097). For this reason, a more conclusive determination of the type of lattice present in these blends should be carried out by employing the electron microscopy tilting method outlined in Section 3.1.3 and used in Appendix B to show that neat block copolymers having spherical domains exhibit a BCC lattice structure. Such a study remains to be performed for copolymer/homopolymer blends. It is interesting to recall that the results of Shibayama et al. [116] (from SAXS based volume fraction calculations) indicated that a SC lattice was also present in their blends of SB diblock copolymer and preferential solvent (n-tetradecane, a preferential solvent for PB). The reasons for the different lattice structures of neat copolymers and copolymers blended with a preferential solvents (such as homopolymer), surely must lie in the different chain packing requirements. The block chains comprising the matrix phase in neat block copolymers must fill the matrix phase uniformly (i.e., a constant segment density must be maintained) due to incompressibility. This requires that some chains be deformed to fill the interstices between the spherical domains, which is entropically unfavorable. The lattice structure which requires the least deformation of these chains (BCC) is the one which is energetically favored. In contrast, the matrix block chains of copolymer/homopolymer blends do not have to fill the matrix uniformly. Local variations in block chain segment density can be compensated for by the mobile homopolymer chains.

# C H A P T E R VI

## COMPARISON OF EXPERIMENTAL RESULTS AND THEORETICAL PREDICTIONS FOR SPHERICAL MICELLAR SYSTEMS

In this chapter, the experimental results presented in Chapter V for poly(styrene-butadiene) diblock copolymer/polystyrene homopolymer blends exhibiting spherical micelles will be critically compared to the predictions of the Leibler, Orland, and Wheeler (LOW) theory of micelle formation in diblock copolymer/homopolymer blends [112], as extended by Roe [133] to allow for the case of asymmetrical copolymers and the possibility of homopolymer residing in the micelle core. The theory of micelle formation presented by Whitmore and Noolandi [131] is essentially the same as the LOW theory, and is therefore expected to give similar results.

At a fixed volume fraction  $\phi$  of copolymer and a fixed temperature (i.e., a fixed polystyrene-polybutadiene interaction energy density) the parameters which characterize the structure of the micellar system are: (1)  $p$ , the number of copolymer chains per micelle, (2)  $\zeta$ , the fraction of copolymer chains which aggregate into micelles, (3)  $\eta_A$ , the fraction of PS monomers in the corona which belong to copolymer chains, and (4)  $\eta_B$ , the fraction of the micelle core which is made up of PB monomers. The equilibrium values of  $p$ ,  $\zeta$ ,  $\eta_A$ , and  $\eta_B$  can be found by minimizing the total free energy of the micellar system with respect to these quantities. Roe [133] has recast the free energy equations of the LOW theory in terms of molecular volumes and root mean square end to end

distances of the individual homopolymer chains and copolymer blocks, thereby avoiding the somewhat ambiguous concept of segment size and the number of segments per molecule (see Equation 3.12). He has also replaced the interaction parameter  $\chi$  with  $\Delta$ , the interaction energy density (see Equation 3.13). Roe has written a computer program to perform the free energy minimization, from which the equilibrium values of  $p$ ,  $\zeta$ ,  $\eta_A$ , and  $\eta_B$  can be obtained, for a given copolymer/homopolymer blend, as a function of copolymer concentration and temperature. Roe has kindly made this program available to the author. All of the theoretical predictions of micellar structure presented in this chapter have been calculated using this program. The parameters which must be input to the program include the temperature, the volume fraction of copolymer monomers, the molecular weights of the homopolymer and copolymer blocks, the PS and PB specific volumes as a function of temperature, the PS-PB interaction energy density as a function of temperature, and the root mean square end to end distances and molecular volumes of the PS and PB chains.

The specific volume ( $\text{cm}^3/\text{g}$ ) of PB as a function of temperature is given in the Polymer Handbook [142]

$$V_{\text{PB}} = 1.0968 + (8.24 \times 10^{-4})T \quad (6.1)$$

while the specific volume of PS as a function of temperature, above its glass transition temperature, has been given by Richardson and Savill [143]

$$v_{PS} = 0.9217 + (5.412 \times 10^{-4})T + (1.687 \times 10^{-7})T^2 \quad (6.2)$$

where  $T$  is in  $^{\circ}\text{C}$ . The PS-PB interaction energy density as a function of temperature has been determined by Roe and Zin [134], from cloud point measurements, to have the functional form given previously by Equation 3.15. In addition, the unperturbed root mean square end to end distances of PS [142] and PB [142,144] have been found to have the following form (recall Section 5.2.3),

$$\langle r^2 \rangle_{PB}^{1/2} = 0.89 M_{PB}^{1/2} \quad (6.3a)$$

$$\langle r^2 \rangle_{PS}^{1/2} = 0.67 M_{PS}^{1/2} \quad (6.3b)$$

and the molecular volumes of the PS and PB chains are given by the relation

$$v_i (\text{\AA}^3) = \frac{M_i (\text{Kg/mole})}{\rho_i (\text{g/cm}^3) 0.602} \quad (6.4)$$

In this chapter, the comparison of the experimental results of Chapter V to the theoretical predictions of the LOW theory, as modified by Roe, will be divided into four sections. The first section examines the critical micelle concentration, the second section examines phase mixing, i.e., the values of  $\eta_B$  and  $\zeta$ , the third section examines the size of micelle cores, and the last section examines the thickness of micelle coronae.



### 6.1 Critical Micelle Concentration

In this section, the experimentally determined critical micelle concentrations, as a function of homopolymer and copolymer block molecular weights, will be compared to the predictions of the LOW theory, as modified by Roe. The theory predicts that the cmc decreases with increasing homopolymer molecular weight. In addition, the cmc is predicted to increase with increasing PS block length (i.e., the amount of PS in the copolymer) and decreasing copolymer weight (for constant copolymer composition). These are the same trends observed experimentally. For example, the critical micelle concentrations determined experimentally for copolymers SB 10/10, SB 40/10, and SB 20/20 (at 115 °C) as a function of homopolystyrene molecular weight are shown in Figure 6.1 (solid lines) along with the predictions of the LOW theory (dashed lines). The predicted cmc values are in qualitative agreement with those found experimentally. However, it is immediately apparent, from Figure 6.1, that the LOW theory predicts cmc values which are 1-2 orders of magnitude smaller than those observed experimentally. This has also been found by Roe [133] (from plots of  $I(0)$  versus copolymer concentration) for poly(styrene-butadiene) diblock copolymers in polybutadiene homopolymer. One possible explanation for this discrepancy could be that the value of the interaction energy density used in the calculations is larger than the actual value at 115 °C, which would lead to lower cmc values. For example, increasing the temperature at which the LOW calculations are made from 115 °C to 150

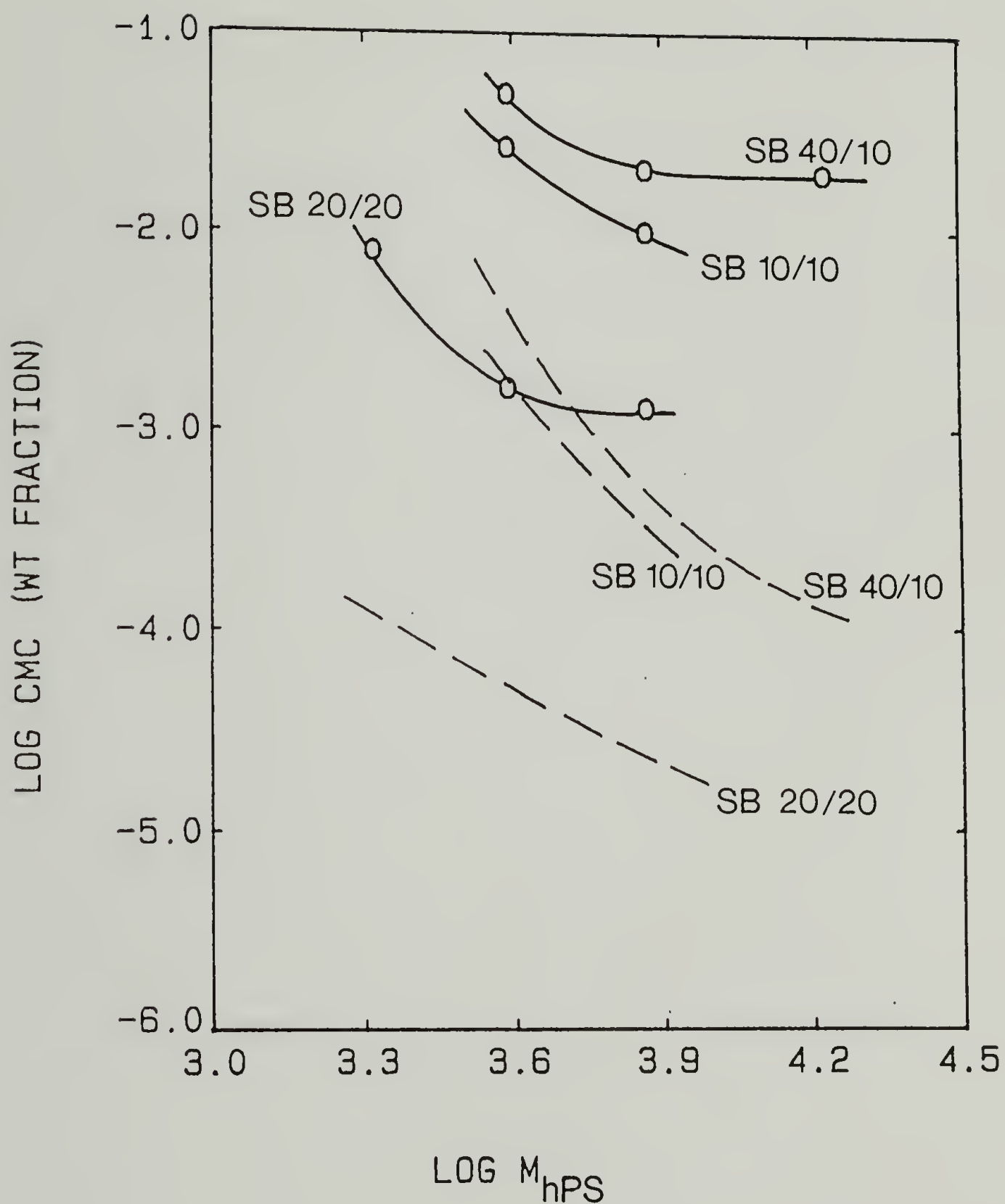


Figure 6.1 Comparison of experimentally determined (solid lines) and theoretically predicted (dashed lines)  $cmc$  values for SB 10/10, SB 40/10, and SB 20/20 at 115 °C.

$^{\circ}\text{C}$ , which corresponds to decreasing the interaction energy density from 0.79 to 0.72 cal/cm<sup>3</sup> (within the error in the measurement of the interaction energy density), results in a calculated cmc of 0.8 wt% SB 20/20 in 2100 PS homopolymer, which agrees with the cmc found experimentally. Alternatively, one or more of the expressions used in the LOW theory for calculating the various contributions to the micelle free energy (such as the interfacial energy, the deformation energy, or the entropy of mixing) could be inexact. For example, the theory assumes that the corona region has a uniform density of homopolymer chains, which may not be the case. If these expressions lead to a calculated micelle free energy which is too large, the theory would predict cmc values which are too small.

## 6.2 Phase Mixing

It was observed experimentally, using SAXS invariant analysis, that some mixing of the PS and PB chains, beyond that due to the cmc, sometimes occurred. In all of the cases where this additional mixing occurred, it was determined, by a combination of SAXS invariant analysis and PY modeling of the SAXS patterns, that the main type of mixing was an increase in the amount of free copolymer (above the cmc) dissolved in the copolymer matrix. For example, Figure 6.2 shows the experimentally determined values of  $\zeta$ , the fraction of copolymer which forms micelles, and  $n_B$ , the fraction of the micelle core consisting of PB blocks (at 115  $^{\circ}\text{C}$ ), for copolymer SB 20/20 ( $\approx 12.5$  wt%) as a function of

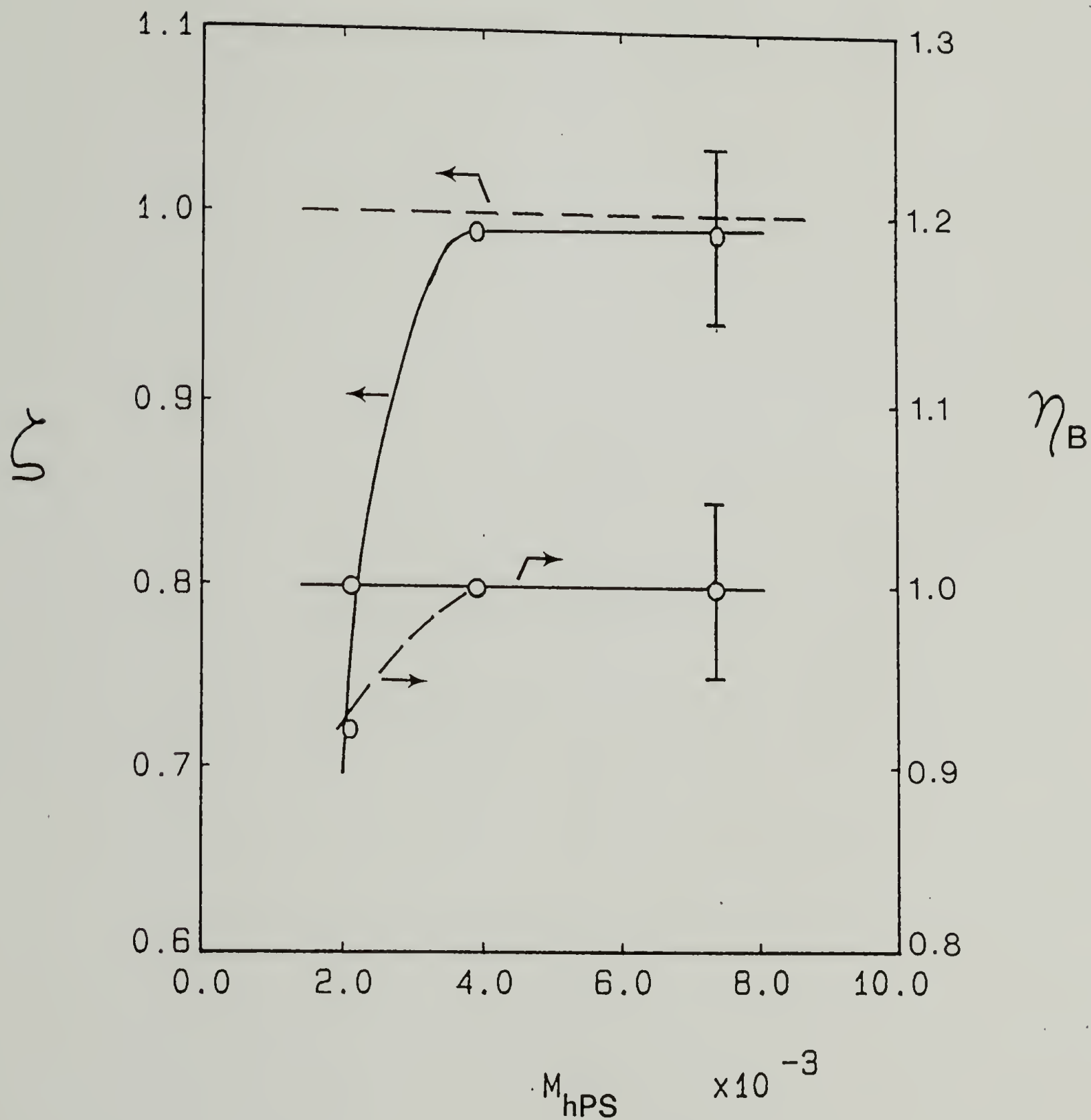


Figure 6.2 Comparison of experimentally determined (solid lines) and theoretically predicted (dashed lines) values of  $\zeta$  and  $\eta_B$  for SB 20/20 ( $\approx 12.5$  wt%) at  $115^\circ\text{C}$  as a function of  $M_{hPS}$ .



homopolystyrene matrix molecular weight. While  $\zeta$  was found to decrease markedly from 0.99 for 7400 PS homopolymer to 0.71 for 2100 PS homopolymer,  $\eta_B$  was found to remain approximately constant at unity. The dashed lines in Figure 6.2 show the predictions of the LOW theory at 115 °C:  $\zeta$  is predicted to remain approximately constant at unity, while  $\eta_B$  is predicted to decrease to a value of 0.93 for 2100 PS homopolymer. In other words, the LOW theory predicts that as the homopolymer molecular weight is decreased to 2100, the majority of phase mixing (at 115 °C) is due to a slight mixing of homopolymer into the micelle core, which disagrees with the experimental findings. However, since the theory greatly underestimates the critical micelle concentration at 115 °C (as the results of Figure 6.1 showed), it is also expected to underestimate the amount of free copolymer at 115 °C.

Figure 6.3 shows the values of  $\zeta$  and  $\eta_B$  predicted by the LOW theory as a function of temperature for 12.5 wt% SB 20/20 in 2100 PS homopolymer. It is apparent that the value of  $\eta_B$  decreases only slightly with temperature, while  $\zeta$  decreases rather abruptly above 180 °C. Therefore, the experimentally observed structure of the blend at 115 °C corresponds to the structure predicted for a much higher temperature (about 190 °C), i.e., a lower value of the interaction energy density. Similar comparisons are obtained for other blends. For example, Figure 6.4 shows the predicted values of  $\zeta$  and  $\eta_B$  as a function of temperature for 17.6 wt% SB 40/10 in 17000 PS homopolymer. In this case, the amount of homopolymer in the core is predicted to be essentially zero at all temperatures. This is a result

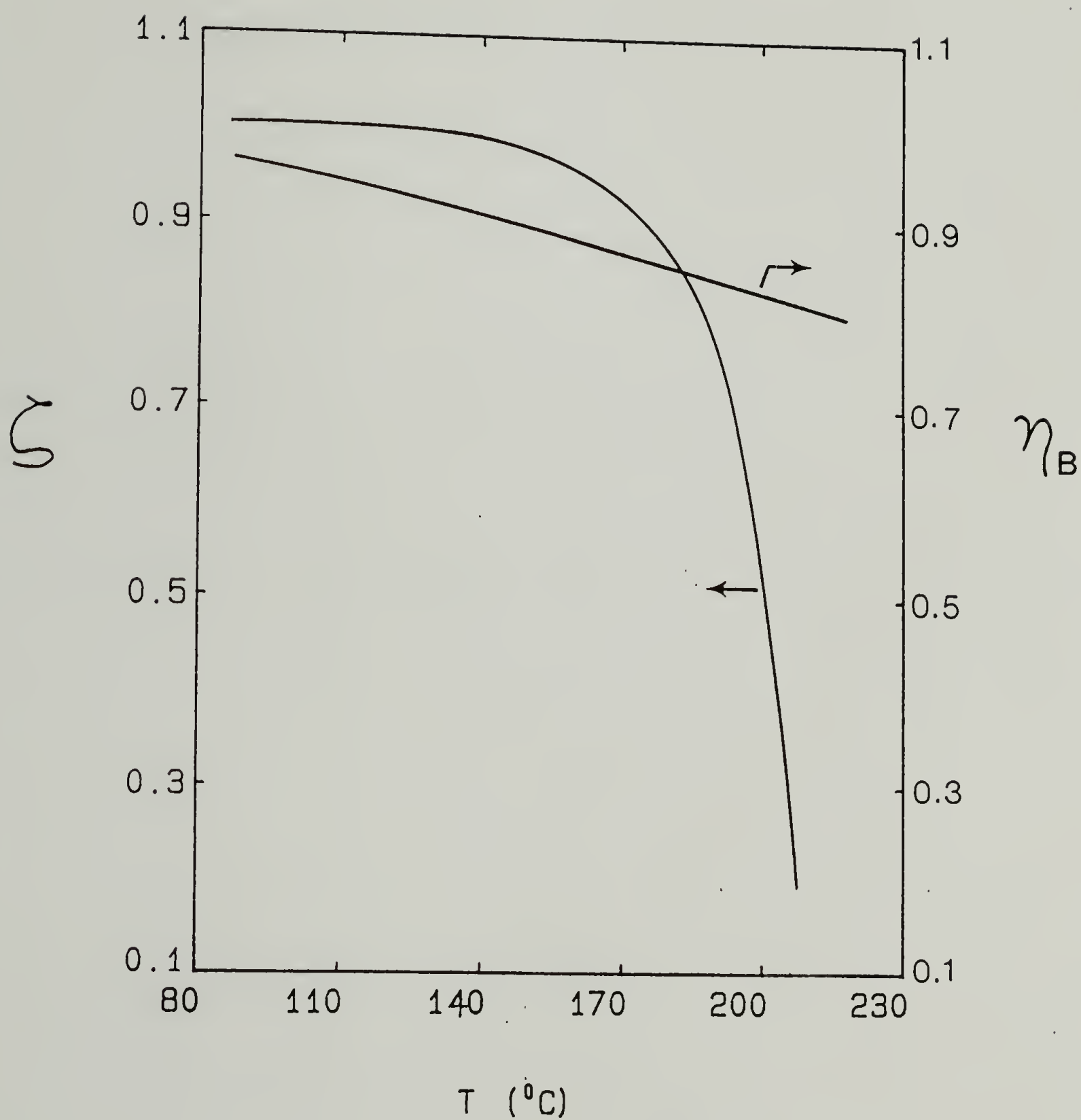


Figure 6.3 Predicted values of  $\zeta$  and  $\eta_B$  as a function of temperature for 12.5 wt% SB 20/20 in 2100 PS.

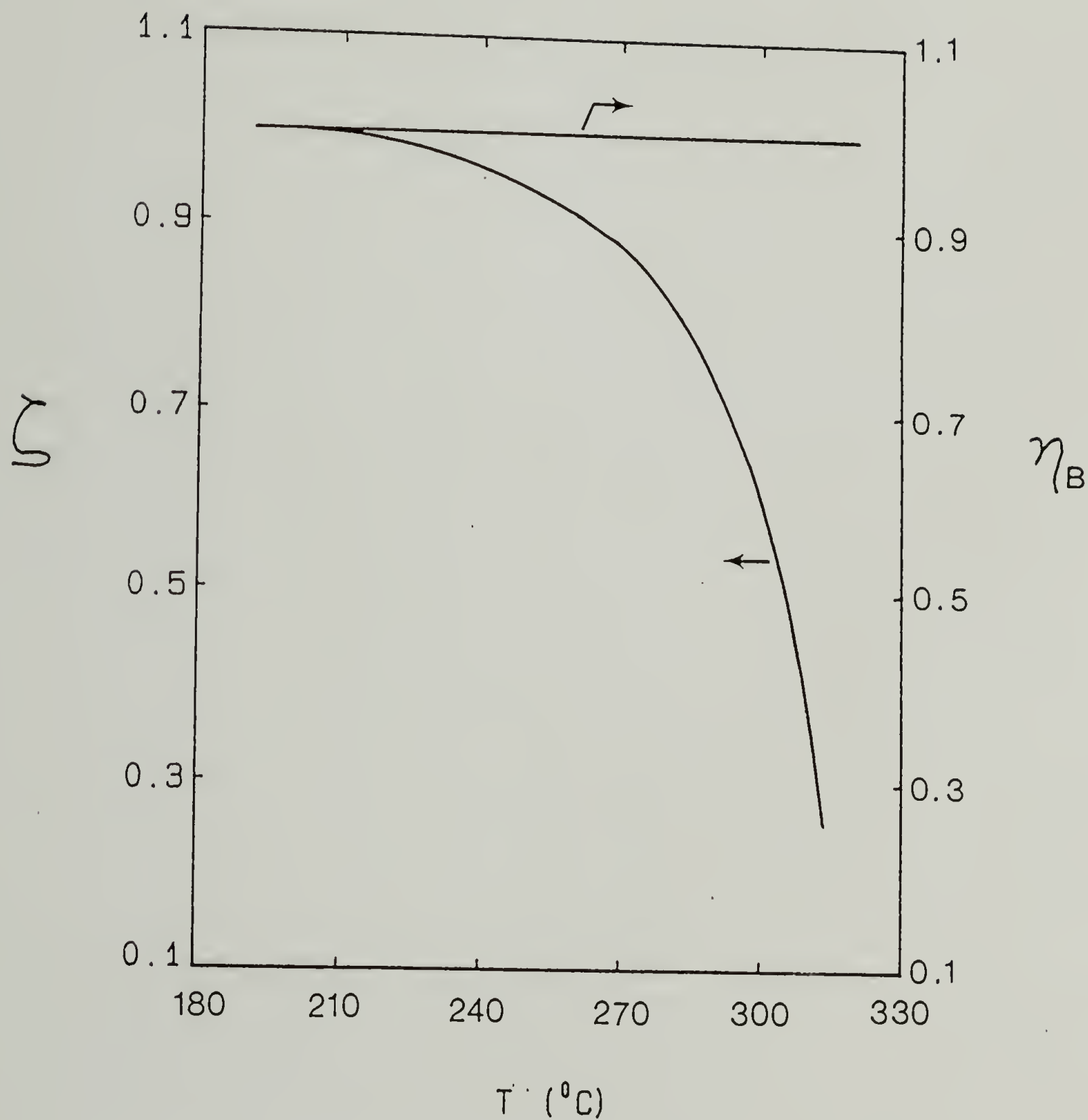


Figure 6.4 Predicted values of  $\zeta$  and  $\eta_B$  as a function of temperature for 17.6 wt% SB<sup>B</sup> 40/10 in 17000 PS.

of the higher ratio of homopolystyrene to PB block molecular weights (i.e., higher PB block-PS homopolymer incompatibility) for this blend compared to that of SB 20/20 in 2100 PS. Again, the value of  $\zeta$  is predicted to decrease rather abruptly above a certain temperature, about 270 °C for this blend. The values of  $\zeta$  and  $\eta_B$  determined experimentally for 17.6 wt% SB 40/10 in 17000 PS at 115 °C were 0.46 and 1.0 respectively, which correspond to the predicted structure at about 300 °C. Again, since the theory greatly underestimates the cmc for this blend at 115 °C, it is also expected to underestimate the amount of free copolymer at 115 °C.

In summary, even when the molecular weight of the homopolystyrene is low (2100), the LOW theory predicts that the type of phase mixing which should occur near the dissolution temperature is predominantly that due to an increase in the concentration of free copolymer. This is the same trend observed experimentally, although the temperature at which this mixing is observed (115 °C) is appreciably less than the theoretically predicted dissolution temperature. As discussed previously, this could be due to using too high a value for the interaction energy density in the calculations, or alternatively, the free energy expressions used in the LOW theory could be inexact. At this time, it is not possible to determine which of these factors is responsible for the discrepancy between the experimental results and the theoretical predictions. It is also possible that non-equilibrium structures, characteristic of a higher temperature, could somehow be frozen in during solvent casting; however, it is expected that the



subsequent annealing treatment, in addition to the relatively low copolymer and homopolymer molecular weights employed, allow equilibrium structures (for 115 °C) to be obtained.

The volume fraction of free copolymer,  $\phi_{\text{free}}$ , versus the overall copolymer volume fraction,  $\phi_{\text{overall}}$ , for 12.5 wt% SB 20/20 in 2100 PS at 190 °C and 17.6 wt% SB 40/10 in 17000 PS at 300 °C predicted by the LOW theory is shown in Figure 6.5. At concentrations below the cmc, the free copolymer and overall copolymer volume fractions are equal; however, the volume fractions of free copolymer are predicted to decrease for copolymer volume fractions greater than the cmc. Experimentally, it was observed however that at overall copolymer concentrations greater than the cmc, the concentration of free copolymer for these blends was actually greater than the cmc. If the cmc is a true first order phase transition, then the volume fraction of free copolymer in the homopolymer matrix should be independent of the copolymer concentration above the cmc. However, the experimental results indicate that the volume fraction of free copolymer in the matrix increases markedly for these blends as the overall concentration of copolymer increases. This leads one to the conclusion that the cmc transition observed for these copolymer/homopolymer blends is not a true first order phase transition. Therefore, phase diagrams such as those proposed by Roe and Zin [126] (see Figure 3.6), which are based on first order phase transitions, are not necessarily valid in the micellar region. Indeed, Leibler et al. [112] point out that because only finite sized micelles occur at the cmc, properties only exhibit rapid

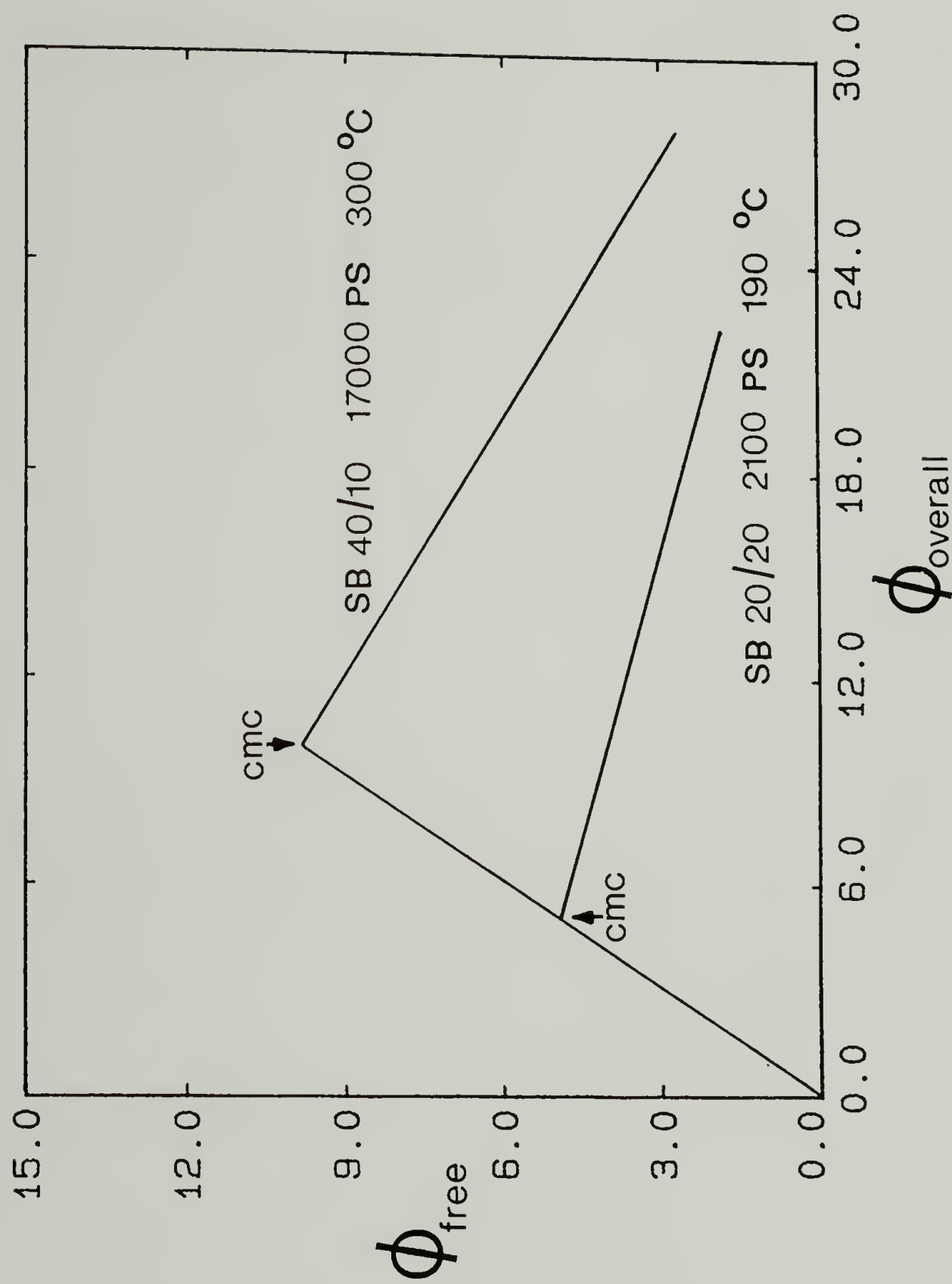


Figure 6.5 Predicted values of free copolymer volume fraction as a function of overall copolymer volume fraction for 12.5 wt% SB 20/20 in 2100 PS at 190 °C and 17.6 wt% SB 40/10 in 17000 PS at 300 °C.

continuous variations through the cmc instead of discontinuous changes at a sharp transition point. This implies that the cmc transition is not a true first order phase transition. The LOW theory predicts an increasing volume fraction of dissolved copolymer in the homopolymer matrix with increasing overall copolymer volume fraction, especially when the product  $XN$  is small (i.e., high temperatures or low copolymer molecular weight). The subsequent loss in free energy, due to the reduction in the total number of micelles, is compensated for by an increase in the entropy of the surrounding homogeneous mixture.

### 6.3 Core Size

The micelle core radii predicted by the LOW theory (dashed lines) for copolymers SB 40/10, SB 20/20, and SB 80/80 as a function of homopolymer molecular weight are compared to the experimental results (solid lines) in Figure 6.6. In all cases, the experimental core radii are slightly smaller than predicted, with the difference between the theoretical and experimental values decreasing with increasing homopolymer molecular weight. In addition, the predicted values of the scaling exponent  $\gamma$  ( $R_c \propto M_{hPS}^\gamma$ ) are 0.067, 0.045, and 0.070, compared to the experimental values of 0.16, 0.22, and 0.14 for copolymers SB 40/10, SB 20/20, and SB 80/80 respectively. The reason that the core radius is dependent on homopolymer molecular weight was discussed previously in Section 5.2. Briefly, as the ratio of homopolystyrene to PS block molecular weight decreases, the entropic effects tending to drive the

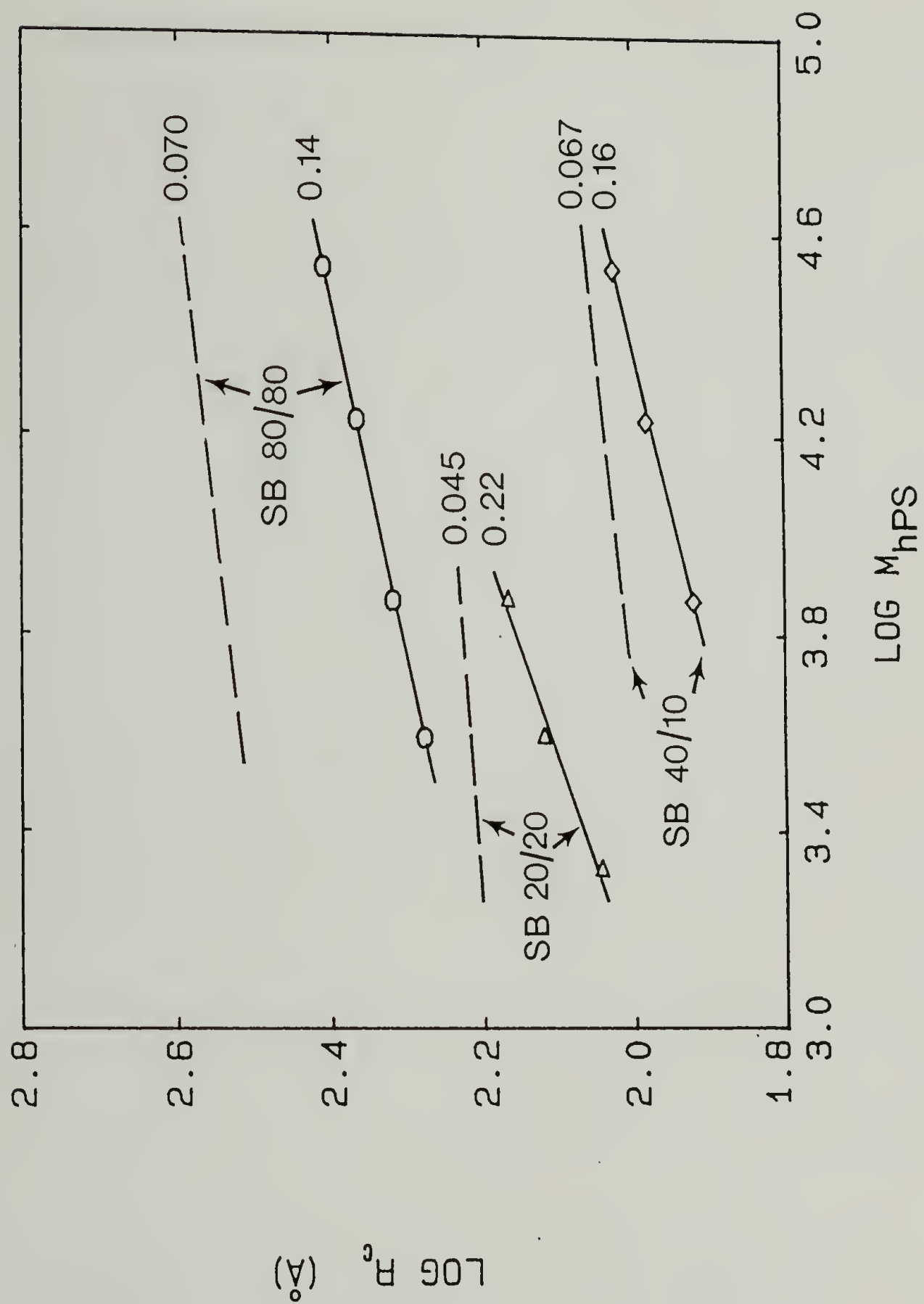


Figure 6.6 Comparison of experimentally determined (solid lines) and theoretically predicted (dashed lines) micelle core radii as a function of  $M_{hPS}$  for SB 40/10, SB 20/20, and SB 80/80 at 115 °C.



homopolymer density towards a more uniform value increase. A more uniform value of homopolymer density can be obtained by maximizing the volume fraction of the corona region, which may be accomplished, in part, by decreasing the core radius, resulting in a larger number of smaller micelle cores. Evidently, the effect of homopolymer molecular weight on the micelle core size is appreciably greater than predicted by the LOW theory. This relatively rapid increase of core radius with homopolymer molecular weight observed experimentally is thought to be an equilibrium effect. As discussed in Section 3.1.2, it has consistently been found that the spherical domains in block copolymer systems having high molecular weights and/or large polystyrene contents (i.e., not at equilibrium) are smaller than predicted by equilibrium theories of domain formation [11,72,85,95]. Therefore, it is expected that non-equilibrium effects, associated with increasing homopolystyrene molecular weight, would cause the micelle core radii to increase more slowly with homopolystyrene molecular weight than predicted by theory; however, this is opposite to what is found.

Figure 6.7 shows a comparison of the theoretically predicted (dashed line) and experimentally determined (solid line) micelle core radii as a function of the PS block length, using the results for copolymers SB 10/10, SB 23/10, SB 40/10, and SB 60/10 in 7400 PS homopolymer. Once again, the experimental core radii are slightly smaller (14-27%) than predicted, with the difference increasing with increasing PS block molecular weight. In addition, the scaling exponent  $\alpha$  ( $R_c \propto M_{PS}^\alpha$ ) predicted by the LOW theory (-0.048) has a much smaller

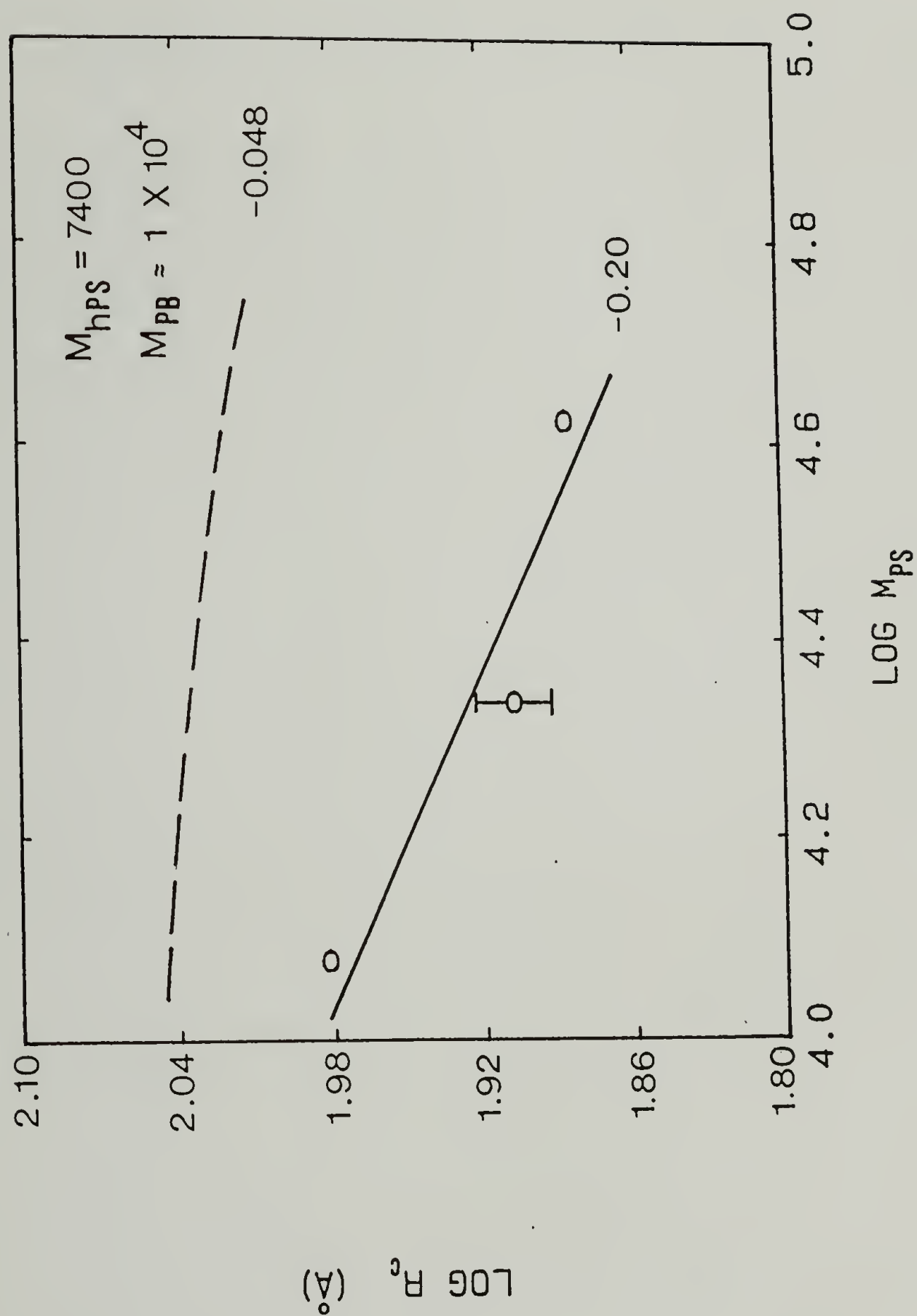


Figure 6.7 Comparison of experimentally determined (solid line) and theoretically predicted (dashed line) core radii as a function of  $M_{PS}$  for SB 10/10, SB 23/10, SB 40/10, and SB 60/10 at 115 °C.

absolute value than that found experimentally ( $-0.20$ ). Therefore, the effect of PS block length on micelle core radii appears to be much greater than predicted by the theory. This is in accord with the larger than predicted dependence of  $R_c$  on the ratio ( $M_{hPS}/M_{PS}$ ) observed previously.

A comparison of the effect of PB block length on core size as predicted by the LOW theory (dashed line) and determined experimentally (solid line) is shown in Figure 6.8 for the copolymers SB 10/10, SB 20/20, SB 40/40, and SB 80/80 in 7400 PS homopolymer. The core radii have been scaled by  $M_{PS}^\alpha$  to eliminate the effect of PS block length, where the values of  $\alpha$  are those determined previously in Figure 6.7. The scaling exponent  $\beta$  ( $R_c \propto M_{PB}^\beta$ ) is predicted to be 0.62, in very good agreement with the value of 0.60 determined experimentally. However, the absolute values of the core radii found experimentally for these blends are once again less than that predicted by the theory, as shown by the results presented in Figure 6.9, with the difference increasing with copolymer molecular weight. This is a direct result of the relatively large dependence of core radius on PS block molecular weight found experimentally.

#### 6.4 Corona Thickness

A comparison of the experimental (solid line) and theoretically predicted (dashed line) effect of homopolystyrene molecular weight on the corona thickness is shown in Figure 6.10 for copolymers SB 20/20 and

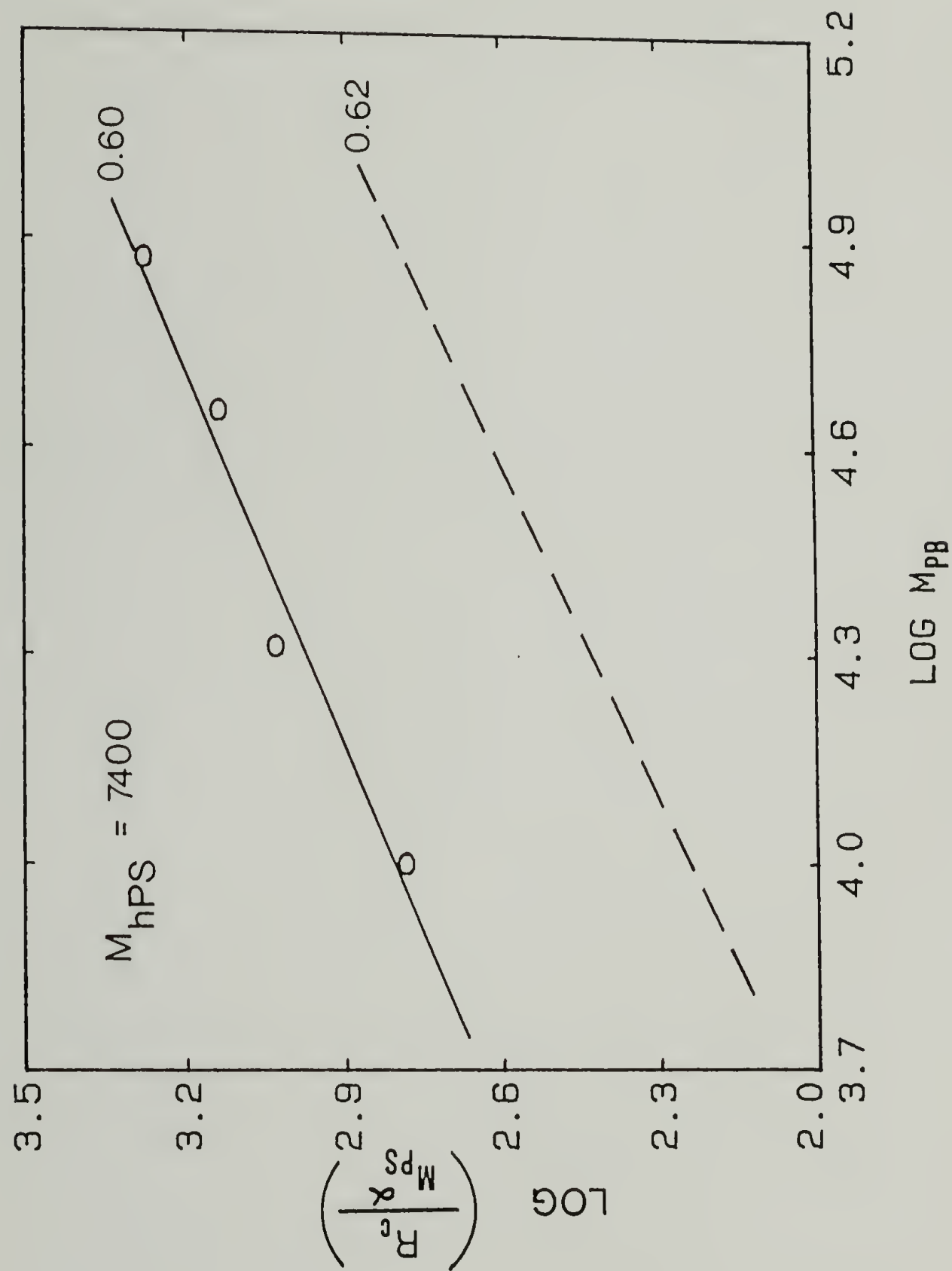


Figure 6.8 Comparison of experimentally determined (solid line) and theoretically predicted (dashed line) core radii as a function of  $M_{PB}$  for SB 10/10, SB 20/20, SB 40/40, and SB 80/80 at 115 °C.



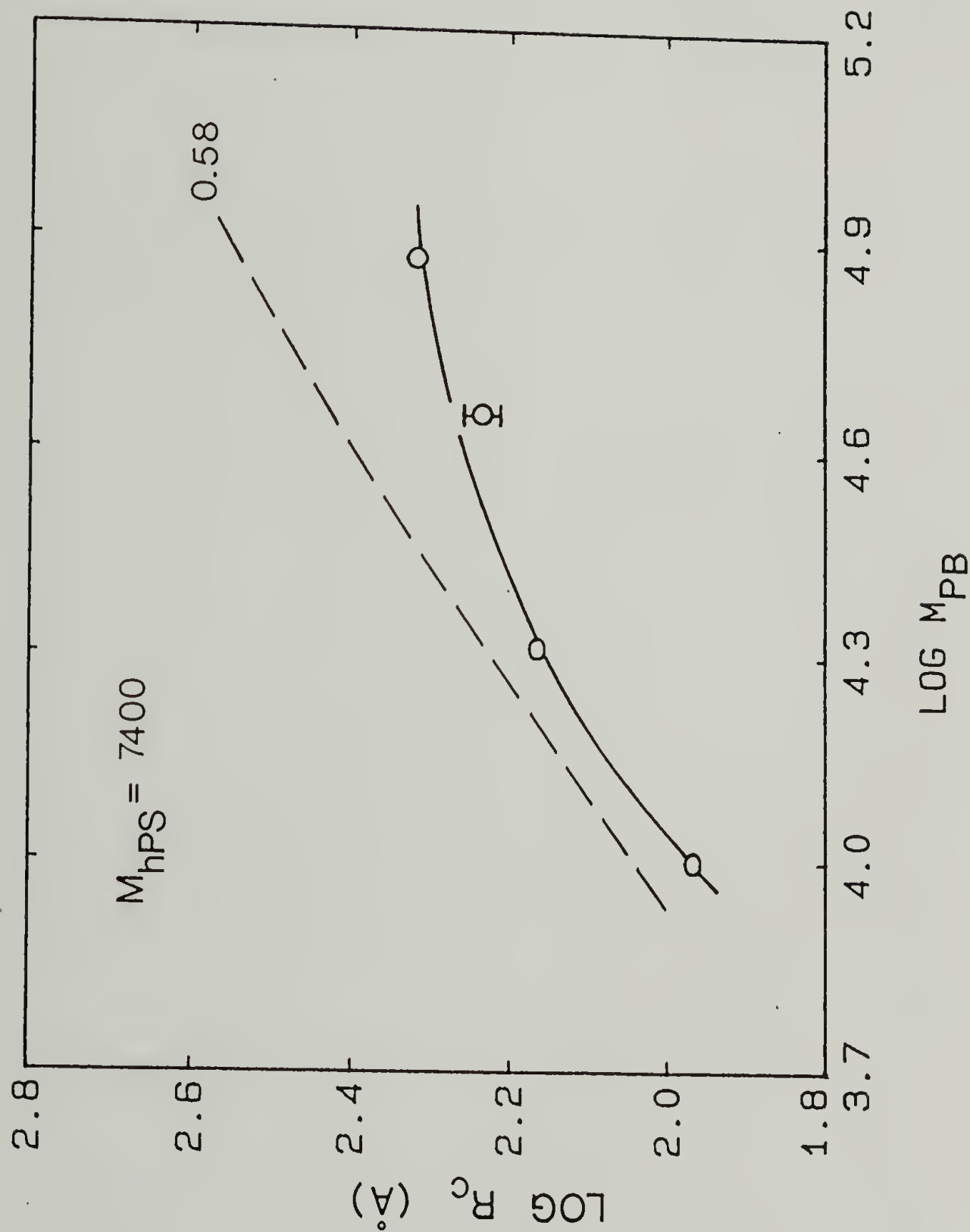


Figure 6.9 Comparison of experimentally determined (solid line) and theoretically predicted (dashed line) core radii as a function of  $M_{PB}$  for SB 10/10, SB 20/20, SB 40/40, and SB 80/80 at 115°C.

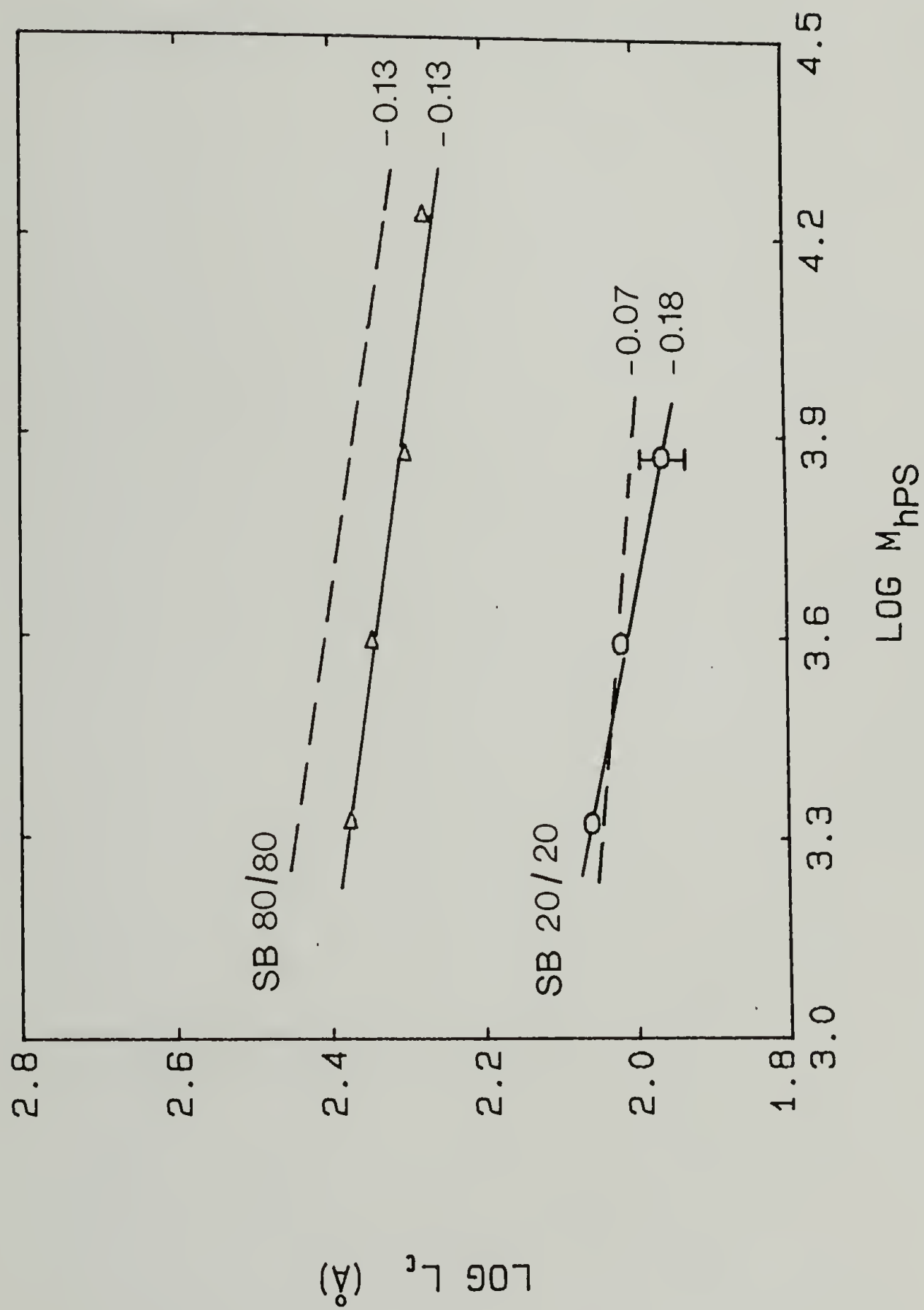


Figure 6.10 Comparison of experimentally determined (solid lines) and theoretically predicted (dashed lines) corona thickness as a function of  $M_{hPS}$  for copolymers SB 20/20 and SB 80/80 at 115 °C.

SB 80/80. For SB 80/80, the experimental and theoretically predicted values of the scaling exponent  $\epsilon$  ( $L_c \propto M_{hPS}^\epsilon$ ) are both  $-0.13$ . In addition, the magnitudes of the corona thickness values agree fairly well, with the experimental values being slightly smaller ( $\approx 15\%$ ) than predicted. This is expected since the corona thickness was determined from the value of the effective hard sphere radius used in the PY modeling. The micelles must overlap slightly before the intermicelle repulsion (arising from a loss of entropy of mixing when the homopolymer is forced out of the overlapping coronae) prevents them from approaching any closer. Since the corona thickness determined from the PY modeling is approximately equal to the unperturbed root mean square end to end distance of the PS blocks, the intermicelle repulsion occurs when the distance between the surfaces of neighboring micelle cores is about twice the end to end distance of the PS blocks. Decreasing the ratio  $M_{hPS}/M_{PS}$  results in an increased swelling of the PS blocks with homopolystyrene, thereby increasing the distance at which the intermicelle repulsion occurs. For copolymer SB 20/20, the experimental value of  $\epsilon$  was found to be  $-0.18$ , which is somewhat less than the theoretically predicted value of  $-0.07$ , although it must be kept in mind that there is a relatively large error in the experimentally determined value of  $\epsilon$  ( $\pm 0.07$ ). In addition, the experimental and theoretically predicted values of the corona thickness agree very well.

Figure 6.11 shows a comparison of the experimental and theoretically predicted corona thickness as a function of the PS block length for copolymers SB 10/10, SB 20/20, SB 40/40, and SB 80/80 in 7400

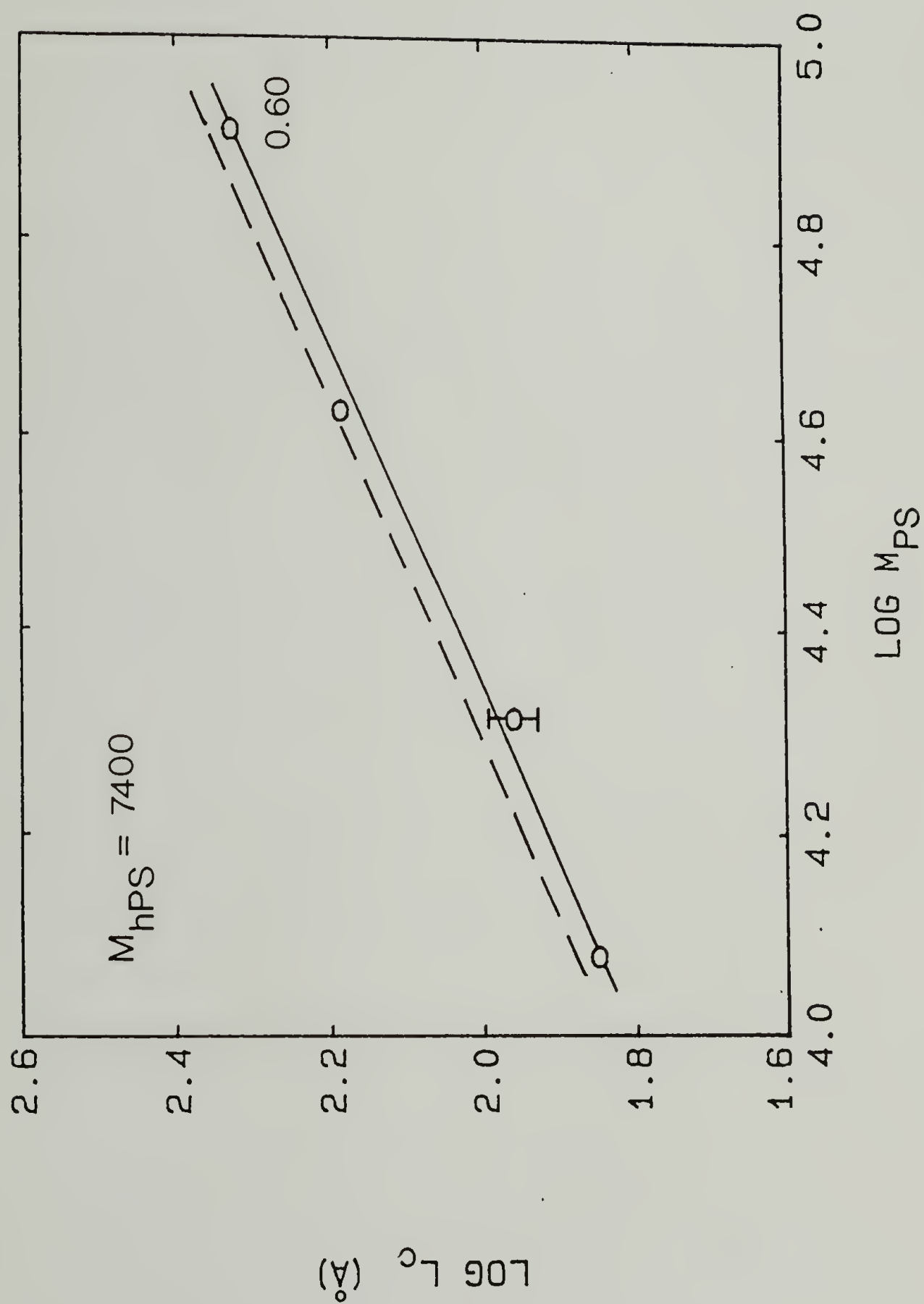


Figure 6.11 Comparison of experimentally determined (solid line) and theoretically predicted (dashed line) corona thickness as a function of  $M_{PS}$  for copolymers SB 10/10, SB 20/20, SB 40/40 and SB 80/80 at 115°C.



PS homopolymer. Good agreement is seen in both the magnitude of the corona thickness and the scaling of corona thickness with PS block molecular weight. Once again, the experimental corona thickness is slightly smaller than predicted by theory. The scaling exponent  $\delta$  ( $L_C \propto M_{PS}^\delta$ ) is found to be 0.60 both experimentally and theoretically.

The volume fraction of homopolystyrene in the micelle core, determined experimentally and predicted theoretically, for copolymer SB 80/80 as a function of homopolystyrene molecular weight is shown in Figure 6.12. The concentration of homopolymer in the core determined by experiment is greater than that predicted by the LOW theory, even though the thickness of the corona is approximately the same in both cases. This is a result of the experimental core radii for SB 80/80 (i.e., the number of copolymer chains per micelle) being appreciably smaller than predicted by the theory.

In conclusion, the LOW theory correctly predicts the qualitative trends of micelle structure as a function of homopolymer and block molecular weights observed experimentally. For example, the theory predicts that the micelle core radius should increase with increasing homopolystyrene or PB block molecular weight, but decrease with increasing PS block molecular weight. The dependence of  $R_C$  on  $M_{PB}$  is predicted to obey the scaling law  $R_C \propto M_{PB}^\beta$  where  $\beta = 0.06$ , which is in good agreement with the experimental results. However, the dependence of  $R_C$  on  $M_{hPS}$  and  $M_{PS}$  for the copolymer/homopolymer blends studied is predicted to obey the scaling laws  $R_C \propto M_{hPS}^\gamma$  and  $R_C \propto M_{PS}^\alpha$  where  $\gamma$  is predicted to be about 0.06 and  $\alpha$  is predicted to be -0.05, compared to

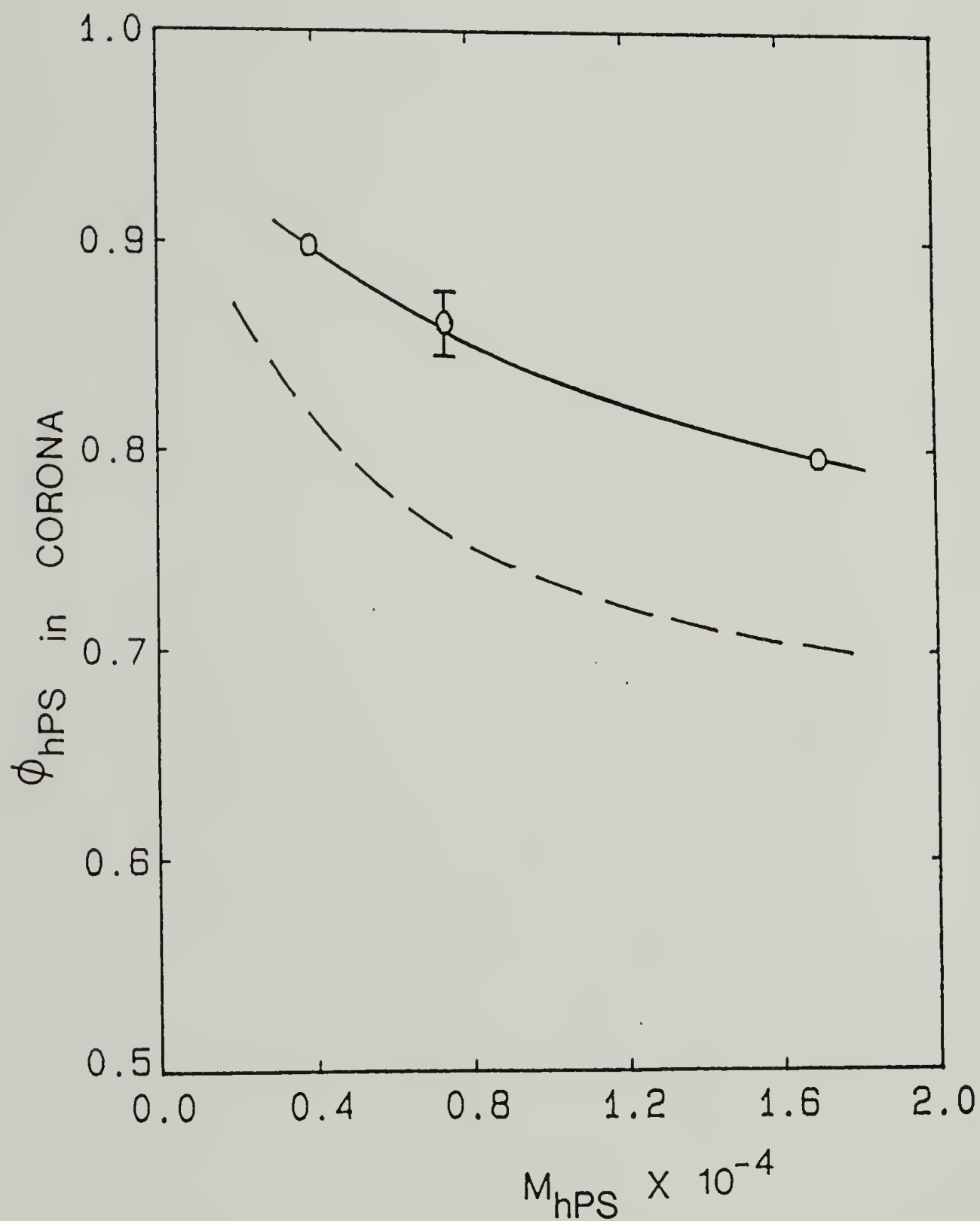


Figure 6.12 Comparison of experimentally determined (solid line) and theoretically predicted (dashed line) value of homopolystyrene volume fraction in the corona as a function of  $M_{\text{hPS}}$  for copolymer SB 80/80 at 115 °C.

the experimentally determined values of  $\gamma = 0.17 \pm 0.04$  and  $\alpha = -0.20 \pm 0.05$ . Therefore, the radius of the micelle core is found to be much more dependent on the ratio  $M_{\text{hPS}}/M_{\text{PS}}$  than predicted. It is believed that this is an equilibrium effect and not an artefact of the sample preparation technique. In contrast, the micelle corona thickness as a function of  $M_{\text{hPS}}$  predicted by the LOW theory is in very good agreement with that found experimentally.

The most notable discrepancy between the experimental results and the predictions of the LOW theory is the amount of free copolymer present at 115 °C. For example, although the qualitative dependence of the cmc on homopolymer and block molecular weights observed experimentally is correctly predicted, the theory predicts cmc values at 115 °C which are at least an order of magnitude smaller than those observed experimentally at 115 °C (i.e., the copolymer and homopolymer are more compatible than predicted). Consequently, the theory also underestimates the amount of free copolymer as a function of overall copolymer concentration. In other words, the structures observed experimentally at 115 °C correspond to structures predicted for higher temperatures. This discrepancy could be attributed to using too high a value for the interaction energy density in the LOW calculations. Alternatively, one or more of the free energy expressions used in the LOW theory could be inexact. At the present time, it is not possible to determine which of these factors is responsible for the discrepancy between the experimental results and the predictions of the LOW theory. It is also possible that non-equilibrium structures, characteristic of a

temperature greater than 115 °C, could be frozen in during the solvent casting; however, it is believed that the subsequent annealing treatment, in addition to the relatively low molecular weights employed, allow equilibrium structures (at the annealing temperature of 115 °C) to be obtained. It should also be stated that the LOW theory predicts that for the blends studied the predominant form of phase mixing which occurs, upon increasing the temperature, is due to an increasing concentration of free copolymer, rather than mixing of homopolymer into the micelle core. The phase mixing observed at 115 °C for the blends studied conforms to this prediction. The amount of homopolystyrene in the PB micelle cores was determined to be small in all cases.



## C H A P T E R   V I I

### STRUCTURE OF POLY(STYRENE-BUTADIENE) DIBLOCK COPOLYMER/POLYSTYRENE HOMOPOLYMER BLENDS EXHIBITING NON-SPHERICAL MICELLES

As stated in Chapter 5, micelles in block copolymer/homopolymer blends are not necessarily spherical. In this chapter, electron microscopy evidence for cylindrical micelles and lamellar type structures, such as spherical vesicles or multilayered structures, will be presented. It will be shown that transitions in micelle shape can result from increasing the molecular weight of the homopolystyrene matrix and/or from increasing the polybutadiene block molecular weight, even though the overall volume fraction of copolymer is kept constant at a relatively small value. These transitions can be explained in terms of the general rule of domain morphology as a function of microphase volume fractions put forth by Molau [32] for neat block copolymers, and later extended by Sadron [64] to the case of block copolymers in preferential solvents. In addition, it is observed that these transitions from spherical to non-spherical micelles are accompanied by an increase in the turbidity of the blends as a result of the increasing scale of the phase separated structures. Without the electron microscopy evidence however, this could be incorrectly attributed to a macrophase separation of the polystyrene homopolymer or the formation of an additional mesophase. For this reason, the micellar regions of block copolymer/homopolymer phase diagrams based on cloud point measurements alone are somewhat tentative.

### 7.1 Transition in Micelle Shape with Homopolymer Molecular Weight

As shown by the inset electron micrograph in the upper left corner of Figure 7.1, a blend containing 5.7 wt% copolymer SB 20/20 in 7400 PS homopolymer exhibited spherical micelles. However, when the molecular weight of the homopolystyrene matrix was increased, wormlike or cylindrical micelles occurred, as shown by the micrograph of 7.4 wt% SB 20/20 in 17000 PS in Figure 7.1. As in the case of spherical micelles, the core of the cylindrical micelle is made up of polybutadiene blocks, while a corona consisting of polystyrene blocks and homopolystyrene surrounds the core. While the blend containing spherical micelles was transparent, the blend containing cylindrical micelles was turbid. This is easily understood since the scale of the phase separated structure (i.e., the micelle core size) for the blend with cylindrical micelles is on the order of a few tenths of a micron, and thus, is expected to scatter light much more than the blend having spherical micelles, for which the scale of the phase separated structure is only a few hundred Angstroms. Without the electron microscopy evidence however, this turbidity with increasing polystyrene homopolymer molecular weight could have been incorrectly interpreted as resulting from a macrophase separation of the polystyrene homopolymer or the formation of an additional mesophase. However, as the electron micrograph in Figure 7.1 shows, the cylindrical micelles are more or less uniformly distributed throughout the homopolymer matrix. No large regions containing exclusively polystyrene homopolymer are observed by electron microscopy.



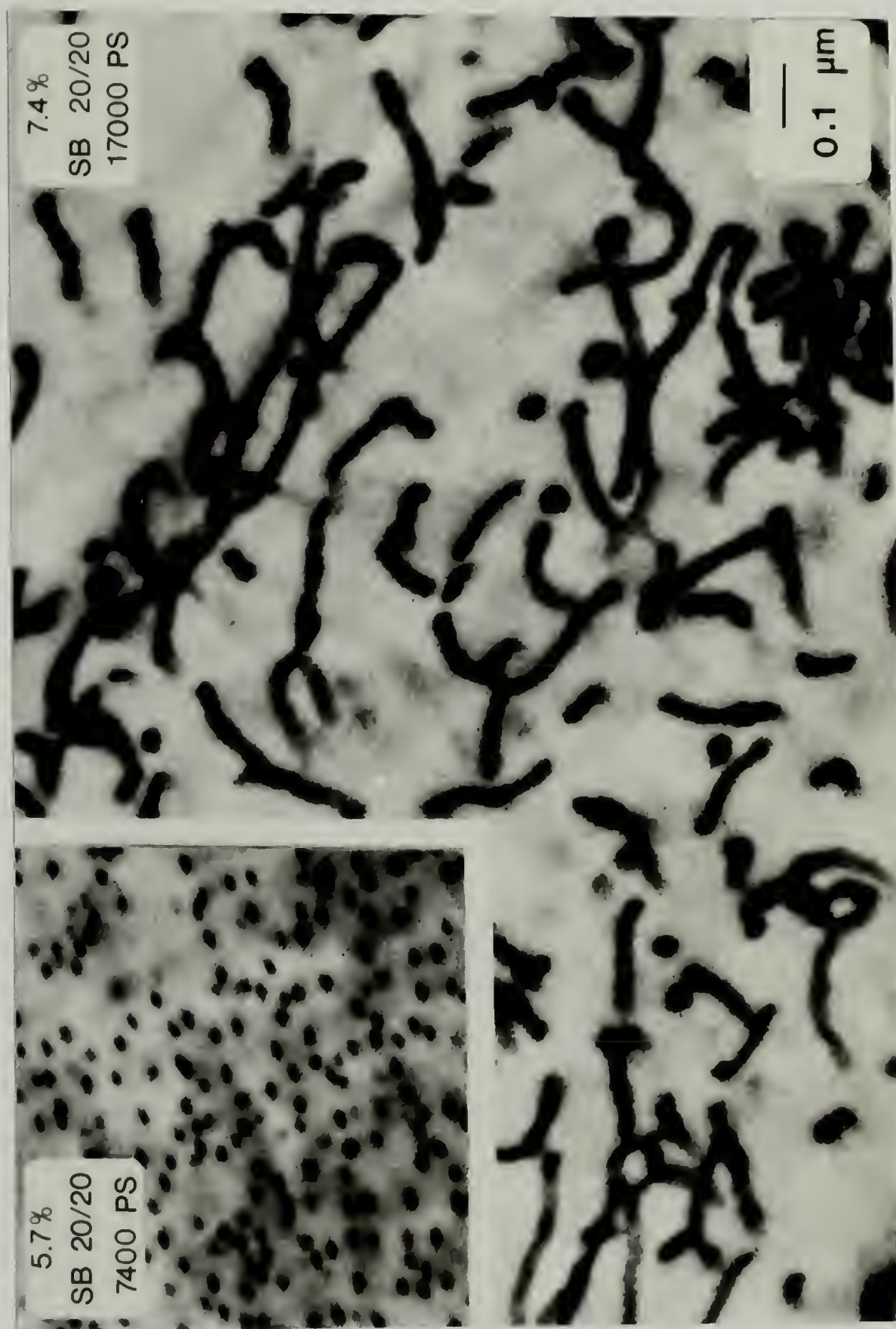


Figure 7.1 Electron micrographs showing the transition from spherical micelles for the blend containing 5.7 wt% SB 20/20 in 7400 PS to cylindrical micelles for the blend containing 7.4 wt% SB 20/20 in 17000 PS.

In other words, a single mesophase having block copolymer aggregates suspended in a homopolymer matrix occurs for 7.4 wt% SB 20/20 in 17000 PS.

The shape of the micelles in blends containing copolymer SB 40/40 was also observed to change from spherical to cylindrical as the homopolymer molecular weight was increased. For homopolymer molecular weights less than 17000, spherical micelles were observed; however, depending on the copolymer concentration, blends of SB 40/40 in 17000 PS exhibited spherical and/or cylindrical micelles, as shown in Figure 7.2. For 5.0 wt% copolymer, only spherical micelles were present, while for 9.8 wt% copolymer a small number of short cylinders were observed. When the copolymer concentration was increased to 18.2 wt%, most of the copolymer formed cylindrical micelles (this blend is also turbid). When the homopolymer molecular weight was increased even further, another structural transition occurred, as shown by the micrograph in Figure 7.3 for 5.0 wt% SB 40/40 in 35000 PS homopolymer. The polybutadiene phase separated structures seen in this micrograph are portions of approximately 0.5 micron diameter spherical vesicles in which the vesicle wall is made up of polybutadiene block chains. This structure is illustrated schematically in Figure 7.4. The thickness of the vesicle wall (250 Å) is about 1.3 times the unperturbed end to end distance of the PB block chains, which are thought to be arranged similarly to the block chains in lamellar structures of neat block copolymers. Next to the interior and exterior of the vesicle walls there is a corona region containing both PS block chains and PS



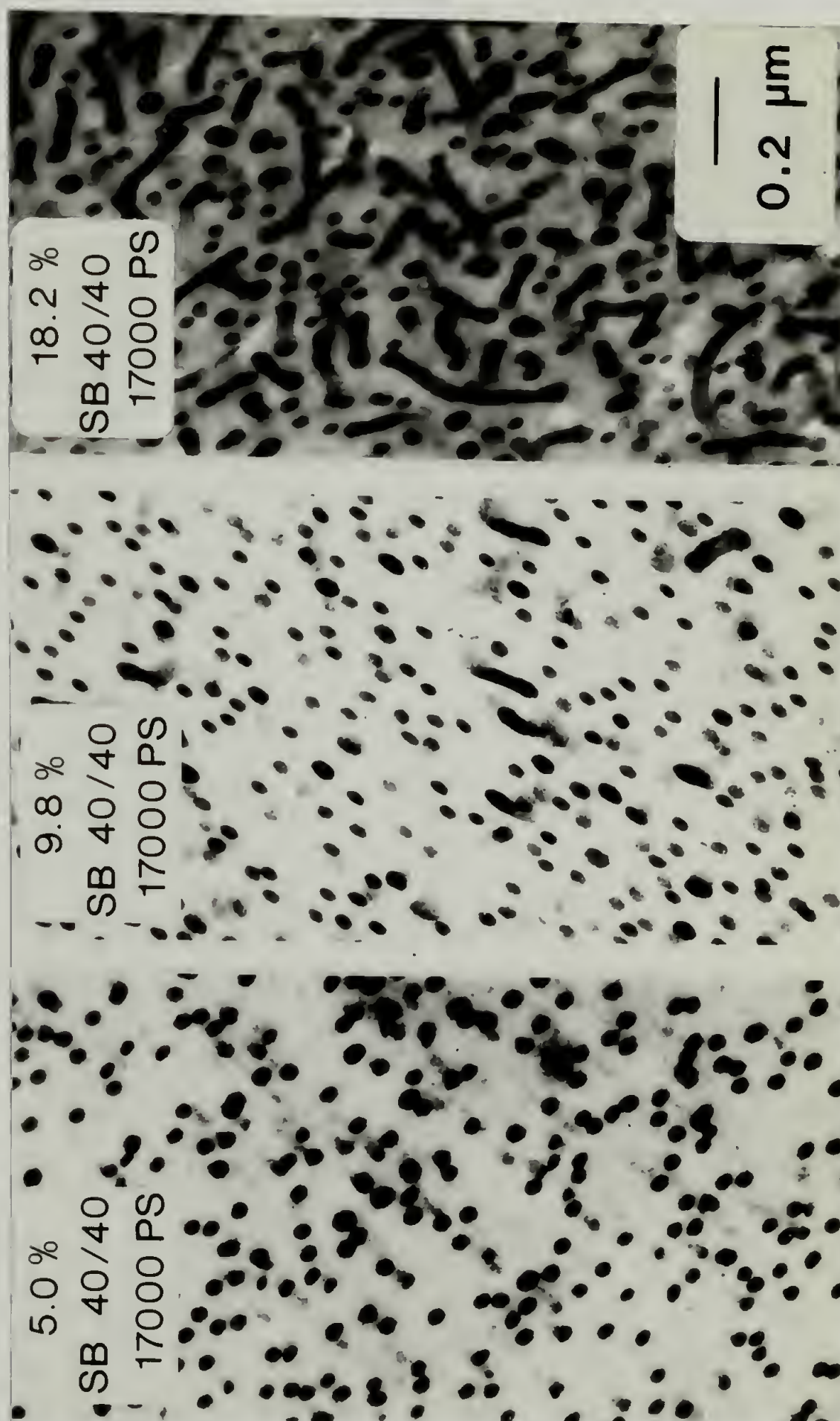


Figure 7.2 Electron micrographs of SB 40/40 in 17000 PS showing the transition from spherical to cylindrical micelles with increasing copolymer concentration (a) 5.0 wt%, (b) 9.8 wt%, and (c) 18.2 wt%.



Figure 7.3 Electron micrograph showing the spherical vesicle morphology of 5.0 wt% SB 40/40 in 35000 PS.

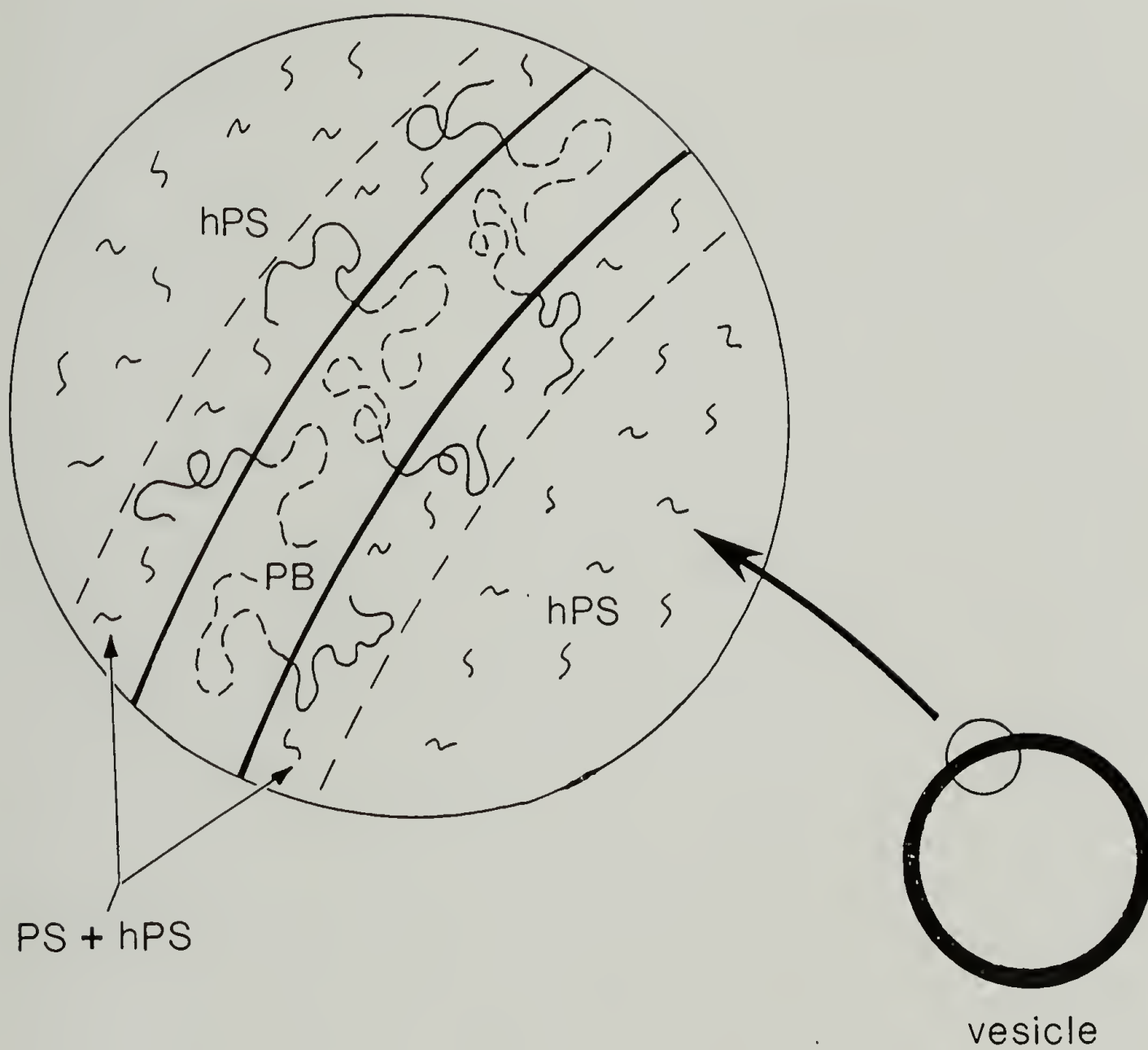


Figure 7.4 Schematic showing the arrangement of the copolymer and homopolymer chains in the spherical vesicle morphology.



homopolymer, similar to the corona region of spherical and cylindrical micelles. As expected from the scale of the phase separation, this blend is also turbid.

These transitions in structure with homopolymer molecular weight are similar to those observed for neat block copolymers [32] and block copolymer/solvent systems [64] as a function of the volume fractions of the microphases. As discussed in Section 3.2, these transitions can be intuitively understood in terms of interface curvature and packing requirements of the blocks in the domain space. Consider the situation of a neat copolymer in which the two blocks have nearly the same volume (SB 20/20 or SB 40/40 for example) and which forms a lamellar domain structure having a planar interface, where the space available to the blocks on either side of the interface is comparable. Now when a preferential solvent is added to the domains of one of the blocks, it has the effect of increasing the effective volume fraction (i.e., molecular volume) of that block, and the interface becomes curved so that the space available on the convex side (containing both block chain and preferential solvent) is larger than that available on the concave side. Therefore, cylindrical or spherical microdomains are formed, depending on the amount of added solvent, with the microphase having the smaller volume fraction occupying the concave side of the interface. In the case of the micellar systems, the two volume fractions which must be considered are the relative volume fractions of the micelle made up by the core  $v_f^{\text{core}}$  (which should not be confused with the definition of core



volume fraction  $\phi$  used in previous chapters) and the corona regions  $v_f^{\text{corona}}$  given by

$$v_f^{\text{core}} = \left[ \frac{R_c}{(R_c + L_c)} \right]^3 \quad (7.1)$$

$$v_f^{\text{corona}} = \left[ \frac{(R_c + L_c)^3 - R_c^3}{(R_c + L_c)^3} \right] \quad (7.2)$$

where  $R_c$  is the radius of the micelle core and  $L_c$  is the thickness of the micelle corona region (see Figure 5.2).

The results of Chapter 5 showed that as the homopolymer molecular weight is increased, the spherical micelle core radius increases while the corona thickness decreases, both of which serve to increase the relative core volume fraction  $v_f^{\text{core}}$ . Considering the volume fractions at which the transitions in domain shape occur for neat block copolymers and block copolymer/solvent blends, it could be anticipated that when  $v_f^{\text{core}}$  becomes greater than about 0.2, a transition from spherical to cylindrical micelles should occur. Likewise, when  $v_f^{\text{core}}$  becomes greater than about 0.35, a transition from cylindrical to lamellar micelles (such as vesicles or multilayered structures) should occur. From the data presented in Figure 5.19 for 12.3 wt% SB 20/20 in 7400 PS ( $R_c = 147$  Å,  $L_c = 92$  Å),  $v_f^{\text{core}}$  is calculated to be  $0.23 \pm 0.02$ . Similarly, the core volume fraction for this same copolymer in 2100 PS and 3900 PS is calculated to be 0.12 and 0.19 respectively. Extrapolating the results of Figures 5.20 and 5.21 yields a spherical micelle core radius of 166 Å and a corona thickness of 79 Å for SB 20/20 in 17000 PS homopolymer,

giving a calculated core volume fraction of 0.31, assuming spherical micelles. However, for this blend, cylindrical micelles occur, as would be expected for  $v_f^{\text{core}}$  equal to 0.31. A similar transition from spherical to cylindrical micelles has been observed previously by Canham et al. [107] for SBS triblock copolymers containing 30% PS in ethyl acetate, a selective solvent for the PS blocks. Although the transition for this system was found to occur as a result of increasing the temperature, the underlying cause was also an increase in the relative volume fraction of the micelle core. Increasing the temperature caused the solvent to be less selective for the PS block, resulting in an increasing swelling of the polybutadiene core with solvent.

From the results presented in Chapter 5,  $v_f^{\text{core}}$  for copolymer SB 40/40 in 3900 PS and 7400 PS is calculated to be 0.11 and 0.16 respectively. Extrapolating the results of Figures 5.20 and 5.21 (which are for 10 wt% copolymer) yields  $R_c = 190 \text{ \AA}$  and  $L_c = 115 \text{ \AA}$  for SB 40/40 in 17000 PS yielding a core volume fraction of  $0.24 \pm 0.02$ . Again, this is near the volume fraction expected for the transition from spherical to cylindrical micelles. As discussed previously, Figure 7.2 shows that the micelles in blends of SB 40/40 in 17000 PS change from spherical to cylindrical as the concentration of copolymer increases from 5 to 18 wt%. This can be explained by the data of Figure 5.12, which shows that the core radius increases about 10% over this concentration range for copolymer SB 20/20. The same phenomenon is expected to occur for copolymer SB 40/40. A 5% decrease in the core radius (190  $\text{\AA}$ ) used previously in calculating the core volume fraction of SB 40/40 in 17000

PS (which was for 10 wt% copolymer) would result in a core volume fraction of about 0.23 at 5 wt% copolymer. Similarly a 5% increase in the core radius would result in a core volume fraction of about 0.26 at 18 wt% copolymer. This slight increase in the core volume fraction with copolymer concentration is presumably responsible for the transition in micelle shape. While one type of structure should have a slightly lower free energy, and thus, be expected to occur exclusively, the difference in free energy between the spherical and cylindrical micellar structures near the transition may be small enough that a metastable (i.e., non-equilibrium) morphology, in which both spherical and cylindrical micelles coexist, may be present.

The spherical vesicles observed in Figure 7.3 for SB 40/40 in 35000 PS homopolymer can be thought of as lamellar structures since the ratio of vesicle diameter to vesicle wall thickness is large, and thus, the domain curvature is relatively small. Extrapolating the results of Figures 5.20 and 5.21 indicate that if spherical micelles occurred for this blend, the core radius and corona thickness would be 212 Å and 92 Å respectively, yielding a  $v_f^{\text{core}}$  of 0.34, which is approximately the volume fraction at which the transition from cylindrical to lamellar structures is expected to occur.

## 7.2 Transition in Micelle Shape With Polybutadiene Block Length

Increasing the length of the polybutadiene block length with respect to the polystyrene block length will also increase the PB core



volume fraction, and is therefore expected to induce a transition in micelle shape. The micelles in blends of SB 10/10 in 3900 PS and 7400 PS (see Figure 5.32) are spherical. On the other hand, the micrograph in Figure 7.5 shows that 18.4 wt% SB 10/23 in 3900 PS has an onion-like structure in which multiple layers of concentric polybutadiene spherical shells are present. This is similar to the structures observed by Bradford [119], Gebizlioglu et al. [120], and Argon et al. [121] in blends of poly(styrene-butadiene) block copolymers in high molecular weight homopolystyrenes. However, in the blends studied here, no large areas of nearly pure homopolymer are observed; rather, the morphology is uniform throughout the entire sample. The distance between the concentric PB layers suggests that a significant amount of homopolymer is contained (solubilized) between them. It is expected that this blend would exhibit the single shell vesicle structure, similar to that in Figure 7.3, for lower copolymer concentrations. A rough estimate of the core volume fraction, had the micelles been spherical, can be obtained by equating the core radius and corona thickness to the mean square end to end distances of the PB and PS blocks respectively (see Table 5.1). The results of Chapter 5 showed this to be a reasonable approximation. This leads to a  $v_f^{\text{core}}$  of  $0.30 \pm 0.05$ , which is near the volume fraction at which the transition from a cylindrical to lamellar domain structure is expected to occur. Reducing the homopolymer molecular weight should cause an increase in the corona thickness and a decrease in the core size, resulting in a reduction of the core volume fraction. Therefore, a transition from this lamellar-type structure to polybutadiene



cylinders or spheres should occur. Indeed, as the micrograph in the upper right corner of Figure 7.5 shows, a blend containing 17.8 wt% SB 10/23 in 2100 PS exhibits spherical micelles. In order for this copolymer to form spherical micelles, the fraction of homopolystyrene in the micelle corona must be quite large ( $> 85\%$ ). As expected from the scale of the phase separation, this blend is transparent, while the former blend is slightly turbid.

Figure 7.6 shows an electron micrograph of 13 wt% SB 10/65 in 2100 PS. While SB 10/23 in this same homopolymer exhibited spherical domains, the blend containing SB 10/65 has a lamellar structure as a result of the increased PB block length. The large distance between the PB lamellae, relative to their width, indicates that a large amount of homopolystyrene is contained between them. It should be remarked that the morphology of this blend is uniform throughout the entire sample. On the other hand, a blend containing 4.0 wt% SB 10/65 in 7400 PS, exhibits two distinct mesophases, as shown in Figure 7.7, corresponding to mesophases  $M_1$  and  $M_2$  of the phase diagrams proposed by Roe and Zin [126] for block copolymer/homopolymer blends (see Figure 3.6).

Mesophase  $M_1$  consists of microdomains of the block copolymer swollen with homopolymer, while mesophase  $M_2$  contains micellar aggregates of the block copolymer suspended in the homopolymer. In the case of the present blend, mesophase  $M_1$  has the same spherical domain morphology as the pure block copolymer, except that the polystyrene spheres are slightly swollen with polystyrene homopolymer. Mesophase  $M_2$  contains isolated spherical vesicles having polybutadiene walls suspended in a



Figure 7.5 Electron micrographs showing the multiple layer structure of 18.4 wt% SB 10/23 in 3900 PS and the spherical micelle structure of 17.8 wt% SB 10/23 in 2100 PS (shown at the same magnification).



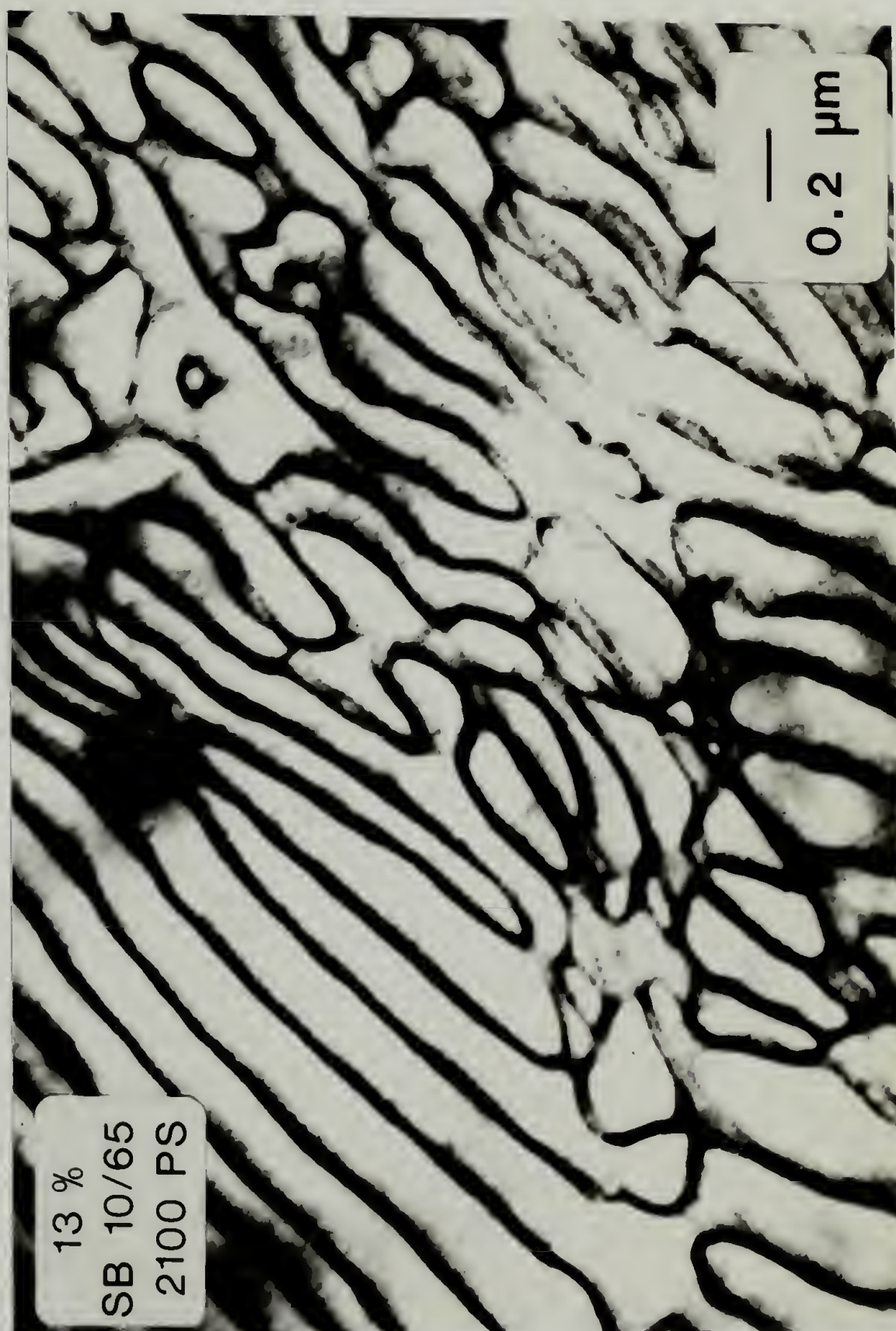


Figure 7.6 Electron micrograph showing the lamellar structure of 13 wt% SB 10/65 in 2100 PS.

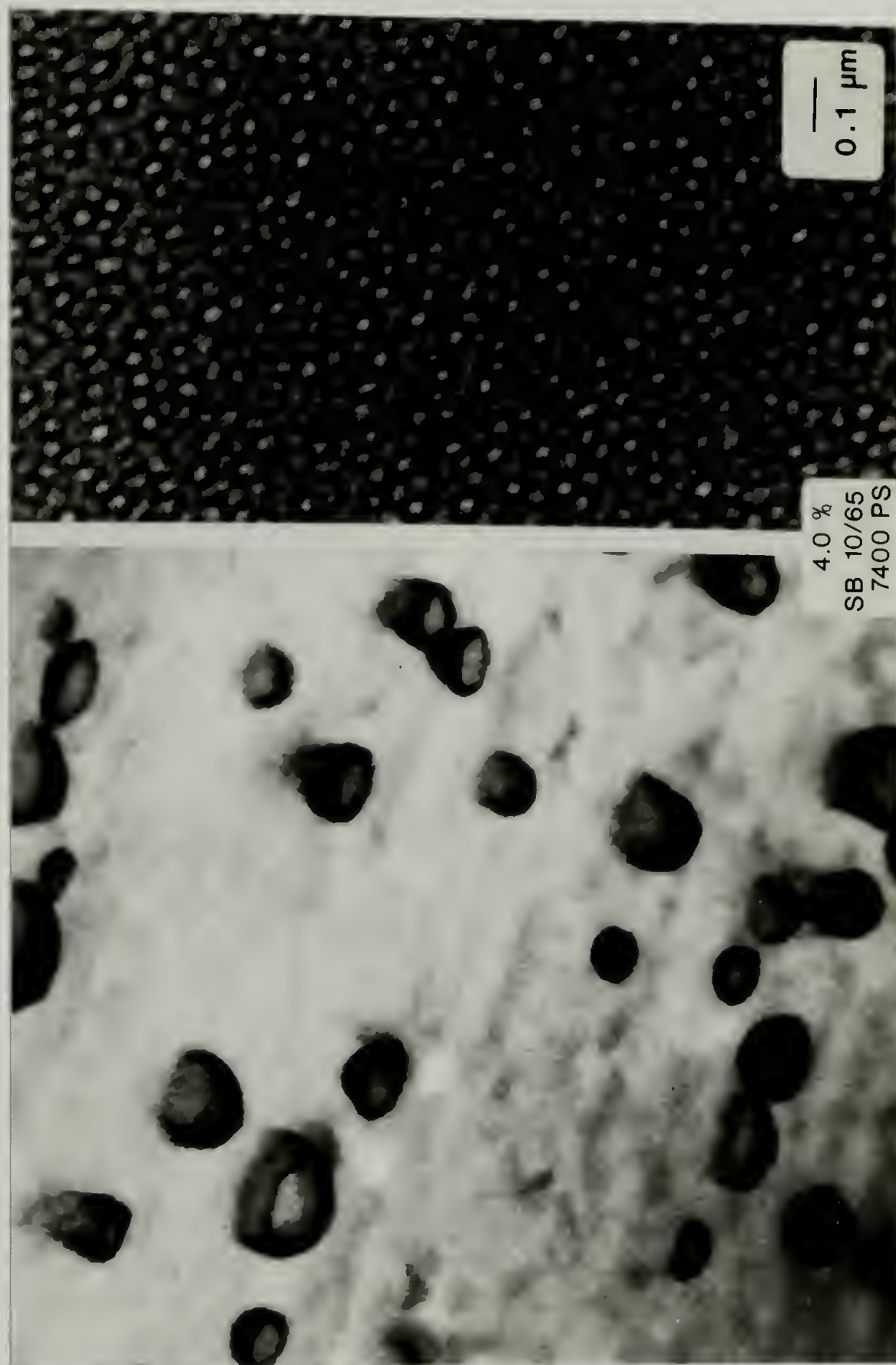


Figure 7.7 Electron micrographs of the two mesophases in the blend containing 4.0 wt% SB 10/65 in 7400 PS (shown at the same magnification).



homopolystyrene matrix. This is the only blend studied which exhibited two distinct mesophases. Evidently, increasing the molecular weight of the PB block relative to the PS block shifts the boundary between the two phase region containing mesophases  $M_1$  and  $M_2$  and the single phase region containing  $M_2$  (line FI of Figure 3.6) to significantly smaller copolymer compositions.

It is interesting to note that the structures observed in these block copolymer/homopolymer blends are similar to the structures encountered in lipid (hydrocarbon amphiphiles)-water systems [146,147]. The major forces which govern the self assembly of fluid lipids into well defined structures have their origin in the hydrophobic interactions between the hydrocarbon tails, which induce them to associate, and the hydrophilic nature of the head groups, which requires them to be in contact with water. Israelachvili et al. [146] have shown that, similar to the case of block copolymer/homopolymer blends, geometric and packing considerations determine whether spherical micelles, non-spherical micelles, or bilayers (vesicles) form. The important geometric and packing properties of lipids are governed by the optimal surface area  $a_0$  per head group (which is dependent on surface tension, and the electrostatic and steric interactions between the head groups), the volume  $v$  of the hydrocarbon chains, and the maximum length  $l$  that the hydrocarbon chains can assume. Spherical micelles are favored when  $a_0$  is large (usually because of charged head groups) and  $v$  is small, while bilayers (vesicles) are favored for lipids having small head group areas and/or bulky hydrocarbon chains. In addition,

multilayered structures can form for high lipid concentrations, just as they do for block copolymer/homopolymer blends having large copolymer concentrations.

The present results are summarized in Figure 7.8 which shows the locations of the transitions between spherical, cylindrical, and lamellar (vesicle or multilayered) morphologies as a function of  $M_{hPS}/M_{PS}$  and the composition of the copolymer. The data from several copolymer/homopolymer blends are shown; the circular data points correspond to blends having spherical micelles, the triangular data points correspond to blends having cylindrical micelles, and the diamond shaped data points correspond to blends having lamellar type structures. The transitions in micelle shape are found to be correlated with the relative volume fractions of the core and corona regions, in analogy with the transitions found in neat copolymers and copolymer/solvent systems. At core volume fractions  $v_f^{core}$  less than about 0.2, spherical micelles are favored, while for  $v_f^{core}$  between about 0.2 and 0.35 cylindrical micelles occur, and for  $v_f^{core}$  greater than 0.35 lamellar type structures occur. The micelle core volume fraction can be increased by increasing the homopolymer molecular weight, resulting in a decreased corona thickness and increased core radius as a result of entropy of mixing effects, and/or by increasing the PB block length (PB composition) of the copolymer. In addition, it is observed that these transitions from spherical to non-spherical micelles are accompanied by an increase in the turbidity of the blends as a result of the increased scale of the phase separated structures. Without the electron

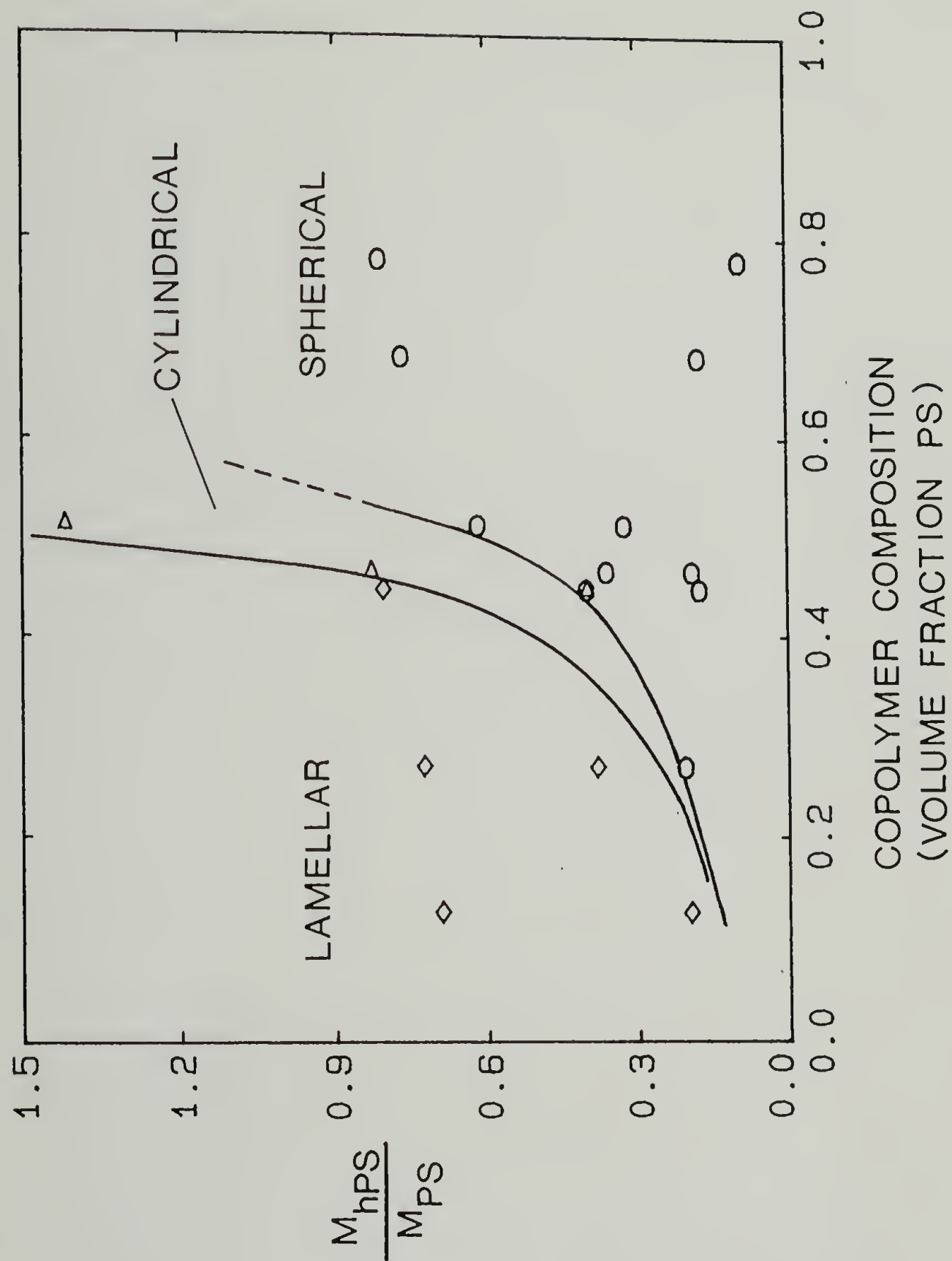


Figure 7.8 Block copolymer/homopolymer micellar structure as a function of homopolymer molecular weight and copolymer composition.

microscopy evidence however, this turbidity could be incorrectly attributed to a macrophase separation of the polystyrene homopolymer or the formation of an additional mesophase. For this reason, the micellar regions of block copolymer/homopolymer phase diagrams based on cloud point measurements alone are somewhat tentative.



## C H A P T E R   V I I I

### CONCLUSIONS AND FUTURE WORK

In this chapter, the main conclusions of this dissertation are reviewed; in addition, suggestions for future work are presented.

#### 8.1 Conclusions

A powerful new experimental methodology employing both small angle x-ray scattering (SAXS) and electron microscopy (EM) has been developed, from which the structure of block copolymer/homopolymer blends exhibiting spherical micelles can be completely characterized. The SAXS data from these blends has been modeled successfully using the Percus-Yevick (PY) hard sphere fluid approximation in order to account for the interparticle interference contributions to the scattered intensity. The validity of this model for the analysis of small angle scattering from block copolymer/homopolymer blends exhibiting spherical micelles was demonstrated first by Kinning and Thomas [124] in 1984. Since then, other researchers [130] have also employed this approach to analyze the small angle scattering from block copolymer micelles. By combining this modeling with SAXS invariant analysis and quantitative analysis of EM images, the following structural parameters can be obtained: (1) critical micelle concentration, (2) micelle core radius, (3) polydispersity in core radius, (4) micelle corona thickness, (5) amount of homopolymer dissolved in the micelle core, (6) concentration of free

unaggregated copolymer, (7) concentration of homopolymer in the micelle corona, and (8) the packing mode of spherical micelles exhibiting long range order. The work presented in this dissertation marks the first time that the micelle corona thickness, the concentration of free copolymer, and the concentration of homopolymer in the micelle corona have been experimentally determined for block copolymer micelles in a homopolymer matrix. The combination of EM and SAXS is a necessary part of the methodology employed since EM provides direct evidence of micelle shape, and the PY model used to quantitatively analyze the SAXS data is only applicable for the case of spherical micelles. In addition, a rigorous sample preparation technique was used to assure that equilibrium structures were obtained, enabling the predictions of the Leibler, Orland, and Wheeler (LOW) theory of micelle formation in block copolymer/homopolymer blends [112] to be critically tested. A wide range of poly(styrene-butadiene) diblock copolymers and polystyrene homopolymers were employed in this study.

It was observed, by both small angle x-ray scattering and transmission electron microscopy, that blends of poly(styrene-butadiene) block copolymers and polystyrene homopolymers have the following structure as a function of copolymer concentration in the micellar region of the phase diagram: at copolymer concentrations below the critical micelle concentration, the copolymer and homopolymer form a homogeneous mixture. When the copolymer concentration is increased beyond the cmc, aggregates form, having cores consisting of PB block chains surrounded by a corona region containing both PS block chains and

homopolystyrene, which are suspended in the homopolymer matrix with no long range order. These aggregates can be in the form of spherical or cylindrical micelles, or lamellar type structures (such as spherical vesicles or multilayered structures) depending on the copolymer concentration and the molecular weights of the homopolymer and the copolymer blocks. In the case of spherical micelles, a transition from a disordered liquid-like arrangement to an ordered SC lattice of micelles was observed by both SAXS and EM as the copolymer concentration was increased further. This transition was found to occur when the effective hard sphere volume fraction of micelles exceeded approximately 0.5, as predicted by Leibler and Pincus [135].

The critical micelle concentration was observed to increase with decreasing homopolymer or copolymer molecular weights (at fixed copolymer composition) and increasing PS block length (amount of PS in copolymer). These are the same trends predicted by the LOW theory of micelle formation in block copolymer/homopolymer blends; however, the cmc values predicted by theory are consistently one to two orders of magnitude smaller than observed experimentally.

The experimental results indicate that at 115 °C the micelle core radius scales with the homopolymer and copolymer block molecular weights as

$$R_c \propto M_{hPS}^{\gamma} M_{PS}^{\alpha} M_{PB}^{\beta}$$

where  $\gamma = 0.17 \pm 0.04$ ,  $\alpha = -0.20 \pm 0.05$ , and  $\beta = 0.60 \pm 0.08$ . These values are in relatively good agreement with those determined from the SANS data of Selb et al. [128] for poly(styrene-butadiene) block



copolymer/polybutadiene homopolymer blends exhibiting spherical micelles. In addition, the corona thickness was found to scale with the homopolystyrene and PS block molecular weights as

$$L_c \propto M_{hPS}^{\epsilon} M_{PS}^{\delta}$$

where  $\epsilon = -0.17 \pm 0.07$  and  $\delta = 0.60 \pm 0.06$ . This is the first time that these corona thickness exponents have been experimentally determined.

Although there is qualitative agreement between the experimentally determined values of  $\alpha$ ,  $\gamma$ ,  $\beta$ ,  $\epsilon$ , and  $\delta$ , and those predicted by the LOW theory of micelle formation, there exists some quantitative differences, particularly in the absolute magnitudes of  $\gamma$  and  $\alpha$ . For example, the LOW theory predicts that for the copolymer/homopolymer blends investigated (at 115°C)  $\gamma \sim 0.06$  and  $\alpha \sim -0.05$ . In other words, the entropy of mixing effects which cause the micelle core radius to decrease as the ratio ( $M_{hPS}/M_{PS}$ ) decreases are stronger than predicted by the theory. This leads to smaller micelle core radii than predicted when  $M_{hPS}$  is small or  $M_{PS}$  is large. On the other hand, the LOW theory correctly predicts the magnitude of the corona thickness and how it scales with  $M_{hPS}$  and  $M_{PS}$ .

By a combination of PY hard sphere modeling of SAXS data and SAXS invariant analysis the concentration of homopolymer in the micelle core was found to be small ( $\leq 5\%$ ) for all copolymer/homopolymer blends investigated, which is in agreement with the predictions of the theory. However, the experimental results indicated that when ( $M_{hPS}/M_{PS}$ ) was small or ( $M_{PS}/M_{PB}$ ) was large, the concentration of free copolymer at 115°C can greatly exceed the cmc, as the overall copolymer concentration is



increased. This is not predicted by the LOW theory, although the theory does predict a slight increase in the concentration of free copolymer in the homopolymer matrix. These results imply that the cmc is not a true first order phase transition.

The transitions in structure, observed by EM, from spherical micelles to cylindrical micelles to lamellar (vesicles or multilayer) structures with increasing  $M_{hPS}$  and/or increasing  $M_{PB}$  are well explained in terms of interface curvature and chain packing requirements (i.e., the microphase volume fractions), in exactly the same manner as for neat block copolymer and block copolymer/solvent systems. The PY hard sphere modeling of the SAXS curves provides a quantitative determination of the relative volume fractions of the core and corona regions as a function of homopolymer and copolymer block molecular weights, and thus, allows one to predict, a priori, the micelle structure for a particular copolymer/homopolymer blend.

## 8.2 Future Work

One of the main reasons for morphological studies is the determination of structure-property relationships. Therefore, it would be advantageous to examine in more detail the physical properties of the block copolymer/homopolymer blends investigated here. For example, one would like to know how the shape and arrangement of the polybutadiene microdomains effects mechanical properties. It may be that for equivalent PB volume fractions, one morphology may be more efficient

than another in initiating and blunting crazes in the PS matrix, thereby improving toughness. In addition, it has been shown that the optical properties of the blends are also highly dependent in the shape and arrangement of the PB microdomains. Another property of interest is the rheological behavior of these blends above the polystyrene  $T_g$ . It is expected that the relaxation time (i.e., viscosity) should increase markedly as the spherical micelles overlap and form an ordered macrolattice. A transition from viscous liquid to gel like behavior should be observed. Still another property of interest is that of transport. For example, blends in which the PB domains are continuous, even though the PB volume fraction is small (see Figure 7.6 for example), should possess relatively high rates of small molecule gas transport. The effect of temperature on the structure of the copolymer/homopolymer blends was not investigated in the present study. However, the dependence of morphology and physical properties on temperature is an area which deserves considerable attention in any future study.

For blends exhibiting ordered arrangements of spherical micelles, volume fraction calculations favored the existence of a SC lattice, in contrast to the BCC lattice structure of neat copolymers. A conclusive determination of the lattice type in these blends should be made using the same electron microscopy tilting method employed in Appendix B for neat copolymers. In addition, the underlying reasons for the different lattice structure in neat block copolymers and in block copolymer/homopolymer blends is a topic which should be pursued further.

The causes of the discrepancies between the experimental results and the predictions of the LOW theory should also be investigated further, in particular the disagreement in the values of the cmc and the amount of free copolymer, and the dependence of the micelle core radius on the molecular weight of the homopolystyrene and PS block.

In addition, the effect of block copolymer molecular architecture on block copolymer/homopolymer phase diagrams, including the micellar structure, could be studied using, for example, tri-block or star block copolymers. It is imperative that such studies employ SAXS, light scattering, and EM. Studies of block copolymer/homopolymer phase diagrams and micellar structure for AB copolymer/C homopolymer blends would also be interesting to study, particularly for the case where homopolymer C is miscible (i.e., a good solvent, instead of a theta solvent) with one of the copolymer blocks.

## REFERENCES

1. A. Guinier and G. Fournet, Small Angle Scattering of X-Rays, Wiley; New York (1955).
2. L. Rayleigh, "The Incidence of Light Upon a Transparent Sphere of Dimensions Comparable with the Wavelength." Proc. Roy. Soc. (London), A84, 25-46 (1911).
3. F. Zernike and J. A. Prins, "Die Beugung von Rontgenstrahlen an Flussigkeiten als Effekt der Molekulanordnung." Z. Phys., 41, 184-194 (1927).
4. J. M. Ziman, Models of Disorder, Cambridge University Press; Cambridge (1979).
5. J. A. Barker and D. Henderson, "What is "Liquid"? Understanding the States of Matter." Rev. Mod. Phys., 48, 587-671 (1976).
6. L. S. Ornstein and F. Zernike, "Accidental Deviations of Density and Opalescence at the Critical Point of a Single Substance." Proc. Akad. Sci. (Amsterdam), 17, 793-806 (1914).
7. J. K. Percus and G. J. Yevick, "Analysis of Classical Statistical Mechanics by Means of Collective Coordinates." Phys. Rev., 110, 1-13 (1958).
8. M. S. Wertheim, "Exact Solution of the Percus-Yevick Integral Equation for Hard Spheres." Phys. Rev. Lett., 10, 321-323 (1963).
9. E. Thiele, "Equations of State for Hard Spheres." J. Chem. Phys., 39, 474-479 (1963).



10. N. W. Ashcroft and J. Lekner, "Structure and Resistivity of Liquid Metals." *Phys. Rev.*, 145, 83-90 (1966).
11. T. Hashimoto, M. Fujimura, and H. Kawai, "Domain-Boundary Structure of Styrene-Isoprene Block Copolymer Films Cast From Solutions. 5. Molecular Weight Dependence of Spherical Microdomains." *Macromol.*, 13, 1660-1669 (1980).
12. A. Vrij, "Mixtures of Hard Spheres in the Percus-Yevick Approximation. Light Scattering at Finite Angles." *J. Chem. Phys.*, 71, 3267-3270 (1979).
13. P. van Beurten and A. Vrij, "Polydispersity Effects in the Small-Angle Scattering of Concentrated Solutions of Colloidal Spheres." *J. Chem. Phys.*, 74, 2744-2748 (1981).
14. O. Glatter and O. Kratky, Small Angle X-Ray Scattering, Academic Press; New York (1982).
15. P. W. Schmidt, "Collimation Corrections in Small Angle X-Ray Scattering." *Acta Cryst.*, 19, 938-942 (1965).
16. J. S. Lin, C. R. Von Bastian, and P. W. Schmidt, "A Modified Method for Slit-Length Collimation Corrections in Small-Angle X-Ray Scattering." *J. Appl. Cryst.*, 7, 439-442 (1974).
17. O. Glatter, "A New Iterative Method for Collimation Correction in Small-Angle Scattering." *J. Appl. Cryst.*, 7, 147-153 (1974).
18. C. G. Vonk, "A Procedure for Desmearing X-Ray Small-Angle Scattering Curves." *J. Appl. Cryst.*, 4, 340-342, (1971).

19. O. Kratky, I. Pilz, and P. J. Schmitz, "Absolute Intensity Measurement of Small Angle X-Ray Scattering by Means of a Standard Sample." *J. Colloid and Int. Sci.*, 21, 24-34 (1966).
20. I. Pilz and O. Kratky, "Absolute Intensity Measurements of Small-Angle X-Ray Scattering by Means of a Standard Sample, II." *J. Colloid and Int. Sci.*, 24, 211-218 (1967).
21. I. Pilz, "Absolute Intensity Measurement of Small Angle X-Ray Scattering by Means of a Standard Sample, III." *J. Colloid and Int. Sci.*, 30, 140-144 (1969).
22. R. W. Hendricks, "A Unified Theory of Absolute Intensity Measurements in Small Angle X-Ray Scattering." *J. Appl. Cryst.*, 5, 315-324 (1972).
23. C. G. Vonk, "A General Computer Program fo the Processing of Small Angle X-Ray Data." *J. Appl. Cryst.*, 8, 340-341 (1975).
24. A. Guinier, X-Ray Diffraction, W. H. Freeman and Co.; San Francisco (1963).
25. G. Porod, "Die Rontgenkleinwinkelstreuung von Dichtgepackten Kolloiden Systemen. I. Teil." *Kolloid-Z.*, 124, 83-114 (1951); "Die Rontgenkleinwinkelstreuung von Dichtgepackten Kolloiden Systemen. II. Teil." *Kolloid-Z.*, 125, 51-57 (1952); "Die Rontgenkleinwinkelstreuung von Dichtgepackten Kolloiden Systemen. III. Teil." *Kolloid-Z.*, 125, 108-122 (1952).
26. W. Ruland, "Small-Angle Scattering of Two-Phase Systems: Determination and Significance of Systematic Deviations from Porod's Law." *J. Appl. Cryst.*, 4, 70-73 (1971).

27. C. G. Vonk "Investigation of Non-Ideal Two-Phase Polymer Structures by Small-Angle X-Ray Scattering." J. Appl. Cryst., 6, 81-86 (1973).
28. J. T. Koberstein, B. Morra, and R. S. Stein, "The Determination of Diffuse Boundary Thickness of Polymers by Small-Angle X-Ray Scattering." J. Appl. Cryst., 13, 34-45 (1980).
29. T. Hashimoto, A. Todo, H. Itoi, and H. Kawai, "Domain-Boundary Structure of Styrene-Isoprene Block Copolymer Films Cast From Solutions. 2. Quantitative Estimation of the Interfacial Thickness of Lamellar Microphase Systems." Macromol., 10, 377-384 (1977).
30. R. J. Roe, M. Fishkis, and J. C. Chang, "Small-Angle X-Ray Diffraction Study of Thermal Transition in Styrene-Butadiene Block Copolymers." Macromol., 14, 1091-1103 (1981).
31. M. Szwarc, M. Levy, and J. Milkovich, "Polymerization Initiated by Electron Transfer to Monomer. A New Method of Formation of Block Copolymers." J. Am. Chem. Soc., 78, 2656-2657 (1956).
32. S. L. Aggarwal, Ed., Block Polymers, Plenum Press; New York (1970).
33. G. E. Molau, Ed., Colloidal and Morphological Behavior of Block Copolymers, Plenum Press; New York (1971).
34. M. J. Folkes and A. Keller in Physics of Glassy Polymers, R. N. Haward, Ed., Applied Science Publishers; London, 548-597 (1973).

35. B. R. M. Gallot, "Preparation and Study of Block Copolymers with Ordered Structures." *Adv. Polym. Sci.*, 29, 85-156 (1978).
36. I. Goodman, Ed., Developments in Block Copolymers 1., Applied Science Publishers; New York (1982).
37. A. Skoulios, G. Finaz, and J. Parrod, "Obtention de Gels Mesomorphes dans les Melanges de Copolymeres Sequences Styrolene-Oxyde d'Ethylene avec Different Solvents." *Comptes. Rendes.*, 251, 739-743 (1960).
38. A. Skoulios and G. Finaz, "Influence de la Nature du Solvent sur la Structure des Gels Mesomorphes d'un Copolymer Sequence Styrolene-Oxyde d'Ethylene." *Comptes. Rendes.*, 252, 3467-3469 (1961).
39. G. Finaz, A. Skoulios, and C. Sadron, "Obtention de Polymeres Organises par Polymerization de Solutions Concentrees d'un Copolymere Sequence Styrolene-Oxyde d'Ethylene." *Comptes. Rendes.*, 253, 265-267 (1961).
40. V. Luzzati, H. Mustacchi, and A. Skoulios, "The Structure of the Liquid-Crystal Phase of Some Soap+Water Systems." *Disc. Faraday Soc.*, 25, 43-50 (1958).
41. V. Luzzati, H. Mustacchi, A. Skoulios, and F. Husson, "La Structures des Colloides d'Association. I. Les Phases Liquide-Cristallines des Systems Amphiphile-Eau." *Acta. Cryst.*, 13, 660-667 (1960).



42. F. Husson, H. Mustacchi, and V. Luzzati, "La Structure des Colloides d'Association. II. Description des Phases Cristallines de Plusiers Systems Amphiphile-Eau: Amphiphiles, Anioniques, Cationiques, Non-Ioniques." *Acta. Cryst.*, 13, 668-677 (1960).
43. K. Kato, "Osmium Tetroxide Fixation of Rubber Latices." *J. Polym. Sci., Part B*, 4, 35-38 (1966).
44. K. Kato, "The Osmium Tetroxide Procedure for Light and Electron Microscopy of ABS Plastics." *Polym. Eng. and Sci.*, 8, 38-39 (1967).
45. E. Vanzo, "Ordered Structures of Styrene-Butadiene Block Copolymers." *J. Polym. Sci.*, (A-1)4, 1727-1730 (1966).
46. E. B. Bradford and E. Vanzo, "Ordered Structures of Styrene-Butadiene Block Copolymers in the Solid State." *J. Polym. Sci.*, (A-1)6, 1661-1670 (1968).
47. E. W. Fischer, "Structures in Styrene-Butadiene Block Copolymers." *J. Macromol. Sci., Chem.*, A2(6), 1285-1288 (1968).
48. H. Hendus, K.-H. Illers, and E. Ropte, "Strukturuntersuchungen an Styrol-Butadien-Styrol Blockcopolymeren." *Kolloid Z.u.Z. Polymere*, 216, 110-119 (1967).
49. J. F. Beecher, L. Marker, R. P. Bradford, and S. L. Aggarwal, "Morphology and Mechanical Behavior of Block Copolymers." *Am. Chem. Soc. Polym. Prep.*, 8, 1532-1538 (1967); "Morphology and Mechanical Behavior of Block Copolymers." *J. Poly. Sci.*, C26, 117-134 (1969).

50. T. Inoue, J. Soen, and H. Kawai, "Electron Microscopic Texture of A-B Type Block Copolymers of Isoprene with Styrene." *J. Polym. Sci.-Polym. Lett.*, 6, 75-81 (1968); "Thermodynamic Interpretation of Domain Structure in Solvent-Cast Films of A-B Type Block Copolymers of Styrene and Isoprene." *J. Polym. Sci.: Part A*, 2(7), 1283-1302 (1969).
51. M. Matysuo, S. Sagae, and H. Asai, "Fine Structures of Styrene-Butadiene Block Copolymer Films Cast From Toluene Solutions." *Polymer*, 10, 79-87 (1969).
52. P. R. Lewis and C. Price, "Morphology of ABA Block Copolymers." *Nature*, 223, 494-495 (1969).
53. A. Douy, R. Mayer, J. Rossi, and B. Gallot, "Structure of Liquid Crystalline Phases from Amorphous Block Copolymers." *Molec. Cryst. and Liq. Cryst.*, 7, 103-126 (1969).
54. M. Hoffman, G. Kampf, H. Kromer, and G. Pampus, "Kinetics of Aggregation and Dimensions of Supramolecular Structure in Non-crystalline Block Copolymers." *Adv. in Chem., Multicomponent Polymer Series*, 99, 351-357 (1971).
55. G. Kampf, M. Hoffman, and H. Kromer, "Konformation, Übermolekulare Struktur und Weitreichende Ordnung in Nichtkristallinen und Nichtstereospezifischen Polymeren Teil I. Sichtbare Übermolekulare Nichtkristallinen Blockcopolymeren." *Ber. Bunsen-Gesellschaft*, 74, 851-859 (1970).

56. H. Kromer, M. Hoffman, G. Kampf, "Konformation, Übermolekulare Struktur und Weitreichende Ordnung in Nichtkristallinen und Nichtstereospezifischen Polymeren Teil II. Die Übermolekulare Struktur von Blockcopolymeren als Folge einer Unverträglichkeit der Sequenzen und der Molekularen Konformation." Ber. Bunsen-Gesellschaft, 74, 859-865 (1970).
57. J. Dlugosz, A. Keller, and E. Pedemonte, "Electron Microscope Evidence of a Macroscopic Single Crystal From a Three Block Copolymer." Kolloid Z.Z. Polym., 242, 1125-1130 (1970).
58. P. R. Lewis and C. Price, "The Morphology of  $(\text{Styrene})_x(\text{Butadiene})_y$  Block Copolymers." Polymer, 12, 258-270 (1971).
59. A. Douy and B. Gallot, "Study of Liquid-Crystalline Structure of Polystyrene-Polybutadiene-Polystyrene Block Copolymers by Small Angle X-Ray Scattering and Electron Microscopy." Molec. Cryst. Liq. Cryst., 14, 191-207 (1971).
60. A. Douy and B. Gallot "Polybutadiene/Polystyrene/Polybutadiene Block Copolymers." Makromol. Chem., 156, 81-115 (1972).
61. G. Kampf, H. Kromer, and M. Hoffman, "Long-Range Order of Supramolecular Structures in Amorphous Butadiene-Styrene Block Copolymers." J. Macromol. Sci.-Phys., B6(1), 167-190 (1972).
62. T. Uchida, T. Saen, T. Inoue, and H. Kawai, "Domain Structure and Bulk Properties of Solvent-Cast Films of A-B-A Block Copolymers of Styrene-Isoprene-Styrene." J. Polym. Sci.: Part A, 2(10), 101-121 (1972).

63. A. Douy and B. Gallot, "Study of Organized Structures of Polystyrene/Polybutadiene/Polystyrene Block Copolymers." *Makromol. Chem.*, 165, 297-312 (1973).
64. C. Sadron and B. Gallot, "Heterophases in Block Copolymer/Solvent Systems in the Liquid and in the Solid State." *Makromol. Chem.*, 164, 301-332 (1973).
65. M. J. Folkes, A. Keller, and F. P. Scalisi, "An Extrusion Technique for the Preparation of 'Single-Crystals' of Block Copolymers." *Kolloid Z.u.Z. Polymere*, 251, 1-4 (1973).
66. J. Dlugoz, M. J. Folkes, and A. Keller, "Macrolattice Based on a Lamellar Morphology in an SBS Copolymer." *J. Polym. Sci.: Part A-2*, 11, 929-938 (1973).
67. E. Pedemonte, G. Dondero, G. C. Alfonso, and F. deCandia, "Three-Block Copolymers: Morphologies and Stress-Strain Properties of Samples Prepared Under Various Experimental Conditions." *Polymer*, 16, 531-538 (1975).
68. G. Hadziioannou, A. Mathis, and A. Skoulios, "Obtention de <<Monocristaux>> de Polymeres Trisequences Styrene/Isoprene/Styrene par Cisaillement Plan." *Colloid Polym. Sci.*, 257, 136-139 (1979).
69. E. Helfand and Y. Tagami, "Theory of the Interface between Immiscible Polymer. II." *J. Chem. Phys.*, 56, 3592-3601 (1972).
70. E. Helfand, "Block Copolymer Theory. III. Statistical Mechanics of the Microdomain Structure." *Macromol.*, 8, 552-556 (1975).



71. E. Helfand and Z. R. Wasserman, "Block Copolymer Theory. 4. Narrow Interphase Approximation." *Macromol.*, 9, 879-888 (1976).
72. E. Helfand and Z. R. Wasserman, "Block Copolymer Theory. 5. Spherical Domains." *Macromol.*, 11, 960-966 (1978).
73. E. Helfand and Z. R. Wasserman, "Block Copolymer Theory. 6. Cylindrical Domains." *Macromol.*, 13, 994-998 (1980).
74. E. Helfand and Z. R. Wasserman in Developments in Block Copolymers I., I. Goodman, Ed., Applied Science Publishers, London (1982).
75. D. J. Meier, "Theory of Block Copolymers I. Domain Formation in A-B Block Copolymers." *J. Polym. Sci.:Part C*, 26, 81-98 (1969).
76. D. J. Meier, "A Theory of the Morphology of Block Copolymers." *Am. Chem. Soc. Polym. Prep.*, 11, 400-405 (1970).
77. D. J. Meier in Block and Graft Copolymers, J. J. Burke and V. Weiss, Eds., Syracuse University Press, New York (1973).
78. D. J. Meier, "A Theory of the Interface in Block Copolymers." *Am. Chem. Soc. Polym. Prep.*, 15, 171-176 (1974).
79. T. Hashimoto, M. Shibayama, M. Fujimura, and H. Kawai in Block Copolymers. Science and Technology, D. J. Meier, Ed. Harwood Academic Publishers, New York (1981).
80. L. Leibler, "Theory of Microphase Separation in Block Copolymers." *Macromol.*, 13, 1602-1617 (1980).
81. K. M. Hong and J. Noolandi, "Theory of Phase Equilibria in Systems Containing Block Copolymers." *Macromol.*, 16, 1083-1093 (1983).

82. P. G. de Gennes, "Theory of X-Ray Scattering by Liquid Macromolecules With Heavy Atom Labels." *J. Phys. (Paris)*, 31, 235-238 (1970).
83. P. G. de Gennes, Scaling Concepts in Polymer Physics, Cornell University Press; Ithaca, NY (1979).
84. R. W. Richards and J. L. Thomason, "A Small Angle Neutron Scattering Investigation of Block Copolymers of Styrene and Isoprene in the Solid State." *Polymer*, 22, 581-589 (1981).
85. R. W. Richards and J. L. Thomason, "Small-Angle Neutron Scattering Study of Block Copolymer Morphology." *Macromol.*, 16, 982-992 (1983).
86. A. Douy and B. Gallot, "A New Structure for Polystyrene-Polybutadiene Block Copolymers: A Smectic E Type Structure." *Makromol. Chem.*, 182, 265-268 (1981).
87. E. Pedemonte, A. Turturro, V. Bianchi, and P. Devetta, "The Cubic Structure of a SIS Three Block Copolymer" *Polymer*, 14, 145-150 (1973).
88. F. S. Bates, R. E. Cohen, and C. V. Berney, "Small-Angle Neutron Scattering Determination of Macrolattice Structure in a Polystyrene-Polybutadiene Diblock Copolymer." *Macromol.*, 15, 589-592 (1982).
89. D. B. Alward, D. J. Kinning, E. L. Thomas, and L. J. Fetters, "Effect of Arm Number and Arm Molecular Weight on the Solid-State Morphology of Poly(styrene-isoprene) Star Block Copolymers." *Macromol.*, 19, 215-224 (1986).

90. D. J. Kinning, E. L. Thomas, D. B. Alward, L. J. Fetters, and D. L. Handlin, "Sharpness of the Functionality Induced Structural Transition in Poly(styrene-isoprene) Star Block Copolymers." *Macromol.*, 19, 1288-1290 (1986).
91. E. L. Thomas, D. B. Alward, D. J. Kinning, D. C. Martin, D. L. Handlin, and L. J. Fetters, "The Ordered Bicontinuous Double Diamond Structure of Star Block Copolymers-A New Equilibrium Microdomain Morphology." Accepted for publication in *Macromol.* (1986).
92. D. Herman, Masters Thesis, University of Massachusetts (Amherst), (1986).
93. H. Hasegawa, T. Hashimoto, D. J. Kinning, and E. L. Thomas, to be published.
94. R. J. Roe "Examination of Errors in the Determination of Phase Boundary Thickness by Small Angle X-Ray Scattering." *J. Appl. Cryst.*, 15, 182-189 (1982).
95. F. S. Bates, C. V. Berney, and R. E. Cohen, "Microphase Structure of Solvent-Cast Diblock Copolymers and Copolymer-Homopolymer Blends Containing Spherical Microdomains." *Macromol.*, 16, 1101-1108 (1983).
96. G. Hadziioannou and A. Skoulios, "Molecular Weight Dependence of Lamellar Structure in Styrene/Isoprene Two and Three-Block Copolymers." *Macromol.*, 15, 258-262 (1982).

97. R. W. Richards and J. L. Thomason, "Small-Angle Neutron Scattering Measurement of Block Copolymer Interphase Structure." *Polymer*, 24, 1089-1096 (1983).
98. M. Fujimura, H. Hashimoto, K. Kurahashi, T. Hashimoto, and H. Kawai, "Domain-Boundary Structure of Styrene-Isoprene Block Copolymer Films Cast From Solutions. 6. Effect of Temperature on Spherical Microdomain Structure." *Macromol.*, 14, 1196-1202 (1981).
99. R. J. Roe, "Phase Diagram of Polymer Blends Containing Block Copolymers." *Polym. Eng. and Sci.*, 25(17), 1103-1109 (1985).
100. Z. Tuzar and P. Kratochvil, "Block and Graft Copolymer Micelles in Solution." *Adv. in Coll. and Int. Sci.*, 6, 201-232 (1976).
101. C. Price, "Micelle Formation by Block Copolymers in Organic Solvents." *Pure and Appl. Chem.*, 55(10), 1563-1572 (1983).
102. C. Price in Developments in Block Copolymers-1." I. Goodman, Ed., Applied Science Publishers, Barking (1982).
103. H. G. Elias, "Nonionic Micelles." *J. Macromol. Sci., Chem.*, A7(3), 601-622 (1973).
104. J. Plestil and J. Baldrian, "Small-Angle X-ray Scattering of the Block Copolymer Polystyrene/Polybutadiene/Polystyrene in Ethyl Methyl Ketone." *Makromol. Chem.*, 174, 183-191 (1973).
105. J. Plestil and J. Baldrian, "Determination of the Structure Parameters of Styrene/Butadiene Block Copolymers in Heptane by Means of Small-Angle X-ray Scattering." *Makromol. Chem.*, 176, 1009-1028 (1975).



106. C. Booth, De V. T. Naylor, C. Price, N. S. Rajab, and R. B. Stubbersfield, "Investigation of the Size Distribution of Non-Ionic Micelles Formed from a Polystyrene-Polyisoprene Block Copolymer in N,N-Dimethylacetamide." J. C. S. Faraday I, 74, 2352-2362 (1978).
107. P. A. Canham, T. P. Lally, C. Price, and R. B. Stubbersfield, "Formation of Worm-like Micelles from a Polystyrene-Polybutadiene-Polystyrene Block Copolymer in Ethyl Acetate." J. C. S. Faraday I, 76, 1857-1867 (1980).
108. C. Price, A. L. Hudd, and B. Wright, "The Concentration Dependence of the Angular Dissymmetry of Light Scattering by Micelle Solutions." Polymer, 23, 170-173 (1982).
109. T. Kotaka, T. Tanaka, M. Hattori, and H. Inagaki, "Block Copolymer Micelles in Dilute Solution." Macromol., 11, 138-145 (1978).
110. P. Marie, R. Duplessix, Y. Gallot, and C. Picot, "Micellar Solutions Obtained with Amphiphilic Block Copolymers in the Presence of Water, Oil, and Alcohol. 1. Small Angle Neutron Scattering Structure Investigation in the Case of Poly(2-vinylpyridine-b-ethylene oxide) Block Copolymers." Macromol., 12, 1180-1186 (1979).
111. J. Noolandi and K. M. Hong, "Theory of Block Copolymer Micelles in Solution." Macromol., 16, 1443-1448 (1983).

112. L. Leibler, H. Orland, and J. C. Wheeler, "Theory of Critical Micelle Concentration for Solutions of Block Copolymers." *J. Chem. Phys.*, 79, 3550-3557 (1983).
113. P. G. de Gennes in Solid State Physics, Academic Press; New York, Suppl. 14 (1978).
114. Z. Tuzar, A. Sikora, V. Petrus, and P. Kratochvil, "Anomalous Behavior of Solutions of Styrene-Butadiene Block Copolymers in Some Solvents." *Makromol. Chem.*, 178, 2743-2746 (1977).
115. M. Gervais and B. Gallot, "Phase Diagram and Structural Study of Polystyrene-Poly(ethylene oxide) Block Copolymers. 2. Systems Polystyrene-Poly(ethylene oxide)/Solvent of the Poly(ethylene oxide) Block." *Makromol. Chem.*, 174, 193-214 (1973).
116. M. Shibayama, T. Hashimoto, and H. Kawai, "Ordered Structures in Block Polymer Solutions. 1. Selective Solvents." *Macromol.*, 16, 16-28 (1983).
117. G. E. Molau and W. M. Wittbrodt, "Colloidal Properties of Styrene-Butadiene Block Copolymers." *Macromol.*, 1, 260-264 (1968).
118. T. Inoue, T. Soen, T. Hashimoto, and H. Kawai, "Studies on Domain Formation of the A-B Type Block Copolymers from its Solutions. Ternary Polymer Blends of the Styrene-Isoprene Block Copolymers with Polystyrene and Polyisoprene." *Macromol.*, 3, 87-92 (1970).
119. E. B. Bradford in Colloidal and Morphological Behavior of Block and Graft Copolymers, Plenum Press; New York (1971).

120. O. S. Gebizlioglu, A. S. Argon, and R. E. Cohen "Crazing and Plastic Deformation in a Block Copolymer-Glassy Homopolymer System." Polym. Prep., 22(2), 257-258 (1981).
121. A. S. Argon, R. E. Cohen, O. S. Gebizlioglu, and C. E. Schwier, "Crazing in Block Copolymers and Blends." Adv. in Polym. Sci., 52/53, 275-334 (1983).
122. D. J. Meier, "The Solubilization of Homopolymers by Block Copolymers." Polym. Prep., 18, 340-345 (1977).
123. H. Hashimoto, M. Fujimura, T. Hashimoto, and H. Kawai, "Domain-Boundary Structure of Styrene-Isoprene Block Copolymer Films Cast From Solutions. 7. Quantitative Studies of Solubilization of Homopolymers in Spherical Domain Systems." Macromol., 14, 844-851 (1981).
124. D. J. Kinning and E. L. Thomas, "Hard-Sphere Interactions Between Spherical Domains in Diblock Copolymers." Macromol., 17, 1712-1718 (1984).
125. W. C. Zin and R. J. Roe, "Phase Equilibria and Transition in Mixtures of a Homopolymer and a Block Copolymer. 1. Small-Angle X-Ray Scattering Study." Macromol., 17, 183-188 (1984).
126. R. J. Roe and W. C. Zin, "Phase Equilibria and Transition in Mixtures of a Homopolymer and a Block Copolymer. 2. Phase Diagram." Macromol., 17, 189-194 (1984).

127. M. D. Whitmore and J. Noolandi, "Theory of Phase Equilibria in Block Copolymer-Homopolymer Blends." *Macromol.*, 18, 2486-2497 (1985).
128. J. Selb, P. Marie, A. Rameau, R. Duplessix, and Y. Gallot, "Study of the Structure of Block Copolymer-Homopolymer Blends Using Small Angle Neutron Scattering." *Polym. Bull.*, 10, 444-451 (1983).
129. D. Rigby and R. J. Roe, "Small-Angle X-Ray Scattering Study of Micelle Formation in Mixtures of Butadiene Homopolymer and Styrene-Butadiene Block Copolymer." *Macromol.*, 17, 1778-1785 (1984).
130. D. Rigby and R. J. Roe, "Small-Angle X-Ray Scattering Study of Micelle Formation in Mixtures of Butadiene Homopolymer and Styrene-Butadiene Block Copolymer. 2. Effects of Block Lengths." *Macromol.*, 19, 721-728 (1986).
131. M. D. Whitmore and J. Noolandi, "Theory of Micelle Formation in Block Copolymer-Homopolymer Blends." *Macromol.*, 18, 657-663 (1985).
132. E. Helfand and A. M. Sapse, "Theory of Unsymmetric Polymer-Polymer Interfaces." *J. Chem. Phys.*, 62, 1327-1331 (1975).
133. R. J. Roe, "Small-Angle X-Ray Scattering Study of Micelle Formation in Mixtures of Butadiene Homopolymer and Styrene-Butadiene Block Copolymer. 3. Comparison with Theory." *Macromol.*, 19, 728-731, (1986).



134. R. J. Roe and W. C. Zin, "Determination of the Polymer-Polymer Interaction Parameter for the Polystyrene-Polybutadiene Pair." *Macromol.*, 13, 1221-1228 (1980).
135. L. Leibler and P. A. Pincus, "Ordering Transition of Copolymer Micelles." *Macromol.*, 17, 2922-2924 (1984).
136. L. J. Fetters, "Procedures for Homogeneous Anionic Polymerization." *J. Res. Nat. Bur. Stand.*, 70A, 421-433 (1966).
137. L. J. Fetters, "Synthesis of Block Polymers by Homogeneous Anionic Polymerization." *J. Polym. Sci.: Part C*, 26, 1-35 (1969)
138. L. J. Fetters and M. Morton in Macromolecular Synthesis, V. 4, W. J. Bailey, Ed., John Wiley and Sons; New York (1972).
139. M. Morton and L. J. Fetters, "Anionic Polymerization of Vinyl Monomers." *Rubb. Chem. Tech.*, 48, 359-400 (1975).
140. D. B. Alward, Ph. D. Dissertation, Polymer Science and Engineering Dept., University of Massachusetts (Amherst), 1984.
141. P. R. Bevington, Data Reduction and Error Analysis for the Physical Sciences, McGraw-Hill; New York (1969).
142. J. Brandrup and E. H. Immergut, Polymer Handbook, 2nd Ed., Wiley; New York (1975).
143. M. J. Richardson and N. G. Savill, "Volumetric Properties of Polystyrene: Influence of Temperature, Molecular Weight and Thermal Treatment." *Polymer*, 18, 3-9 (1977).
144. N. Hadjichristidis, X. Zhongde, and L. J. Fetters, "The Characteristic Ratios of Stereoirregular Polybutadiene and Polyisoprene." *J. Polym. Sci. (Phys)*, 20, 743-750 (1982).

145. C. V. Berney, R. E. Cohen, F. S. Bates, "Sphere Sizes in Diblock Copolymers: Discrepancy Between Electron Microscopy and Small-Angle Scattering Results." *Polymer*, 23, 1222-1226 (1982).
146. J. N. Israelachvili, D. J. Mitchell, and B. W. Ninham, "Theory of Self-Assembly of Hydrocarbon Amphiphiles into Micelles and Bilayers." *J. Chem. Soc., Faraday Trans II.*, 72, 1525-1568 (1976).
147. J. N. Israelachvili, S. Marcelja, and R. G. Horn, "Physical Principles of Membrane Organization." *Quart. Rev. of Biophys.*, 2, 121-200 (1980).
148. J. E. Sax and J. M. Ottino, "Modeling of Transport of Small Molecules in Polymer Blends: Application of Effective Medium Thoery." *Polym. Eng. and Sci.*, 23, 165-176 (1983).
149. H. T. Davis, "The Effective Medium Theory of Diffusion in Composite Media." *J. Am. Ceramic Soc.*, 60, 499-501 (1977).
150. C. Maxwell, Treatise on Electricity and Magnetism Vol. I, Oxford University Press; London (1873).
151. L. Rayleigh, "On the Influence of Obstacles Arranged in Rectangular Order Upon the Properties of a Medium." *Phil. Mag.*, 34, 481-502 (1892).
152. J. E. Sax, Ph. D. Thesis, University of Massachusetts, Amherst (1984).
153. R. M. Felder and G. S. Huvarad in Methods of Experimental Physics, 16C, R. Fava, Ed., Academic Press; New York (1980).

154. C. H. Y. Chen Tsai, E. L. Thomas, and W. J. MacKnight, "Structure and Morphology of Segmented Polyurethanes. III. Electron Microscopy and Small Angle X-Ray Scattering Studies of Amorphous Random Segmented Polyurethanes." *Polymer*, 27, 659-666 (1986).
155. J. E. Sax and J. M. Ottino, "Influence of Morphology on the Transport Properties of Polystyrene/Polybutadiene Blends. 1. Experimental Studies." *Polymer*, 26, 1073-1080 (1985).
156. N. Shah, J. E. Sax, and J. M. Ottino, "Influence of Morphology on the Transport Properties of Polystyrene/Polybutadiene Blends. II. Modeling Results." *Polymer*, 26, 1239-1246 (1985).
157. F. Annighofer and W. Gronski, "Blockpolymers of Styrene and Isoprene With Variable Interphase: Morphology and Dynamic Viscoelastic Behavior." *Coll. and Int. Sci.*, 261, 15-25 (1983).

## A P P E N D I X    A

### Effect of Morphology on the Transport of Small Molecule Gases in Block Copolymers

#### Introduction

The interaction of transport and morphology in multiphase polymer systems arises under many practical conditions; for example, in devolatilization in polymer blends, and in the design of membranes, photographic films, coatings, packaging materials, and protective clothing to name but a few. Nevertheless, there have been few combined studies of transport and morphology in multiphase polymer blends, with only simple diffusion and morphological models being considered.

Recently, Sax and Ottino [148] have presented models for predicting the effective diffusion coefficient of small molecule gases in two phase polymer blends exhibiting small scale order, but large scale disorder. As shown in Figure A.1 (taken from this work), for the case of alternating lamellar domains, the structure is considered to consist of small (relative to the size of the sample) grains, in which there is a high degree of order, oriented randomly with respect to each other so that macroscopically the structure is isotropic. The models predict that the effective diffusion coefficient is not only a function of the volume fractions of the phases, but is also highly dependent on the domain morphology. Especially important in determining the



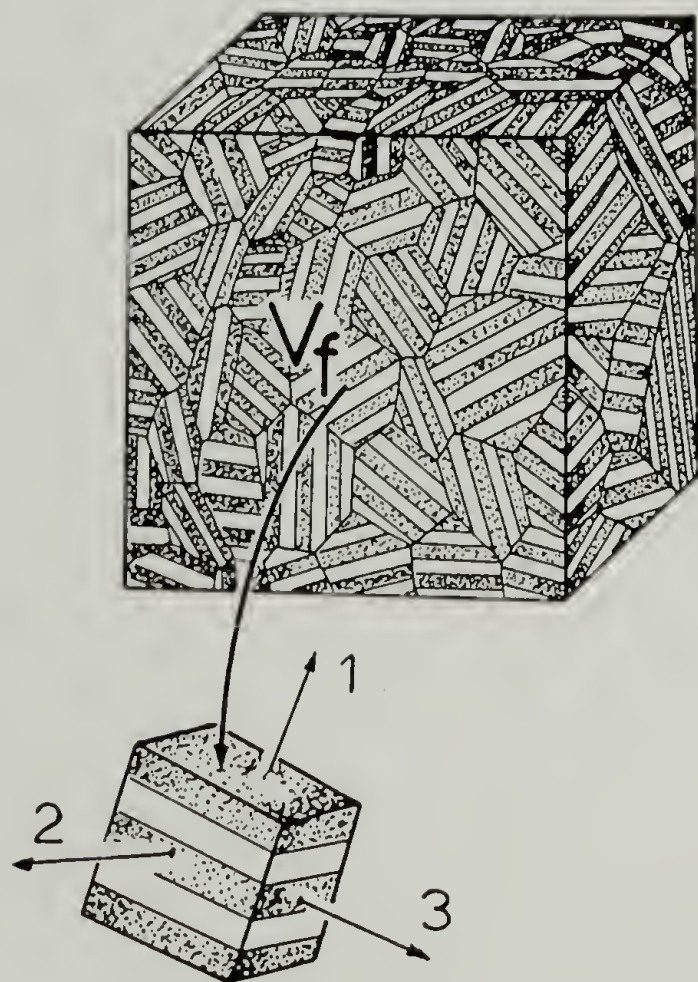


Figure A.1 Structured composite having random orientation of ordered lamellar grains. The grain volume,  $V_f$ , is much smaller than the volume of the sample (taken from Sax and Ottino [148]).

transport behavior is the connectivity of the more diffusive (conductive) phase. Therefore, transport measurements can provide guidance in cases where other experimental techniques do not indicate which of the two phases is continuous. The models can predict the effective diffusion coefficient,  $D_{\text{eff}}$ , as a function of composition for spherical, cylindrical, and lamellar domains. These are exactly the type of domain structures often encountered for ordered block copolymers. Therefore, these materials should serve as model experimental systems with which to test the predictions of Sax and Ottino's models. In addition, by employing different casting solvents, the domain morphology of block copolymers (i.e., the connectivity of the phases) can be systematically altered, enabling the effect of morphology on transport to be independently investigated.

### Review of the Models

Assuming Fickian diffusion, the transport behavior within the small-scale ordered grain is assumed to be given by

$$\underline{J} = -\underline{D} \cdot \nabla C \quad (\text{A1})$$

where  $\underline{J}$  is the flux vector,  $\underline{D}$  is the diffusion tensor, and  $C$  is concentration. As shown by Sax and Ottino [148], if there is random orientation of the grains the effective diffusion coefficient is given

simply by the average of the diffusion coefficients in the principal directions

$$D_{\text{eff}} = (1/3) (D_{11} + D_{22} + D_{33}). \quad (\text{A2})$$

For example, in the alternating lamellar grains of Figure A.1, the diffusion coefficients along the principal directions are given by

$$D_{11} = D_B ([ (1-\phi_B) Sx + \phi_B ] [ S(1+\phi_B(1-S)/S) ])^{-1} \quad (\text{A3})$$

$$D_{22} = D_{33} = D_B [ (1-\phi_B) Sx + \phi_B ] / [ S(1+\phi_B(1-S)/S) ] \quad (\text{A4})$$

where  $\phi_A$  and  $\phi_B$  are the volume fractions of phases A and B,  $S = S_A/S_B$ , and  $x = D_A/D_B$ .  $S_A$  and  $S_B$  are the penetrant solubilities, and  $D_A$  and  $D_B$  are the penetrant diffusion coefficients in components A and B.

Equations A3 and A4 were obtained by combining the classical results for electrical conductivity in layered domains (i.e., series and parallel laws) with the fact that the driving force for diffusion is the gradient of chemical potential rather than the gradient of concentration [149].

Solutions for the effective dielectric permeability of a dilute suspension of spheres [150] and a cubic lattice of cylinders [151] have long since been known, from which expressions for the effective diffusion coefficients for these structures can also be obtained. The corrections to these solutions, taking into account the actual cubic lattice packing of spherical domains and the hexagonal packing of cylindrical domains, is expected to be small. Therefore, in terms of

predicting diffusion behavior, these microstructure models are a good approximation to the equilibrium microstructures observed in block copolymers. Incorporation of these microstructure equations into Equation A2 provides simple models for predicting effective diffusion equations for materials having small scale order and large scale disorder. The equations given by Sax and Ottino for spheres (A5), cylinders (A6), and lamellae (A7) are:

$$D_{\text{eff}}^S = \frac{D_c (1 + 3\phi_d (\frac{\bar{s}\bar{x} + 2}{\bar{s}\bar{x} - 1} - \phi_d)^{-1})}{\bar{s}(1 + \phi_c(1 - \bar{s})/\bar{s})} \quad (\text{A5})$$

$$D_{\text{eff}}^C = [\bar{s}(1 + \phi_c(1 - \bar{s})/\bar{s})]^{-1} D_c \left[ (1/3)[(1 - \phi_d) + \phi_d \bar{x}\bar{s}] + (2/3)[1 + 2\phi_d (\frac{\bar{s}\bar{x} + 1}{\bar{s}\bar{x} - 1} - \phi_d + 0.3 \frac{\bar{s}\bar{x} - 1}{\bar{s}\bar{x} + 1} \phi_d^4 + .013 \frac{\bar{s}\bar{x} - 1}{\bar{s}\bar{x} + 1} \phi_d^8)^{-1}] \right] \quad (\text{A6})$$

$$D_{\text{eff}}^L = \frac{D_B ((1/3)[((1 - \phi_B)/Sx) + \phi_B]^{-1} + (2/3)[(1 - \phi_B)Sx + \phi_B])}{S(1 + \phi_B(1 - S)/S)} \quad (\text{A7})$$

where c is the continuous phase, d is the dispersed phase, and  $\bar{s}$  and  $\bar{x}$  are defined as

$$\bar{s} = \text{solubility ratio } (S_d/S_c)$$

$$\bar{x} = \text{diffusivity ratio } (D_d/D_c)$$



## Experimental

The molecular characteristics of the poly(styrene-butadiene) block copolymers used for this study are listed in Table A1. Except for samples SB 22/10 and SBS Kraton<sup>R</sup>, these are the same samples that were used previously in this dissertation to study the structure of block copolymer/homopolymer blends. The molecular weights and compositions of the copolymers were determined by a combination of GPC and UV absorption analysis as described in Section 4.1. All of these copolymers with the exception of the SBS Kraton<sup>R</sup>, which was obtained from Shell Co., were prepared by Dr. L. J. Fetters of Exxon Research and Engineering Company using the butyl lithium initiated anionic synthesis technique outlined in Section 4.1.

The polystyrene and polybutadiene homopolymers used to obtain the pure component diffusion properties were Lustrex<sup>R</sup> polystyrene, obtained from Monsanto, which had a weight average molecular weight of 250,000, and Diene 35 NFA/AC, an alkyl lithium polymerized polybutadiene made by Firestone Synthetic Rubber and Latex Company, which had a weight average molecular weight of 182,000.

Films, approximately 0.5 mm thick, for morphological characterization and diffusion measurements were prepared by slow casting from a 3% w/v solution in toluene over a period of one week followed by 125 °C annealing for 3 days. This sample preparation technique was utilized in order to obtain, as near as possible, equilibrium microstructures. Electron microscopy and SAXS were performed

TABLE A1

Characteristics of poly(styrene-butadiene) block copolymers

Sample	Designation	M <sub>n</sub> PS (Kg/mole)	M <sub>n</sub> PB (Kg/mole)	Ø <sub>PS</sub>	morphology
SB 60/10	A	56.6	10.9	.818	PB spheres
SB 40/10	B	42.0	10.3	.779	PB cylinders
SB 23/10	C	22.2	9.0	.682	PB cylinders
SB 22/10	D	21.7	10.1	.651	OBDD
SB 10/10	E	12.0	10.0	.512	Disordered
SB 20/20	F	20.5	20.5	.465	Lamellar
SB 40/40	G	42.3	45.0	.447	Lamellar
SB 80/80	H	81.0	74.5	.486	Lamellar
SB 80/80 MEK	I	81.0	74.5	.486	PB spheres
SBS Kraton	J	30	70	.27	PS cylinders
SB 10/65	K	10.7	63.1	.127	PS spheres

in the manner described previously in Sections 4.3 and 4.4.

The measurement of effective diffusion coefficients and solubilities utilized  $\text{CO}_2$  in a constant pressure sorption apparatus which consisted of a gas delivery system and a Cahn Model 2000 electrobalance. The details of this apparatus have been given elsewhere [152]. The mass of the sample as a function of diffusion time was monitored within 2 micrograms continuously and output to a chart recorder and an Apple 2e minicomputer. Sorption and desorption measurements were made at approximately 25 °C and from subatmospheric to atmospheric pressures. Sample dimensions were typically 1 cm X 1 cm X 0.05 cm so that they could be approximated as semi-infinite slabs. The calculation of effective diffusion coefficients from sorption and desorption curves for this geometry have been described by Felder and Huvard [153]. Four different methods of calculating effective diffusion coefficients from the mass versus time curves have been employed here: initial slope, half-time, moment, and limiting slope methods. Solubility coefficients were determined from the equilibrium weight gain or loss.

### Results and Discussion

Electron micrographs of the block copolymer samples listed in Table A1 are shown in Figure A.2 (the letters on the micrographs refer to the sample designation given in Table A1). The domain morphology of each sample, determined from an inspection of these micrographs, is also



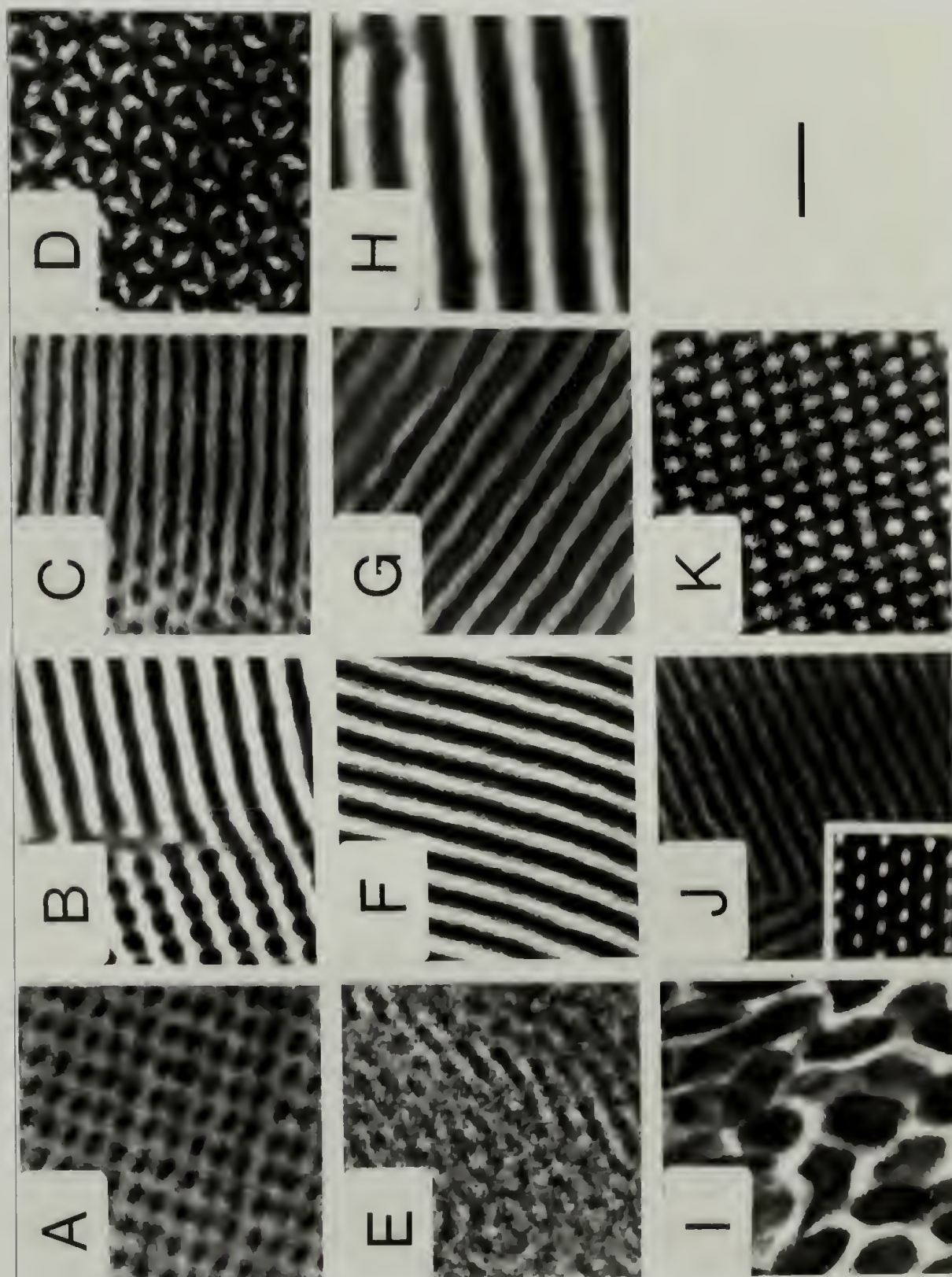


Figure A.2 Electron micrographs of the block copolymer samples. The letters refer to the designation given in Table A1. The magnification bar corresponds to 1000 Å except for D and E, for which it corresponds to 667 Å.



listed in Table A1. Except for samples SB 80/80 MEK and SB 10/10, the morphologies are those expected considering the relative volume fractions of the two components.

Sample SB 22/10 exhibits the recently discovered [91] ordered bicontinuous double diamond structure in which the polybutadiene and polystyrene phases are both continuous. The structure consists of two translationally displaced, mutually interwoven, but unconnected three dimensional networks of polybutadiene (minority phase) rods embedded in a polystyrene matrix. Each of the separate polybutadiene networks has the symmetry of a double diamond cubic lattice.

Although one might expect SB 10/10 to have a lamellar domain structure, it exhibits a rather disordered phase separated structure (see Figure A.2) reminiscent of that seen by Chen-Tsai [153] in amorphous random segmented polyurethanes having total molecular weights of about 20,000. Further annealing had no effect on the SB 10/10 structure. Hadziioannou and Skoulios [96] have observed similar disordered structures in poly(styrene-isoprene) di- and tri- block copolymers having approximately 50% polystyrene, for which the total molecular weights were less than about 20,000 and 40,000 respectively. This was explained in terms of a melting transition between an ordered lamellar structure and a disordered phase separated structure.

While sample SB 80/80 cast from toluene has the expected alternating lamellar morphology for this composition, the same sample cast from methyl ethyl ketone (SB 80/80 MEK), a preferential solvent for the polystyrene block, has the morphology of nearly spherical

polybutadiene domains in a continuous matrix of polystyrene (see Figure A.2). The effective diffusion coefficient of this copolymer cast from the different solvents should therefore show a marked difference, even though the composition is constant.

The transport properties of the pure components, which are needed in the model calculations, have been determined previously by Sax and Ottino [155] using the same apparatus used here. It was found that the transport of  $\text{CO}_2$  in polystyrene and polybutadiene at pressures less than one atmosphere and at approximately 25 °C was Fickian (the curves of dimensionless mass versus time for the sorption and desorption runs were found to be superimposable) and that the effective diffusion coefficient was independent of the penetrant concentration. The pure component effective diffusion and solubility coefficients determined by the four aforementioned methods are listed in Table A2. Good agreement between the methods is found; in particular, the values determined from the half time and moment method are virtually identical.

Sorption and desorption experiments were also performed for the block copolymer samples; the values of  $D_{\text{eff}}$  determined by all four methods, as well as  $S_{\text{eff}}$ , are listed in Table A2. The values found by the sorption and desorption experiments were the same within the error of the measurements; therefore, the values listed in Table A2 are averages of the sorption and desorption values. Although the methods give values for  $D_{\text{eff}}$  which are within approximately 30% of each other for a given sample, the values of  $D_{\text{eff}}$  determined by the initial slope method are always found to be greater than those determined by the

limiting slope method (the half time and moment methods give intermediate values). Sax and Ottino [155] found the opposite trend in mechanically interdispersed blends of polystyrene and polybutadiene. This was attributed to the presence of the more conductive phase at the surface of the sample leading to a relatively rapid weight increase during the initial portion of the experiment. Near the end of the experiment, domains of the more conductive phase are near equilibrium while the domains of the less conductive phase are still sorbing a significant amount of the penetrant. Thus, the weight increase with time near the end of the experiment is relatively slow. This effect should be more pronounced the larger the less conductive domains are. It was later predicted by unsteady-state modeling of disordered composites [156] that the initial slope method should yield higher values of the effective diffusion coefficient when the less conductive phase is the majority phase, but that the limiting slope method should yield higher values of the effective diffusion coefficient when the more conductive phase is the majority phase. The reason that the initial slope method consistently yielded smaller effective diffusion coefficients for the present samples is not clear, although undoubtedly the length scale of the domain structure is much smaller in block copolymers than in blends. In addition, blends have a rather random phase separated structure, whereas block copolymers exhibit very regular phase separated structures.

The values of the effective solubilities for these samples are plotted as a function of composition in Figure A.3. The straight line

TABLE A2

Transport data for pure components and block copolymers

<u>Sample Designation</u>		$D_{\text{eff}} \text{ (cm}^2\text{/s)} \pm 15\%$				$S_{\text{eff}} \pm 5\%$
		Initial	Half	Moment	Limiting	$(\text{cm}^3_{\text{STP}}/\text{g atm})$
		slope	time		slope	
Polystyrene		4.8E-8	4.7E-8	4.7E-8	5.3E-8	1.90
Polybutadiene		3.6E-6	3.1E-6	3.1E-6	2.9E-6	0.78
SB 60/10	A	7.4E-8	7.7E-8	8.2E-8	8.7E-8	1.62
SB 40/10	B	1.4E-7	1.6E-7	1.7E-7	1.9E-7	1.48
SB 23/10	C	2.6E-7	2.8E-7	2.9E-7	3.1E-7	1.10
SB 22/10	D	4.5E-7	4.7E-7	4.8E-7	5.3E-7	0.92
SB 10/10	E	2.5E-7	3.1E-7	3.5E-7	4.1E-7	1.02
SB 20/20	F	5.8E-7	6.4E-7	6.4E-7	7.1E-7	1.17
SB 40/40	G	5.5E-7	6.1E-7	6.4E-7	7.3E-7	1.26
SB 80/80	H	6.0E-7	6.3E-7	6.6E-7	7.3E-7	1.30
SB 80/80 MEK	I	2.2E-7	2.4E-7	2.6E-7	2.8E-7	1.13
SBS Kraton	J	1.3E-6	1.4E-6	1.5E-6	1.7E-6	1.01
SB 10/65	K	1.9E-6	2.1E-6	2.2E-6	2.5E-6	0.91



represents the predicted solubility based on the additivity rule:

$$S_{\text{eff}} = \phi_A S_A + \phi_B S_B \quad (\text{A8})$$

While the values of  $S_{\text{eff}}$  are all found to be somewhat less than that predicted by Equation A8, except for three samples (SB 10/10, SB 22/10, and SB 23/10) the values of  $S_{\text{eff}}$  agree, within the error of the measurements, to the predictions of the additivity rule. The reason for the negative deviation, in the case of samples SB 10/10, SB 22/10, and SB 23/10 is not immediately apparent, although the reason may lie in the low molecular weights of these samples, and hence, the fact that these samples have a relatively large amount of interfacial material.

Figure A.4 shows the measured effective diffusion coefficients, taken as the average given by the four different methods, as a function of composition for the samples listed in Table A1. Also shown in Figure A.4 are the predicted effective diffusion coefficients as a function of composition for different domain morphologies as predicted by the models of Sax and Ottino. Good agreement between the experimental and predicted effective diffusion coefficients as a function of copolymer morphology is seen in the case of samples having spherical, cylindrical, or lamellar domains.

The four samples containing approximately 50% polystyrene were examined with the intention of studying the effect of the interfacial region on diffusion, while maintaining a lamellar structure (however, as shown by the micrograph in Figure A.2, SB 10/10 did not have a lamellar

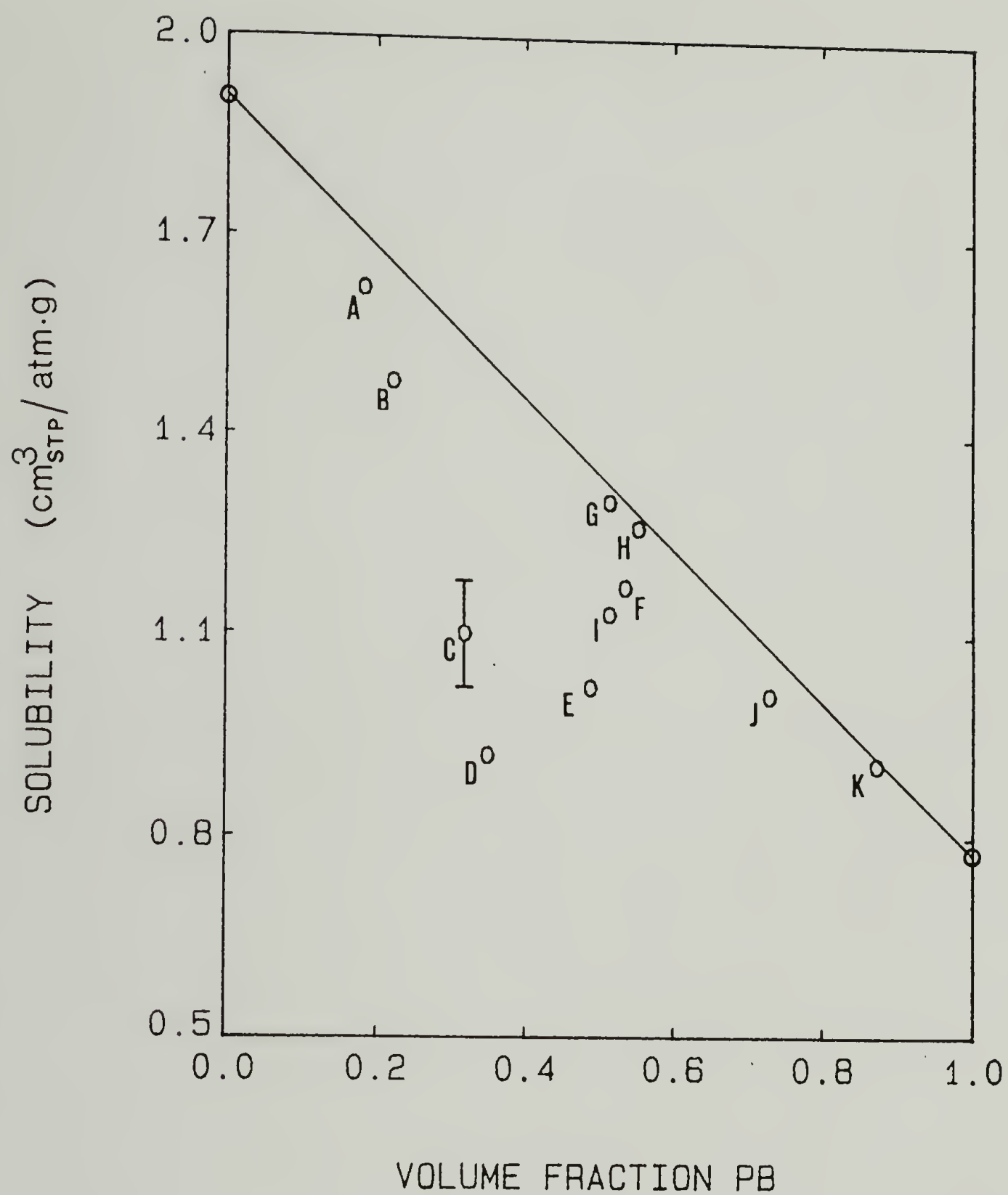


Figure A.3 Effective solubility coefficients as a function of composition. The bar in measurement C indicates representative errors.

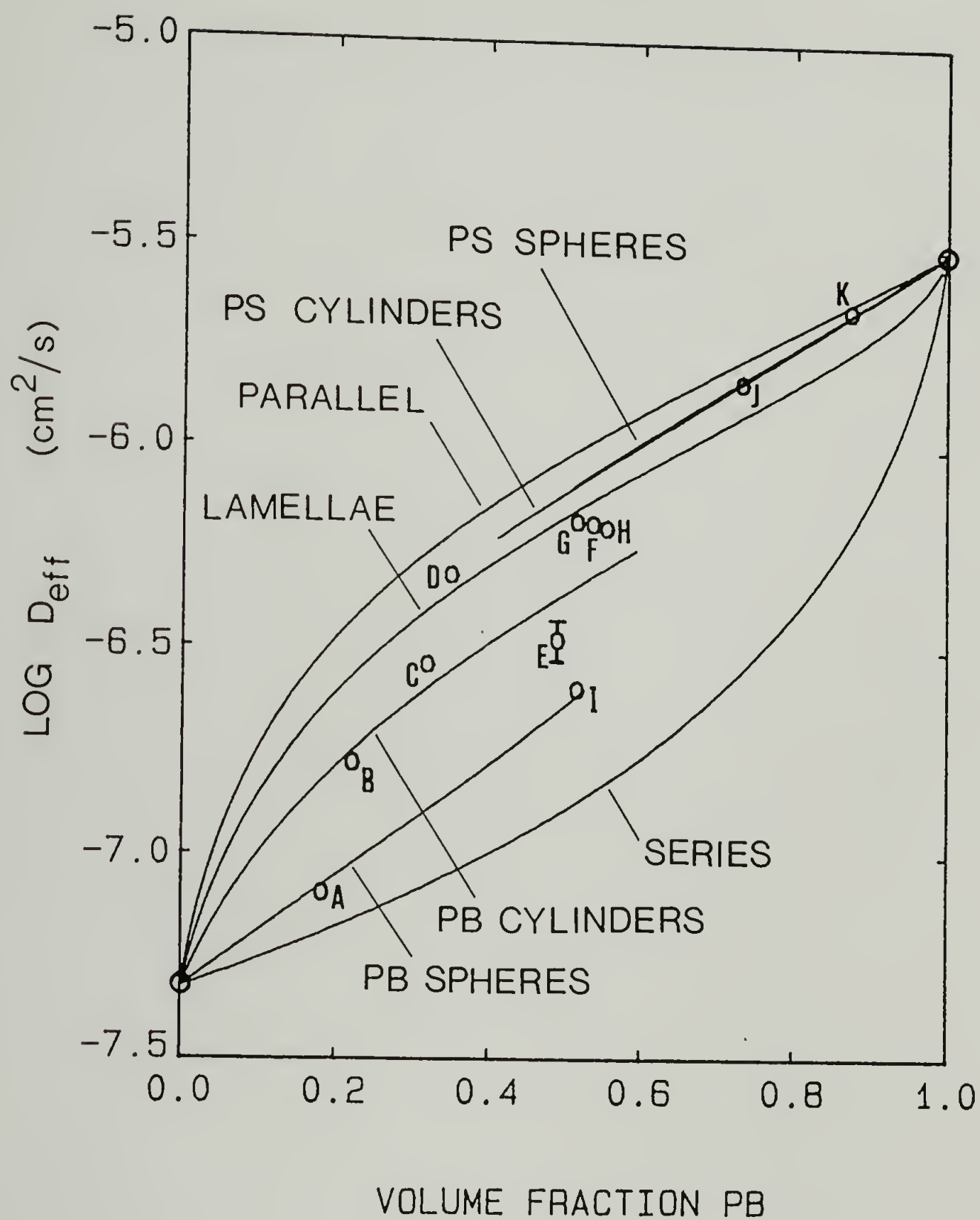


Figure A.4 Effective diffusion coefficients as a function of composition and morphology. The bar in measurement E indicates representative errors.

structure). In order to determine the change in diffusion coefficients arising solely from changes in the amount of interfacial material, it is necessary for the samples studied to possess the same amount of orientation of lamellar grains. While some workers [29] have been able to produce samples in which the lamellae are parallel to the film surface, the present samples possessed little, if any, preferential orientation, as SAXS patterns obtained with the beam normal and parallel to the film surface showed little difference.

It has been shown experimentally that, above about 10,000 molecular weight, the interface thickness  $t$  changes little with molecular weight [11,29,30,95,97] being about 20 Å. On the other hand, the lamellar spacing should increase with about the  $2/3$  power of molecular weight. Therefore, the volume fraction of interfacial material, given by  $2t/d_1$  where  $d_1$  is the lamellar spacing, should decrease with the molecular weight of the copolymer. The lamellar spacings obtained from the positions of the SAXS lattice peaks were 375, 600, and 810 Å giving interfacial volume fractions of 0.11, 0.07, and 0.05 for samples SB 20/20 (F), SB 40/40 (G), and SB 80/80 (H) respectively.

Within the error of the transport measurements, no effect of interfacial volume fraction on the effective diffusion coefficient was observed, although a rather limited range of interfacial volume fractions were examined. A better experimental system to test for the effect of interface might be that of graded block copolymers in which the change from one type of monomer unit in the chain to another is not



abrupt but has a region of controlled width over which the composition changes gradually. Annighofer and Gronski [157] have produced such copolymers consisting of styrene and isoprene in which the interfacial volume fraction was as high as 0.66.

The lack of preferential alignment of the lamellar domains manifests itself in the measured values of  $D_{\text{eff}}$ , as well as in the SAXS experiments. If the lamellar domains were aligned parallel to the film surface, then one would expect to observe  $D_{\text{eff}}$  values as predicted by the series law. The agreement between the experimental  $D_{\text{eff}}$  values and those predicted assuming a random orientation of grains is further evidence of the lack of significant orientation of the lamellar domains in these samples over the length scale of the film thickness.

It should be noted that sample SB 10/10, which had a rather disordered phase separated structure, had a measured  $D_{\text{eff}}$  much lower than the other samples containing 50% polystyrene. Evidently, the connectivity of the polybutadiene phase in this disordered structure is appreciably less than that of the lamellar structure. This is also apparent in the electron micrographs.

Electron microscopy showed that by changing the casting solvent from toluene to methyl ethyl ketone the morphology of sample SB 80/80 could be changed from alternating lamellae to isolated spheroidal polybutadiene domains embedded in a continuous polystyrene matrix. This change in morphology, i.e. in the connectedness of the more diffusive polybutadiene phase, shows up remarkably well in the diffusion measurements. The average value of the effective diffusion coefficient

dropped from  $6.5\text{E-}7$  for the toluene cast film to  $2.5\text{E-}7$  for the film cast from MEK. In addition, the value of  $D_{\text{eff}}$  for the MEK cast film agreed rather well to that predicted for spherical polybutadiene domains.

Also noteworthy is the difference in the diffusion coefficients of samples SB 22/10 and SB 23/10. Although their compositions are nearly the same, the measured values of  $D_{\text{eff}}$  differ by over 65%, which can be explained very nicely in terms of sample morphology. As seen by the micrographs in Figure A2, sample SB 23/10 exhibits the morphology of polybutadiene cylinders, and the measured value of  $D_{\text{eff}}$  for this sample agrees rather well with that predicted for this structure. Sample SB 22/10, on the other hand, has the ordered bicontinuous double diamond structure in which the more diffusive polybutadiene exists as a three dimensional continuous phase compared to the one dimensional continuous polybutadiene cylinders of sample SB 23/10. Therefore, the increase in  $D_{\text{eff}}$  for SB 22/10 is to be expected. Indeed, the effective diffusion coefficient of SB 22/10 is slightly greater than that predicted for a lamellar morphology of the same composition.

### Conclusions

Two main conclusions can be drawn from this study: (1) The morphology of two phase block copolymers, in addition to their composition, plays a large role in determining their transport properties. Especially important is the connectivity of the more

diffusive (conductive) phase. Increasing the connectedness of this phase will increase the effective diffusion coefficient; conversely, decreasing its connectedness will decrease the effective diffusion coefficient. No effect of interfacial volume fraction on the effective diffusion coefficient was found, although the solubilities of the samples with the larger interfacial volume fractions were observed to be less than that predicted by the additivity rule; and (2) the highly simplified models presented by Sax and Ottino for predicting the diffusion properties of materials having small scale order and large scale disorder work very well for the case of ordered two phase block copolymers. It should be noted that the models neglect the effect of orientation of the ordered grains, the effect of interfacial material, and the individual phase continuity across grain boundaries which is often observed for block copolymers. In addition, the models assume that the transport behavior in the polybutadiene and polystyrene microdomains is the same as that in the pure components, which may not be the case. Although the models could be improved to account for these effects, they seem to do quite well as they are.

## A P P E N D I X    B

### BCC Lattice Structure of Diblock Copolymers Exhibiting Spherical Microdomains

#### Introduction

As discussed in section 3.1.3, the type of lattice structure present in styrene-diene block copolymers forming spherical microdomains is still an active and somewhat controversial topic which warrants further investigation. The present work combines quantitative electron microscopy and SAXS studies on spherical microdomain samples which have been carefully prepared in such a manner as to produce a high degree of long range order. It is conclusively proven that a BCC lattice structure exists in both of the poly(styrene-butadiene) diblock copolymers studied, one containing polystyrene spheres and the other containing polybutadiene spheres. The novel feature of this study is the quantitative electron microscopy employing a tilt-rotate specimen holder whereby the (100), (110), and (111) projections of the lattice are all obtained from a single ordered grain. In addition, the SAXS patterns contain four well-defined lattice peaks indicating a very high degree of long range order.



### Experimental

Two different SB diblock copolymers, designated SB 10/110 and SB 60/10, were studied. Their molecular characteristics are given in Table B1. Sample SB 10/110 was an experimental polymer provided by Dr. D. L. Handlin, Jr. of Shell Development Company, while sample SB 60/10 was synthesized by Dr. L. J. Fetters of Exxon Research and Engineering Company and is the same copolymer used previously in the studies of micelle formation. Sample synthesis and characterization, sample preparation, electron microscopy, and SAXS were performed as described in Chapter 4. The electron microscopy tilt studies were performed using a side entry goniometer and tilt-rotate specimen holder which allowed the sections to be rotated  $\pm 180$  degrees and tilted about a chosen axis by  $\pm 60$  degrees.

### Results and Discussion

The corrected SAXS curves for samples SB 10/110 and SB 60/10 are shown in Figure B.1. The scattered intensity is given as the log of the number of counts recorded at a particular scattering vector  $Q$  ( $4\pi\sin\theta/\lambda$ ). Both samples exhibit at least three well defined interparticle interference peaks associated with the macrolattice of spherical microdomains (see arrows). In addition, there are weaker, broad peaks at higher angles attributed to intraparticle sphere

TABLE B1 Molecular characteristics of block copolymers

Sample	$M_n$ PS (Kg/mole)	$M_n$ PB (Kg/mole)	wt% PS	vol% PS	$M_w/M_n$
SB 10/110	10.5	113	8.48	7.43	1.06
SB 60/10	56.6	10.9	83.9	81.8	1.04

TABLE B2 SAXS lattice spacings

Sample	Reflection	$Q(\text{\AA}^{-1})$	$d(\text{\AA})$	$d_n/d_1$
SB 10/110	1	.0160	393	1.00
	2	.0226	279	.710
	3	.0273	230	.585
SB 60/10	1	.0210	299	1.00
	2	.0299	210	.702
	3	.0364	172	.577
	4	.0427	147	.492

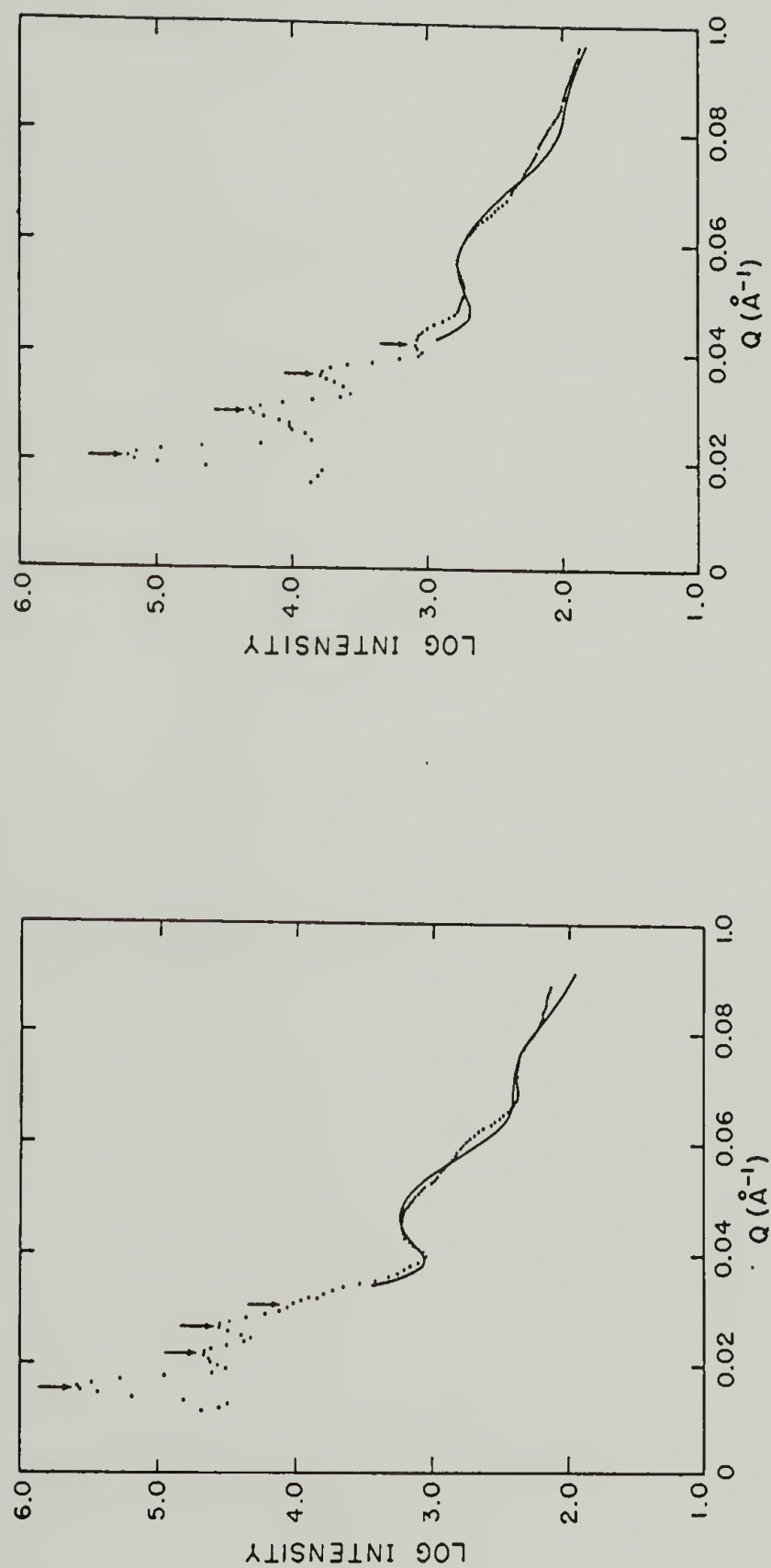
**a****b**

Figure B.1 Corrected SAXS curves for (a) SB 10/110 and (b) SB 60/10. The solid lines show the sphere scattering fit to the data, taking into account the distribution in sphere sizes.

scattering. Table B2 gives the  $Q$  values of the lattice peaks along with the corresponding spacings determined from Bragg's law. The relative spacings of the reflections are also listed. Comparing these relative spacings to those of the different cubic lattices listed in Table 2.1 reveals excellent agreement for both the SC and BCC lattice. The arrows in Figure B1 indicate the predicted positions of the first four lattice reflections for the SC and BCC packing modes. Since the seventh order reflection would need to be resolved in order to distinguish between SC and BCC, the assignment of a particular lattice requires additional information.

By performing tilting experiments in the electron microscope, a systematic series of two dimensional projections can be obtained from a given area from which the three dimensional structure can be conclusively determined. Figure B.2 shows the (100), (110), and (111) projections for the SC, BCC, and FCC lattices. In each case, the unit cell has been outlined and the projected distances between neighboring spheres are indicated. Of course, both SC and BCC lattices exhibit square (100), rectangular (110), and hexagonal (111) projections; however, it is possible to distinguish between the packing modes using the tilt method shown schematically in Figure B.3. An area (single grain) of section in the correct orientation to give a square projection (i.e. (100) projection) is first located. This section is then tilted about the two different axes designated [10] and [11] in Figure B.3. Tilting about the [10] axis is equivalent to tilting about the [100] SC axis or the [110] BCC axis. Similarly, tilting about the [11] axis is



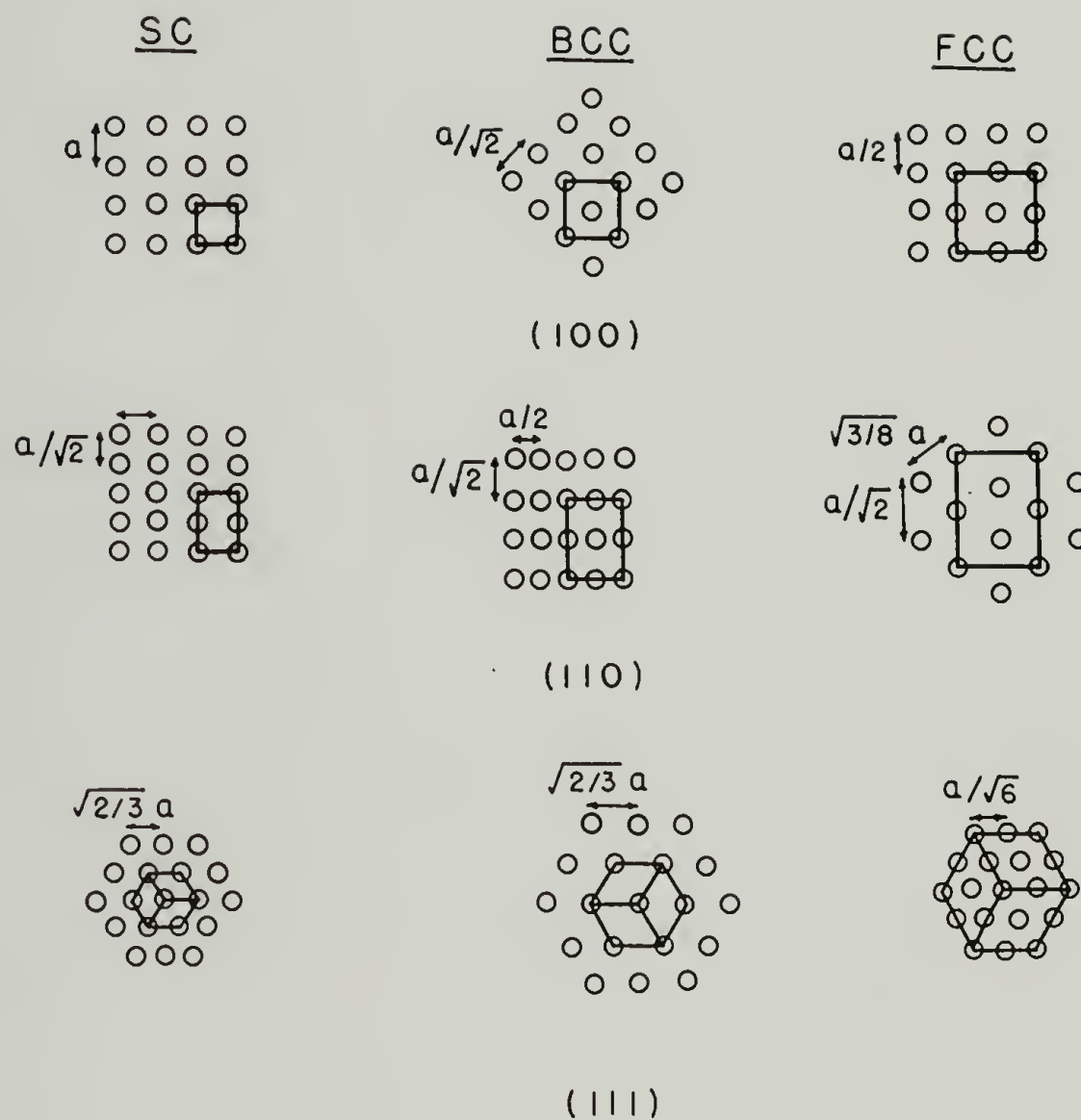


Figure B.2 (100), (110), (111) projections of a SC, BCC, and FCC lattice showing the unit cells (outlined) and relative projected intersphere distances. The square arrays of the (100) projections have been drawn the same size leading to different unit cell sizes for the three lattice types. Subsequent projections have been scaled accordingly.

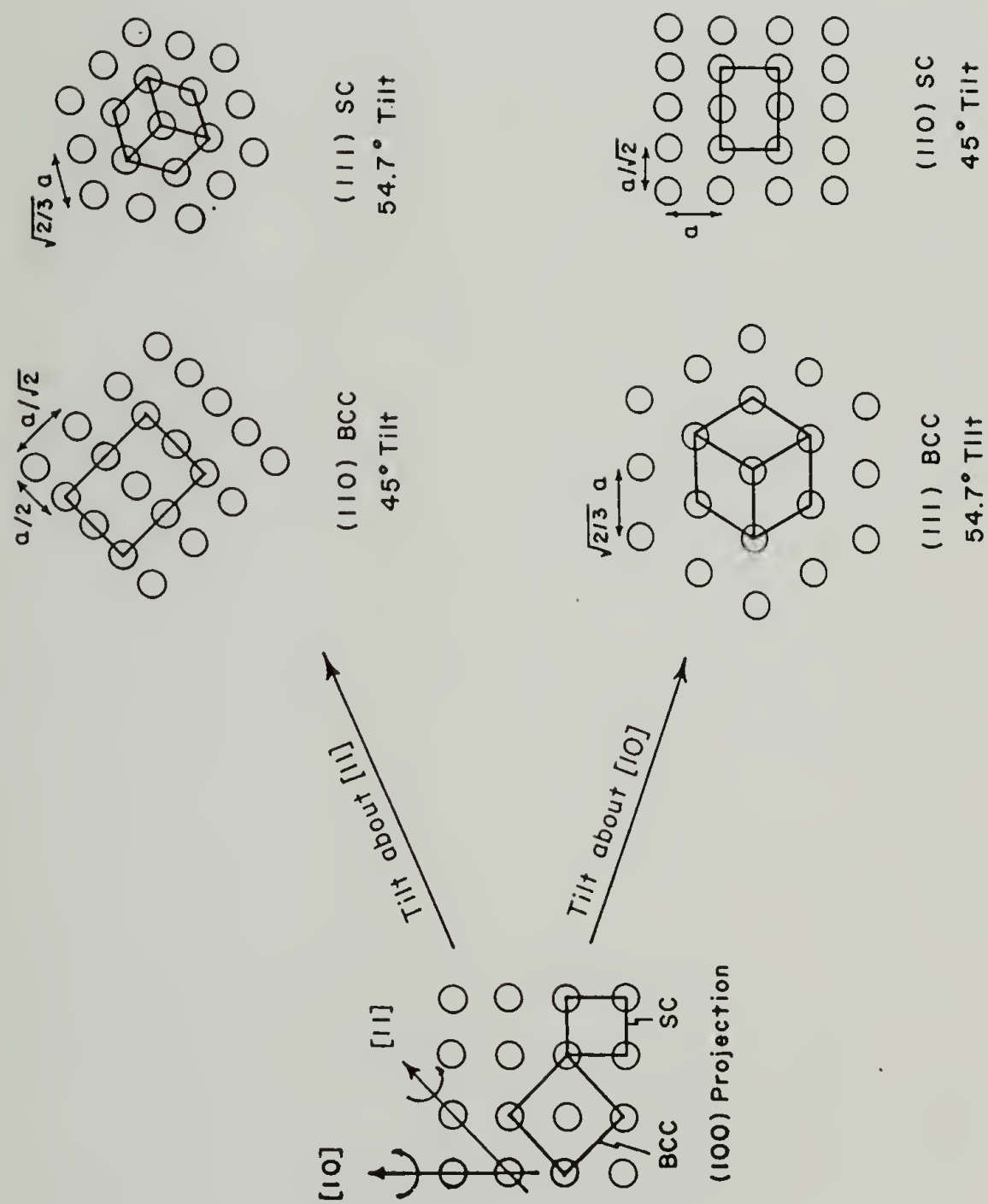


Figure B.3 Schematic of tilting experiments performed in the electron microscope.

equivalent to tilting about the  $[110]$  SC axis or the  $[100]$  BCC axis. Therefore, as shown in Figure B.3, tilting about the  $[10]$  or  $[11]$  axis will produce different projections depending on the lattice type. For example, a 45 degree tilt about the  $[10]$  axis produces a rectangular array of spheres if the lattice is SC, while a 54.7 degree tilt about this same axis produces a hexagonal array if the lattice is BCC. Conversely, a 45 degree tilt about the  $[11]$  axis will produce a rectangular array if the lattice is BCC, while a 54.7 degree tilt about this axis will produce a hexagonal array if the lattice is SC.

Figure B.4 shows the results of such an exercise for sample SB 10/110. Starting with the square projection observed in micrograph B.4a, the section was tilted about the two axes indicated by  $[10]$  and  $[11]$ . A 53 degree tilt about the  $[10]$  axis produced the hexagonal projection observed in micrograph B.4b, while a 46 degree tilt about the  $[11]$  axis produced the rectangular projection observed in micrograph B.4c (the section was rotated 45 degrees clockwise prior to tilting). These observations prove the existence of a BCC lattice for SB 10/110, consistent with the SAXS results.

Optical diffraction patterns obtained from the negatives of these micrographs are shown in each figure, substantiating the macrolattice structure. Each micrograph in Figure B.4 was taken from the same area (ordered grain) of a single section as evidenced by the two dark marks present on all three micrographs (see arrows). These marks are probably due to the osmium tetroxide staining, and help to provide landmarks by which the same area of the section may be located in each micrograph;

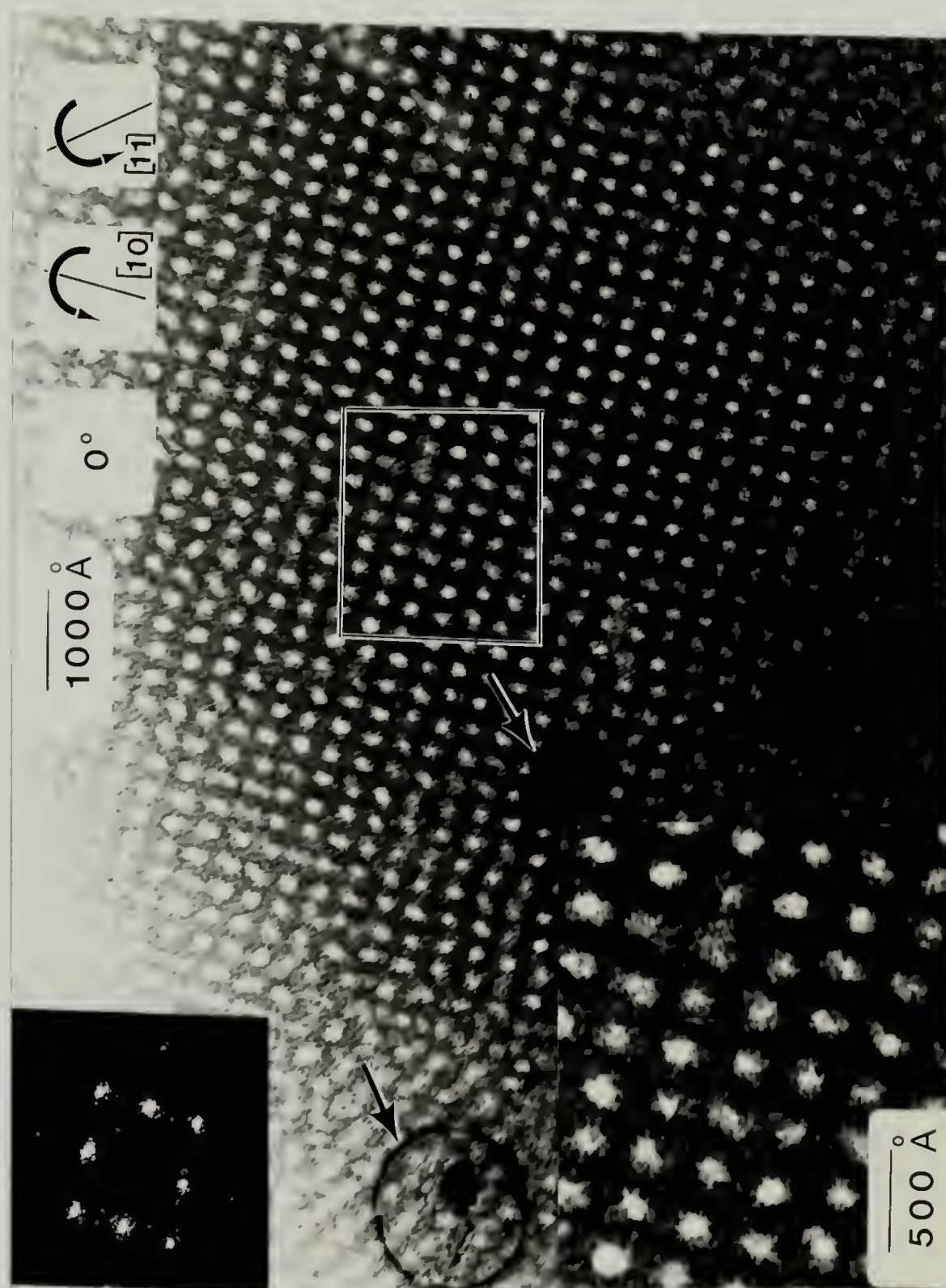


Figure B.4a Electron micrograph showing the (100) projection of the BCC macrolattice for SB 10/110.



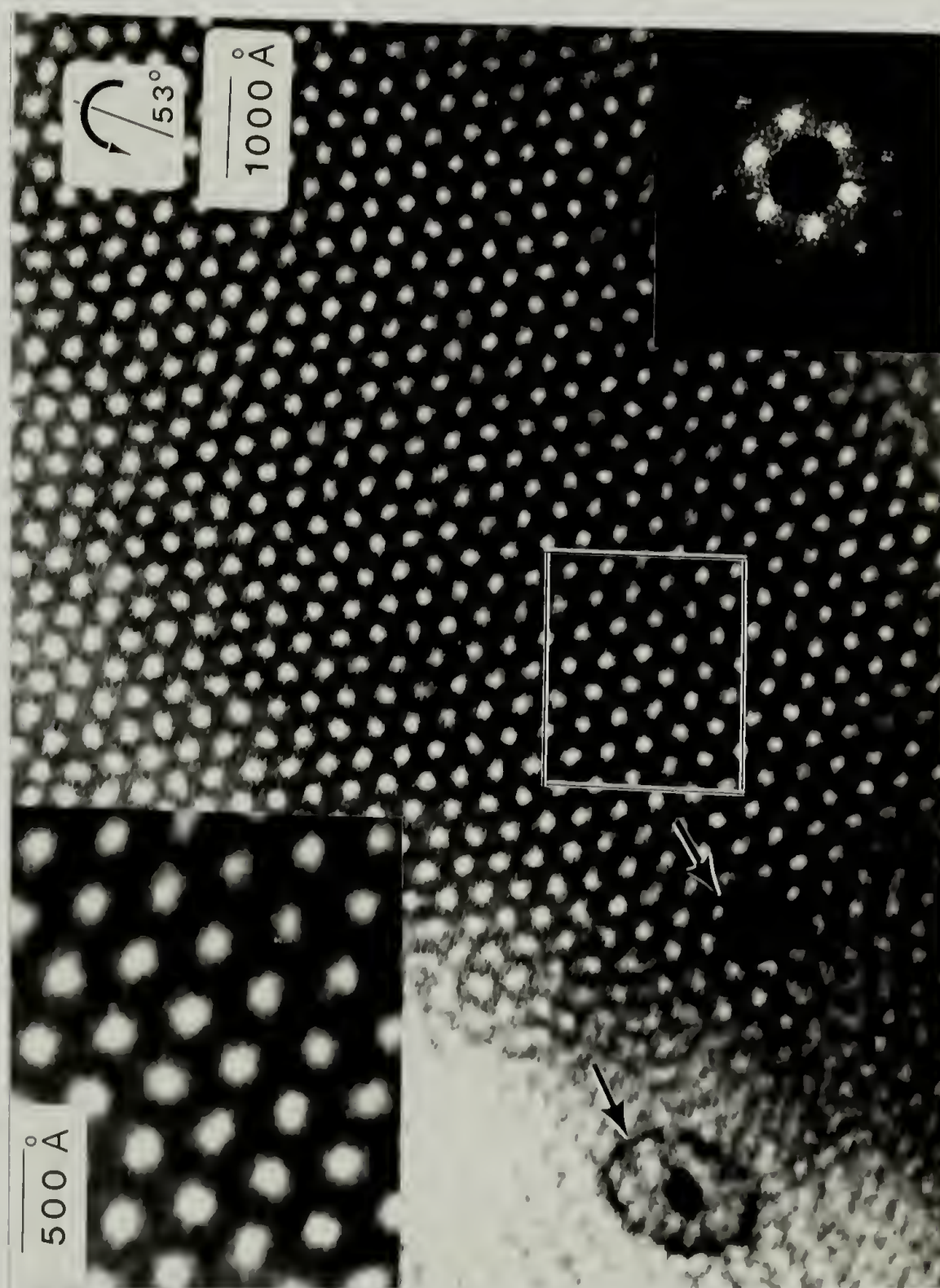


Figure B.4b Electron micrograph showing the (111) projection of the BCC macrolattice for SB 10/110.

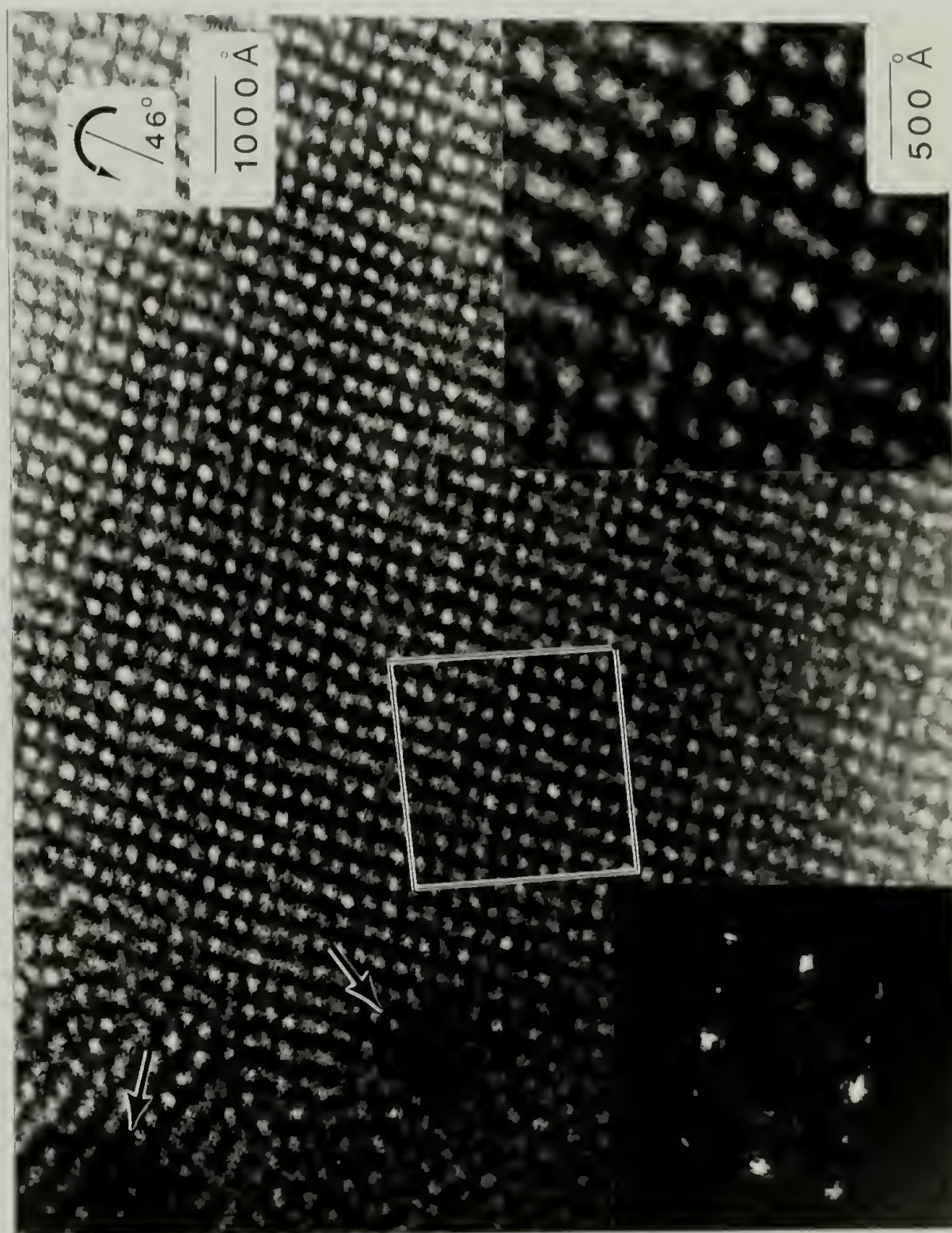


Figure B.4c Electron micrograph showing the (110) projection of the BCC macrolattice for SB 10/110.



such an area has been outlined and enlarged. Such landmarks can be purposely introduced and used to confirm the axis and amount of tilt (which was read from the side entry goniometer of the electron microscope) between different micrographs of the tilt series. For example, the three dark circular regions observed in micrographs B.5a and b are 1000 Å diameter polystyrene spheres which were deposited on the section after staining. As in Figure B.4a and b, a SB 10/110 section giving a square projection was tilted about the [10] axis to produce a hexagonal projection, the amount of tilt read from the goniometer being 56 degrees. By triangulating between the positions of the three spheres in each micrograph, the tilt axis and amount of tilt can be independently determined. This is particularly easy for the case of Figure B.5 since a line drawn between the 1000 Å polystyrene spheres marked 1 and 2 conveniently lies along the assumed tilt axis. Therefore, the distance between these spheres should not change upon tilting, which is indeed found to be the case, confirming that the tilt is about the [110] BCC axis. In addition, the cosine of the tilt angle can be determined from the ratio of the lengths of the perpendicular from sphere 3 to the line joining spheres 1 and 2. In this manner, the tilt angle was found to be 55.5 degrees which agrees rather well with the tilt angle read from the goniometer.

Further confirmation of the BCC lattice structure is obtained by comparing the measured relative projected distances between neighboring spheres to those predicted for the different lattices (see Figure B.2). The projected intersphere distances measured from the micrographs in

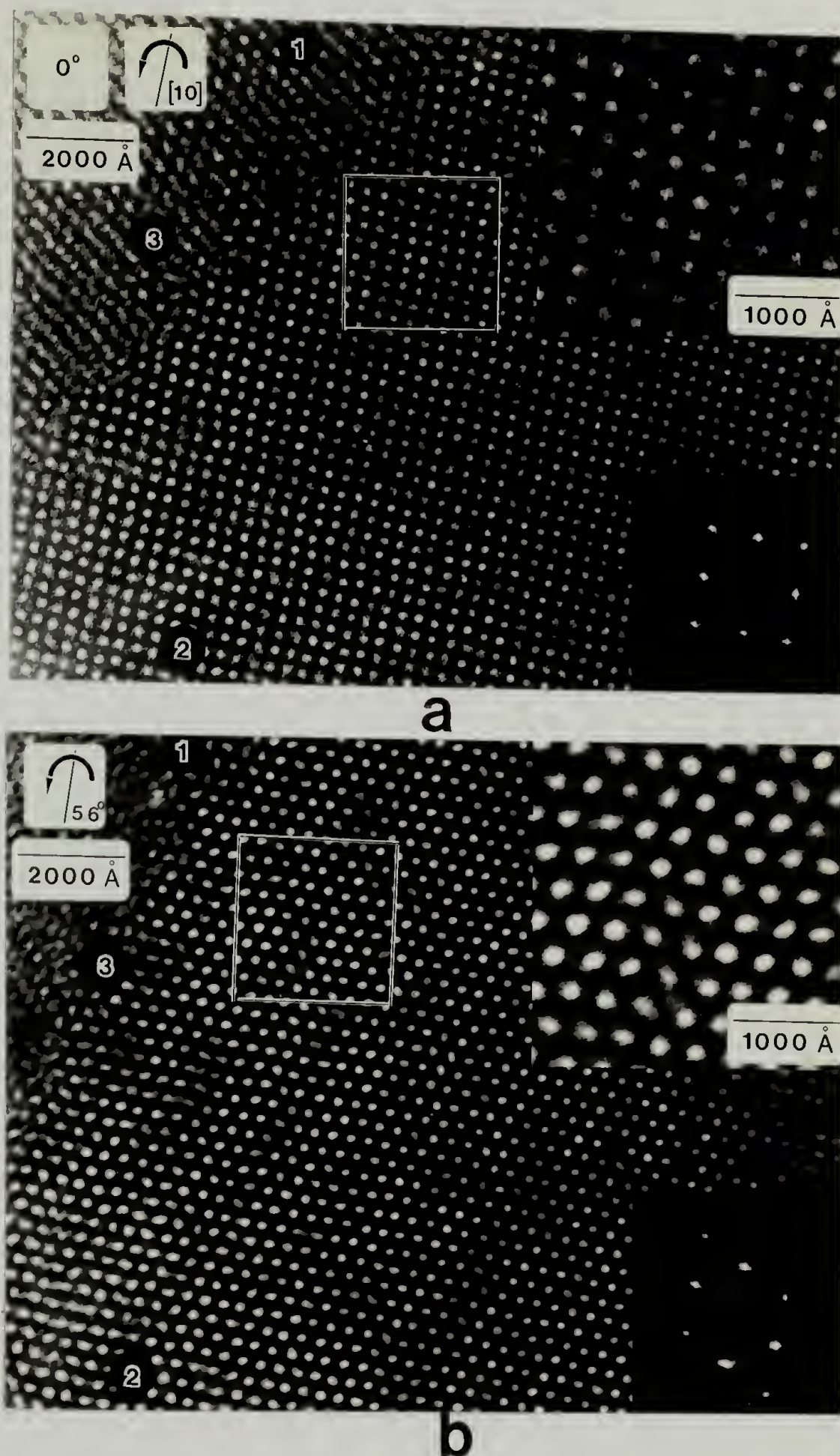


Figure B.5 Electron micrographs showing the (a) (100), and (b) (111) projections of the BCC macrolattice for SB 10/110. The dark circular regions labeled 1, 2, and 3 are 1000 Å PS spheres deposited on the section to confirm the axis and magnitude of tilt between the two projections.



TABLE B3 Comparison of intersphere distance for the various  
projections of SB 10/110

Micrograph	Array	(hkl)	d Projected Inter-	(d/a)	(d/a)
		Projection	sphere distance (Å)	calc.	BCC
B4a	square	(100)	300	.707*	.707
B4b	hexagonal	(111)	350	.825	.816
B4c	rectangular	(110)	281 x 216	.509x.663	.500x.707
B5a	square	(110)	312	.707**	.707
B5b	hexagonal	(111)	352	.798	.816

\*with a = 424 Å

\*\*with a = 441 Å

Figures B.4 and B.5 are listed in Table B3, which also gives the dimensions normalized with respect to the size of the BCC unit cell calculated from the (100) projection. Comparing these normalized dimensions to those predicted for the BCC lattice shows good agreement. It should be noted that the (100) projection shown in Figure B.4a is not exactly a square array. The average dimensions in the [10] and [01] directions are 320 and 280 Å. Most likely, this is due to a slight deformation of the section during microtoming. The value of 300 Å given in Table B3 is thus an average value.

The results of the tilting experiments for sample SB 60/10 were essentially identical to those of sample SB 10/110. Moreover, with knowledge of the sample structure (and the particular axis of tilt and (hkl) projection) it is straightforward to determine the section thickness by noting the degree of distortion of the projection with amount of tilt from the (symmetrical) ideal projection setting. For example, a section giving a (100) projection, shown in Figure B.6a, was tilted 49 degrees about the [110] BCC axis to produce the slightly distorted (111) projection observed in Figure B.6b. Assuming the normal to the projection in B6b to be 5.7 degrees off of the [111] axis, measurement of the long axis of the ellipse (normal to the [110] direction) yields a 500 Å thick section in the boxed area, i.e. about 1.5 unit cells thick. In addition, both the distortion of the hexagonal projection and the axial ratio of the elliptical projections are seen to increase on proceeding from the top right to the bottom left of the

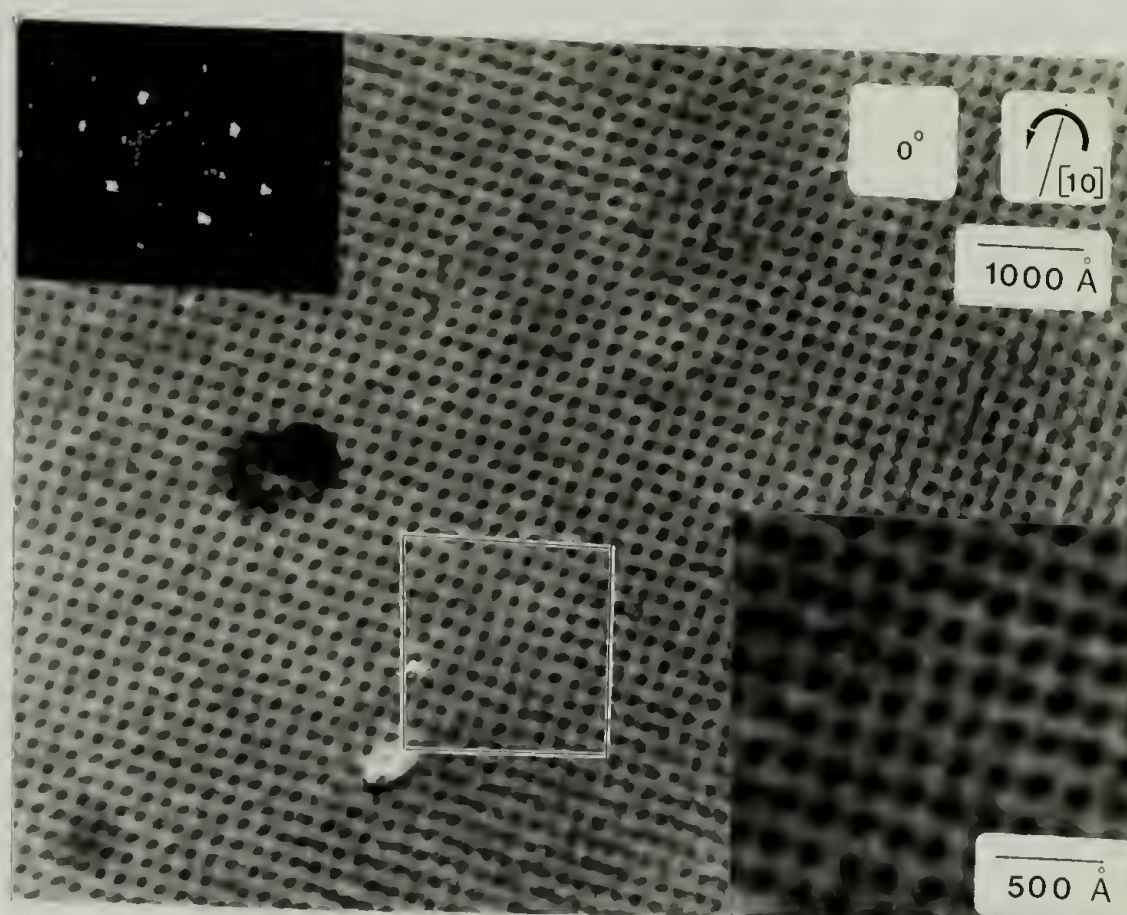
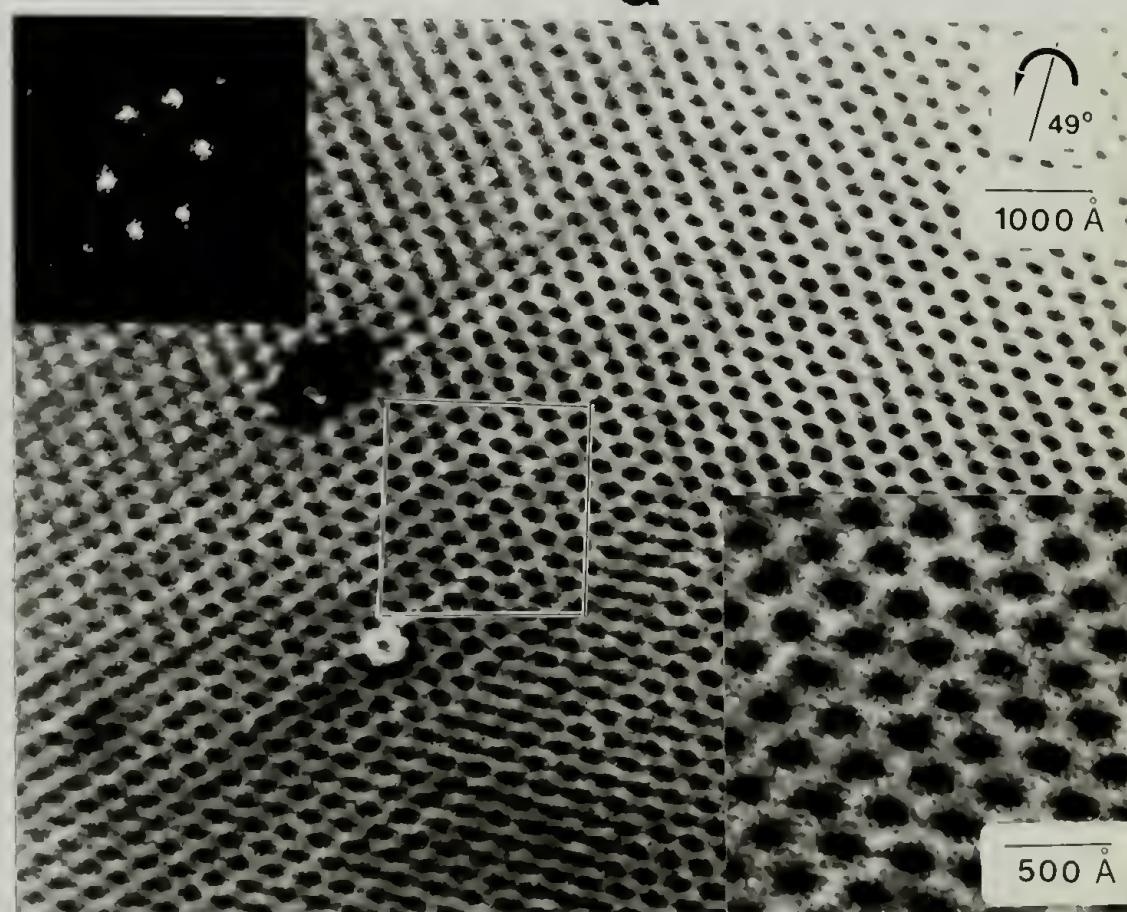
**a****b**

Figure B.6 Electron micrographs showing the (a) (100), and (b) near (111) projections of the BCC macrolattice for SB 60/10.



micrograph, while the overall intensity level decreases, as a result of increasing section thickness.

It is also informative to compare the values of the BCC unit cell size ( $a$ ) and the sphere radius ( $R$ ) measured from the electron micrographs to the values determined from SAXS (see Table B4). The values of  $a$  from SAXS were obtained from the slope of a  $d_{hkl}$  versus  $(h^2 + k^2 + l^2)^{-1/2}$  plot. The SAXS sphere sizes were obtained by fitting the scattering predicted from a polydisperse system of spheres to the scattering data in the higher angle region where the type II distortions have caused the interparticle interference factor to approach unity. The solid lines in Figure B.1a and b show the best fit of the theoretical sphere scattering to the actual data, obtained by adjusting  $\bar{R}$ , the average sphere radius, and  $\sigma_R$ , the standard deviation of the gaussian used to approximate the distribution in sphere size. The comparison shows that the sizes of the unit cell as well as the sphere radii determined by electron microscopy are between 20 and 30% smaller than those determined by SAXS, for both polystyrene and polybutadiene spheres. These observations can be explained by a uniform contraction of the section, arising from either the osmium tetroxide staining process and/or from exposure to the electron beam in the microscope. A similar observation has been reported previously by Berney et al. [145] who found that polybutadiene sphere sizes for several different SB diblock copolymers measured by electron microscopy were on the average 23% smaller than the sphere sizes determined by SANS. These authors



TABLE B4      Comparison of EM and SAXS results

	SB 10/110	SB 60/10
$a_{\text{SAXS}} (\text{\AA})$	556	423
$a_{\text{EM}} (\text{\AA})$	441	300
% difference	21	29
$\bar{R}_{\text{SAXS}} (\text{\AA})$	116	95
$\sigma_R (\text{\AA})$	13	12
$\bar{R}_{\text{EM}} (\text{\AA})$	86	67
% difference	26	29

attributed this discrepancy to the osmium tetroxide staining. Therefore, if accurate lattice spacings and sphere radii are desired, small angle scattering is the preferred technique; nevertheless, electron microscopy can provide accurate relative dimensions within a section and positive lattice identification.



